AD-A055 409 COASTAL ENGINEERING RESEARCH CENTER FORT BELVOIR VA F/G 8/3
WAVE TRANSFORMATION AT ISOLATED VERTICAL PILES IN SHALLOW WATER--ETC(U)
MAR 78 R J HALLERMEIR, R E RAY

UNCLASSIFIED CERC-TP-78-1 NL

1 OF 2
AD
A055409

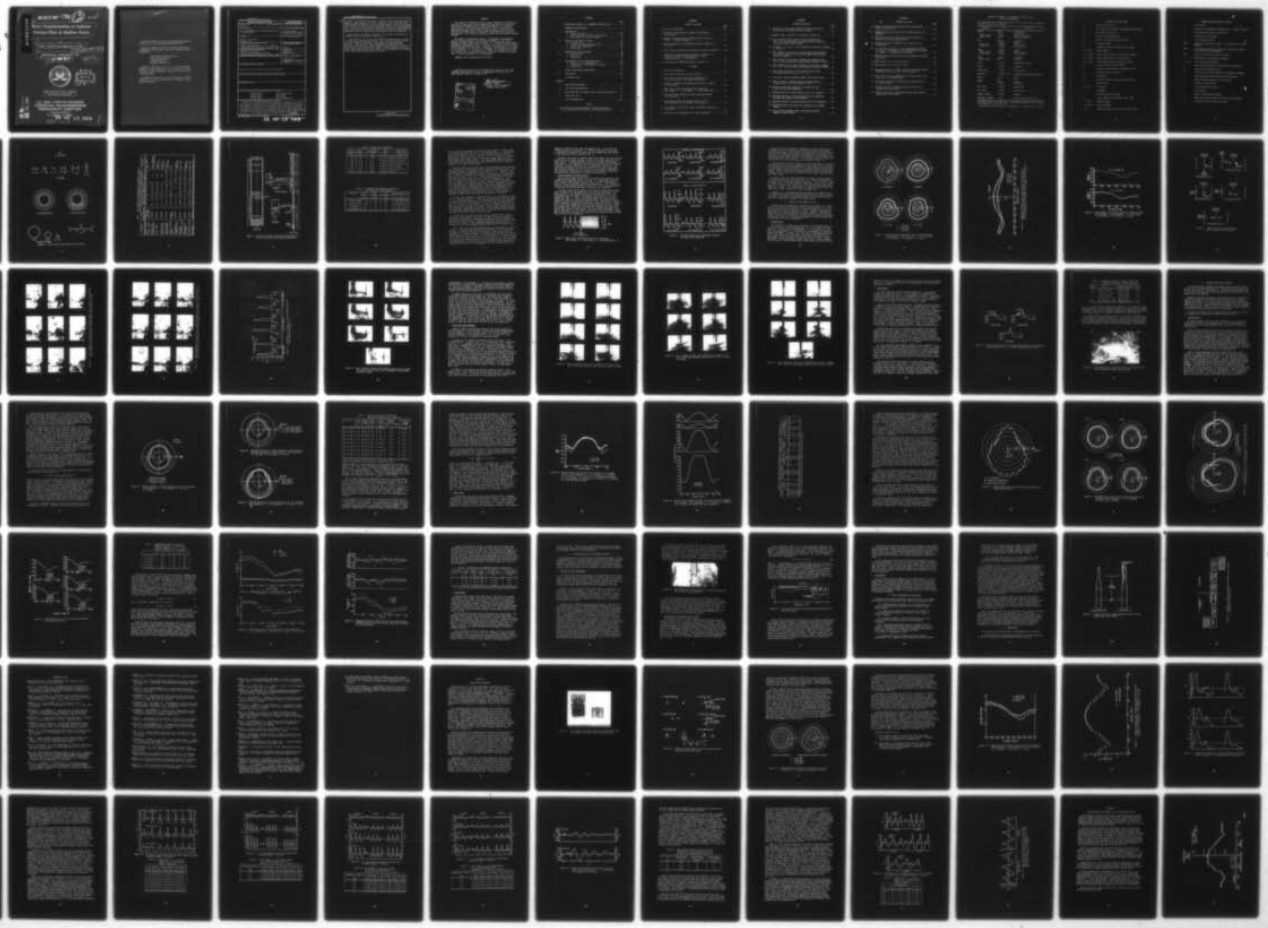


F
5409

FOR FURTHER TRAN[illegible] (12) TP 78-1

(6)

Wave Transformation at Isolated Vertical Piles in Shallow Water

(10)

by

Robert J. Hallermeier and Robert E. Ray

(9) (14) CERC-TP-78-1

TECHNICAL PAPER NO. 78-1

(11) MARCH 1978

(12) 190 p.

Approved for public release; distribution unlimited.

U.S. ARMY, CORPS OF ENGINEERS
COASTAL ENGINEERING RESEARCH CENTER
Kingman Building
Fort Belvoir, Va. 22060

UNCLASSIFIED

SECURITY CLASSIFICATION OF THIS PAGE *(When Data Entered)*

REPORT DOCUMENTATION PAGE

READ INSTRUCTIONS BEFORE COMPLETING FORM

1. REPORT NUMBER: TP 78-1	2. GOVT ACCESSION NO.
3. RECIPIENT'S CATALOG NUMBER	
4. TITLE *(and Subtitle)*: WAVE TRANSFORMATION AT ISOLATED VERTICAL PILES IN SHALLOW WATER	5. TYPE OF REPORT & PERIOD COVERED: Technical Paper
	6. PERFORMING ORG. REPORT NUMBER
7. AUTHOR(s): Robert J. Hallermeier Robert E. Ray	8. CONTRACT OR GRANT NUMBER(s)
9. PERFORMING ORGANIZATION NAME AND ADDRESS: Department of the Army Coastal Engineering Research Center (CERRE-CP) Kingman Building, Fort Belvoir, Virginia 22060	10. PROGRAM ELEMENT, PROJECT, TASK AREA & WORK UNIT NUMBERS: A31222
11. CONTROLLING OFFICE NAME AND ADDRESS: Department of the Army Coastal Engineering Research Center Kingman Building, Fort Belvoir, Virginia 22060	12. REPORT DATE: March 1978 13. NUMBER OF PAGES: 187
14. MONITORING AGENCY NAME & ADDRESS*(if different from Controlling Office)*	15. SECURITY CLASS. *(of this report)*: UNCLASSIFIED 15a. DECLASSIFICATION/DOWNGRADING SCHEDULE

16. DISTRIBUTION STATEMENT *(of this Report)*

Approved for public release, distribution unlimited.

17. DISTRIBUTION STATEMENT *(of the abstract entered in Block 20, if different from Report)*

18. SUPPLEMENTARY NOTES

19. KEY WORDS *(Continue on reverse side if necessary and identify by block number)*

Channeled piles	Wave direction gage
Circular piles	Wave forces
Surface effects	Wave runup
Velocity head	Wave transformation

20. ABSTRACT *(Continue on reverse side if necessary and identify by block number)*

Water level was measured within the flanges of a channeled pile, or near the surface of a circular pile, for isolated piles in a periodic wave train. Measurements are plotted as 160 patterns of crest height versus orientation with respect to wave direction. All patterns have a maximum at the front, facing into the wave, and a lesser maximum at the rear. Intervening minimums are symmetrically located at the sides of the pattern, usually slightly toward the rear. As wave height increases, the front maximum becomes higher,

(continued)

DD FORM 1 JAN 73 1473 EDITION OF 1 NOV 65 IS OBSOLETE

UNCLASSIFIED

SECURITY CLASSIFICATION OF THIS PAGE *(When Data Entered)*

depending on calculated velocity head. The angular width of the front maximum depends on channel geometry of the pile, tending to be very broad for a pile without channels and narrow for a pile with deep channels. With H-piles having deep channels, the pattern minimums occur farther forward than with unchanneled piles. Geometrically similar piles of different size result in similar patterns. The patterns for finned and smooth circular piles are similar, except that the finned pile results in slightly higher and narrower front and rear maximums.

Applications of the reported conclusions to the design of nearshore pile-supported structures are briefly discussed.

Twelve different vertical piles were tested, including circular, circular with radial fins, and various H-sections. Pile cross section and water depth were small compared to wavelength, corresponding to typical nearshore situations. Electrical gage records and photos show complicated surface effects occur near the piles. Crest stagnation can be similar at circular and channeled piles with three stagnation regimes: smooth, breaking, and jetting runup. Smooth runup occurred in most tests, with a nonbreaking bow wave formed at the front of the pile during peak forward flow.

PREFACE

This report is published to assist coastal engineers and scientists dealing with wave action at pile-supported structures by providing results from a laboratory study of wave transformation at a variety of vertical piles. The tests were conducted at the U.S. Army Coastal Engineering Research Center (CERC) during an effort to develop a nearshore wave direction gage utilizing wave transformation at a surface-piercing pile. The study was carried out under the wave dynamics program of CERC.

The report was prepared by Robert J. Hallermeier, Oceanographer, Coastal Processes Branch, with assistance by Robert E. Ray, Civil Engineer, Coastal Design Criteria Branch. Dr. Hallermeier worked under the general supervision of Dr. C.J. Galvin, Jr., Chief, Coastal Processes Branch, who initiated the study. The tests were performed by J.C. Jones, R.J. Karlitskie, R.E. Ray, and C.R. Schweppe, with continuing assistance by R.P. Stafford. J.C. Ahlquist, D.C. Fresch, B.H. Gwinnup, L.B. Keely, C.F. Thomas, and S.B. Ward assisted with the data reduction and display, and J.T. Dayton assisted with the photography.

Comments on this publication are invited.

Approved for publication in accordance with Public Law 166, 79th Congress, approved 31 July 1945, as supplemented by Public Law 172, 88th Congress, approved 7 November 1963.

JOHN H. COUSINS
Colonel, Corps of Engineers
Commander and Director

CONTENTS

TABLES

CONTENTS

TABLES--Continued

FIGURES

CONTENTS

FIGURES--Continued

CONTENTS

FIGURES--Continued

CONVERSION FACTORS, U.S. CUSTOMARY TO METRIC (SI) UNITS OF MEASUREMENT

U.S. customary units of measurement used in this report can be converted to metric (SI) units as follows:

Multiply	by	To obtain
inches	25.4	millimeters
	2.54	centimeters
square inches	6.452	square centimeters
cubic inches	16.39	cubic centimeters
feet	30.48	centimeters
	0.3048	meters
square feet	0.0929	square meters
cubic feet	0.0283	cubic meters
yards	0.9144	meters
square yards	0.836	square meters
cubic yards	0.7646	cubic meters
miles	1.6093	kilometers
square miles	259.0	hectares
knots	1.8532	kilometers per hour
acres	0.4047	hectares
foot-pounds	1.3558	newton meters
millibars	1.0197×10^{-3}	kilograms per square centimeter
ounces	28.35	grams
pounds	453.6	grams
	0.4536	kilograms
ton, long	1.0160	metric tons
ton, short	0.9072	metric tons
degrees (angle)	0.1745	radians
Fahrenheit degrees	5/9	Celsius degrees or Kelvins[1]

[1]To obtain Celsius (C) temperature readings from Fahrenheit (F) readings, use formula: $C = (5/9)(F - 32)$.

To obtain Kelvin (K) readings, use formula: $K = (5/9)(F - 32) + 273.15$.

SYMBOLS AND DEFINITIONS

a	circular pile radius
B	beat length between first and second wave harmonics
b	half-width of wave tank
C_D	empirical drag coefficient
D	draft of a surface-piercing obstacle
d	stillwater depth
E	eccentric setting on wavemaker drive wheel
$F = U^2/g\ell$	Froude number
$F_a = U^2/2ga$	Froude number based on circular pile diameter
$F_D = u^2/gD$	Froude number based on obstacle draft
$F_t = U^2/gt$	Froude number based on obstacle thickness
f_D	drag force per unit pile length
G	distance from wavemaker to measurement point
g	acceleration due to gravity
H	wave height
h	horizontal semiaxis of water particle orbit
j	integer index
$k = 2\pi/L$	wave number
L	wavelength
ℓ	characteristic flow length
Q	trough depth below stillwater level (SWL)
$R = U\ell/\nu$	Reynolds number
$S = HL^2/2d^3$	Stokes parameter
$S(\alpha)$	symmetric series curve fit to peak water data

SYMBOLS AND DEFINITIONS--Continued

T	wave period
t	obstacle cross-sectional thickness norm to wave direction
U	horizontal fluid speed at wave crest
u	characteristic flow speed
W	crest height above SWL
$W(\alpha)$	peak water above SWL at angle α on circular pile circumference
$\overline{W}(\alpha)$	time-averaged quantity of peak water above SWL at angle α on circular pile circumference
$W(\beta)$	peak water above SWL at pile yaw angle β
X	maximum pile cross-sectional dimension
$Z = a/b$	flow constriction parameter
α	angle specifying point on circular pile circumference
β	yaw angle of noncircular pile
$\overline{\beta}$	average over yaw angles identical according to symmetry
γ	angle specifying front symmetry point of pattern
θ	angle describing geometry of pile channel
ν	kinematic fluid viscosity
π	the transcendental number 3.14 . . .
ρ	fluid density
ϕ	angle locating pattern minimum
χ	angle measuring half-width of pattern's front maximum
ψ	orientation angle in wave basin tests

WAVE TRANSFORMATION AT ISOLATED VERTICAL PILES IN SHALLOW WATER

by
Robert J. Hallermeier and *Robert E. Ray*

I. INTRODUCTION

1. Context of Study.

This report presents the results of a laboratory investigation of wave height measurements at an isolated pile. The investigation was motivated by the possibility that wave transformation near a pile can be used to measure nearshore wave directions (Galvin and Hallermeier, 1972). Usual test situations with a straight wave crest incident on a vertical pile, either smooth or with channels, are shown in Figure 1. Figure 2 shows the cross sections and the types of piles tested. These tests investigated the dependencies of transformed crest height near a pile on incident wave characteristics and on the cross-sectional shape and orientation of the pile. This account completes several brief reports on these data (Galvin and Hallermeier, 1972; Hallermeier, 1976; James and Hallermeier, 1976).

The tests differed from previous laboratory studies of waves on piles in that the pile's effect on the wave was measured, rather than the wave's effect on the pile. Previous studies primarily investigated wave force or pressure on circular vertical piles (Table 1). The report extends the previous work, as indicated in Table 1, by recording water levels at a wide variety of piles, and thoroughly examining the effects of pile orientation with respect to wave direction. The tests were conducted in relatively shallow water with relatively steep waves; the test piles have small cross sections compared to wavelength.

2. Test Situations and Water Level Records.

The tests were conducted in two indoor wave tanks with length, width, and height dimensions of 96 by 1.5 by 2 feet (29.3 by 0.5 by 0.6 meters) and 85 by 14 by 4 feet (25.9 by 4.3 by 1.2 meters), hereafter called the 96-foot tank and the 85-foot tank, respectively. Figure 3 shows plan views of these wave tanks. Each tank had a piston-type wavemaker, a vertical flat plate across the width of the tank, driven horizontally in nearly sinusoidal motion with a set period, T, and amplitude controlled by the radius setting, E, of the rod connecting a rotating drive wheel to the wavemaking plate. At the end opposite the wavemaker, each tank had an unchanging wave absorber, a steep beach of about 3-inch-diameter (0.1 meter) rubble in the 85-foot tank, and a gently inclined plane of permeable rubberized hogshair in the 96-foot tank. A vertical surface-piercing pile was rigidly mounted in the long section of the tanks with constant water depth, d.

The major test conditions are listed in Table 2. These laboratory conditions represent the prototype situations listed in Table 3.

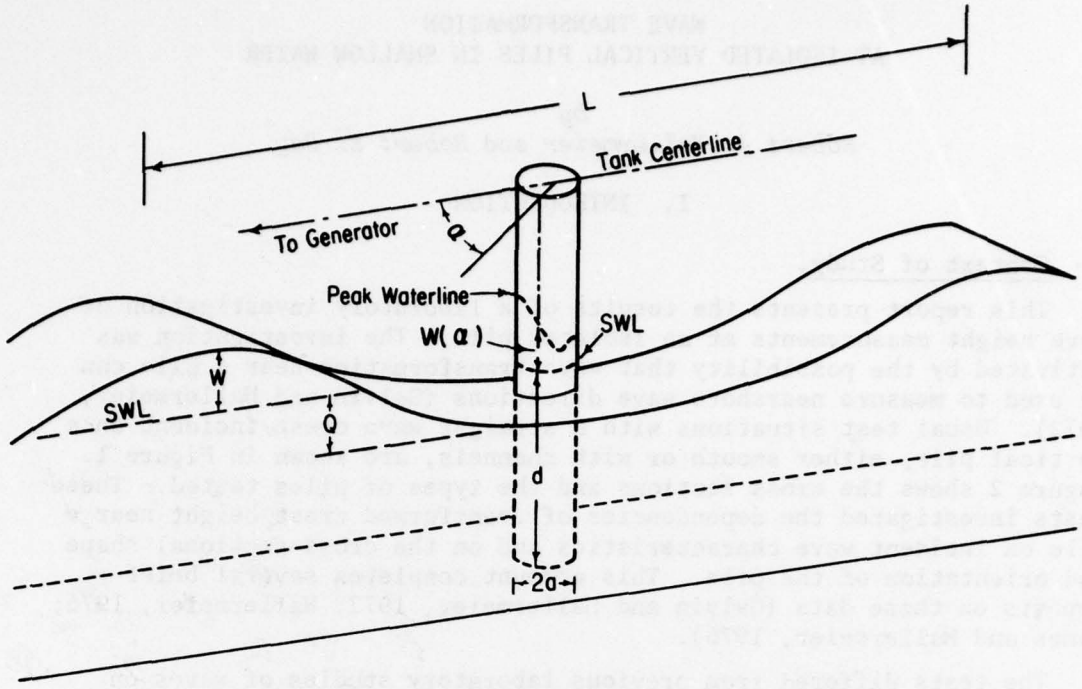

a. Circular Pile.

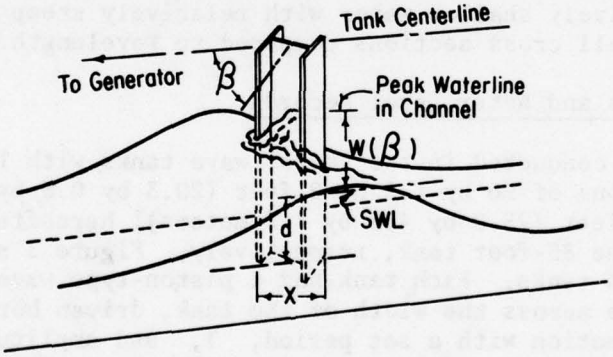

b. Pile with Channels.

Figure 1. Usual test situations.

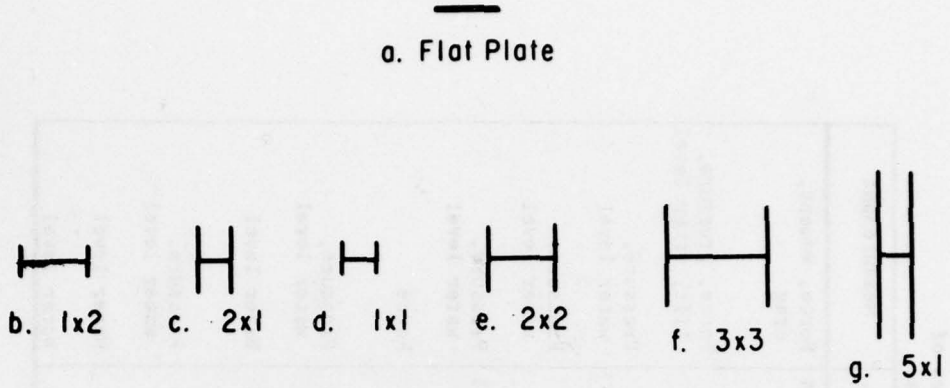

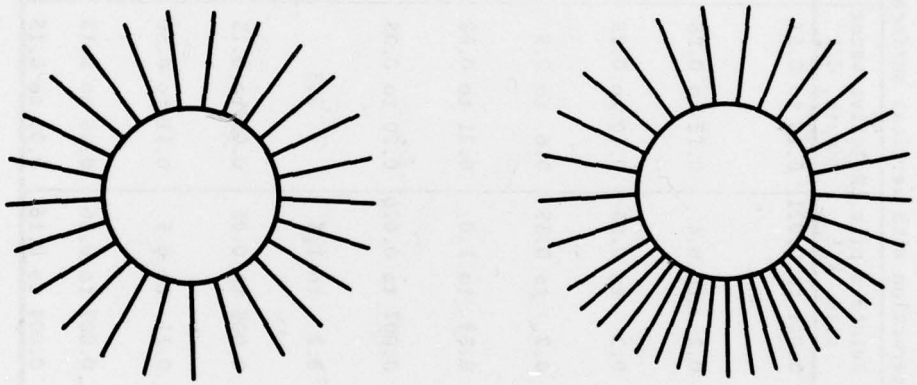

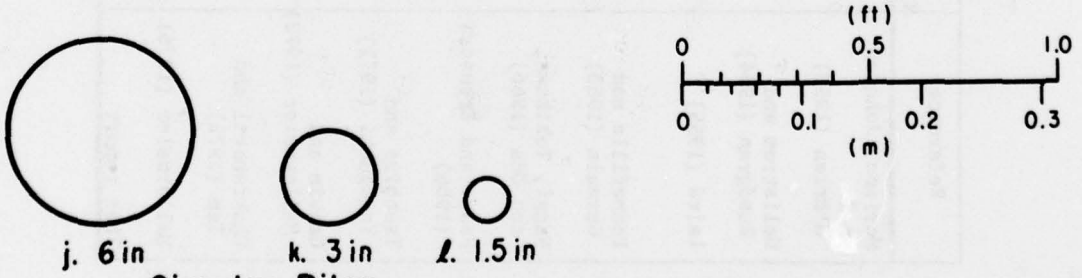

Figure 2. Cross sections and types of piles tested.

Table 1. Test conditions and measurements in laboratory studies of wave interaction with vertical surface-piercing piles.

Reference	Pile cross sections	Relative pile size, X/L	Relative water depth, d/L	Wave steepness, H/L	Measurement
Morison, Johnson, and O'Brien (1953)	Circular, flat plate, H-section	0.011 to 0.021	0.10 to 0.53	0.009 to 0.114	Force, moment, drag
Hellstrom and Rundgren (1954)	Circular	0.2 to 0.4	0.12 to 0.25	0.1	Force, pressure, lift, water level
Laird (1955)	Circular	0.2 to 0.55	0.10 to 0.25	<0.03	Pressure, water level
Bonnefille and Germain (1963)	Circular	0.2 to 0.35	0.6 to 0.9	<0.04	Pressure, water level
Nagai, Tokikawa, and Oda (1966)	Circular	0.33 to 1.0	0.21 to 0.62	0.017 to 0.055	Pressure, water level
Paape and Breusers (1966)	Square, circular	0.007 to 0.026	0.20 to 0.35	0.03 to 0.09	Force
Tsuchiya and Yamaguchi (1971)	Circular	0.2 to 1.3	0.3	0.003 to 0.03	Pressure, water level
Galvin and Hallermeier (1972)	Various	0.005 to 0.05	0.05 to 0.13	0.008 to 0.04	Water level
Chakrabarti and Tam (1975)	Circular	0.11 to 0.5	0.11 to 0.50	0.009 to 0.06	Pressure, water level
Hallermeier (1976)	Circular	0.007 to 0.16	0.05 to 0.13	0.006 to 0.06	Water level
This report	(See Fig. 2)	0.004 to 0.16	0.05 to 0.13	0.006 to 0.06	Water level

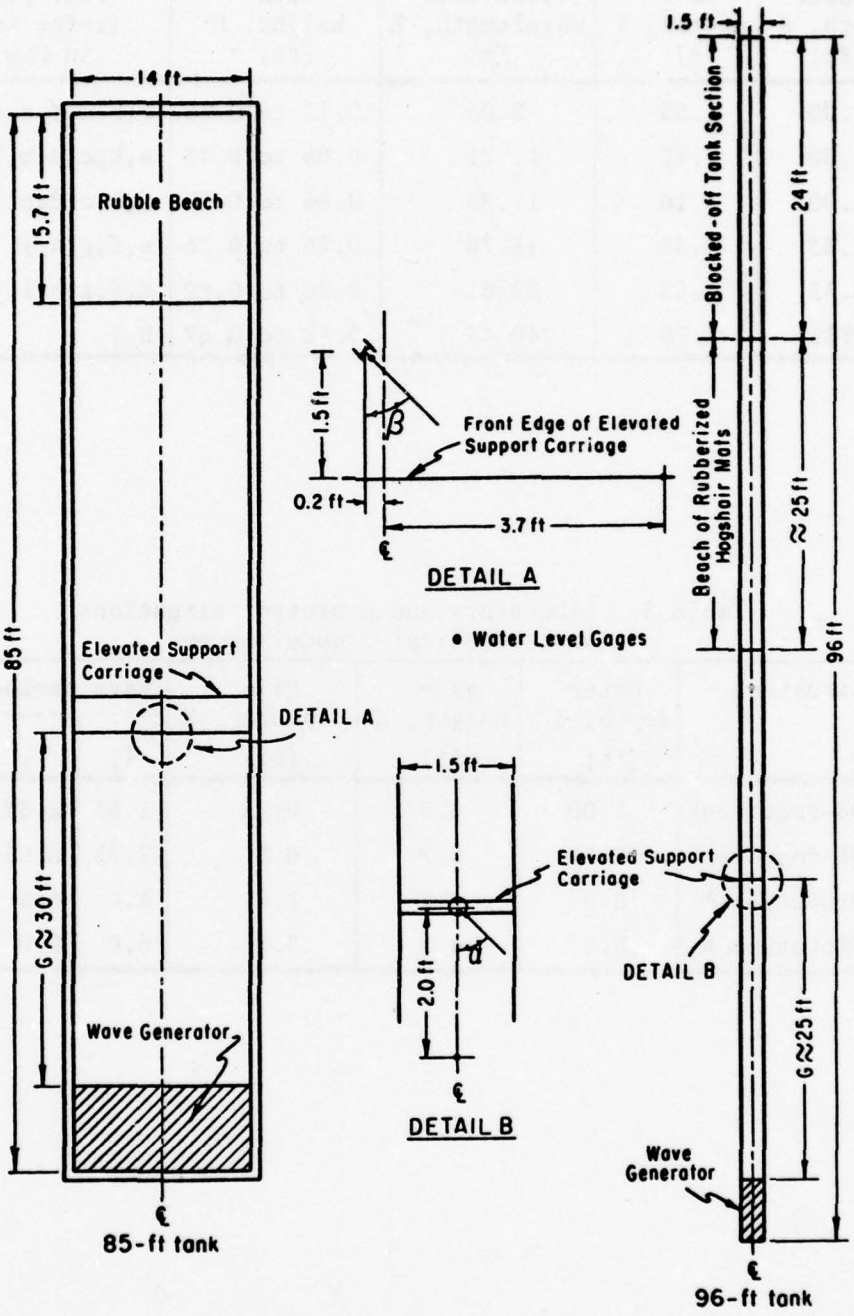

Figure 3. Plan views of the two wave tanks and details of the pile and water level gage configurations.

Table 2. Major test conditions.

Water depth, d (ft)	Wave period, T (s)	Calculated wavelength, L (ft)	Wave height, H (ft)	Test piles (refer to key in Fig. 2)
1.00	1.55	8.06	0.12 to 0.36	a,b,c,d,e,f,k,l
1.00	2.32	12.71	0.08 to 0.43	a,b,c,d,e,k,l
1.00	3.10	17.35	0.06 to 0.31	a,b,c,d,e,f,k,l
2.33	2.35	18.78	0.26 to 0.76	e,f,g,h,j
2.33	3.55	29.61	0.26 to 0.82	e,f,g,h,i,j
2.33	4.70	40.43	0.42 to 0.67	h,j

Table 3. Laboratory and prototype situations with identical Froude number.

Situation	Water depth, d (ft)	Wave height, H (ft)	Pile diameter, X (ft)	Wave periods (s)		
				T_1	T_2	T_3
1. 96-foot tank	1.00	0.3	0.22	1.55	2.32	3.10
2. 85-foot tank	2.33	0.7	0.5	2.35	3.55	4.70
3. Prototype A	8.0	2.4	1.8	4.4	6.6	8.8
4. Prototype B	15.0	4.5	3.3	6.0	9.0	12.0

Each of the four situations has the same Froude number $F = U^2/g\ell$, where U is the maximum particle velocity at the wave crest, g is the acceleration due to gravity, and ℓ is some characteristic flow length, which can be taken to be either the d, X, or H (Table 3). (Several subscripted Froude numbers based on different length scales are used where appropriate in this report.) The Froude number measures the ratio of inertial to gravitational forces and therefore describes stagnation effects in flow with a free surface.

Electrical gages were used for pen-and-ink records of water level in time, according to well-defined Coastal Engineering Research Center (CERC) laboratory procedures (Stafford, Ray, and Jones, 1973). Generally, one gage recorded the transformed wave near the pile, e.g., within a channel, and a second gage recorded the incident wave, between the wavemaker and the pile (see insets in Fig. 3). Several different water level probes were used during the study for more accuracy and compactness. Also, most test data for circular piles consist only of the measured peak water, recorded by the wetting of a paper sleeve wrapped around the pile or by the removal of a powder deposit on the pile. Appendix A discusses the techniques used in measuring water level; these techniques give accurate peak water measurements and are fairly interchangeable. However, the wave gages were calibrated only in still water, so their response to rapid water level fluctuations was not well defined; the measured waveforms have been treated as qualitative information.

The test wave condition is specified by the T,d combination, along with E and the distance, G, from the wave generator to the test pile. G must be specified because of the nonlinearity of the finite-amplitude test waves in fairly shallow water ($d/L < 0.13$) (see the waveforms in App. B). The test pile was near $G = 25$ feet (7.6 meters) and the other wave gage near $G = 23$ feet (7.0 meters) in most 96-foot tank tests; the test waves had smooth and sharp crests. The secondary waveform features are relatively unimportant in this study, since the major data reported are peak water levels caused by the main crest.

In each tank, the wave field was slightly variable due to wave reflection and other effects (see App. B). Most tests were conducted during the approximately steady state attained after the wavemaker had generated at least 20 waves. One-wave tests were conducted in each tank in the brief interval after starting the wavemaker when reflection effects had not yet accumulated and the water surface was glassy smooth.

The 12 test piles had the horizontal cross sections shown to scale in Figure 2. The piles were constructed of Plexiglas, and the flat plate was made of varnished plywood, for stiffness. Noncircular piles are designated HP shapes according to standard usage (American Institute of Steel Construction, Inc., 1970). The H-section piles are named according to the ratio of their flange to web size in inches; e.g., the 5x1 H-pile has deep, narrow channels, and the 1x2 H-pile has shallow, wide channels. The orientation of a noncircular pile is specified by the yaw angle β between the direction of wave propagation and the inward normal to the

channel in which the water level was measured (Fig. 1); the pile was fixed in the tank at a specific β. With a circular pile, the angle α specifies the location of a point on the circumference with respect to the direction of wave incidence (Fig. 1).

Because of the size of available water level gages, the cross sections of most piles are larger by about a factor of two than required by the model scales, if common nearshore piles are considered the prototype (see Table 3). The importance of inaccuracies in modeling the prototype situations in these laboratory tests is evaluated in Section IV. The variations introduced into the wave records by the type of wave gage and its exact location near the test pile are evaluated in Appendix A. Each evaluation indicates the reliability of the reported conclusions concerning wave transformation at surface-piercing piles.

3. Record Analysis and Data Displays.

The electrical gage records show the incident waves generally have a markedly nonsinusoidal profile (see App. B). The primary crests are usually smooth, but secondary crests occur. The flow transformation near the pile can introduce additional complications. This is shown in Figure 4, which displays records of water level in time associated with the incident and transformed waves in several test situations.

Peak water above the stillwater level (SWL) was measured from water level records of the transformed wave; the average crest height, $\overline{W}$, above the SWL is the important dimension of the incident wave. The transformation of the slowly varying peak forward flow at the pile is measured as $\overline{W}(\alpha)$ or $\overline{W}(\beta)$, the average peak water level or crest height above SWL at a certain orientation angle. This method of data reduction retains only the upper envelope of the recorded wave transformation, ignoring the generally complicated trough flow effects. Figure 5 shows the waveform dimensions that have been introduced and shows that the average crest height may be conveniently measured from water level records made with slow chart speed. The crest height measurements were made to one-quarter of the smallest division on the test record. Depending on calibration constant, this quarter division equaled 0.001 to 0.006 foot (0.03 to 0.18 centimeter).

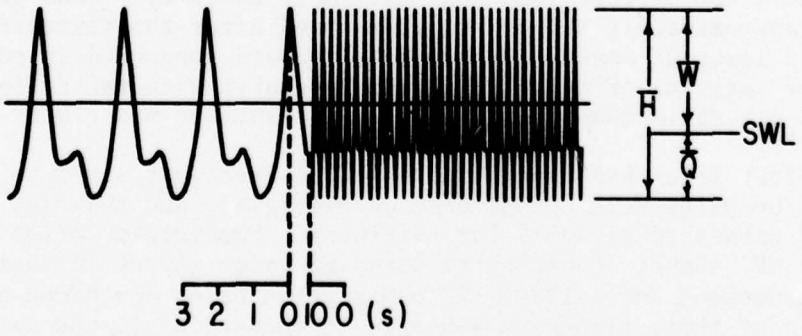

Figure 5. Water level record and measured wave dimensions: Wave height, H, crest height, W, and trough depth, Q.

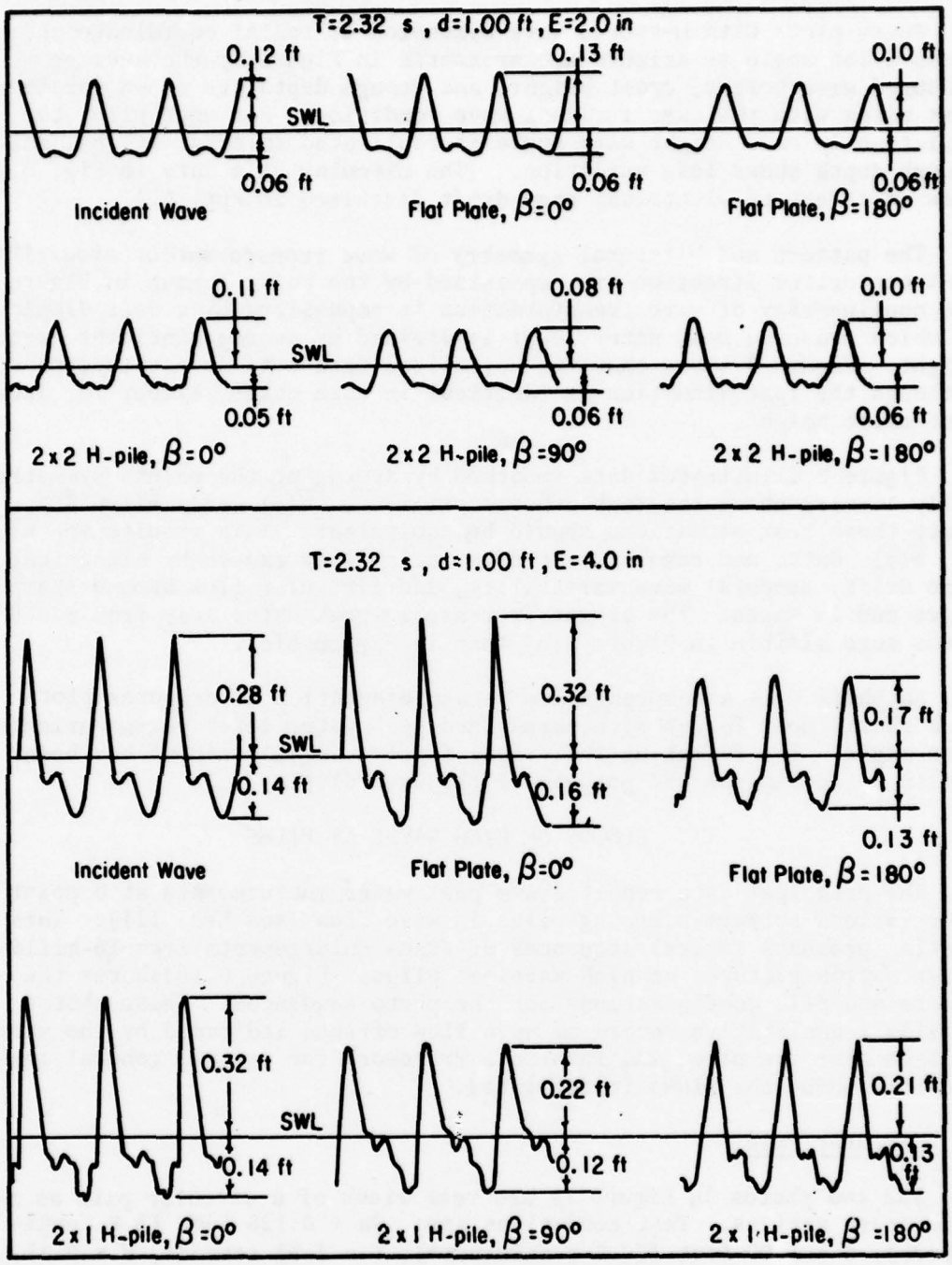

Figure 4. Recorded incident and transformed waveforms in several test situations.

Polar plots with measured wave dimension as radial coordinate and orientation angle as azimuth are presented in Figure 6; the average measured wave height, crest height, and trough depth are shown for four test piles with the same incident wave condition. For each pile, the variation in wave height with angle is replicated in crest height, while trough depth shows less variation. (The circular pile data in Fig. 6,a show an effect of electrical gage drift discussed in App. A.)

The pattern and bilateral symmetry of wave transformation about the tank centerline direction are emphasized by the polar format in Figure 6. The nonlinearity of wave transformation is emphasized by a data display in which measured peak water level is divided by average incident crest height. Figure 7 shows that two normalized data sets do not superpose, although the test situation is identical in both cases, except for incident crest height.

Figure 8 illustrates data smoothed by averaging the points symmetrically located about the tank centerline, i.e., $\overline{W}(\beta)$ and $\overline{W}(360°-\beta)$, since these test situations should be equivalent. This results in $\overline{W}(\overline{\alpha})$ or $\overline{W}(\overline{\beta})$ data, and removes some data variability caused by electrical gage drift, temporal wave variability, and irregular flow around sharp edges and in wakes. The slight increase in peak water away from $\beta = 0°$ seems more visible in Figure 8(b) than in Figure 6(c).

Appendix C is a comprehensive data presentation of computer plots in a rectilinear format with normalized peak water level versus orientation angle. The format of individual figures in this report has been chosen to accomplish the purpose of the data display.

II. PHOTOS OF HIGH WAVES AT PILES

The principal data reported are peak water measurements at a point near various surface-piercing piles in wave flow (see Sec. III). This section presents several sequences of frame enlargements from 16-millimeter motion pictures of high waves at piles. Figure 9 indicates the camera and pile configurations for the photo sequences. These photos provide a qualitative record of wave flow effects indicated by the water surface near the pile, and furnish a framework for several general conclusions about the flows investigated.

1. Circular Pile.

The two photos in Figure 10 are rear views of a circular pile as a wave crest arrives. Test conditions are: $2a = 0.125$ foot (3.8 centimeters), $d = 1.00$ foot (30.5 centimeters), $T = 2.32$ seconds, $H = 0.41$ foot (12.5 centimeters), $W = 0.27$ foot (8.2 centimeters), 32 frames per second film speed. In Figure 10(a), the crest is approaching the pile. The bow wave around the pile's front is particularly visible at the upper right of the frame, and the spilling flow at the pile's sides is noticeable. The flow separates from the pile near $\alpha = \pm 130°$, judging from the breaks in water surface slope. Water flows up the back of the

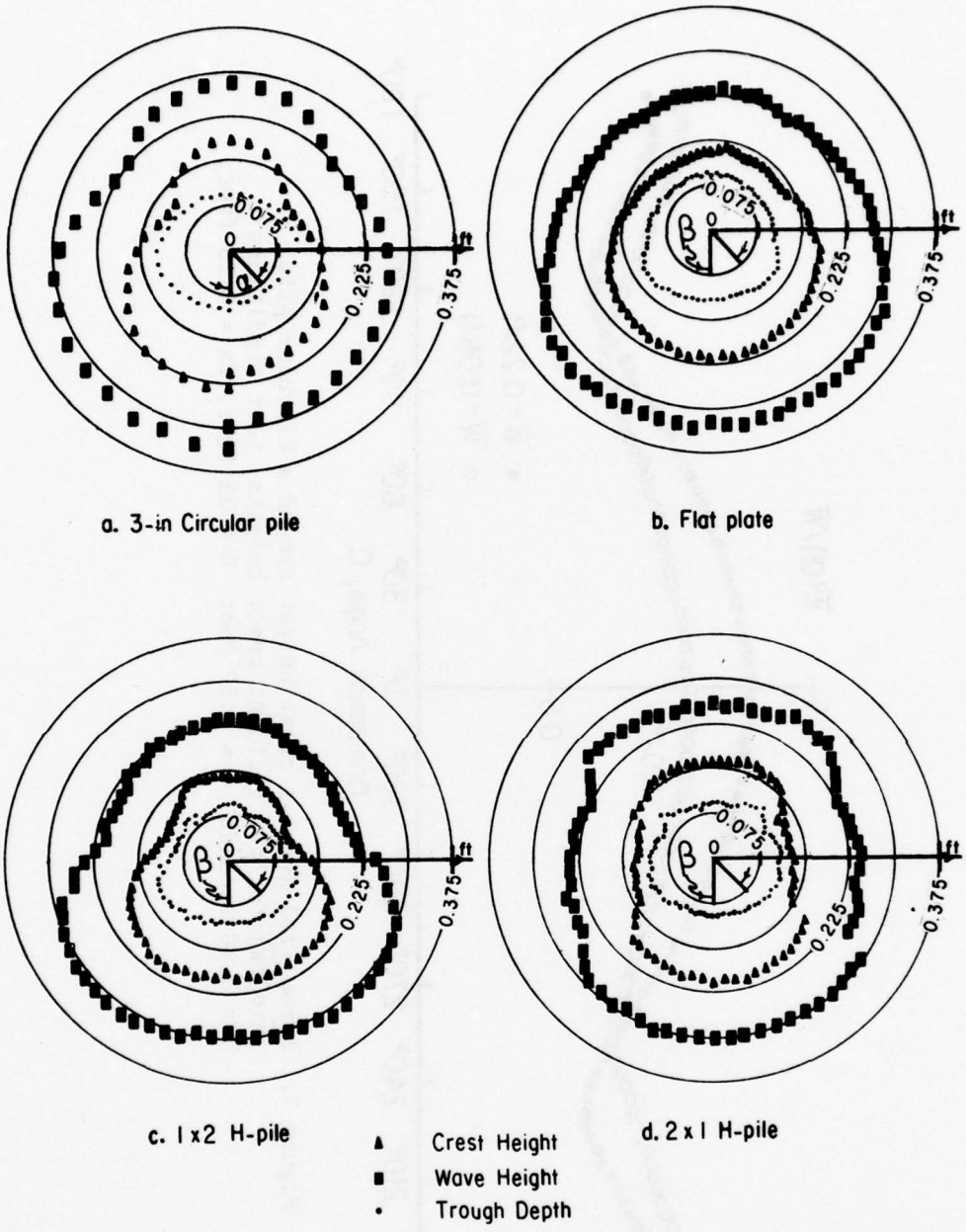

Figure 6. Transformed wave dimensions versus orientation angle for four piles. Test conditions: T = 2.32 seconds, d = 1.00 foot, E = 3.0 inches, G = 25 feet.

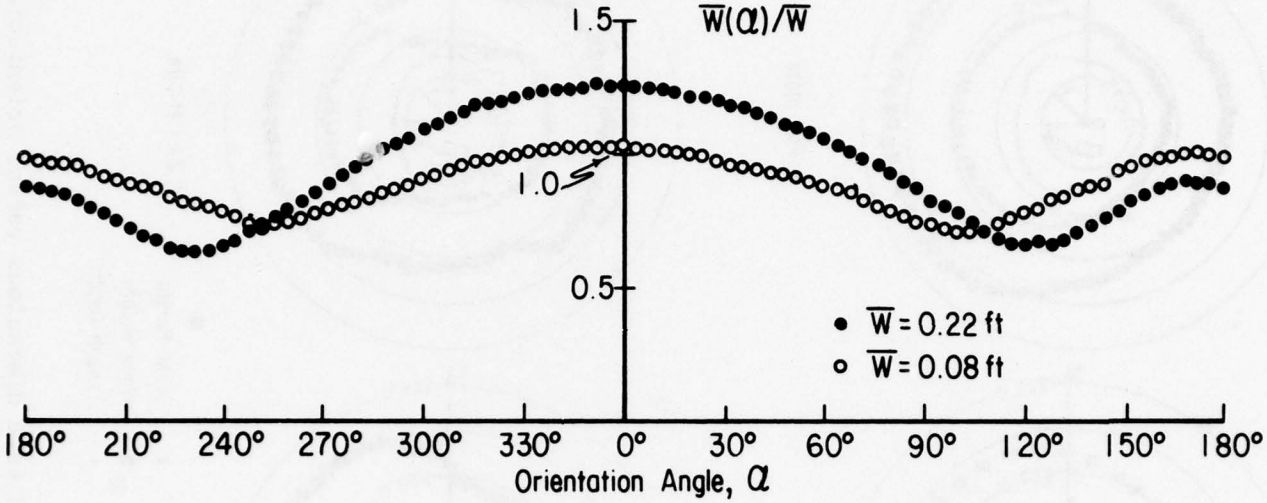

Figure 7. Normalized average crest height around a circular pile $[\overline{W}(\alpha)/\overline{W}]$ for two incident crest heights, test conditions: T = 3.10 seconds, d = 1.00 foot, G = 25 feet, 2a = 0.25 foot.

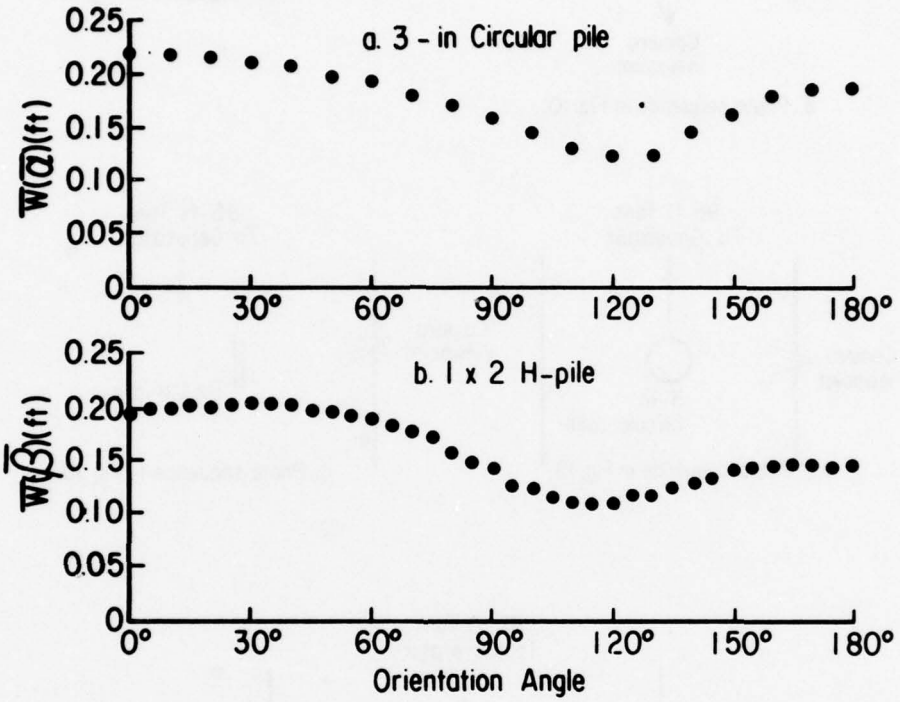

Figure 8. Crest height over the 180° range of orientation angle for two piles. Test conditions: T = 2.32 seconds, d = 1.00 foot, E = 3.0 inches, G = 25 feet.

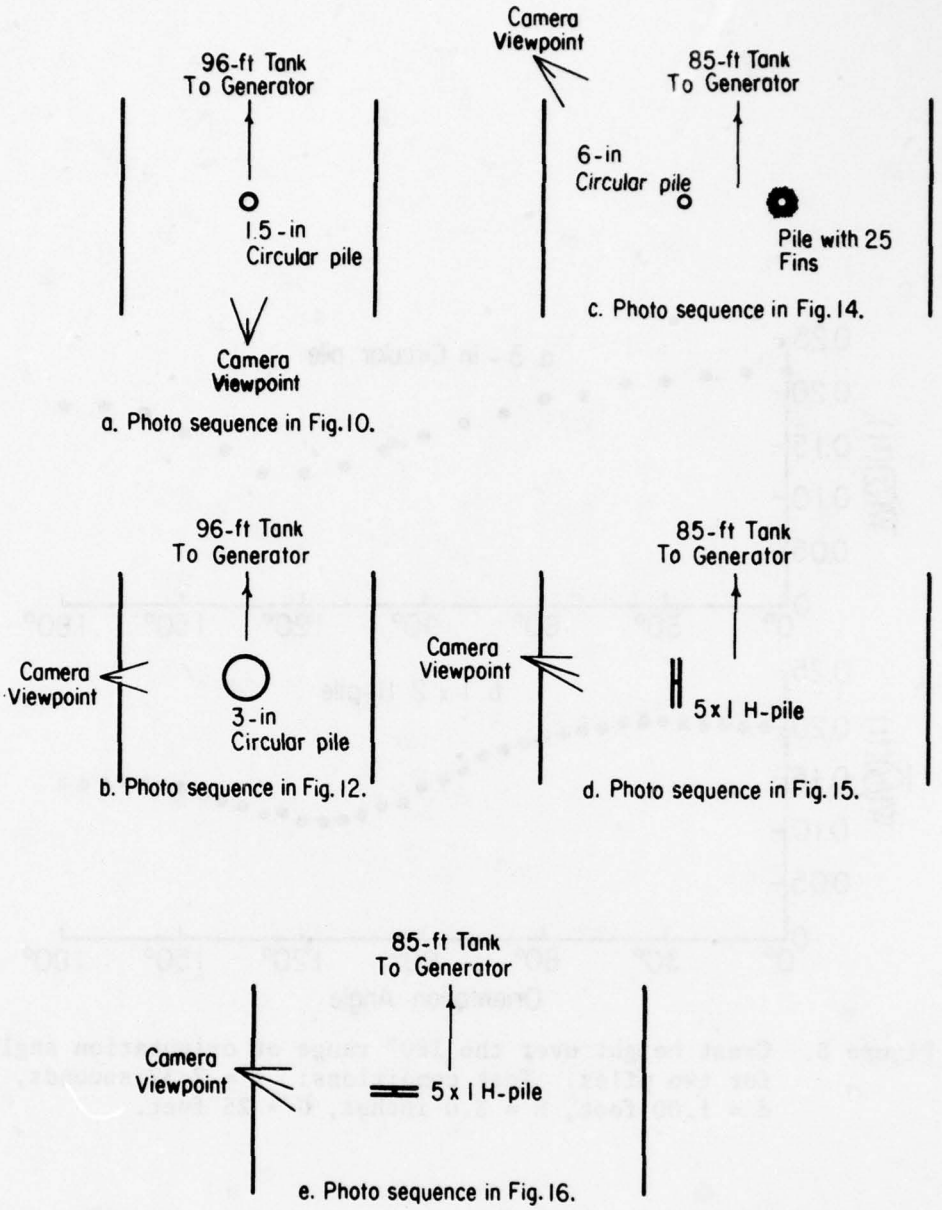

Figure 9. Camera and pile configurations for photo sequences (not to scale).

pile in the wake, which is skewed toward the right of the frame. The crest is at the pile in Figure 10(b), taken one-eighth second later. The top of the bow wave is above the frame. The points of flow separation are farther away from $\alpha = 180°$ than in Figure 10(a), and the wake has become flatter, wider, and skewed toward the left of the frame. Figure 11 shows the pattern of average peak water recorded in the same test situation by wetting a paper sleeve on the pile. This pattern resembles the water levels visible in Figure 10(b), with about the same minimum locations and a low wake skewed to the same side.

The photo sequence in Figure 12 views a circular pile from the side through a wave cycle, starting during trough flow of a wave traveling toward the right. Test conditions are: $2a = 0.25$ foot (7.6 centimeters), $d = 1.00$ foot, $T = 2.32$ seconds, $H = 0.49$ foot (14.9 centimeters), $W = 0.30$ foot (9.2 centimeters), 32 frames per second film speed (Fig. 12 shows every fourth frame). Figure 13 shows the incident waveform and two waveforms recorded on the pile's surface in the same test situation.

These photos show an intricate water surface near the pile. Figure 12(a and b) reveals flow toward the left associated with the wave trough; the water level is higher on the right segment of the pile due to flow stagnation near $\alpha = 180°$. The flow is reversing in Figure 12(c) and has increasing velocity toward the right in the next three frames. Crest stagnation near $\alpha = 0°$ is maximum in Figure 12(f), as is the slope in water level near $\alpha = 90°$. The flow then subsides and is weak in Figure 12(i), which shows practically no relief in water level around the pile. Another definite effect is visible in Figure 12(o), where the higher water level at the left of the pile corresponds to stagnation of the waveform's secondary crest.

The waveforms in Figure 13 complement the pictorial record in Figure 12. The transformed crest recorded at the pile is broader than the incident crest, as flow stagnation increases the duration of peak water. At $\alpha = 0°$, crest height is significantly increased by runup, while peak water at $\alpha = 180°$ is slightly lower than the incident crest. After the main crest passes, the $\alpha = 0°$ waveform shows a small peak, perhaps caused by a splash of falling water; this effect is visible at the left side of Figure 12(j). The lowest part of the incident wave, midway between the main and secondary crests, results in a slight secondary peak in the $\alpha = 180°$ waveform, due to flow stagnation; as this trough passes, recorded water level is nearly the same at $\alpha = 0°$ and at $\alpha = 180°$ (Fig. 12,i). The secondary crest of the incident waveform rises to about SWL, and stagnation results in a higher water level at $\alpha = 0°$ than at $\alpha = 180°$, as in Figure 12(n and o).

2. Circular and Finned Circular Piles.

Figure 14 shows a wave crest in the 85-foot tank simultaneously striking the 6-inch-diameter pile, at the right of the frame, and the pile with 25 radial fins (12 in total diameter). Every eighth frame at 64 frames per second is shown. The wave condition is $d = 2.33$ feet (71.1

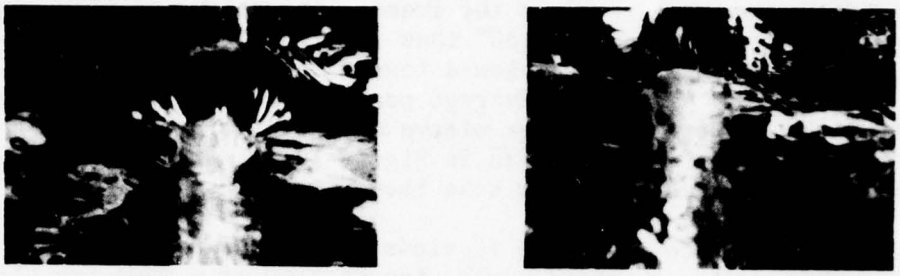

a. b.

Figure 10. Two photos of wake region behind 1.5-inch circular pile with wave crest incident from top of frame: a, 1/8 second before peak crest flow; b, peak crest flow.

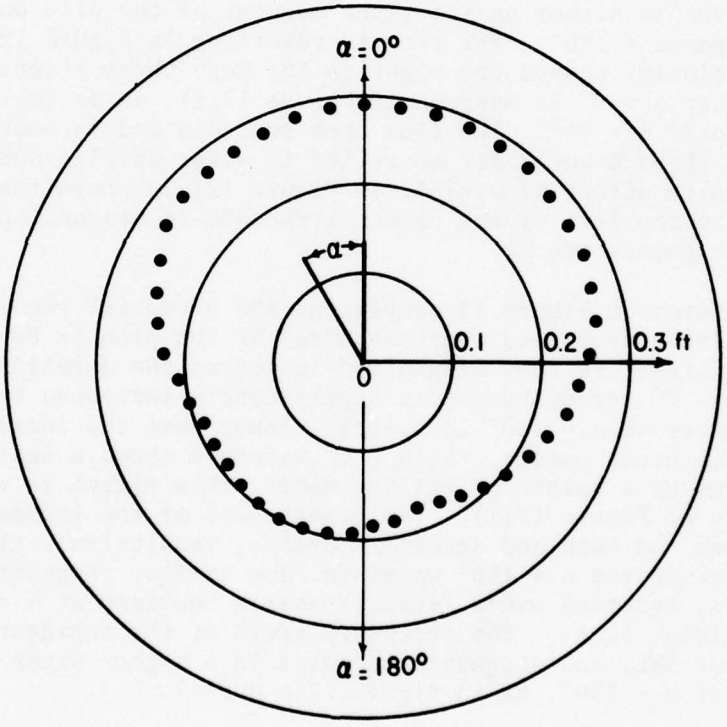

Figure 11. Measured $\overline{W}(\alpha)$ in same test situation as Figure 10.

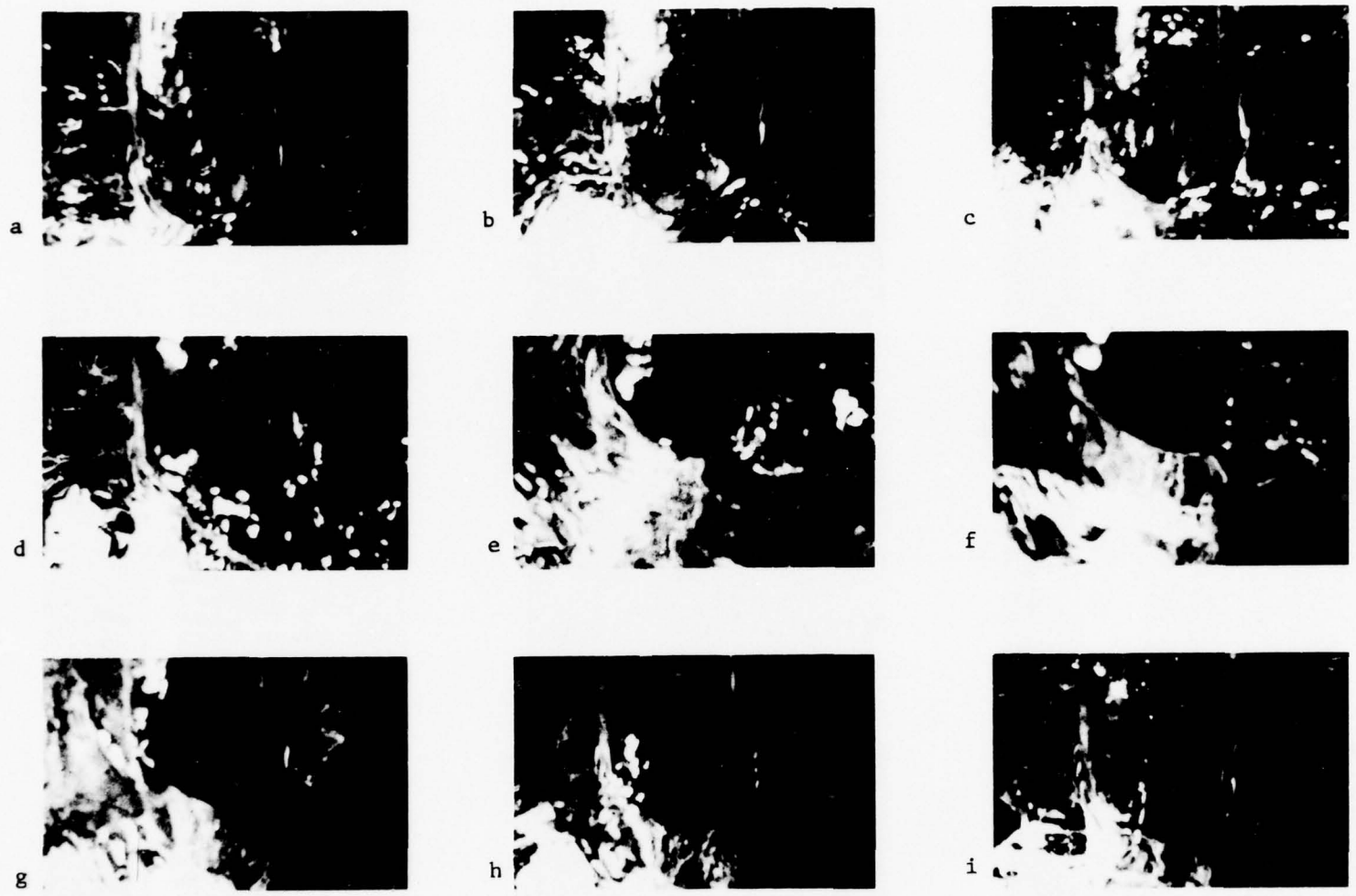

Figure 12. Photo sequence of wave cycle at 3-inch circular pile, with T = 2.32-second wave traveling toward the right and one-eighth second between frames.

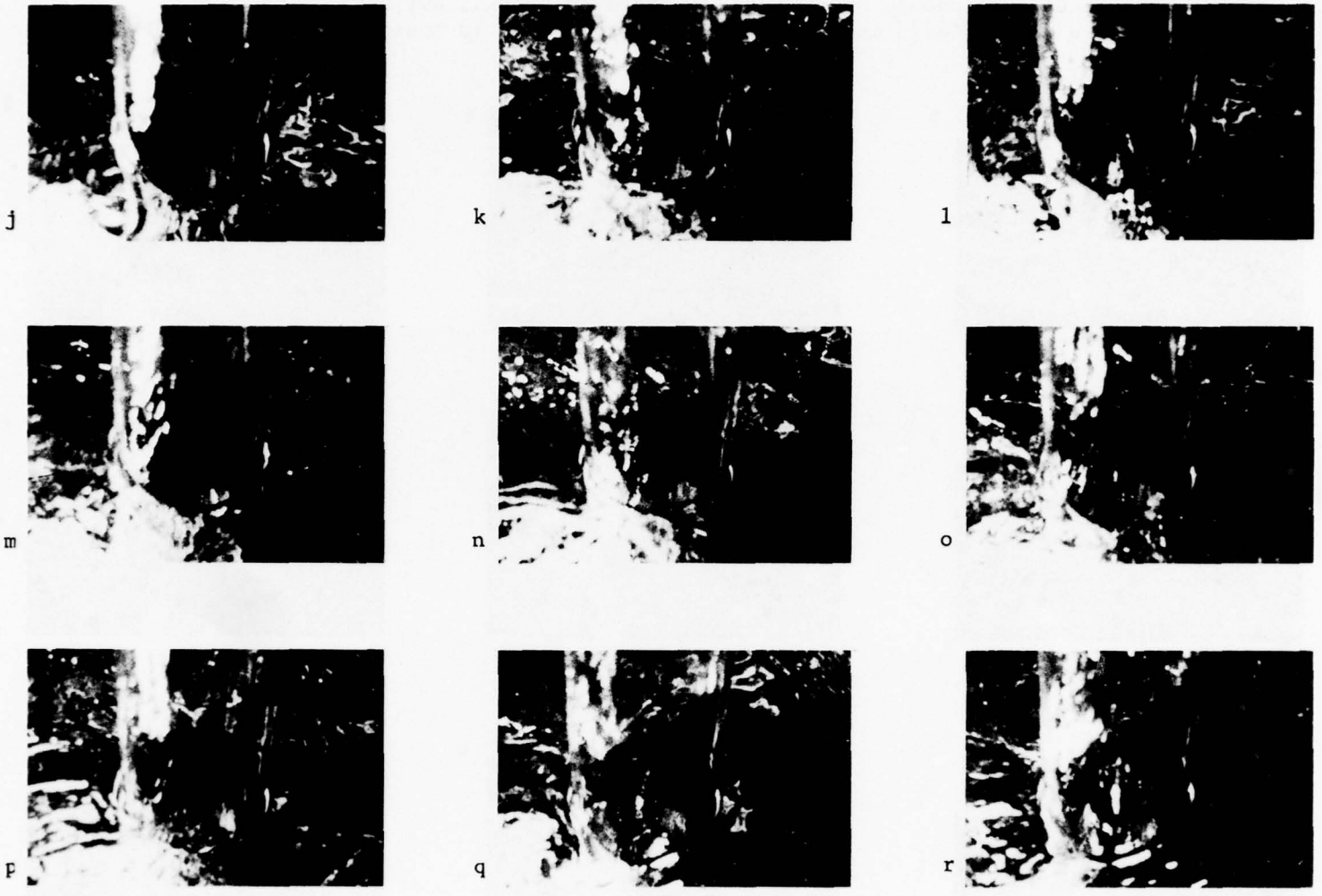

Figure 12. Photo sequence of wave cycle at 3-inch circular pile, with T = 2.32-second wave traveling toward the right and one-eighth second between frames.--Continued

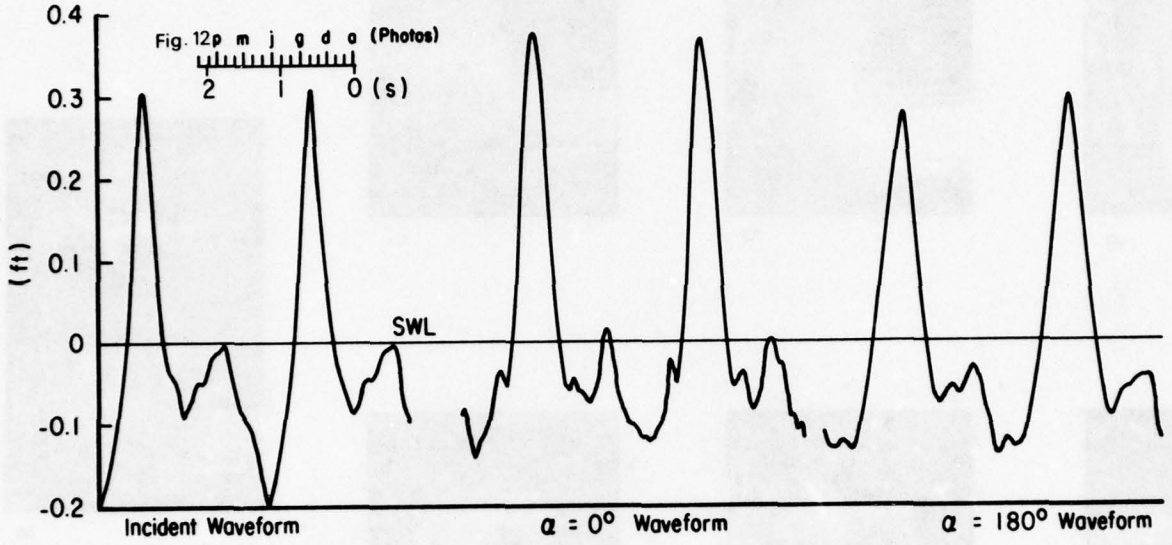

Figure 13. Incident, $\alpha = 0°$, and $\alpha = 180°$ waveforms in same test situation as Figure 12.

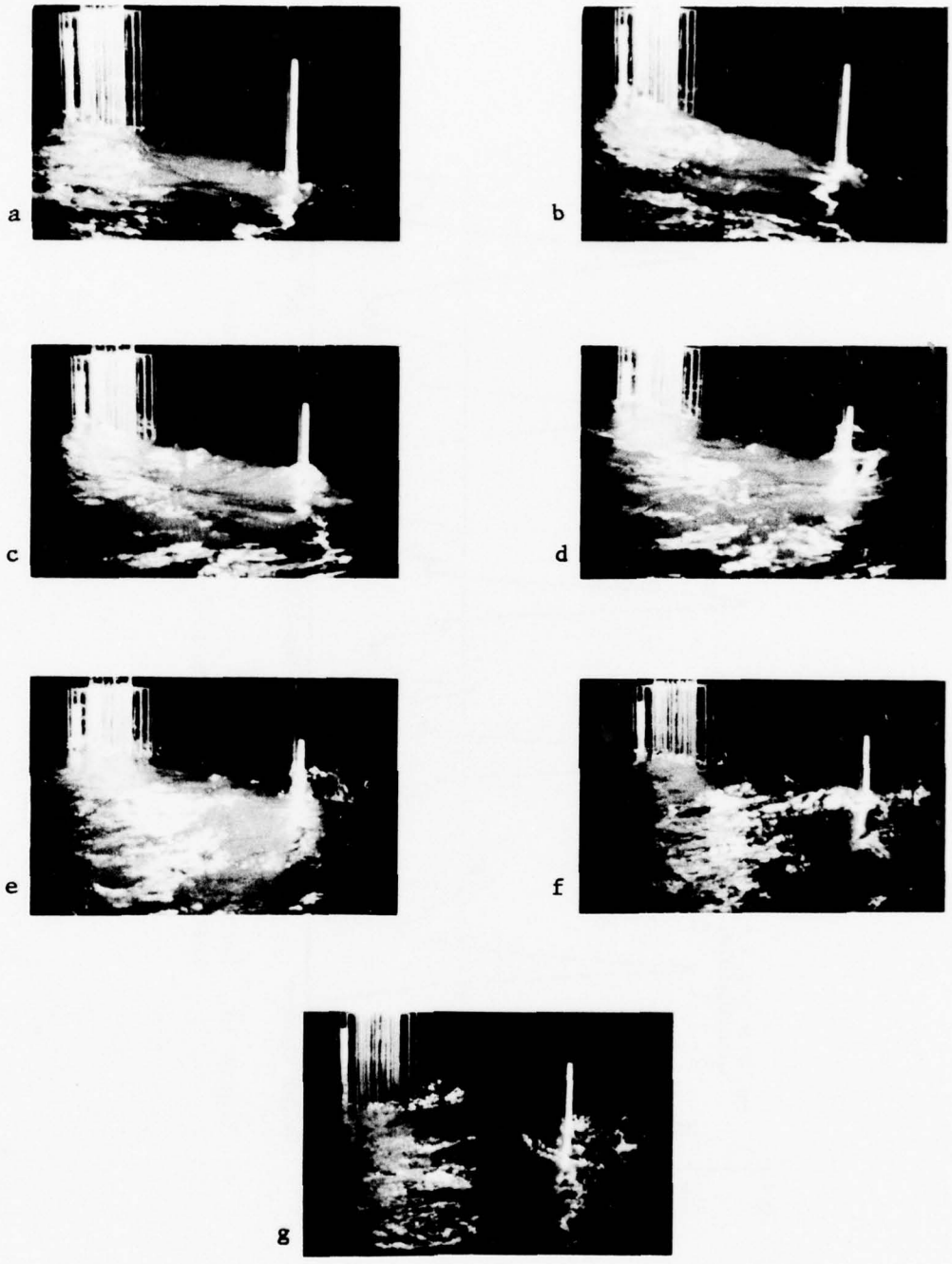

Figure 14. Photo sequence of wave crest striking side-by-side circular and finned circular piles, with one-eighth second between successive frames.

centimeters), T = 3.55 seconds, W = 0.5 foot (15.2 centimeters), and the centers of the two piles are an equal distance from the wave generator (G = 29 feet, 8.8 meters). The white tapes on the two piles extend to the same elevation above the SWL and are located on the face or on the flange directly facing the generator.

In Figure 14(a and b), the crest is approaching, and runup begins in the front channels of the finned pile. In Figure 14(c), runup is occurring on the face of the smooth pile, and a "stairstep" runup is visible in the front channels of the finned pile; this runup has a horizontal free surface and differs between neighboring channels. In Figure 14(d), a distinct bow wave exists forward of the finned pile, while a higher uprush occurs on the smooth pile's face in a thin sheet; the water surface slope at the side of the smooth pile is about twice as great as the side slope at the finned pile. In Figure 14(e), the crest has passed the piles; the water level forward of the finned pile is dropping and the water sheet on the smooth pile's face is falling. The speckles of light on the water surface behind each pile indicate disordered flow in the wake regions. In Figure 14(f), the runup at the front of each pile has dropped farther, and a splash up the rear of each pile is visible. In Figure 14(g), the crest is far beyond the two piles, and a circular splash is radiating outward from the front face of the smooth pile.

3. H-Pile with Deep Channels.

Figure 15 shows a wave incident directly into the deep channel of the 5x1 H-pile ($\beta = 0°$), and Figure 16 shows this pile's flange facing the wave generator, so the visible channel is at $\beta = 90°$ relative to the wave direction. Test conditions are: d = 2.33 feet, T = 3.55 seconds, W = 0.5 foot, 64 frames per second film speed.

In Figure 15, the elapsed time between successive photos is one-sixteenth second. In Figure 15(a to f), the main wave crest is approaching the pile. A secondary crest occurred on the forward face of the main crest. Although barely visible, it caused the noticeable runup in Figure 15(d). In Figure 15(f), the water level in the channel is again the same as the surrounding water level. In Figure 15(h, i, and j), runup is visible at the pile's web, as the main crest approaches the pile. The water surface has a complicated curvature until it becomes horizontal at its maximum (Fig. 15,k), when the wave crest is at the center of the pile. Slight breaking (aeration) commences at the leading edges of the pile in Figure 15(k) and spreads toward the generator as the runup falls in Figure 15(l and m); this breaking is apparently associated with flow reflected from the pile jetting out of the channel. In Figure 15(l, m, and n), the water level in the rear channel is above the surrounding water level.

In Figure 16, the elapsed time between successive photos is one-eighth second. The flange facing the wave generator acts as a flat plate along the wave front. A breaking bow wave grows toward the generator and curls around the pile channel until the crest passes (Fig. 16,e).

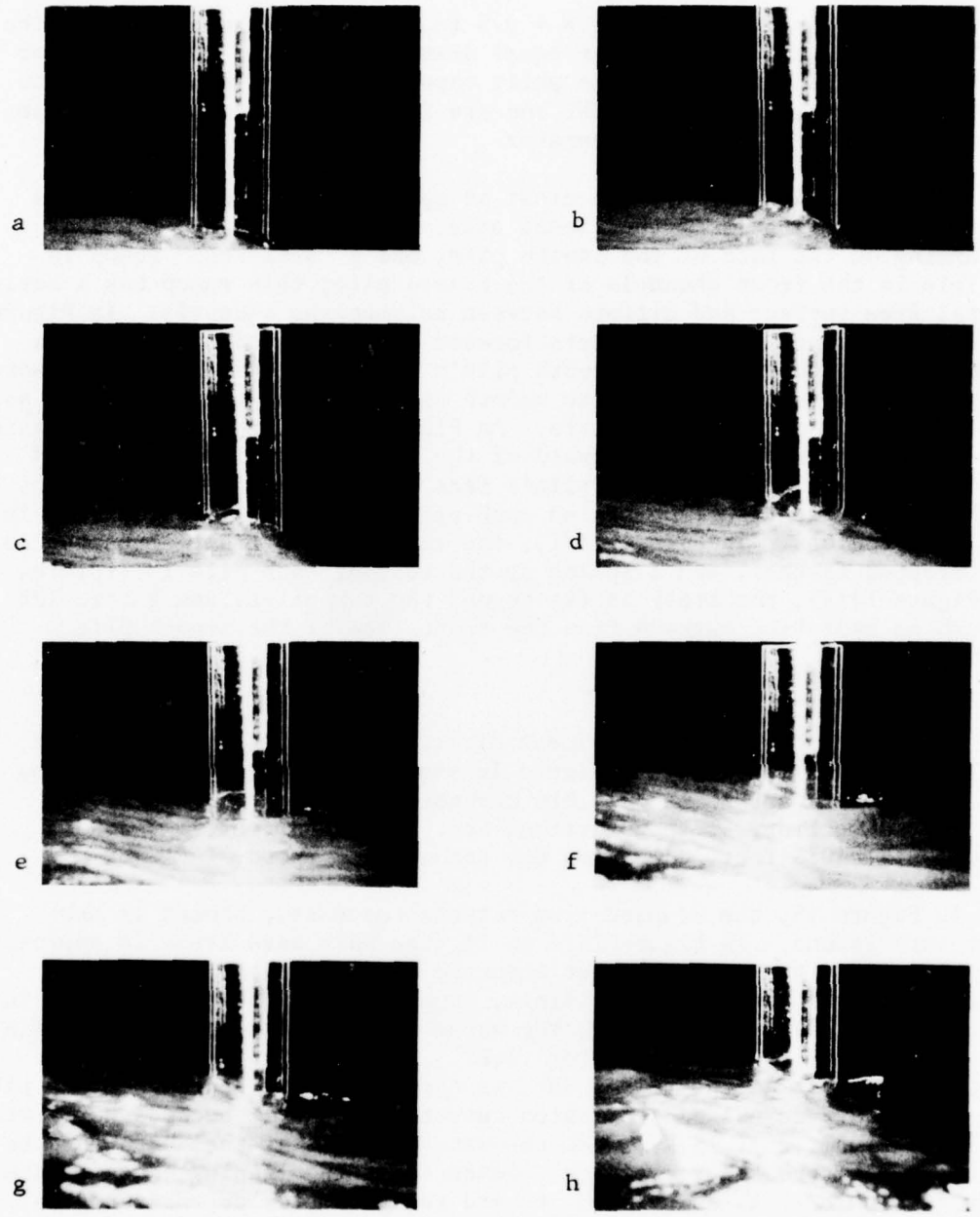

Figure 15. Photo sequence of wave crest incident into channel of 5x1 H-pile, with one-sixteenth second between successive frames.

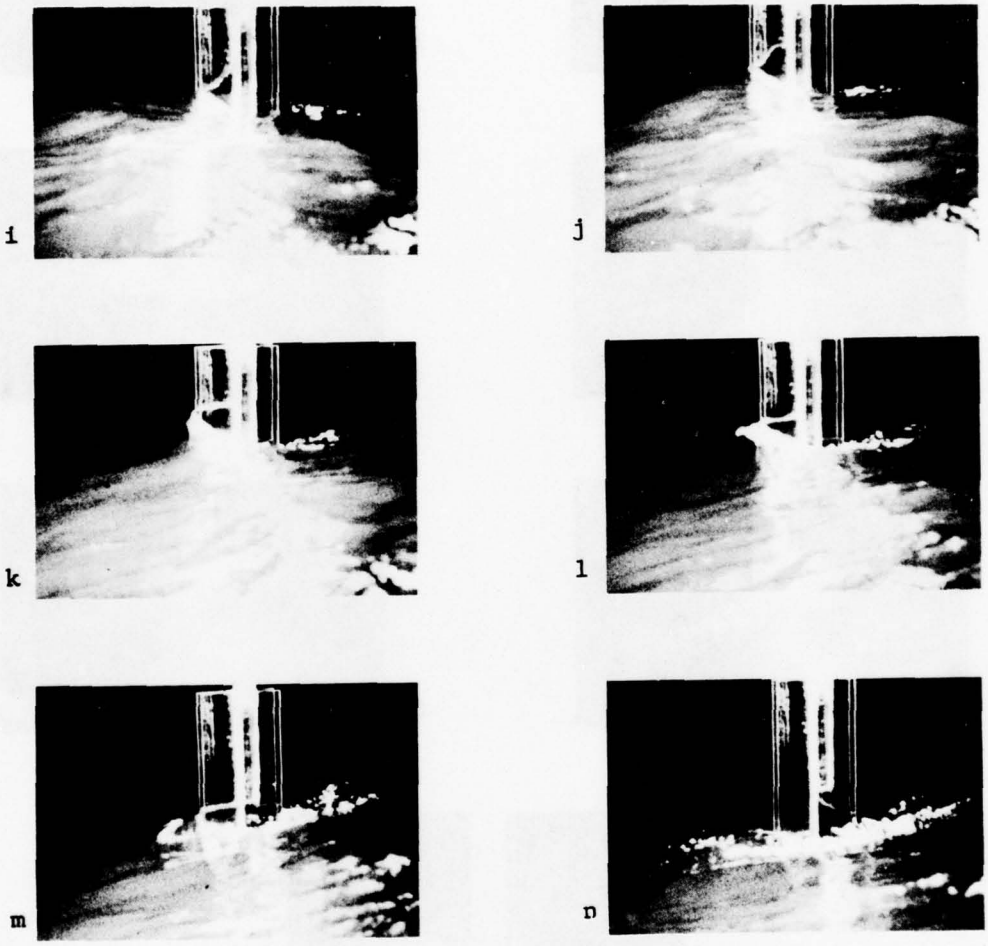

Figure 15. Photo sequence of wave crest incident into channel of 5x1 H-pile, with one-sixteenth second between successive frames. --Continued.

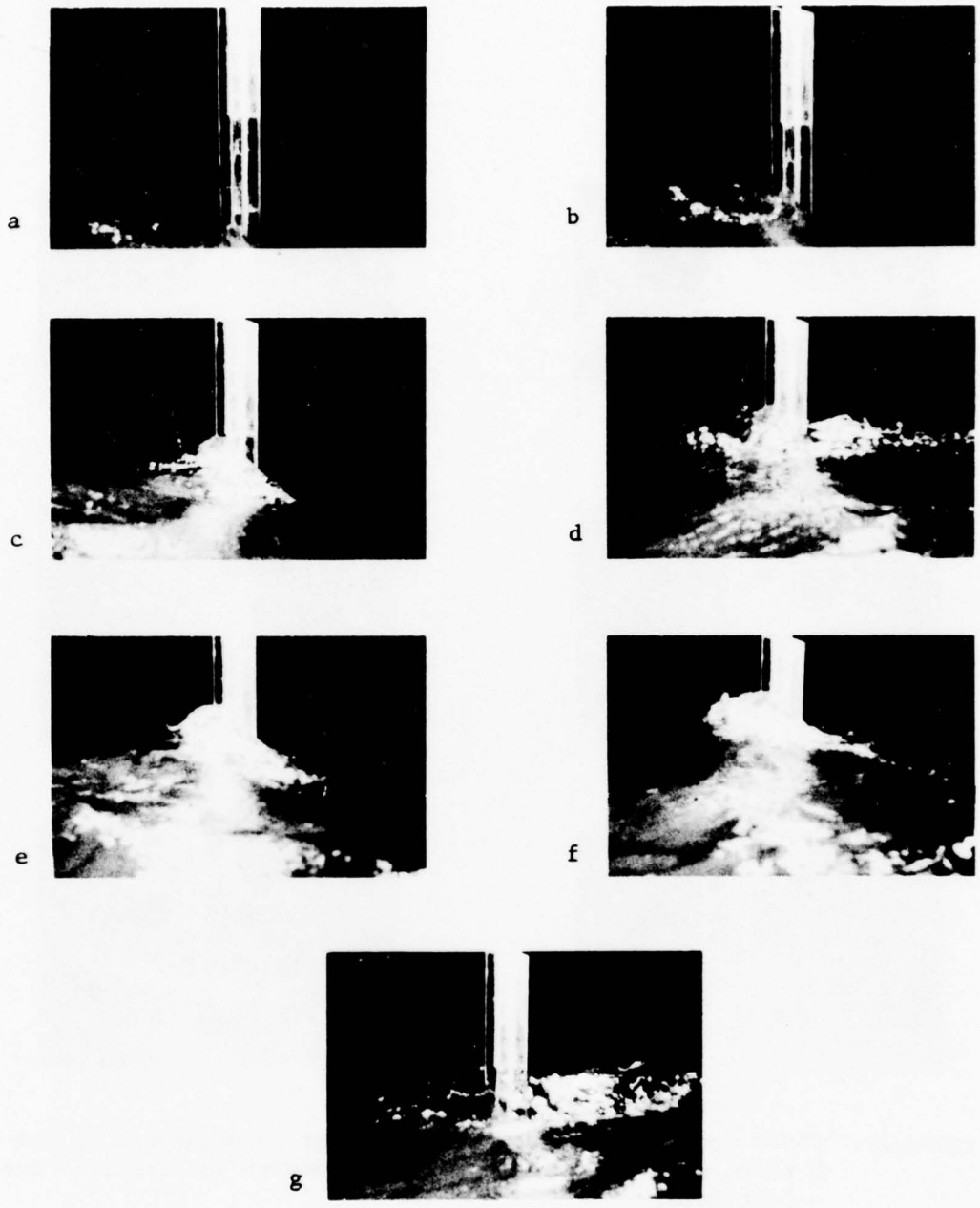

Figure 16. Photo sequence of wave crest incident on 5x1 H-pile, oriented at $\beta = 90°$, with one-eighth second between successive frames.

The water level in the channel is not visible when the bow wave is present (Fig. 16,c, d, and e) but the main flow clearly curves past and does not penetrate the channel.

4. Conclusions.

The photo sequences show free-surface effects at a pile are most marked as the high crest passes. Crest stagnation is significant at circular and channeled piles in the photographed situations. The surface configurations at peak crest flow in Figures 14, 15, and 16 resemble the free surfaces for steady unidirectional flow past a circular surface-piercing pile (see Figs. 21, 22, and 23 in Petryk, 1969).

Dagan and Tulin (1972) analyzed steady two-dimensional, free-surface flow past an obstacle of shallow draft, D. Stagnation effects were found to depend critically on the Froude number based on draft, $F_D = u^2/gD$, where u is incident flow velocity. Figure 17 shows the three stagnation regimes occurring with increasing F_D: (a) a smooth elevation equal to $(u^2/2g)$ in the free surface at the obstacle; (b) a stable breaking wave with a surface elevation somewhat less than $(u^2/2g)$, when F_D rises above 1.4; and (c) at larger F_D, a vertical jet. The photo sequences of wave flows show these three stagnation regimes at the test pile. However, the flow obstacle is thin, rather than of shallow draft, and the important Froude number is based on obstacle diameter. (Dagan, 1975 analyzed the influence of obstacle slenderness on free-surface nonlinear effects.)

Petryk (1969) noted that, in steady unidirectional flow, the free-surface features near a vertical circular pile depend on the Froude number based on pile diameter. For wave flow, Hallermeier (1976) documented effects of the Froude number, $F_a = U^2/2ga$, on the free-surface geometry during peak water. One effect of F_a is directly visible in Figure 14(d): the finned pile is twice the diameter of the circular pile and, at peak flow, the water slope at the side of the finned pile is about half that at the smooth pile, because F_a is halved.

F_a also determines the stagnation regime in a way analogous to F_D in the situation considered by Dagan and Tulin (1972). When F_a increases above unity, the front runup and side slope at a circular pile cease their linear increase with the velocity head, $U^2/2g$, possibly indicating a transition from smooth to breaking runup (Figs. 4 and 5 in Hallermeier, 1976). Smooth runup occurred in most of the present test series. The photos showing breaking and jetting runup are of situations with maximum values of U and F_a.

The stagnation regime occurring in the photo sequences and the calculated value of $F_t = U^2/gt$, where t is obstacle cross-sectional thickness normal to wave direction, are listed in Table 4. Velocity was calculated using McCowan solitary wave theory, since measurements by Le Mehaute, Divoky, and Lin (1968) show this theory accurately gives U for high waves near d/L = 0.08, the condition for all the photos. Table 4 indicates the stagnation regime can be roughly categorized by the value

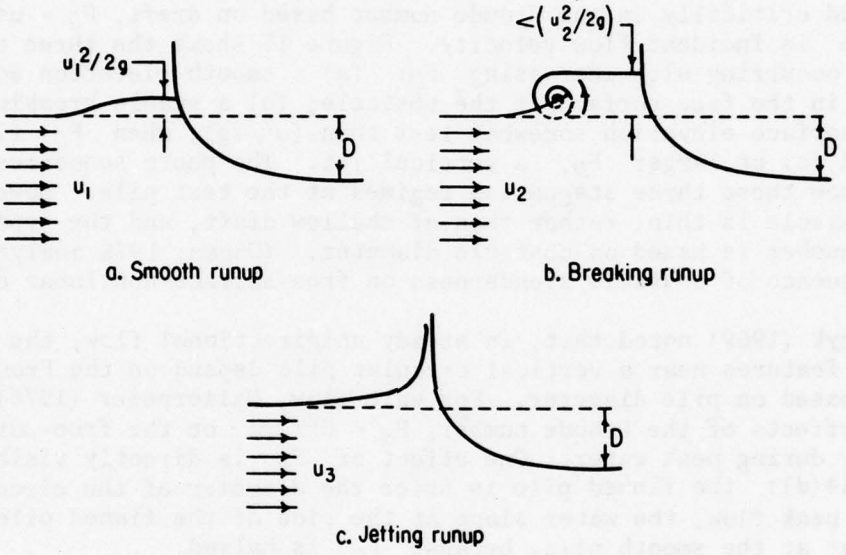

Figure 17. Three runup regimes at a shallow-draft obstacle with increasing flow velocity, $u_1 < u_2 < u_3$ (after Dagan and Tulin, 1972).

Table 4. Stagnation regime and Froude number based on obstacle thickness in photo sequences.

Figure	Pile	Stagnation Regime	U^2/gt
12	3-inch circular	Smooth runup	0.6
14	Pile with 25 fins	Smooth runup	0.6
	6-inch circular	Jetting runup	1.2
15	5x1 H-pile (β = 0°)	Smooth runup	7.2
16	5x1 H-pile (β = 90°)	Breaking runup	1.4

of F_t, but the bluntness and surface complexity of the obstacle clearly have some effects on the stagnation regime. This can be seen by comparing Figures 15(k) and 16(e), where the stagnation regime goes from smooth to breaking runup as F_t decreases, opposite the expected trend.

The photos indicate that wave flow does not directly penetrate the pile's channels at certain orientations. The water level in the channel is horizontal and responds to the sloping exterior flow around the pile. This is clearly shown in Figure 18; the sloping exterior flow causes a "stairstep" variation in water level within the channels around the pile.

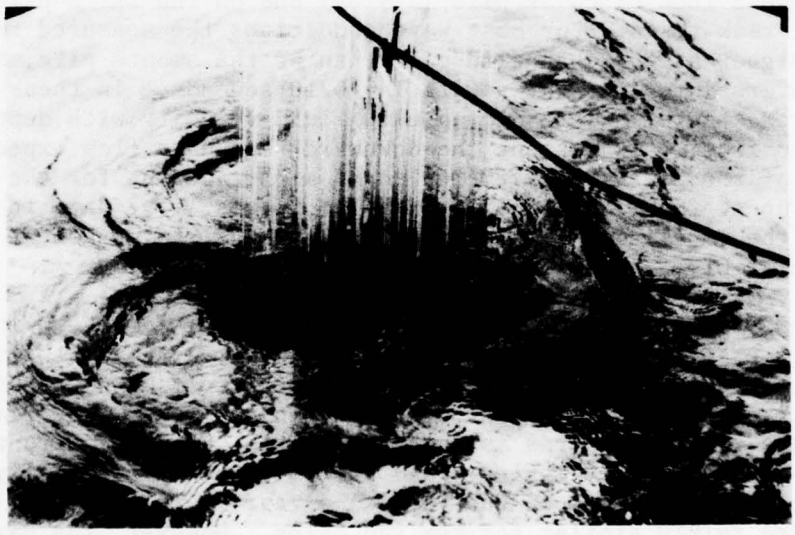

Figure 18. "Stairstep" runup in channels around a pile with 25 fins. Crest incident from upper right of frame.

III. MEASURED PEAK WATER PATTERNS

The preceding photo sequences show complicated free-surface effects in wave flow at surface-piercing piles. The principal data reported are measured peak water (or crest height) at various pile orientations relative to wave direction, which were extracted from the test records of the complex flows investigated.

Appendix C includes data sets of the measured patterns of peak water versus pile orientation for which the test records have satisfactory internal consistency. Still, these sets have a detectable variability: repeated tests result in a slightly different pattern, and, with channeled piles, there can be a ragged variation in measurement with small changes in orientation angle. However, each pile is expected to have a characteristic peak water pattern related to its cross section.

This section presents data to establish general trends and to facilitate comparison of the patterns obtained with various piles.

1. Circular Piles.

The photo sequences show that crest stagnation at a circular pile can be similar to that at a channeled pile. This is established as a quantitative result by comparing peak water at an H-pile to that at a circular pile.

Figure 19 shows measured runup versus wave generator eccentric for waves on the 3-inch circular pile ($\alpha = 0°$) and on the 2x2 H-pile ($\beta = 0°$) in 96-foot tank tests. For most wave conditions the measured runup is slightly higher at the channeled pile than at the smooth pile, although this is reversed for the waves with T = 3.10 seconds. In these long-period waves, there is less decrease in fluid velocity with depth below the free surface; this lessens the downward secondary flow expected at the front of the pile (Petryk, 1969), and might account for the relatively higher runup at the circular pile with long waves. The data in Figure 19 reinforce the conclusion in Section II that crest stagnation at the front of a circular pile is similar to that at a channeled pile.

Figure 20 superposes polar patterns of $[\overline{W}(\alpha)/\overline{W}]$ for the 3-inch circular pile and of $[\overline{W}(\beta)/\overline{W}]$ for the 3x3 H-pile, although the angular variable is fundamentally different (Fig. 1). The four wave conditions cover the range used in the 96-foot tank. In each case, the similarity in the shape of the patterns is notable: there is a broad front maximum region, a rear secondary maximum, and intermediate symmetrically located minimums. The magnitudes of the front and rear maximums and of the minimums are fairly similar for the two piles. However, the maximum in $\overline{W}(\beta)$ can occur away from $\beta = 0°$ and the pattern variation with orientation angle is more regular for the circular pile. Figure 20 partially contradicts the results in Figure 19, showing $\overline{W}(\beta = 0°)$ is larger than $\overline{W}(\alpha = 0°)$ in each case. This disagreement may be due to confinement effects with the 3x3 H-pile in the 96-foot tank (see Sec. IV,1).

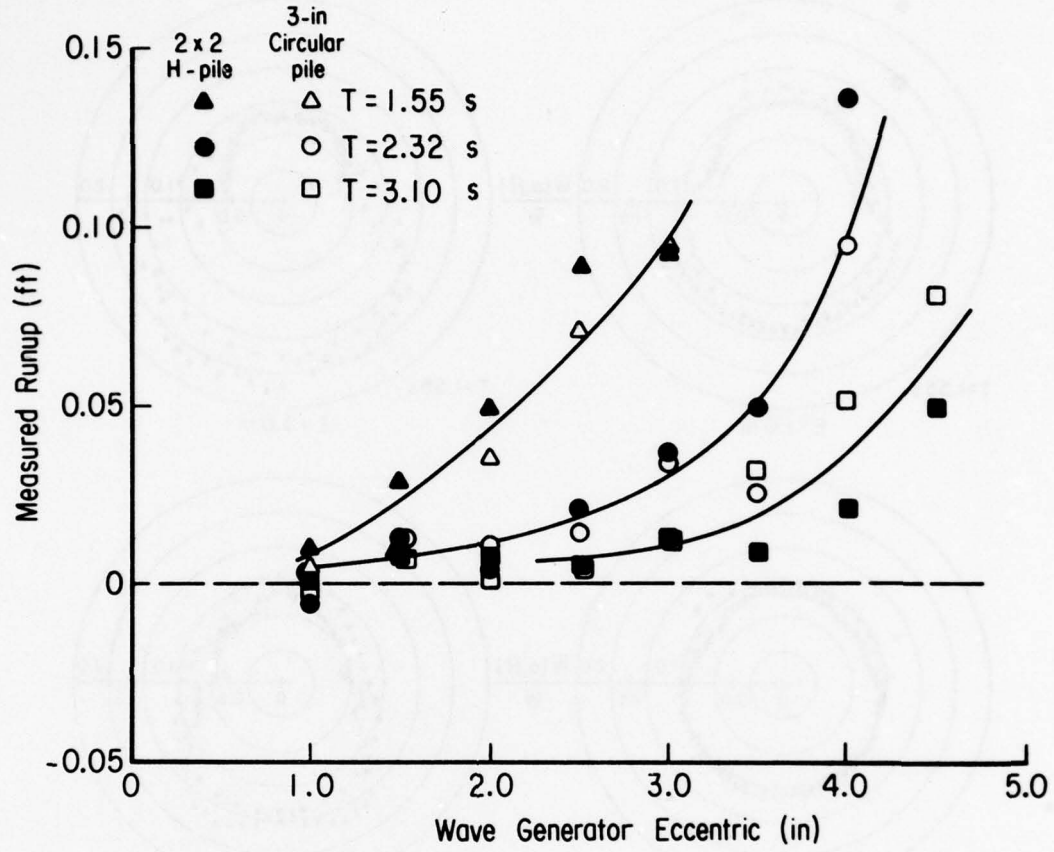

Figure 19. Similar trends in measured runup for various waves at circular pile ($\alpha = 0°$) and H-pile ($\beta = 0°$). Test conditions: d = 1.00 foot, G = 25 feet.

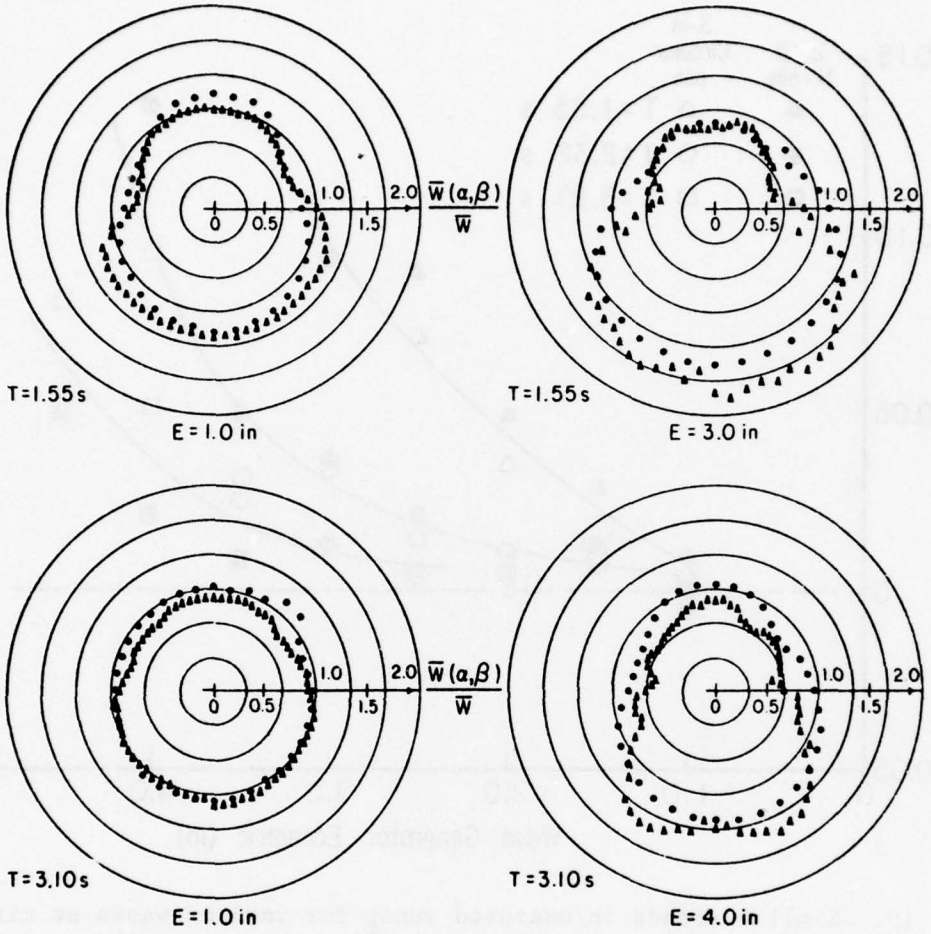

Figure 20. Normalized peak water patterns at circular pile and H-pile in four wave conditions. Test conditions: d = 1.00 foot, G = 25 feet.

Figure 20 shows clear differences in the data variation near the pattern minimums for the two piles. At a circular pile, singularities in the second angular derivative can occur near the water level minimums (Hallermeier, 1976); the minimums then indicate the break in water surface slope associated with flow separation (Longuet-Higgins, 1973). The $\overline{W}(\beta)$ mimimums indicate maximum sheltering of the channel from incident wave action, and must be related to channel geometry.

The calculated velocity head of the incident crest, $U^2/2g$, gives a fairly close upper bound to the front runup of a single crest at a circular pile, $[W(\alpha = 0°)-W]$, for a subset of this study's data considered by Hallermeier (1976). He reported that velocity calculations are somewhat problematic for these tests. For the most part, the wave conditions do not match those included in the stream-function tables of Dean (1974), and the numerical stream-function theory is the only available theory accurate throughout the range of d/L in these tests. Also, the test waves generally have complicated profiles (see App. B). Furthermore, the runup need not be exactly $U^2/2g$, since various regimes of flow stagnation are possible (see Sec. II,4), and the variation of horizontal flow velocity with depth causes downward secondary flow at the front of the pile, which might decrease runup. For these reasons, velocity head calculations have not been made for the complete data.

However, Figures 21, 22, and 23 exhibit trends consistent with crest stagnation causing the front runup; i.e., the peak water level at $\alpha = 0°$ is approximately the incident crest height plus the velocity head. Figure 21 shows three $[\overline{W}(\alpha)/\overline{W}]$ patterns for the 3-inch circular pile in waves of three heights at the same period. Figure 22 shows three $[\overline{W}(\alpha)/\overline{W}]$ patterns at the same pile for waves at three periods with the same height. Figure 23 shows three $[\overline{W}(\alpha)/\overline{W}]$ patterns for the 6-inch circular pile in waves of three heights at the same period.

Linear wave theory provides a first approximation for the peak horizontal velocity at the wave crest:

$$U = (2\pi W/T)\ [\cosh k(W+d)]/\sinh kd\ , \qquad (1)$$

where $k = (2\pi/L)$ is the wave number and $W = H/2$ for the sine wave considered by linear wave theory. The numerical stream-function theory provides a more accurate value of U for waves of finite amplitude (Dean, 1974). Table 5 presents the normalized measured and calculated front runup for the data in Figures 21, 22, and 23. The measured runup is given as $\{[\overline{W}(\alpha = 0°)/\overline{W}]-1\}$, and the calculated runup as $(U^2/2g\overline{W})$, where U has been obtained by interpolation in the stream-function tables (Dean, 1974, Vol. I, pp. 86-91). The measured values are larger than the calculated. Identical trends occur in measurements and calculations: at a given wave period, normalized runup increases with increasing wave height; at a given wave height, normalized runup decreases with increasing wave period. These trends agree with the velocity given by equation (1).

Minimums of $[\overline{W}(\alpha)/\overline{W}]$ generally change location and dimension with changing wave conditions. However, this behavior does not seem to be

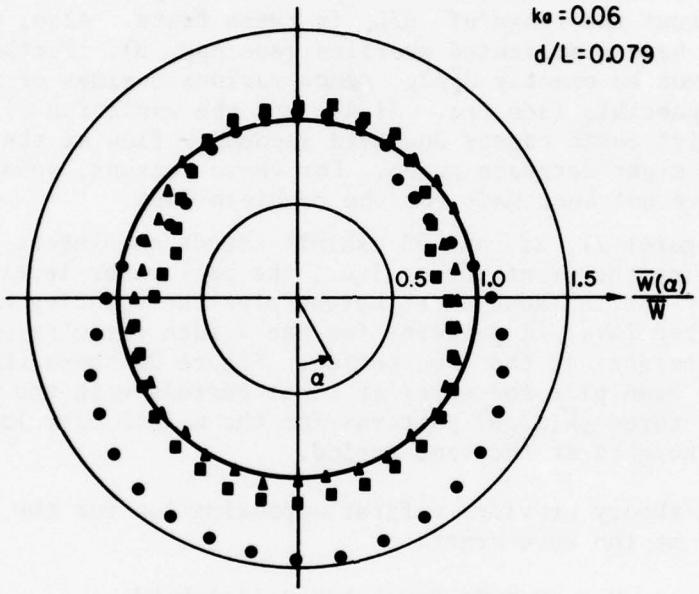

▲ $\overline{W}$=0.048 ft; $\overline{H}$=0.08 ft
■ $\overline{W}$=0.112 ft; $\overline{H}$=0.18 ft
● $\overline{W}$=0.264 ft; $\overline{H}$=0.41 ft

Figure 21. $\overline{W}(\alpha)/\overline{W}$ patterns at 3-inch circular pile as $\overline{W}$ increases. Test conditions: T = 2.32 seconds, d = 1.00 foot, G = 25 feet.

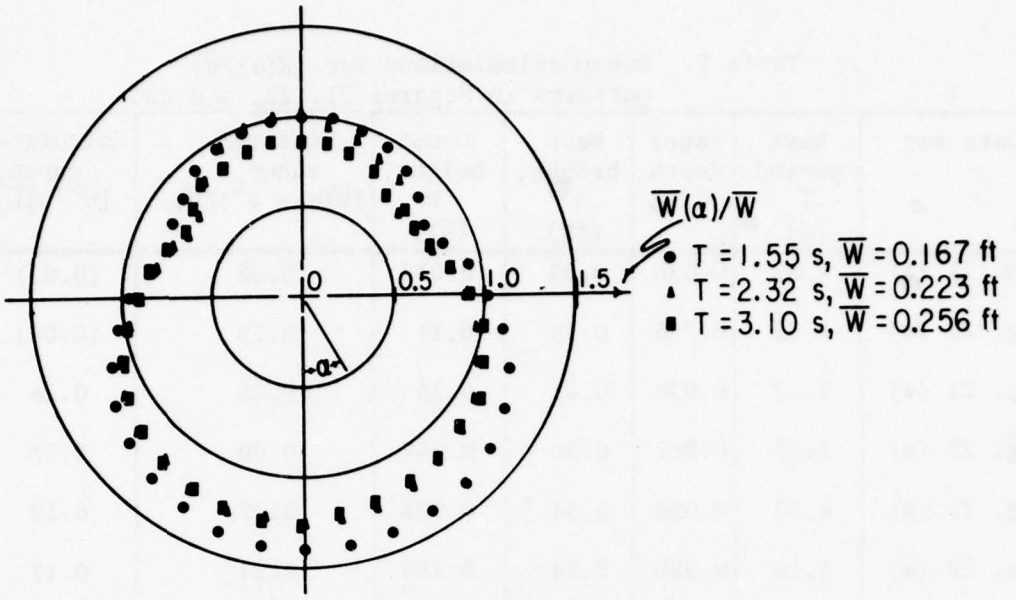

Figure 22. $[\overline{W}(\alpha)/\overline{W}]$ patterns at 3-inch circular pile with identical incident wave height at three periods. Test conditions: $\overline{H}$ = 0.34 foot, d = 1.00 foot, G = 25 feet.

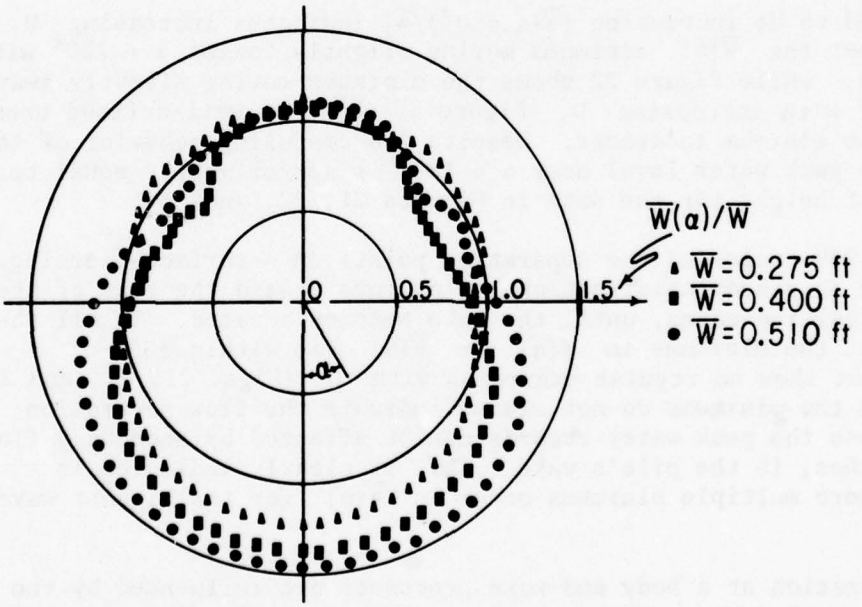

Figure 23. $[\overline{W}(\alpha)/\overline{W}]$ patterns at 6-inch circular pile as $\overline{W}$ increases. Test conditions: T = 3.55 seconds, d = 2.33 feet, G = 19.5 feet.

Table 5. Runup calculations for $[\overline{W}(\alpha)/\overline{W}]$ patterns in Figures 21, 22, and 23.

Data set	Wave period, T (s)	Water depth, d/L_o	Wave height, H (ft)	Crest height, W (ft)	Measured runup, $[\overline{W}(\alpha = 0°)/\overline{W}]-1$	Calculated runup, $[U^2/2g\overline{W}]$
Fig. 21 (▲)	2.32	0.036	0.08	0.048	0.02	(0.02)[1]
Fig. 21 (■)	2.32	0.036	0.18	0.11	0.13	(0.04)
Fig. 21 (●)	2.32	0.036	0.41	0.26	0.43	0.26
Fig. 22 (●)	1.55	0.081	0.34	0.167	0.40	0.23
Fig. 22 (▲)	2.32	0.036	0.34	0.223	0.27	0.19
Fig. 22 (■)	3.10	0.020	0.34	0.256	0.24	0.17
Fig. 23 (▲)	3.55	0.036	0.49	0.275	0.21	0.10
Fig. 23 (■)	3.55	0.036	0.68	0.40	0.36	0.16
Fig. 23 (●)	3.55	0.036	0.85	0.51	0.46	0.23

[1]Value in parentheses calculated from linear wave theory.

simply related to U; increasing $[\overline{W}(\alpha = 0°)/\overline{W}]$ indicates increasing U. Figure 21 shows the $\overline{W}(\alpha)$ minimums moving slightly toward $\alpha = 180°$ with increasing U, while Figure 22 shows the minimums moving slightly away from $\alpha = 180°$ with increasing U. Figure 23 shows no well-defined trend with U in the minimum locations. Despite the confusing behavior of the minimums, the peak water level near $\alpha = 180°$ is approximately equal to the incident crest height for the data in Figures 21, 22, and 23.

Petryk (1969) reported the separation points on a surface-piercing circular pile in steady unidirectional flow move toward the rear of the pile as $(u^2/2ga)$ increases, until the wake becomes aerated. In all the present tests, the minimums in $W(\alpha)$ or $\overline{W}(\alpha)$ lie within $\pm 35°$ of $|\alpha| = 125°$, but show no regular excursion with U (Figs. 21, 22, and 23). This suggests the minimums do not always indicate the flow separation points, because the peak water records can be affected by secondary flow, such as splashes, in the pile's wake. This is clearly indicated in Figure 23, where multiple minimums occur in $\overline{W}(\alpha)$ for the highest wave condition.

Flow separation at a body and wake processes are influenced by the Reynolds number, $R = U\ell/\nu$, where ℓ is a characteristic flow length and ν is kinematic fluid viscosity. The Reynolds number measures the ratio of inertial to viscous forces. The present tests were designed to show prototype stagnation effects, determined by the Froude number, $F = U^2/g\ell$. Since this Froude number is identical in both laboratory and prototype

situations (Table 3), the laboratory Reynolds number is lower than that in the prototype by a factor equal to the length scale raised to the power 1.5. Although this modeling inaccuracy is discussed later in Section IV,2, one effect on the test data is seen in Figure 24. These two $[\overline{W}(\alpha)/\overline{W}]$ data sets are for a circular pile in approximately the same flow situation at two different length scales. All the lengths are about 2.33 times greater in the 85-foot tank test than in the 96-foot tank, while the Froude number, $F_a = (U^2/2ga)$, is nearly the same in the two tests. The two data sets superpose well near the pile's front, but diverge toward the pile's rear. (The noticeable skewness of the 96-foot tank data is probably due to a flow along the wave crest discussed in App. B.) The smoothly sloping pattern around the sides of the pile breaks near $|\alpha| = 130°$ in the 96-foot tank data and near $|\alpha| = 110°$ in the 85-foot tank data. The depths of the minimums and the peak water level in the wake are markedly different in the two tests. Thus, Figure 24 demonstrates both the limitation and the asset of the scaling by Froude number used for these tests. Modeling of the wake details behind the pile was inaccurate, but modeling of the front stagnation effects was accurate.

The peak water patterns have definite value because stagnation effects dominate the patterns of most interest, as the following analysis shows. James and Hallermeier (1976) introduced a method for describing the peak water patterns in terms of a symmetric series

$$S(\alpha) = \sum_{j=0}^{\infty} a_j \cos [j(\alpha-\gamma)] , \qquad (2)$$

where a_j is the amplitude of the jth harmonic and γ is the angle about which the pattern is symmetric. The amplitudes, a_j, and the angle, γ, best describing a set of $W(\alpha)$ data can be determined by using a least squares estimation technique. Three harmonics provide a good fit to $W(\alpha)$ patterns produced by both low and high waves. Figure 25 superposes $W(\alpha)$ patterns for four wave types with the fitted symmetric series. Table 6 lists the wave conditions and the percent of pattern variance in each harmonic. For the two low waves, the second harmonic dominates the $S(\alpha)$ pattern, providing the fit to the front and rear maximums. For the two steep waves, the first harmonic dominates the $S(\alpha)$ pattern, providing the fit to the dominant front maximum. For all four wave types, $S(\alpha)$ fits $W(\alpha)$ fairly well except near the sharp minimums. These data demonstrate that stagnation effects dominate the $W(\alpha)$ pattern when they are significant; this occurs at a circular pile when F_a has a value greater than about 0.1 (Hallermeier, 1976).

2. Other Piles.

The peak water patterns for piles with channels exhibit a somewhat rough variation of measurement with orientation angle. This variability, as mentioned in the discussion of Figure 20, is due to complicated flows caused by the complex obstacle cross section. The variability impedes quantitative analysis of $\overline{W}(\beta)$ pattern features. However, comparing patterns for various piles clarifies some general effects of pile channels.

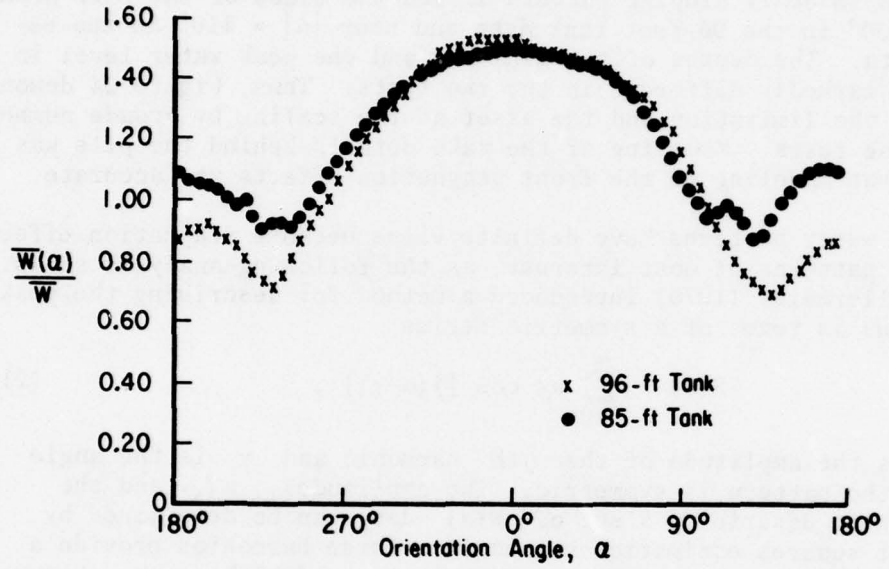

Figure 24. $\overline{W}(\alpha)/\overline{W}$ patterns for the same test situation at two length scales. Test conditions: T = 2.32 seconds, d = 1.00 foot, 2a = 0.25 foot, G = 8.6 feet, $\overline{W}$ = 0.27 foot (96-foot tank); T = 3.55 seconds, d = 2.33 feet, 2a = 0.5 foot, G = 19.5 feet, $\overline{W}$ = 0.49 foot (85-foot tank).

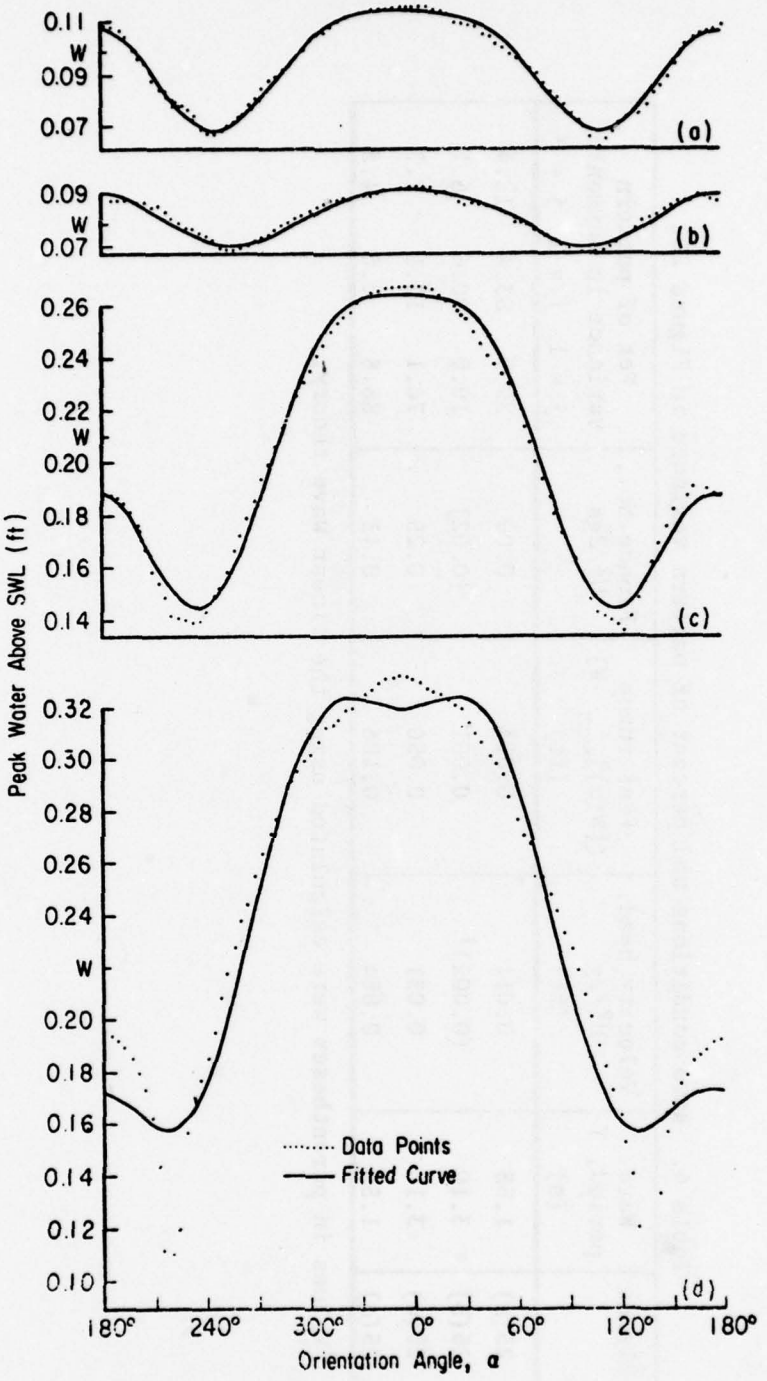

Figure 25. W(α) for four different crests, and curves fitted by symmetric series method. Test conditions: d = 1.00 foot, G = 25 feet, 2a = 0.25 foot; see Table 6 for wave conditions.

Table 6. Wave conditions and percent of pattern variance in Figure 25.

Figure	Wave period, T (s)	Velocity head, $U^2/2g$ (ft)	Peak runup $([W(\alpha)]_{max} - W)$ (ft)	Froude No., $U^2/2ga$	Pct of pattern variance in harmonic: j = 1	j = 2	j = 3
25(a)	1.55	0.011	0.014	0.09	29.9	53.4	15.4
25(b)	3.10	(0.002)[1]	0.001	(0.02)	10.0	80.6	6.1
25(c)	3.10	0.031	0.050	0.25	76.1	15.1	7.7
25(d)	1.55	0.054	0.106	0.43	88.8	0.6	4.3

[1]Values in parentheses were calculated using the linear wave theory.

Figure 26 superposes peak water measurements at the 6-inch circular pile and at the pile with 25 fins, in the side-by-side situation shown in Figure 14. Wave conditions were d = 2.33 feet (71 centimeters), T = 3.55 seconds, E = 4.0 inches (10 centimeters), G = 18 feet (5.5 meters). The finned pile was tested both with a fin forward and with a channel forward; the channel-forward position gives measurements at 0°, ±14.4°, ...; the fin-forward position gives measurements at ±7.2°, ±21.6°, ... The minimums in each pattern are located near ±120°. However, the pattern for the finned pile has higher, narrower front and rear maximums than the pattern for the smooth pile. This increased articulation is a general feature of the peak water patterns for piles with channels, compared to the patterns for smooth piles (circular piles and the flat plate).

The effects of increasing wave height at T = 2.32 seconds on the $[\overline{W}(\beta)/\overline{W}]$ patterns measured with the flat plate, the 1x2 H-pile, and the 2x1 H-pile (with relatively deep channels) are shown in Figure 27. Figure 27(a) shows that the three obstacles have negligible effects for small waves. For each pile, the normalized pattern shows more distinct features as wave height increases. The patterns for the 2x1 H-pile have the most marked features: a front maximum region with a sharp border near $\beta = \pm 55°$, symmetrically located minimums near $\beta = \pm 80°$, and a broad, relatively high rear maximum. For the 1x2 H-pile, the front maximum region is broader with a less distinct edge, the minimums occurring near $\beta = \pm 115°$ are slightly deeper, and the rear secondary maximum is more sharply defined but lower than that for the 2x1 H-pile. At the two H-piles, the maximum water level occurs slightly away from $\beta = 0°$ for the highest wave, due to flow around the leading face and into the front channel. The flat plate gives the smoothest variation of peak water with orientation angle, so the minimums and the rear maximum are not well defined.

Figure 28 shows normalized patterns measured at the same three piles in the highest test waves at two other periods; the features just described are again apparent. However, at T = 3.10 seconds, the 2x1 H-pile causes a deeper minimum than the 1x2 H-pile. At T = 1.55 seconds, the patterns for the H-piles are skewed rather than symmetric in the front maximum region; there is also a slight depression in the center of the rear maximum for the 2x1 H-pile.

Figure 29 presents waveforms measured within the 2x1 H-pile for $\beta = 0°$, 20°, 40°, and 90°. For $\beta = 90°$, the transformed wave has a much broader and lower crest than the incident wave, indicating that peak crest flow bypasses the channel. The other three waveforms are similar to the incident waveform (see App. B, Fig. B-4), although crest height is increased by runup.

The various channeled piles were tested primarily to examine the influence of channel geometry on the angular width of the front maximum region in the peak water pattern. Figure 30(a) defines an angle θ describing the pile channel geometry; the streamline sketches in Figure 30(b) indicate how θ can influence the peak water pattern.

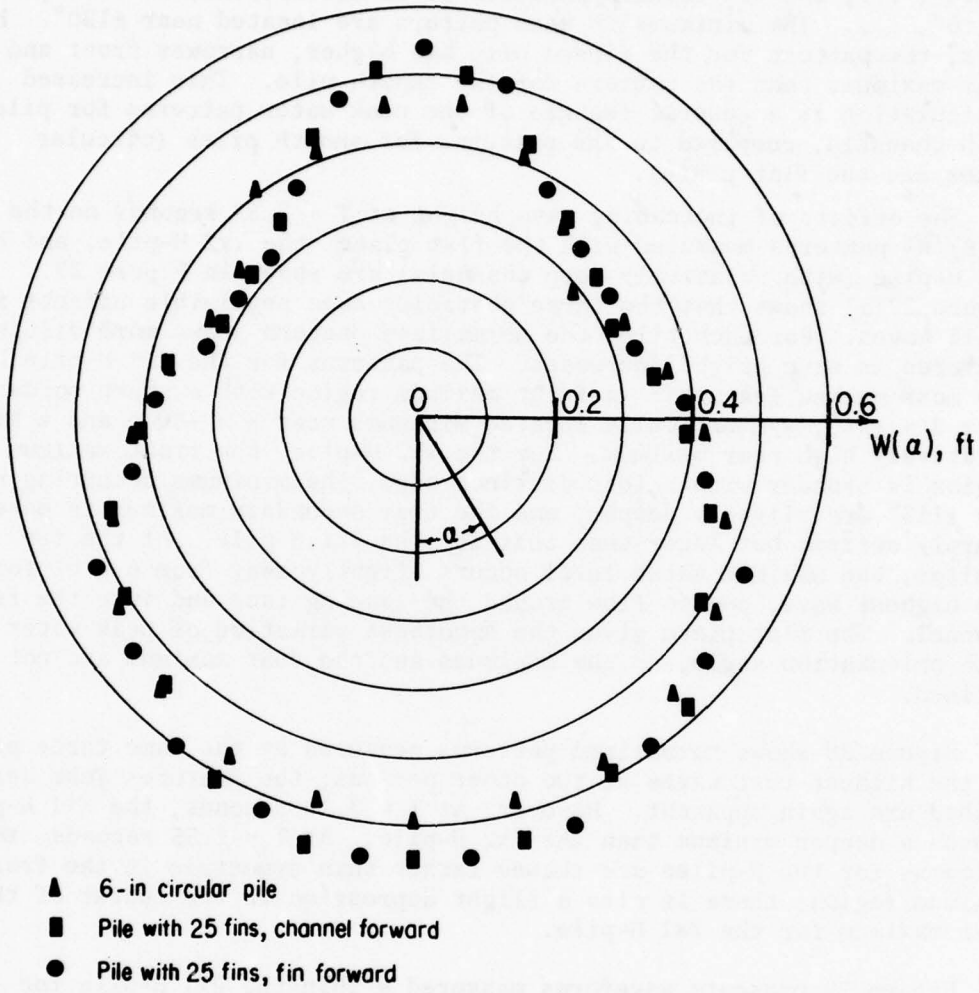

Figure 26. Measured peak water around side-by-side circular and finned circular piles.

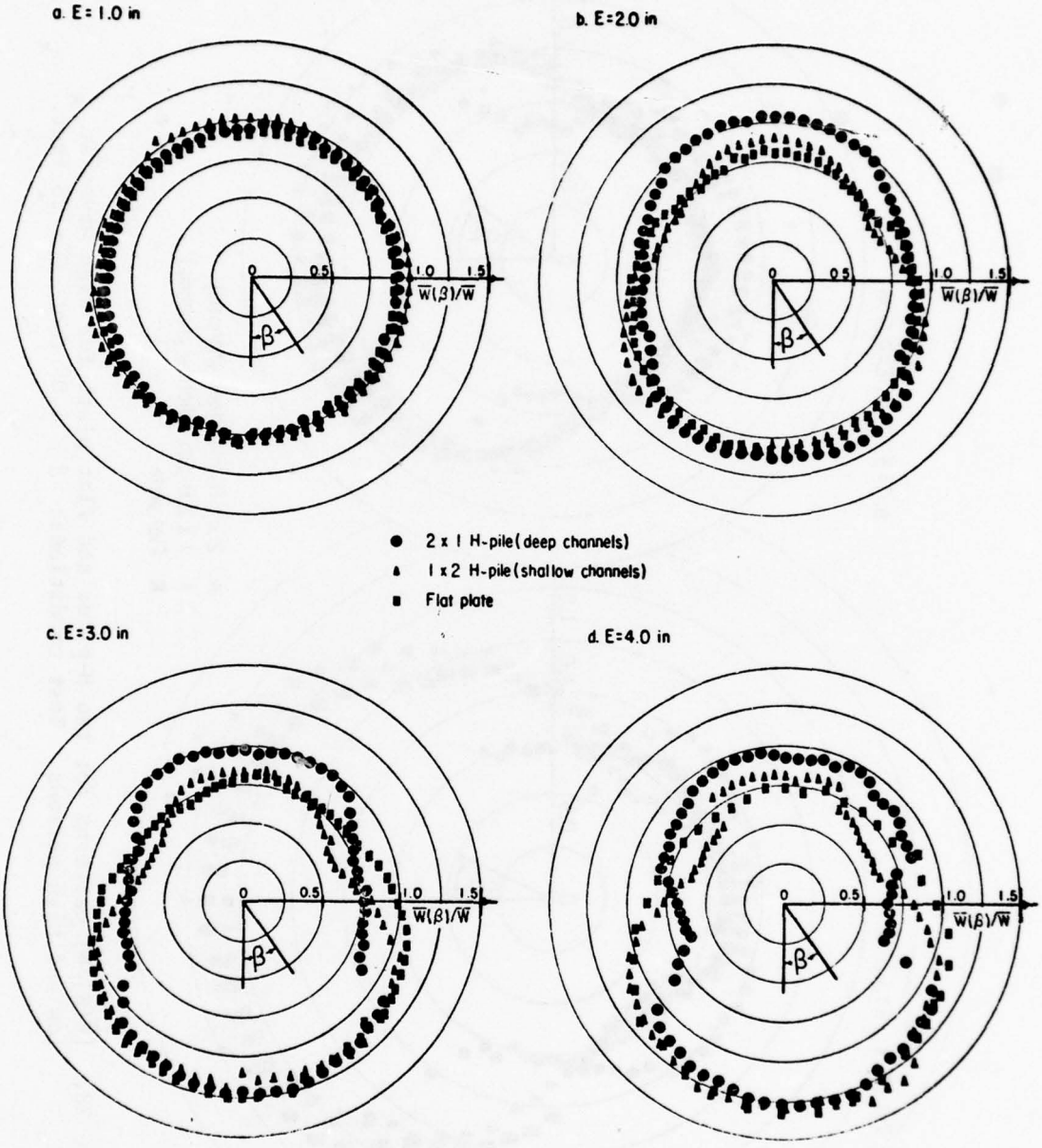

Figure 27. $[\overline{W}(\beta)/\overline{W}]$ patterns for two H-piles and flat plate as $\overline{W}$ increases. Test conditions: T = 2.32 seconds, d = 1.00 foot, G = 25 feet.

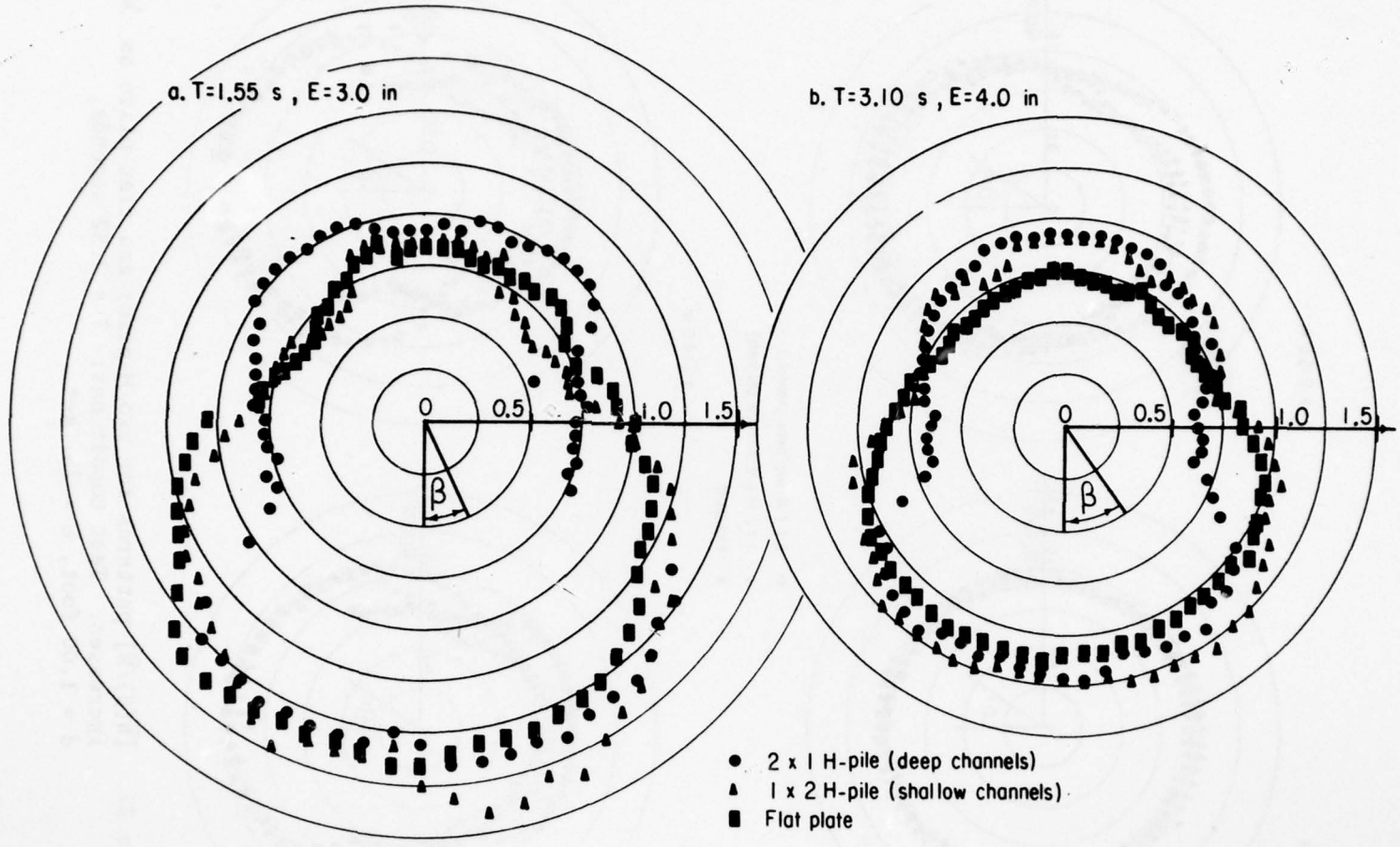

Figure 28. $[\overline{W}(\beta)/\overline{W}]$ patterns for two H-piles and flat plate for high waves at low and high periods. Test conditions: d = 1.00 foot, G = 25 feet.

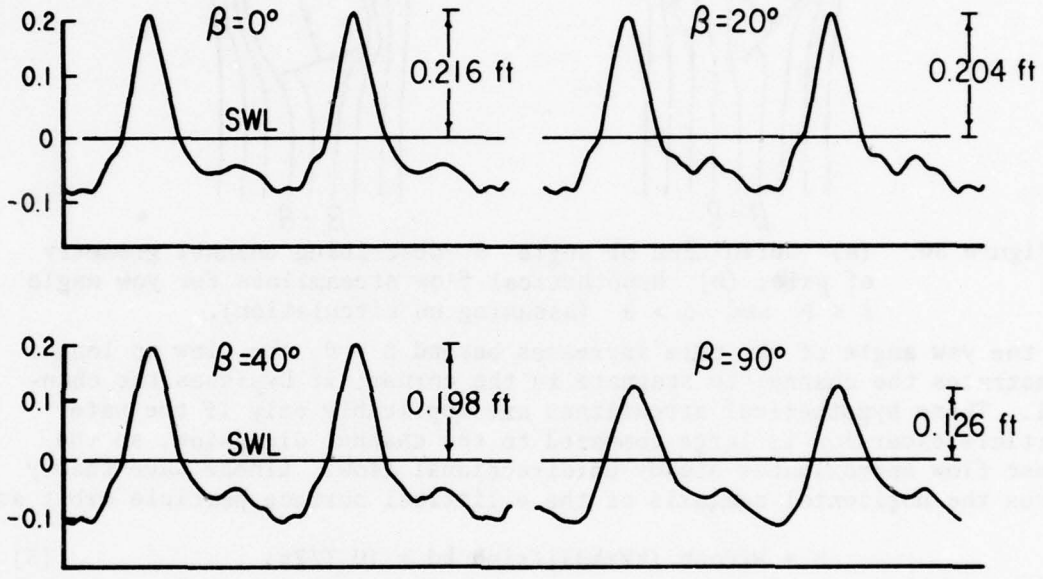

Figure 29. Waveforms measured in channel of 2x1 H-pile at four orientations. Test conditions: T = 2.32 seconds, d = 1.00 foot, G = 25 feet, $\overline{W}$ = 0.18 foot.

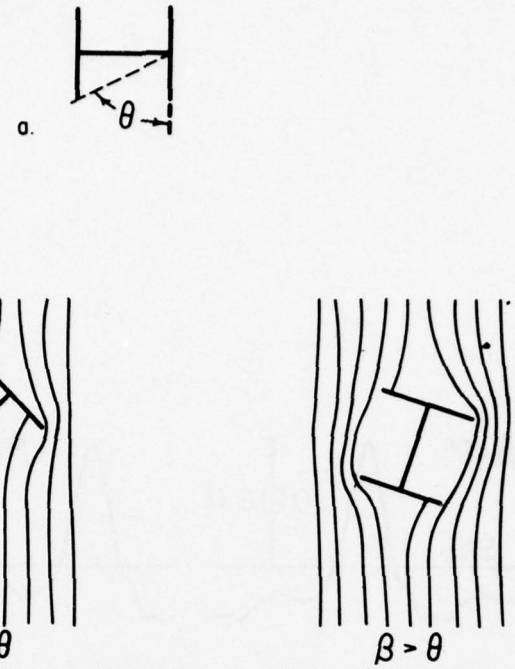

Figure 30. (a) Definition of angle θ describing channel geometry of pile; (b) hypothetical flow streamlines for yaw angle $\beta < \theta$ and $\beta > \theta$ (assuming no circulation).

As the yaw angle of the pile increases beyond $\beta = \theta$, the flow no longer penetrates the channel to stagnate in the corner; it bypasses the channel. These hypothetical streamlines are applicable only if the water particle excursion is large compared to the channel dimension, so the crest flow approximates steady unidirectional flow. Linear wave theory gives the horizontal semiaxis of the elliptical surface particle orbit as

$$h = W[\cosh (kW+kd)]/\sinh kd = (U\,T/2\pi) \; . \qquad (3)$$

Although the test waves were nonlinear, equation (3) gives the order of magnitude of the fluid excursion, showing it is much larger than X for H-piles with high waves at the medium period (T = 2.32 seconds for d = 1.00 foot; T = 3.55 seconds for d = 2.33 feet). Figure 31 shows peak water patterns measured at five H-piles with maximum fluid excursion. (The 3x3 H-pile is excluded because no data are available for the medium period and pile confinement effects also may be significant for this pile; see Sec. IV.)

Table 7 compares the angle θ for these piles with the angular half-width, χ, of the front runup region in Figure 31; χ is defined as the angle at which $\overline{W}(\beta)$ drops below $\frac{1}{2}[\overline{W}(\beta = 0°) + \overline{W}]$. For the relatively ideal situations represented in Figure 31, Table 7 shows a clear relationship between θ and χ. The five (θ, χ) pairs have a correlation coefficient of 0.732, so the hypothesis that there is no linear relationship between θ and χ can be rejected with about 81.3-percent confidence (Sec. 13.4.1 in Freund, .1962).

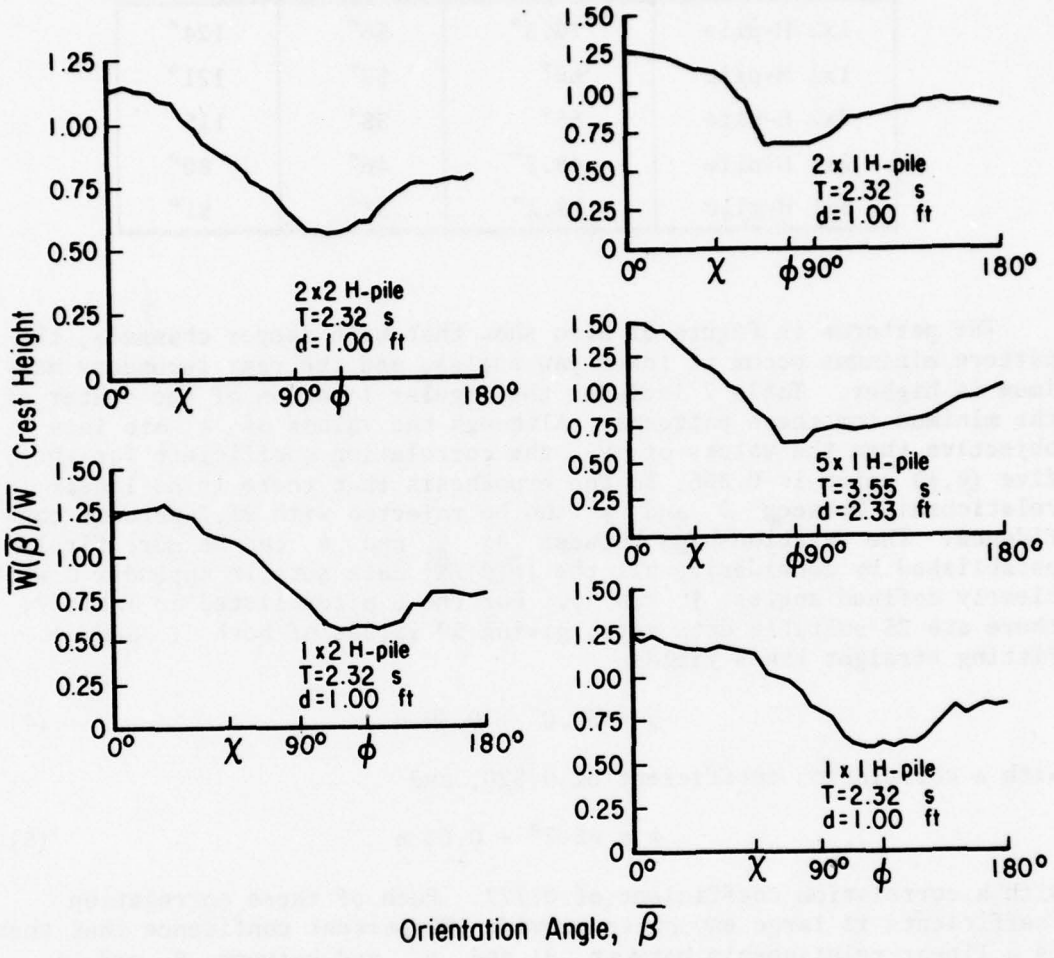

Figure 31. $[\overline{W}(\beta)/\overline{W}]$ patterns for five H-piles with maximum horizontal fluid orbit.

Table 7. Comparison of angles giving pile channel geometry, θ, half-width of front maximum region, χ, and minimum location, ϕ, for Figure 31.

	θ	χ	ϕ
1x2 H-pile	76.3°	56°	124°
1x1 H-pile	65°	59°	121°
2x2 H-pile	65°	38°	115°
2x1 H-pile	48.2°	46°	80°
5x1 H-pile	18.2°	33°	81°

The patterns in Figure 31 also show that with deeper channels, the pattern minimums occur at lower yaw angles, and the rear secondary maximum is higher. Table 7 includes the angular location of the center of the minimum for these patterns. Although the values of ϕ are less objective than the values of χ, the correlation coefficient for the five (θ,ϕ) pairs is 0.866, so the hypothesis that there is no linear relationship between θ and ϕ can be rejected with 93.7-percent confidence. The relationships between θ, χ, and ϕ can be more firmly established by considering all the $[\overline{W}(\beta)/\overline{W}]$ data sets in Appendix C with clearly defined angles χ and ϕ. For the 5 piles listed in Table 7, there are 25 suitable data sets, giving 50 values of both χ and ϕ. Fitting straight lines yields

$$\chi = 36.0° + 0.30\ \theta\ , \qquad (4)$$

with a correlation coefficient of 0.520, and

$$\phi = 65.7° + 0.63\ \theta\ , \qquad (5)$$

with a correlation coefficient of 0.777. Each of these correlation coefficients is large enough to provide 100-percent confidence that there is a linear relationship between θ and χ, and between θ and ϕ. Thus, pile channel geometry definitely affects the shape of the peak water pattern for high waves. This conclusion is consistent with the data in Figures 32, 33, and 34.

Figures 32 and 33 present peak water patterns for piles of similar shape but different sizes; Figure 32 shows data for low and high waves at T = 1.55 seconds incident on the 1x1 and 3x3 H-piles; and Figure 33 shows data for a high wave at T = 3.10 seconds incident on the 1x1 and 2x2 H-piles. The larger pile generally causes a slightly higher front maximum, a more sharply defined front maximum region, and a lower rear maximum; peak forward flow is less obstructed by the smaller pile. However, each pattern of a pair is basically similar to the other.

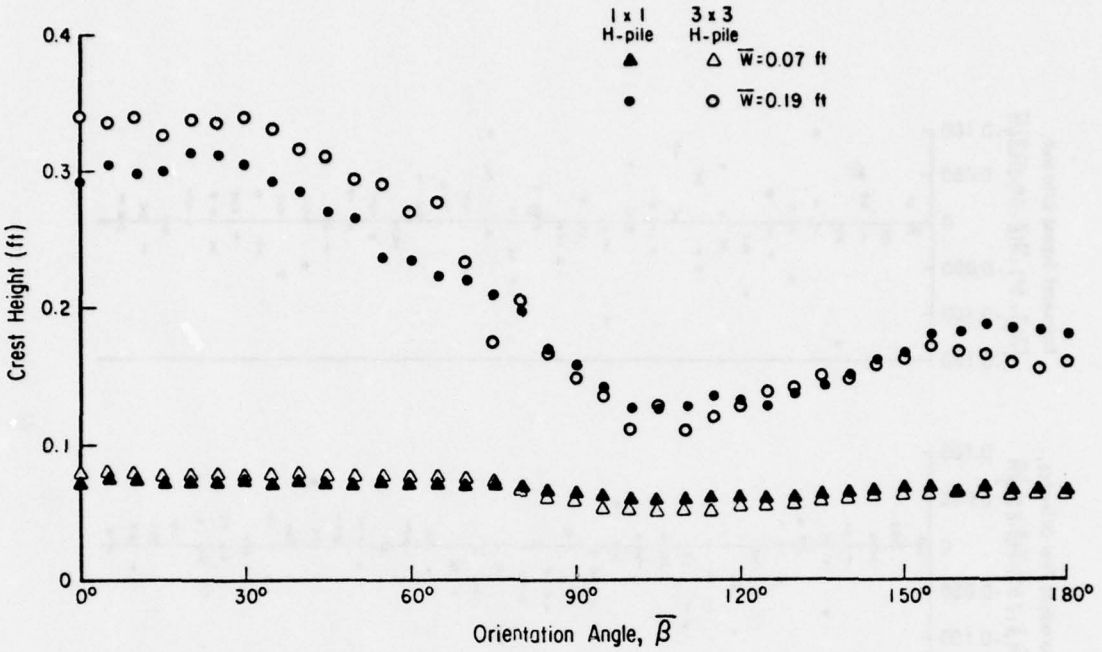

Figure 32. $\overline{W}(\overline{\beta})$ patterns for 1x1 and 3x3 H-piles. Test conditions: T = 1.55 seconds, d = 1.00 foot, G = 25 feet.

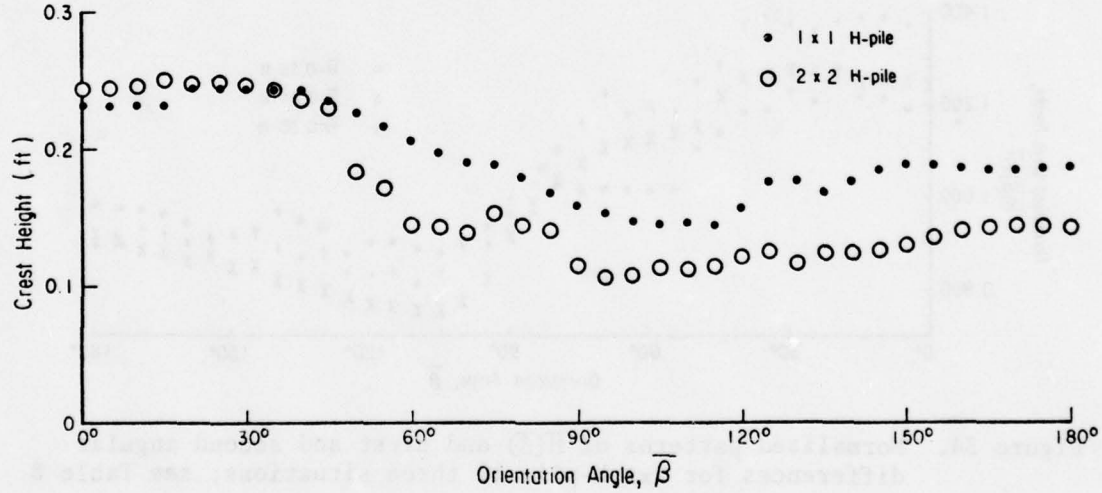

Figure 33. $\overline{W}(\overline{\beta})$ patterns for 1x1 and 2x2 H-piles. Test conditions: T = 3.10 seconds, d = 1.00 foot, G = 25 feet, E = 4.0 inches.

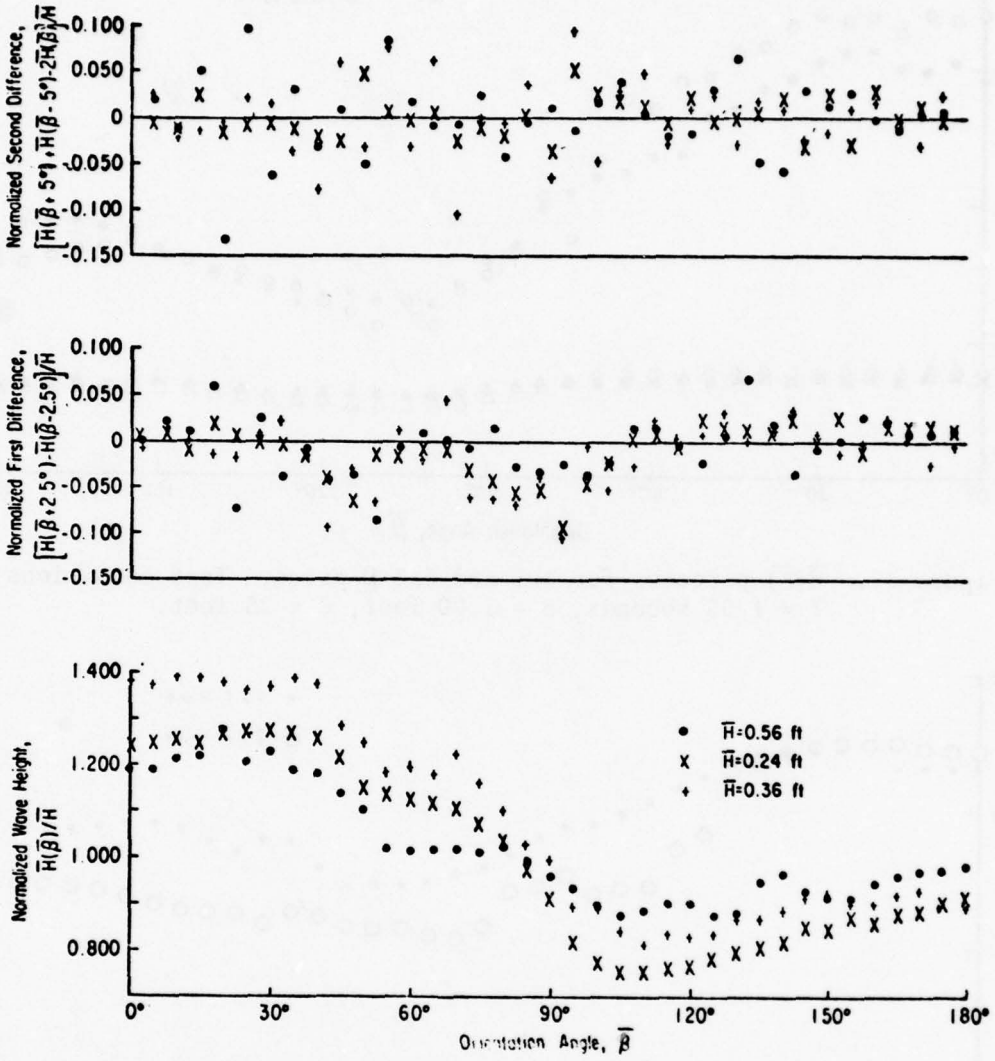

Figure 34. Normalized patterns of $\bar{H}(\bar{\beta})$ and first and second angular differences for 2x2 H-pile in three situations; see Table 8 for test conditions.

Figure 34 concludes the display of effects of pile channels with three data sets for the 2x2 H-pile, two sets from 96-foot tank tests, and the other from an 85-foot tank test. The relative water depth, d/L, is identical for the three tests. The data are presented as $[\bar{H}(\bar{\beta})/\bar{H}]$, because stillwater datum is not clearly indicated on the record of the 85-foot tank test. The Reynolds and Froude numbers for the 85-foot tank test are each bracketed by those for the 96-foot tank tests (see Table 8). The plots of first and second angular differences show scatter but similar data trends, demonstrating that the pattern shapes are similar in these situations.

Table 8. Calculations for $[\bar{H}(\bar{\beta})/\bar{H}]$ patterns in Figure 34.[1]

Data set in Fig. 34	Wave period, T (s)	Water depth, d (ft)	Wave height, $\bar{H}$ (ft)	Calculated Reynolds number, UX/ν	Calculated Froude number, U^2/gX
.	2.35	2.33	0.56	$3.1 \cdot 10^4$	0.33
×	1.55	1.00	0.24	$2.0 \cdot 10^4$	0.14
+	1.55	1.00	0.37	$3.5 \cdot 10^4$	0.43

[1]X = 0.22 foot and velocities calculated using stream-function tables.

3. Conclusions.

The peak water patterns for high waves at thin piles are somewhat independent of pile shape. Basically similar patterns are obtained with circular and channeled piles (Figs. 20 and 26); all patterns show a front maximum region, a lesser maximum at the rear, and intervening symmetrically located minimums. As incident crest height increases, in patterns normalized by crest height, the front maximum becomes higher in a manner consistent with crest stagnation, the rear maximum becomes slightly lower, and the minimums generally become deeper (Figs. 21, 22, 23, 27, and 28).

The patterns show several definite dependencies on pile shape. The pattern minimums are farthest toward the rear for the smooth piles (circular or flat plate), and the minimums are farther toward the front for deeper pile channels (Figs. 26, 27, 28, and 31). Patterns for smooth piles are less articulated than those for channeled piles (Figs. 20, 27, and 28). At H-piles, maximum water level may occur away from $\beta = 0°$ (Figs. 20 and 28). The angular width of the front maximum region is linearly related to an angle measuring the shallowness of the pile channels (Table 7).

Piles of different size but identical shape give very similar peak water patterns (Figs. 21, 23, 32, and 33). Similar stagnation effects are recorded in test situations that are geometrically similar (identical Froude number but different scale), although the Reynolds number has a definite effect on the pattern away from the front maximum region

(Figs. 24 and 34). These results verify that the peak water patterns are primarily caused by crest stagnation at the obstacle, with significant secondary effects of obstacle geometry.

IV. EXTRAPOLATION OF THE LABORATORY RESULTS

The laboratory tests were designed to be approximate models of wave transformation near an isolated, rigid vertical pile in common nearshore situations (Table 3). The conclusions based on the data can be extrapolated to prototype situations if the modeling is essentially valid. The following discussions assess the importance of the pile confinement within a narrow wave tank, and of inaccuracy in modeling the prototype.

1. Effects of Pile Confinement.

In a narrow wave tank, measurements can include effects of the tank walls. Constriction of the flow through the reduced tank cross section causes increased velocity past the pile, so the incident wave does not fully define the flow at the pile. In addition, the bow wave occurring upstream of the pile may be compressed by the confining tank walls. Either effect might influence the peak water measured at the pile.

Taking b to be tank half-width, these effects are partially discribed by a blockage parameter Z equal to a/b or X/2b. If Z is very small, as in the 14-foot-wide tank (85-foot tank) used in this study, effects of pile confinement are negligible. However, the other wave tank (96-foot tank) used was only 1.5 feet wide; Z was usually on the order of 0.1, so flow constriction effects may be significant in the 96-foot tank tests.

Saunders (1957) described a correction procedure for the flow constriction effect, using a calculated Bernoulli contour system for the flow in the reduced section. This procedure is standard for correcting data from tests in unidirectional flows, and may be used to calculate peak water level adjustments caused by flow constriction in the present tests, if maximum crest flow is assumed to be steady unidirectional flow. Using equation 4-4 in Petryk (1969) for open-channel flow, the situation defined by a/b = 0.167, d = 1.00 foot, and F_a = 1.2 results in about a 2-percent reduction of water depth at the pile. This is a relatively minor correction for this example of extreme flow constriction from the present test series. Furthermore, in reporting wind-tunnel tests on the effects of wake splitter plates, Apelt and West (1975) expressed doubt about the applicability of a Bernoulli contour calculation to the case of a bluff body with a trailing plate, and did not attempt to correct their data for flow constriction effects. Similar doubts arise concerning correction calculations for the present tests of piles with leading and trailing sharp edges. For these reasons, the measurements have been reported as recorded, without correcting water level for the flow constriction by the pile.

The bow wave extends laterally about two to three radii away from the test pile (Figs. 10, 12, 14, 15, 16, and 35). Hallermeier (1976) noted that blockages of one-sixth or one-twelfth of the tank by a circular pile resulted in $W(\alpha)$ patterns not revealing different confinement effects; the side slope in $W(\alpha)$ depends on F_a but not on Z. Considering these facts, $Z \leq (1/6)$ seems a reasonable criterion for minor confinement effects. This requirement is satisfied for every test situation except the 3x3 H-pile and the 6-inch-diameter circular pile in the 96-foot tank.

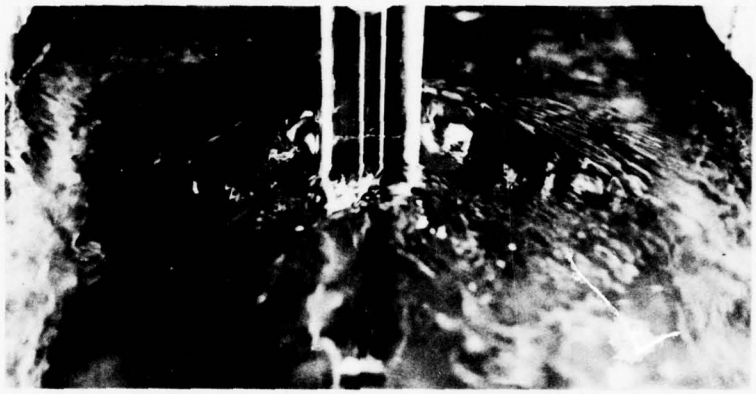

Figure 35. Photo from rear of disturbance at 2x2 H-pile during crest flow in the 1.5-foot-wide tank.

The tests with the 6-inch circular pile in the 96-foot tank ($Z = 0.33$) were discussed in Hallermeier (1976). Effects of pile confinement were negligible because linear wave scattering was the dominant effect in those tests, rather than unidirectional peak crest flow. According to the theoretical results by Spring (1973) for linear wave scattering, situations with certain values of ka and b/L and significantly large Z can be equivalent to an unconfined pile. The tests with the 6-inch circular pile in the 96-foot tank ($ka = 0.5$, $b/L = 0.24$) constitute one of these situations.

2. Inaccuracies in Modeling the Prototype.

The Reynolds number, $R = 2Ua/\nu$, characterizes the important flow effects occurring at a circular pile due to fluid viscosity. Because stagnation effects were of primary importance in the present tests with surface-piercing piles, the laboratory situation was scaled to have the same Froude number as important prototypes; the Reynolds number was lower than in corresponding prototypes by a factor of the length scale to the power 1.5. This factor is between 6 and 60 in the present tests (see Table 3 for the length scales). High ocean waves at typical field piles give $10^4 < R < 10^7$, approximately. Even with the slight exaggeration in pile diameter (Table 3), the present laboratory tests were such that $10^3 < R < 10^5$.

Figure 24 shows an effect of R on the peak water around the rear half of a circular pile, but R has a more fundamental influence. In general, R characterizes the flow regime at a circular pile, as clearly shown in measured drag forces on circular cylinders in unidirectional flow. From first principles, the drag force, f_D, per unit length of a cylinder may be expressed as

$$f_D = 0.5\, C_D\, \rho\, a\, u\, |u| \,, \qquad (6)$$

where ρ is fluid density, u is flow velocity, and C_D is drag coefficient. Roshko (1961) and Schlichting (1968) discussed the distinct unidirectional flow regimes revealed in measured values of C_D at various R (Fig. 36). A subcritical range with $C_D \approx 1.2$ is separated from a transcritical range with $C_D \approx 0.7$ by a supercritical range of varying but lower C_D at Reynolds numbers between $2 \cdot 10^5$ and $3.5 \cdot 10^6$. The C_D measured in wave flow is about the same as that indicated in Figure 36, although the data are scanty (Fig. 7-62 in U.S. Army, Corps of Engineers, Coastal Engineering Research Center, 1977).

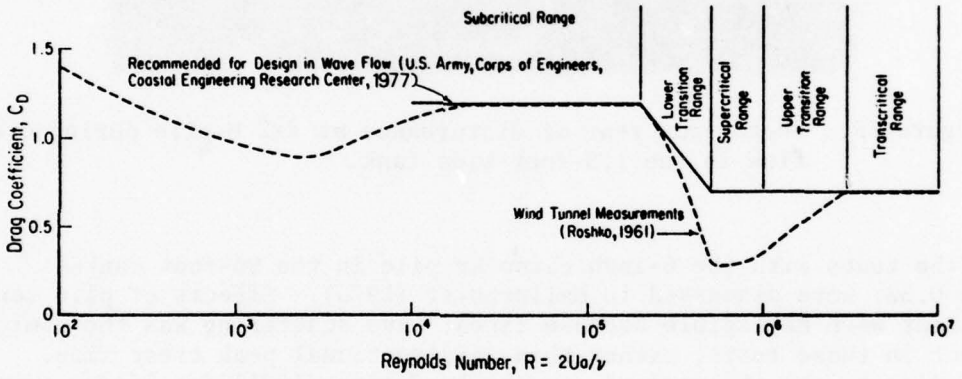

Figure 36. Flow regimes indicated by measured drag coefficient at a circular cylinder.

Roshko (1961) describes the supercritical flow range as characterized by a laminar separation bubble. Proceeding around the pile, the following phenomena occur: laminar flow separation, transition to turbulent flow, flow reattachment, and finally turbulent flow separation. The laboratory test waves were well ordered, whereas natural waves have a somewhat turbulent character, likely to be important to the flow separation process in this supercritical range. Also, the test piles were smooth, whereas realistic models would have a somewhat rough face, also likely to be important beyond the subcritical range. These other modeling inaccuracies would be important if these tests had entered into higher Reynolds number flows.

The reported tests with circular piles all correspond to the subcritical range, having a larger drag coefficient than intense prototype flows. McNown and Keulegan (1959) stated that increasing wake size is associated with a smaller C_D, so the measured laboratory wakes are generally smaller than prototype wakes. Thus, measured peak water around the rear of circular piles is not generally typical of prototypes included in Table 3.

For the noncircular piles tested, the modeling inaccuracies seem to be of minor importance. The piles have small cross sections, measured as X/L, and Section III,2 has pointed out that channel shape has a more important effect than pile size on the shape of the $\overline{W}(\beta)$ pattern with these thin piles. Also, the Reynolds number is less important in flow past a pile with channels, because the sharp edges establish the points of flow separation.

3. Conclusions.

The wave tanks were wide enough that the reported data are free of significant pile confinement effects except for the 3x3 H-pile in the 96-foot tank. Because the Reynolds number is lower for the reported laboratory tests, measured peak water around the rear half of circular piles is not typical of prototype situations in Table 3. However, the identical Froude number in model and prototype implies the conclusions concerning wave stagnation effects at various piles (Sec. III,3) pertain to prototype situations.

V. COASTAL ENGINEERING APPLICATIONS

The data in this report (especially App. C) can be used to improve the solutions for the following coastal engineering design problems:

(a) Determining deck elevations for pile-supported structures in cases where deck elevation is not limited by other design factors.

(b) Improving the design of decks near pile supports in cases where deck elevation will be subject to wave runup at the pile supports.

(c) Estimating height to which different types of corrosion protection is needed on piles and pile-supported structures.

(d) Clarifying the physical processes causing the wide scatter in measured coefficients used for computing wave forces on piles. For example, it appears that runup can significantly affect wave force on piles in shallow water when $F_a = U^2/2ga \simeq 1$ (Hallermeier, 1976).

(e) Suggesting novel pile shapes for special design requirements; e.g., capping a thick concrete pile with a narrower

steel section of equivalent bearing strength to avoid unwanted runup (Fig. 37). If wave direction is nearly constant, as it is in the nearshore zone, web-shaped members may reduce cross section to incoming waves, although transverse oscillations will limit such applications (Apelt and Isaacs, 1968).

(f) Estimating wave direction in the nearshore zone. The following paragraphs review the status of the potential use of wave runup at a pile to estimate wave direction.

As mentioned in Section I, this study is aimed at evaluating the use of wave transformation at a pile in an instrument measuring nearshore wave directions. In this application, maximizing stagnation effects results in a measurable relief in peak water level on a circular pile's circumference. This relief is symmetrical about the direction of surface flow, and wave direction may be estimated by interpolation, using a small number of water level gages on the pile's circumference. James and Hallermeier (1976) reported dependencies of precision in direction estimates on the interpolation method, the angular measurement spacing, the vertical measurement resolution, and the incident wave type. The simplest instrument would use four water level gages spaced 60° apart on the seaward pile half, to measure wave direction within ±3° over a 120° range of incidence. This high measurement precision is needed for nearshore wave directions, since wave refraction limits the range of incident direction. The proposed instrument could measure individual crests, recording direction variations.

The reported data show that a finned circular pile can produce a smaller angular range of maximum runup than a smooth circular pile. However, this increased relief in water level is associated with a more ragged variation of water level with angle. Thus, it seems doubtful that interpolated estimates of wave direction with a small number of water level gages at a finned pile could attain the precision possible using a smooth circular pile.

Figure 38 schematically shows the operation of an automatic direction gage using symmetrical crest transformation at a circular pile. Hallermeier and James (1974) presented an example of the design process for the pile installation, using an estimate of the local wave climate. Major remaining uncertainties about the proposed instrument are a foolproof objective method for recognizing crest incidence, and whether available water level gages have adequate durability and resolution. Development of a prototype instrument is not presently planned.

VI. CONCLUSIONS

The principal conclusions from this investigation are as follows:

a. With high waves at thin surface-piercing piles, crest stagnation is similar at circular and channeled piles (Figs. 14 and 19).

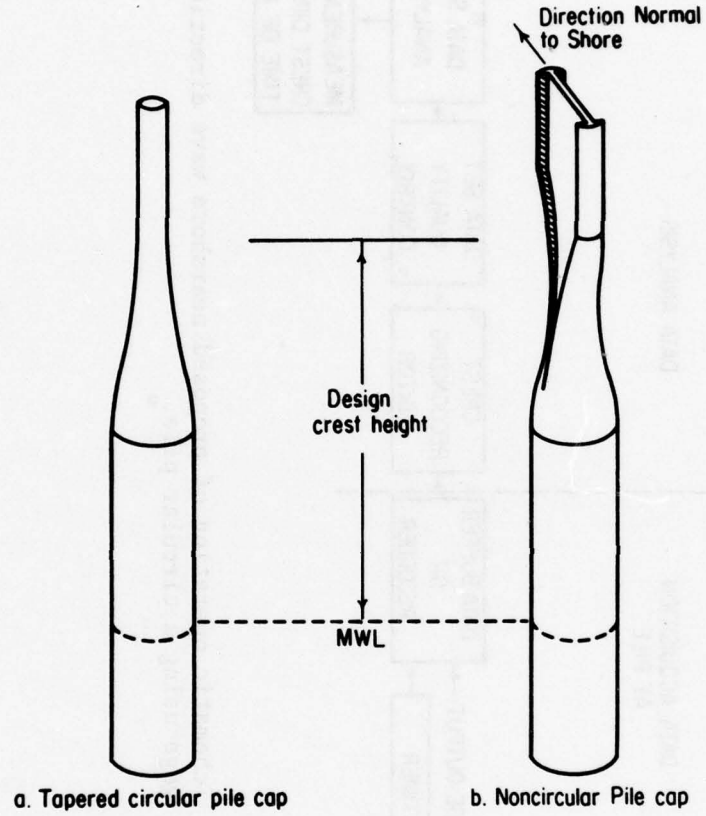

Figure 37. Varying sections to reduce design wave force on pile segment near water surface.

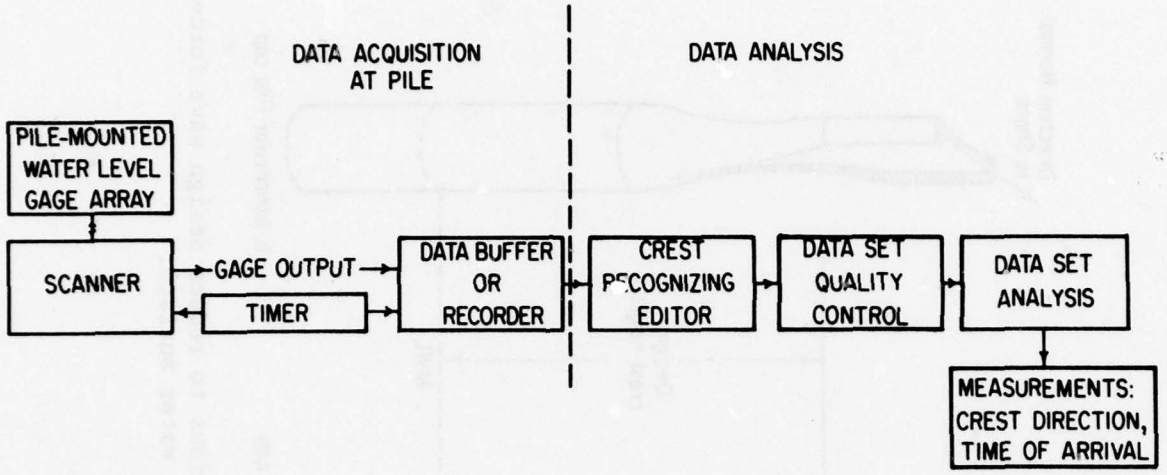

Figure 38. Schematic operation of proposed nearshore wave direction gage using a circular pile.

b. As in steady unidirectional flow, this free-surface flow effect depends on the Froude number based on peak fluid velocity and the thin dimension of the obstacle. Smooth, breaking, or jetting runup can occur, depending on the Froude number and the geometry of the obstacle's front face (Sec. II,4).

c. At a circular pile, wave scattering is overwhelmed by flow stagnation effects when the Froude number, $F_a = (U^2/2ga) \simeq (H^2/La)$, becomes significant compared to unity (Hallermeier, 1976).

d. The patterns of measured crest height versus pile orientation with respect to wave direction are largely independent of pile shape. Basically similar patterns are obtained with smooth and channeled piles; all the patterns have a front maximum region, a lesser maximum at the rear, and intervening symmetrically located minimums (Figs. 20 and 26).

e. With increasing peak fluid velocity, in patterns normalized by incident crest height, the front maximum becomes higher in a manner consistent with crest stagnation, the rear maximum generally becomes lower, and the minimums become deeper (Figs. 21, 22, 23, 27, and 28).

f. Measured runup of a single crest at the front of a thin circular pile agrees well with calculated velocity head, $U^2/2g$ (Fig. 4 in Hallermeier, 1976), while mean measured runup in steady wave action is larger than the calculated velocity head (Table 5). However, velocity calculations are problematic for the test waves.

g. The patterns show several definite effects of pile shape. The angular width of the front maximum region is linearly related to an angle measuring the shallowness of the pile channels (Fig. 30, eq. 4). The pattern minimums are farthest toward the rear for the smooth piles (flat plate and circular piles), and the minimums are farthest toward the front for deeper pile channels (Figs. 20, 27, 28, and 31; eq. 5).

h. Similar stagnation effects are measured in test situations that are geometrically similar (identical Froude number but different scale), although the Reynolds number affects the pattern away from the front maximum region (Figs. 24 and 34). With minor caution, the test results can be extrapolated to prototype situations of interest in coastal engineering (Sec. IV,3).

i. A small number of water level gages on the circumference of a circular pile might be used for high-resolution direction measurements of individual nearshore crests (James and Hallermeier, 1976). Available laboratory data permit making major design choices for a field installation (Hallermeier and James, 1974), although several uncertainties

remain about the design and durability of an automatic instrument for field wave direction measurements (Sec. V).

j. Further study is needed to define surface effects in wave forces on a thin circular pile in shallow water (Sec. V).

LITERATURE CITED

AMERICAN INSTITUTE OF STEEL CONSTRUCTION, INC., *Manual of Steel Construction*, 7th ed., New York, 1970.

APELT, C.J., and ISAACS, L.T., "Hydrodynamic Force Coefficients for Bluff Cylinders of Tee Shape and Their Relevance to Bridge Piers," *Proceedings of the Third Australasian Conference on Hydraulics and Fluid Mechanics*, 1968, pp. 169-174.

APELT, C.J., and WEST, G.S., "The Effects of Wake Splitter Plates on Bluff-body Flow in the Range $10^4 < R < 5 \times 10^4$. Pt. 2," *Journal of Fluid Mechanics*, Vol. 71, Pt. 1, Sept. 1975, pp. 145-160.

BARNARD, B.J.S., and PRITCHARD, W.G., "Cross-waves. Pt. 2. Experiments," *Journal of Fluid Mechanics*, Vol. 55, Pt. 2, Sept. 1972, pp. 245-255.

BONNEFILLE, R., and GERMAIN, R., "Wave Action on Isolated Vertical Cylinders of Large Dimension," *Proceedings of the International Association for Hydraulic Research Congress*, 1963, pp. 311-318.

BOURODIMOS, E.L., "Gravity Wave Shoaling and Transformation in Shallow Water," *Ocean Engineering*, Vol. 1, No. 1, 1968, pp. 39-76.

CHAKRABARTI, S.K., and TAM, W.A., "Wave Height Distribution Around Vertical Cylinder," *Journal of the Waterways, Harbors and Coastal Engineering Division*, Vol. 101, No. WW2, May 1975, pp. 225-230.

CRAPPER, G.D., "Non-linear Capillary Waves Generated by Steep Gravity Waves." *Journal of Fluid Mechanics*, Vol. 40, Pt. 1, Jan. 1970, pp. 149-159.

DAGAN, G., "Waves and Wave Resistance of Thin Bodies Moving at Low Speed: The Free-surface Nonlinear Effect," *Journal of Fluid Mechanics*, Vol. 69, Pt. 2, May 1975, pp. 405-416.

DAGAN, G., and TULIN, M.P., "Two-dimensional Free-surface Gravity Flow Past Blunt Bodies," *Journal of Fluid Mechanics*, Vol. 51, Pt. 3, Feb. 1972, pp. 529-543.

DEAN, R.G., "Presentation of Research Results," SR-1, Vol. I, Stock No. 008-022-00083, "Tabulation of Dimensionless Stream Function Theory Variables," SR-1, Vol. II, Stock No. 008-022-00084, *Evaluation of Water Wave Theories for Engineering Application*, U.S. Government Printing Office, Washington, D.C., Nov. 1974.

DEAN, R.G., and URSELL, F., "Interaction of a Fixed, Semi-Immersed Circular Cylinder with a Train of Water Waves," Technical Report No. 37, Hydraulics Laboratory, Massachusetts Institute of Technology, Cambridge, Mass., 1959.

FREUND, J.E., *Mathematical Statistics*, Prentice-Hall, Englewood Cliffs, N.J., 1962.

GALVIN, C.J., Jr., "Finite-Amplitude, Shallow-Water Waves of Periodically Recurring Form," *Proceedings of the Symposium on Long Waves*, 1971, pp. 1-32.

GALVIN, C.J., Jr., and HALLERMEIER, R.J., "Wave Runup on Vertical Cylinders," *Proceedings of the 13th Conference on Coastal Engineering*, 1972, pp. 1955-1974.

HALLERMEIER, R.J., "Nonlinear Flow of Wave Crests Past a Thin Pile," *Journal of the Waterways, Harbors and Coastal Engineering Division*, Vol. 102, No. WW4, Nov. 1976, pp. 365-377.

HALLERMEIER, R.J., and JAMES, W.R., "Development of a Shallow-Water Wave Direction Gage," *Proceedings of the International Symposium on Ocean Wave Measurement and Analysis*, 1974, pp. 696-712.

HELLSTROM, B., and RUNDGREN, L., "Model Tests on Olands Sondra Grund Lighthouse," Bulletin No. 39, The Institution of Hydraulics, Royal Institute of Technology, Stockholm, Sweden, 1954.

JAMES, D.F., "The Meniscus on the Outside of a Small Circular Cylinder," *Journal of Fluid Mechanics*, Vol. 63, Pt. 4, May 1974, pp. 657-664.

JAMES, W.R., and HALLERMEIER, R.J., "Nearshore Wave Direction Gage," *Journal of the Waterways, Harbors and Coastal Engineering Division*, Vol. 102, No. WW4, Nov. 1976, pp. 379-393.

LAIRD, A.D.K., "A Model Study of Wave Action on a Cylindrical Island," *Transactions of the American Geophysical Union*, Vol. 36, No. 2, 1955, pp. 279-285.

Le MEHAUTE, B., DIVOKY, D., and LIN, A., "Shallow Water Waves: A Comparison of Theories and Experiments," *Proceedings of the 11th Conference on Coastal Engineering*, 1968, pp. 86-107.

LONGUET-HIGGINS, M.S., "The Generation of Capillary Waves by Steep Gravity Waves," *Journal of Fluid Mechanics*, Vol. 16, Pt. 1, May 1963, pp. 138-159.

LONGUET-HIGGINS, M.S., "A Model of Flow Separation at a Free Surface," *Journal of Fluid Mechanics*, Vol. 57, Pt. 1, Jan. 1973, pp. 129-148.

MADSEN, O.S., "Waves Generated by a Piston-Type Wavemaker," *Proceedings of the 12th Conference on Coastal Engineering*, 1970, pp. 589-607.

MADSEN, O.S., "On the Generation of Long Waves," *Journal of Geophysical Research*, Vol. 76, No. 36, Dec. 1971, pp. 8672-8683.

MADSEN, O.S., "A Three Dimensional Wave Maker, Its Theory and Application," *Journal of Hydraulic Research*, Vol. 12, No. 2, 1974, pp. 205-222.

MAHONEY, J.J., "Cross-waves. Pt. 1. Theory," *Journal of Fluid Mechanics*, Vol. 55, Pt. 2, Sept. 1972, pp. 229-244.

McNOWN, J.S., and KEULEGAN, G.H., "Vortex Formation and Resistance in Periodic Motion," *Journal of the Engineering Mechanics Division*, Vol. 85, No. EM 1, Jan. 1959, pp. 1-6.

MEI, C.C., and UNLUATA, U., "Harmonic Generation in Shallow Water Waves," *Waves on Beaches and Resulting Sediment Transport*, Academic Press, New York, 1972, pp. 181-202.

MORISON, J.R., JOHNSON, J.W., and O'BRIEN, M.P., "Experimental Studies of Forces on Piles," *Proceedings of the Fourth Conference on Coastal Engineering*, 1953, pp. 340-370.

NAGAI, S., TOKIKAWA, K., and ODA, K., "Report on the Pier of the Suspension Bridge Connecting the Main Land with Shikoku Island in Japan," Interim Report I, Hydraulics Laboratory, Osaka City University, Osaka, Japan, 1966.

PAAPE, A., and BREUSERS, H.N.C., "The Influence of Pile Dimension on Forces Exerted by Waves," *Proceedings of the 10th Conference on Coastal Engineering*, 1966, pp. 840-849.

PETRYK, S., "Drag on Cylinders in Open Channel Flow," Ph.D. Thesis, Colorado State University, Fort Collins, Colo., 1969.

ROSHKO, A., "Experiments on the Flow Past a Circular Cylinder at Very High Reynolds Number," *Journal of Fluid Mechanics*, Vol. 10, Pt. 3, May 1961, pp. 345-356.

SAUNDERS, H.E., *Hydrodynamics in Ship Design*, Vol. I, Society of Naval Architects and Marine Engineers, New York, 1957.

SCHLICHTING, H., *Boundary-Layer Theory*, 6th ed., McGraw-Hill, New York, 1968.

SPRING, B.H., "Interaction of Plane Water Waves with Vertical Circular Cylinders," Ph.D. Thesis, University of Wisconsin, Madison, Wis., 1973.

STAFFORD, R.P., RAY, R.E.L, and JONES, J.C., "Seven Reports on CERC Laboratory Wave Gages," Laboratory Memorandum, U.S. Army, Corps of Engineers, Coastal Engineering Research Center, Fort Belvoir, Va., 1973.

TSUCHIYA, Y., and YAMAGUCHI, M., "Studies of Wave Forces Exerted on Large Cylindrical Piles (1) - Characteristics of the Distribution of Wave Pressure and the Variation of Water Level," No. 14B, Annual Report of the Disaster Prevention Research Institute, Kyoto University, Kyoto, Japan, 1971, pp. 373-390.

U.S. ARMY, CORPS OF ENGINEERS, COASTAL ENGINEERING RESEARCH CENTER, *Shore Protection Manual*, 3d ed., Vols. I, II, and III, Stock No. 008-022-00113-1, U.S. Government Printing Office, Washington, D.C., 1977, 1,262 pp.

WHITE, R.V., and MILLER, R.L., "Experimental System for the Analysis of Continuously Transforming Impulse Waves." Technical Report No. 10, Fluid Dynamics and Sediment Transport Laboratory, University of Chicago, Chicago, Ill., 1971.

APPENDIX A

WAVE-GAGING TECHNIQUES

Both electrical and "direct" measurement techniques were used to record water levels in the laboratory tests. The electrical gages recorded, on a strip chart, the electrical signal indicating the immersed length of a probe, either by changing resistance (CERC gages) or by changing inductance (the Marsh-McBirney gage). In the direct techniques, wetting of a paper sleeve or erosion of a powder deposit on a circular pile preserved the peak waterline, which was marked with waterproof ink or crayon and then manually measured. This technique measured the entire pile circumference with no important flow obstruction from a sensing probe, but recorded no information on water level variation in time.

The electrical gages were calibrated and used according to well-defined CERC laboratory procedures (Stafford, Ray, and Jones, 1973). Before use, a calibration in still water ensured that the electrical gage had a suitable linear sensitivity through the expected range of water level. After use, the probe was again dipped in still water to ensure there was no appreciable drift of the gage datum or change in sensitivity. There were no major differences in using the resistance or inductance principles of water level measurement; the exact electronics are unimportant. Figure A-1 shows an electronic signal-conditioning unit, a strip-chart recorder, and a standard water level probe. Horizontal cross sections of all the electrical probes used are shown in actual size in Figure A-2.

White and Miller (1971) investigated the physical considerations in an accurate measurement of fluid level by a surface-piercing probe. They determined that the water and probe surfaces must be kept clean, and that the diameter of the probe and the static meniscus between probe and fluid should be minimized. A probe of minimum diameter approximates a needle piercing the fluid surface, rather than a bluff cylinder; this minimizes the possibility of erroneous measurement due to significant flow obstruction by the probe. James (1974) presented a solution for the shape and height of the static meniscus occurring at an extremely thin circular cylinder due to interfacial tension. For probes of about 0.01- to 0.1-inch (0.3 to 3 millimeters) diameter (see Fig. A-2) in water, the effects due to the static meniscus and flow obstruction should be minimal.

Confinement of a probe within a narrow channel was observed to have a significant effect on its electrical characteristics, but each probe used within a channel was statically calibrated while mounted there. Significant measurement error may arise from the static probe calibration. Water draining off the probe may not exactly follow the water surface; this can be significant when the water level is fluctuating rapidly. Dean and Ursell (1959) reported errors in using static calibration factors in wave measurements with a surface-piercing gage.

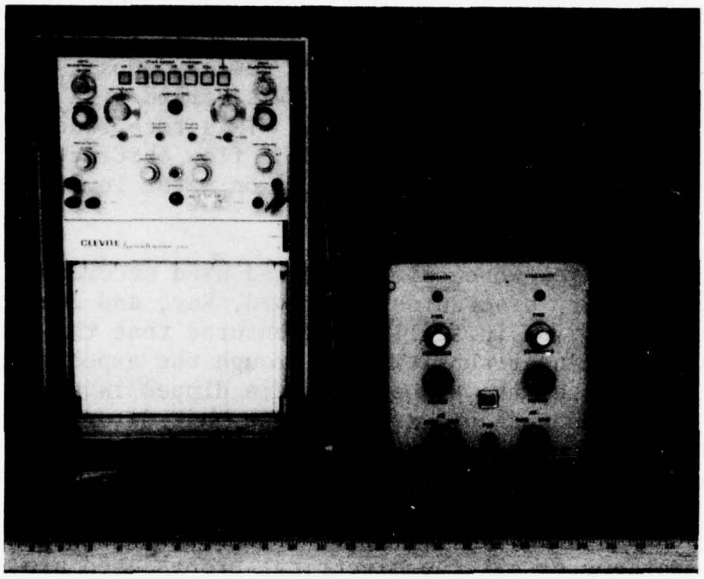

Figure A-1. Two-channel strip-chart recorder, standard CERC water level probe, and probe signal-conditioning unit.

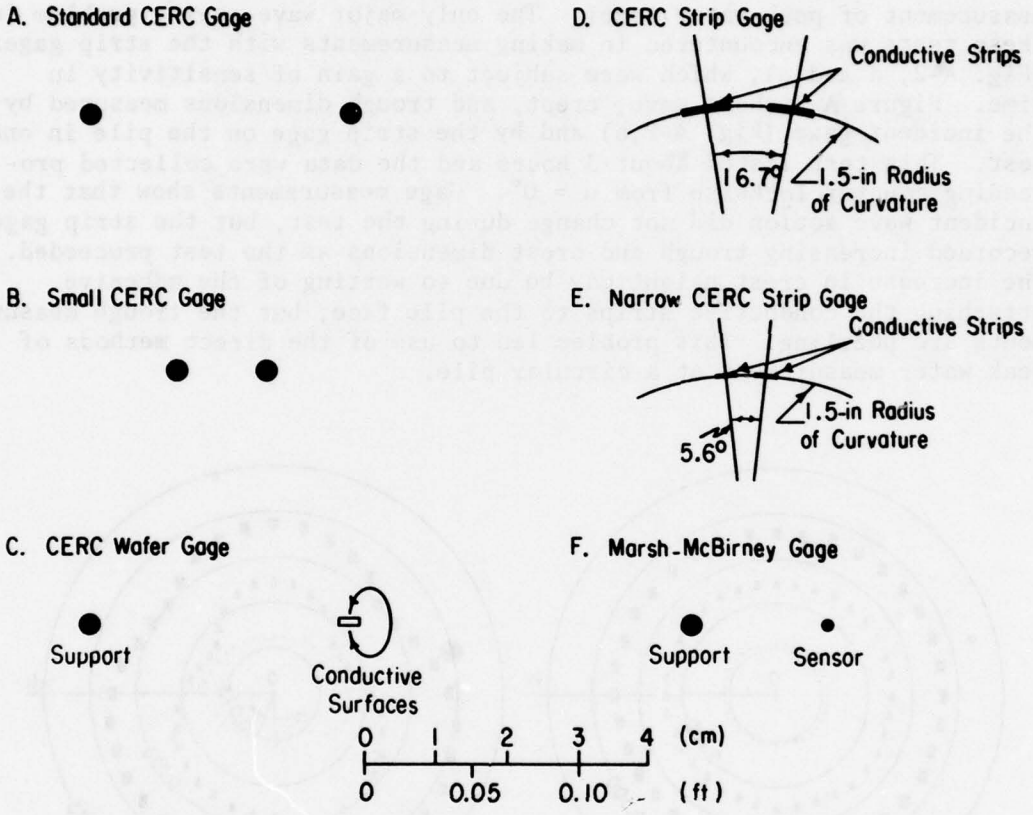

Figure A-2. Horizontal cross sections of electrical water level probes used (in actual size).

Noting this possibility, Bourodimos (1968) used a dynamic calibration technique for water level probes, but did not report the magnitude of difference between dynamic and static calibrations. Dynamic measurement errors were not investigated in the present study, so the measured waveforms have been treated as qualitative data.

The major reported data are peak water levels above SWL, and do not include the uncertain accuracy of the instantaneous water level measurements. Because peak crest flow varies rather slowly, dynamic measurement errors are unimportant and the static calibration ensures accurate measurement of peak water level. The only major wave-gaging problem in these tests was encountered in making measurements with the strip gages (Fig. A-2, d and e), which were subject to a gain of sensitivity in time. Figure A-3 shows wave, crest, and trough dimensions measured by the incident gage (Fig. A-2,a) and by the strip gage on the pile in one test. This test lasted about 3 hours and the data were collected proceeding counterclockwise from $\alpha = 0°$. Gage measurements show that the incident wave action did not change during the test, but the strip gage recorded increasing trough and crest dimensions as the test proceeded. The increase in crest height may be due to wetting of the adhesive attaching the conductive strips to the pile face, but the trough measurements are puzzling. This problem led to use of the direct methods of peak water measurement at a circular pile.

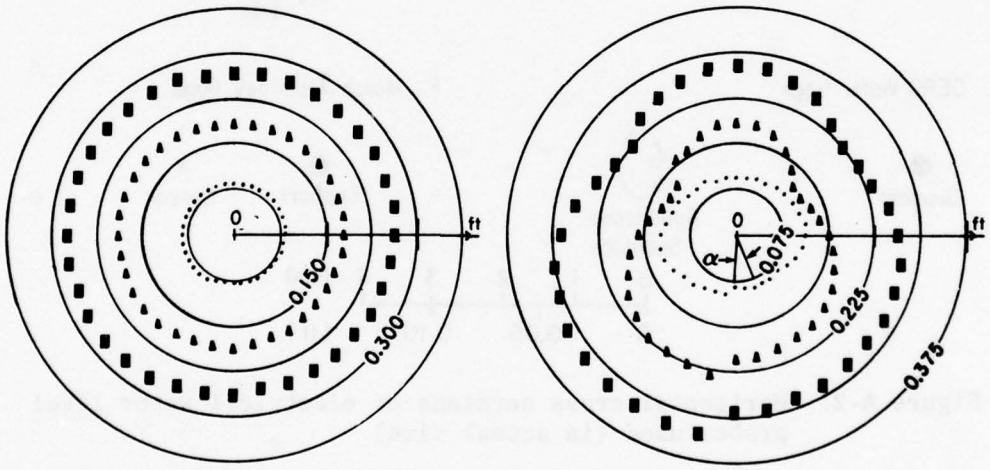

a. Dimensions of Incident Wave.

b. Wave Dimensions on Surface of Circular Pile.

■ Wave Height
▲ Crest Height
• Trough Depth

Figure A-3. Measurement drift shown by strip gage on the 3-inch circular pile in unchanging incident wave action.

Investigations showed good agreement between electrical and direct measurements of peak water. Figure A-4 displays measurements on the 3-inch circular pile by three techniques in nominally the same test conditions. The three patterns show good basic agreement with slight deviations. Differences could occur because the powder erosion measurement is for one wave crest, and because the paper sleeve is rougher than the Plexiglas pile and might cause a different flow boundary layer. Also, the paper might dry slightly before peak water could be marked and the measurement completed.

The importance of another possible effect of materials on the measurements can be assessed from the $\overline{W}(\alpha)$ data in Figure A-5. Here a test was repeated with 40 parts per million of wetting agent, Edwal Kwik-Wet, added to the water to reduce effects of surface tension; observed average peak water was marked on the Plexiglas pile with a crayon. The two patterns were very similar, except that the minimums were higher and more symmetrically located without the wetting agent. From these data, it was concluded that the smoothness of the pile material caused no anomalous effects on the data obtained in the model tests.

A final possible source of variability in $\overline{W}(\beta)$ measurements is the variable probe placement near the pile. The waveforms in Figure A-6 and the associated measurements in Table A-1 provide an estimate of the extreme range in this effect. Four waveforms were obtained deep within and just within the 2x2 H-pile channel at $\beta = 0°$ and $\beta = 90°$; the two other waveforms were obtained relatively near and far from the flat plate oriented at $\beta = 90°$. Although the waveforms show definite qualitative effects of gage placement, the peak water level measurements show less than a 4-percent change, which is considered insignificant compared to the variation in $\overline{W}(\beta)$ over the range of orientation angle.

The major conclusions are:

(a) The waveforms recorded by electrical water level gages are somewhat suspect, because the gage response to changing water level is imperfect in an undefined way;

(b) measurements of crest dimensions (peak water level) from gage records have adequate accuracy; the agreement between direct and electrical measurements of peak water levels is within about 5 percent.

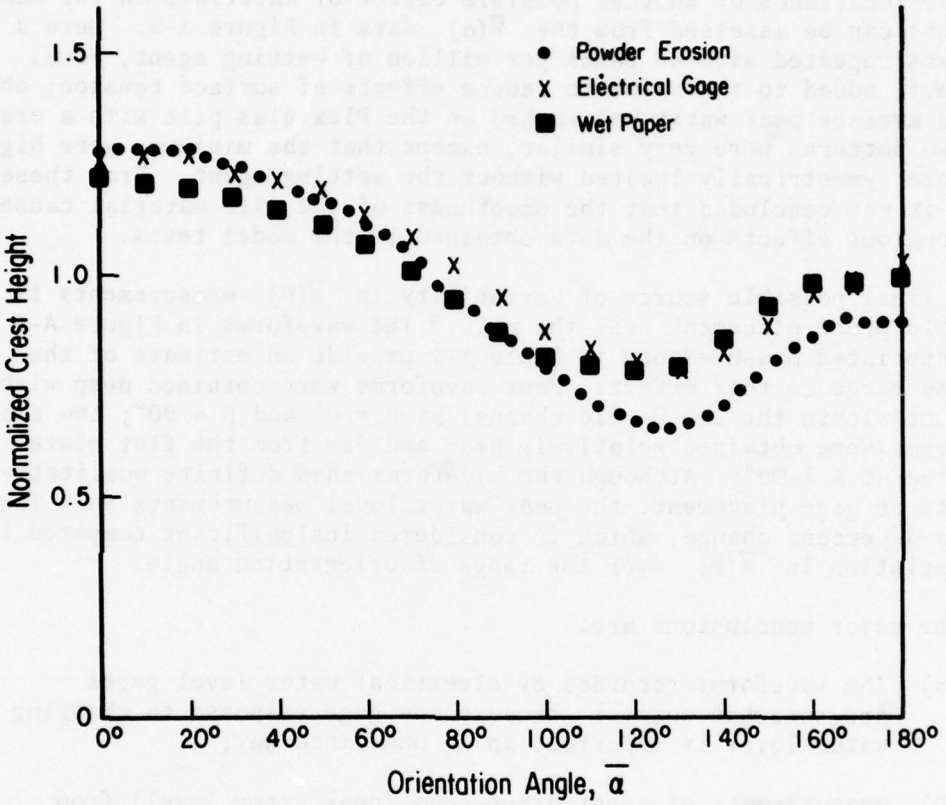

Figure A-4. Peak water level around 3-inch circular pile measured by three techniques. Test conditions: T = 3.10 seconds, E = 4.0 inches, d = 1.00 foot, G = 25 feet.

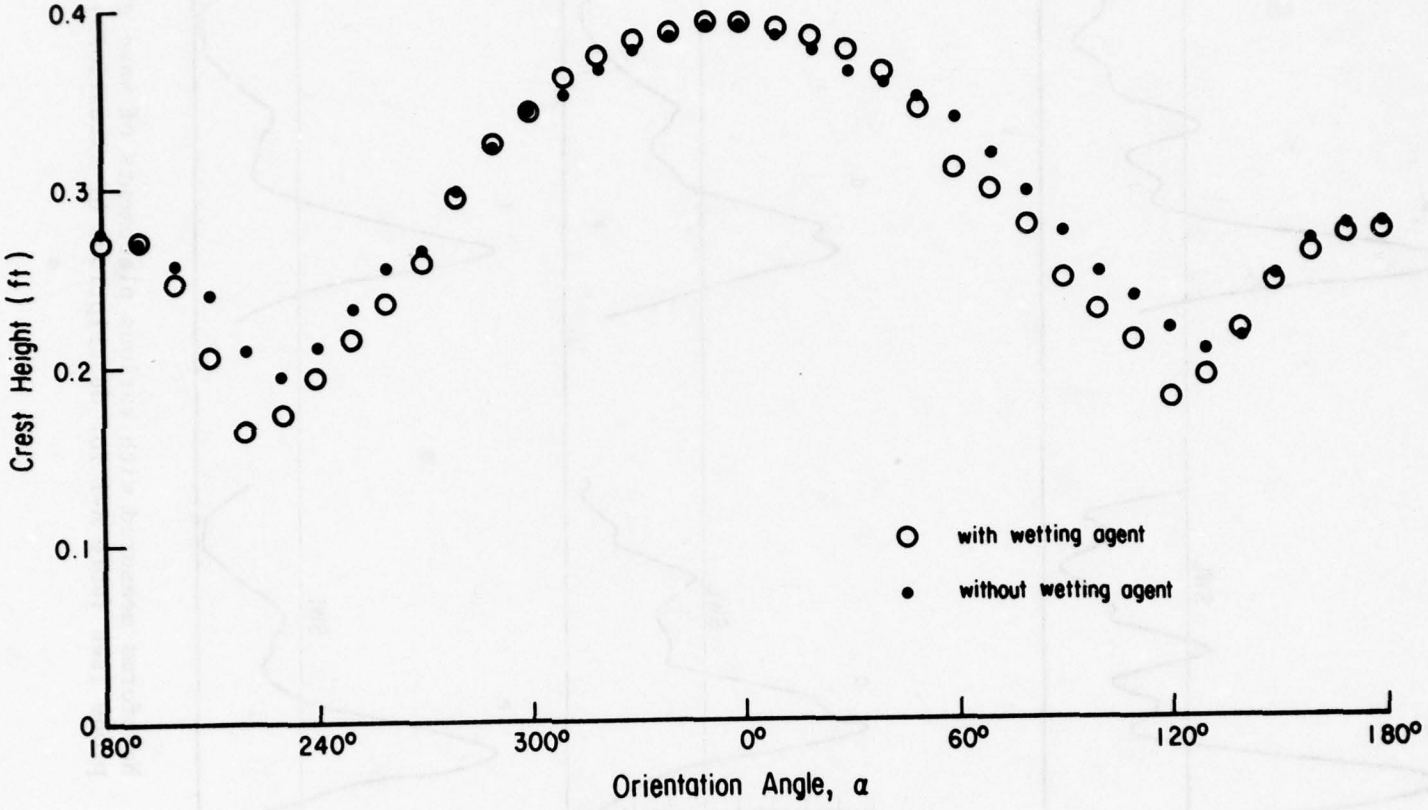

Figure A-5. Effect of wetting agent on observed peak water at 3-inch circular Plexiglas pile. Test conditions: T = 2.32 seconds, d = 1.00 foot, E = 4.0 inches, G = 25 feet.

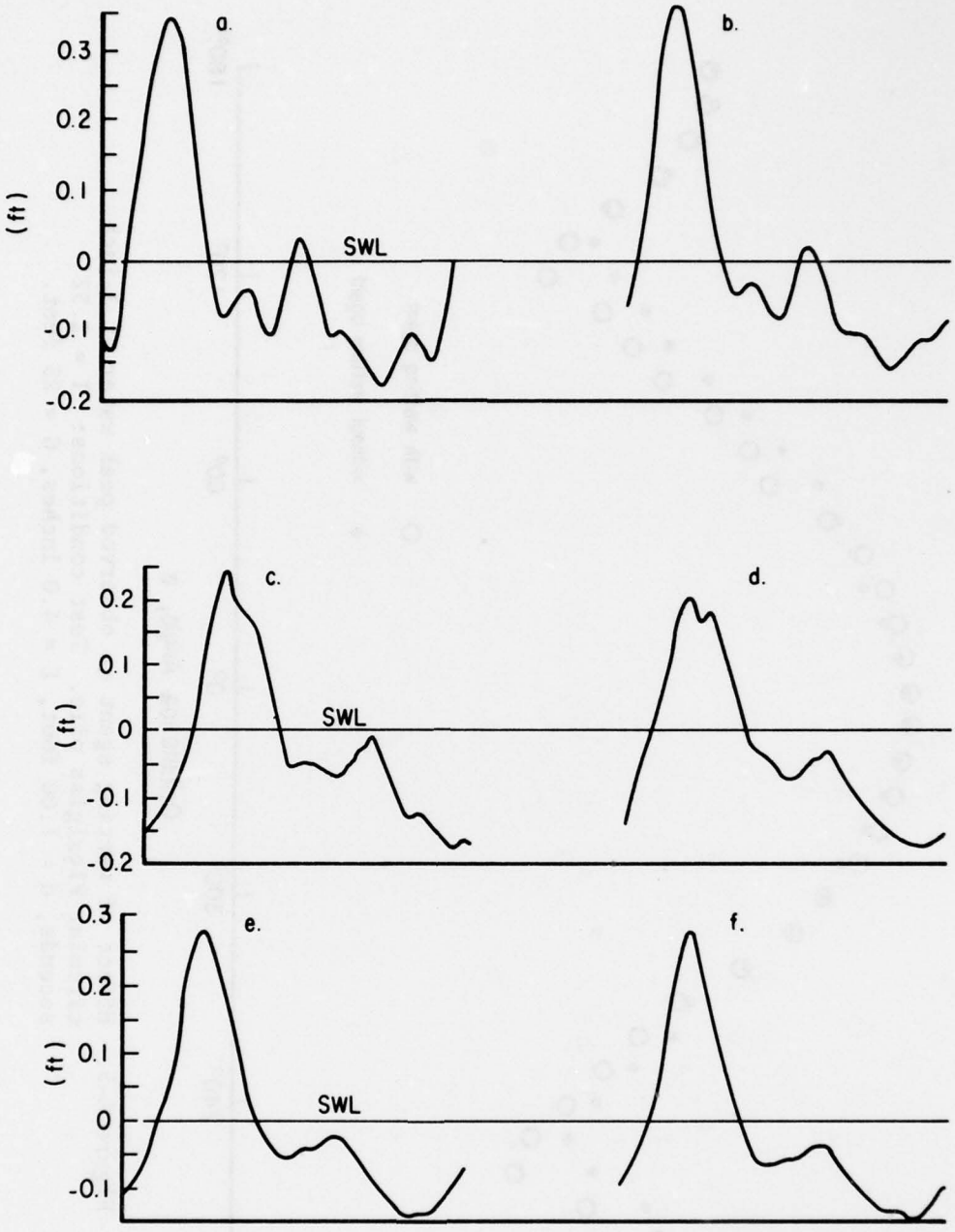

Figure A-6. Waveforms measured with various placements of wave gage probe (see Table A-1 for descriptions of situations).

Table A-1. Probe placement effects on measured wave dimension. Test conditions: T = 2.32 seconds, d = 1.00 foot, E = 4.0 inches, G = 25 feet.[1]

Test situation	Gage location	$\overline{W}(\beta)/\overline{W}$
a. 2x2 H-pile, $\beta = 0°$	Deep within channel	1.26
b. 2x2 H-pile, $\beta = 0°$	Just within channel	1.31
c. 2x2 H-pile, $\beta = 90°$	Deep within channel	0.80
d. 2x2 H-pile, $\beta = 90°$	Just within channel	0.74
e. Flat plate, $\beta = 90°$	0.25 inch from plate	1.03
f. Flat plate, $\beta = 90°$	0.75 inch from plate	1.04

[1]Measurements made using CERC wafer gage (c in Fig. A-2) with resolution of 0.015 W.

APPENDIX B

TEST WAVE CHARACTERISTICS

The following discussion concentrates on wave effects in the 96-foot tank, where most of the reported data were obtained. Regular, high waves were desired for the tests, but the mechanically driven piston generated waves with complicated and variable profiles. Wave variability may be either temporal or spatial. Temporal variability in the wave condition at some point can be caused by irregularities in the generating piston motion over a time large compared to T, or by accumulating reflected wave energy. Figure B-1 shows wave records that should reveal any important temporal variability for a steep wave in the 96-foot tank without a test pile. (The test pile was located near G = 25 feet with the second wave gage close to G = 23 feet in most tests.) There was little change in wave condition when the generator had been running for 1, 5, or 15 minutes, indicating the gently sloping hogshair beach was effectively absorbing incident wave action. Note that the crest height does decrease slightly in time.

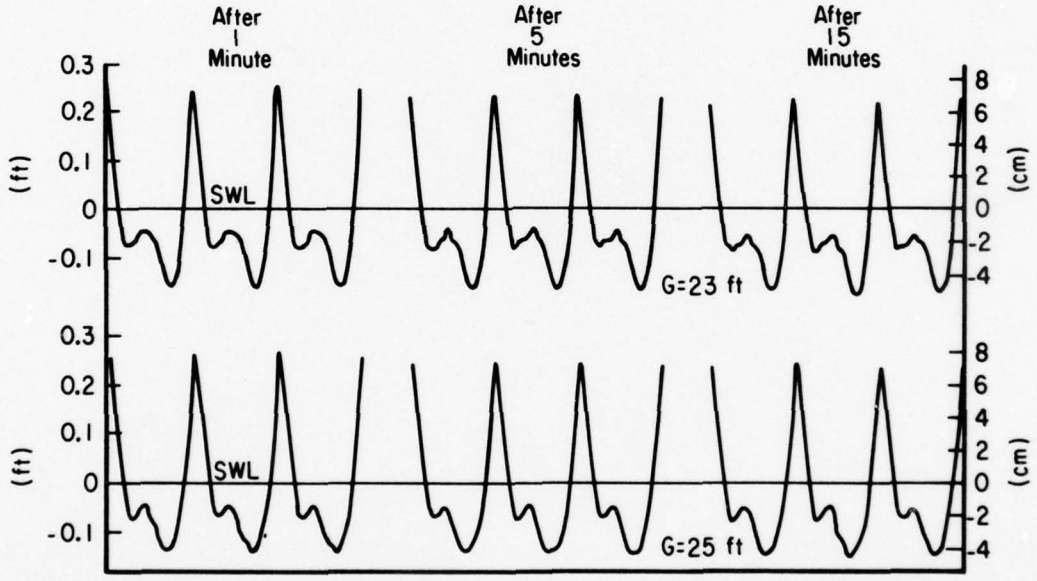

Figure B-1. Changing wave condition in time after start of 96-foot tank generator. Test conditions: T = 2.32 seconds, d = 1.00 foot, E = 4.0 inches.

There was appreciable reflection off some of the larger test piles (e.g., the 3x3 H-pile), which resulted in a slight variation in the incident wave recorded by the second wave gage at various pile orientations. The incident crest height variation approached (0.05 $\overline{W}$), at most, in any reported test; if the gage away from the pile recorded larger

variations in the course of a test, the data set was considered to be of unsatisfactory quality. Variations in $\overline{W}(\alpha)$ or $\overline{W}(\beta)$ over the 360° range of orientation angle were always much larger than the variation in $\overline{W}$. Some tests required 4 hours to obtain a complete data set, but measurements at the beginning and end were usually the same for the same pile orientation. Measurement drift in time was a common problem only with the CERC strip gages (d and e in Fig. A-2); this was evidently due to soaking of the adhesive attaching the strips to the pile face (see Fig. A-3). Thus, temporal wave variability had insignificant effects on the 96-foot tank data.

However, spatial wave variability was marked in the 96-foot tank. Figure B-2 shows the waveform at seven locations along the tank for the highest wave at T = 1.55, 2.32, and 3.10 seconds; measured wave dimensions are listed in Table B-1. In each case, there are notable changes in crest height and curvature and in the secondary details of the waveform; the wave must be regarded as transforming as it propagates in constant water depth. Two possible causes of this are nonlinear wave propagation effects and departures from the ideal in the wave tank (e.g., variations in tank cross section). The 96-foot tank had considerable imperfections but these were not precisely documented. The tank was dismantled after the tests, so this possible cause of spatial wave variability cannot be evaluated.

Figures B-3 to B-6 present waveforms for all the generator settings commonly used in the 96-foot tank tests; measured wave dimensions for Figures B-3, B-4, and B-5 are listed in Tables B-2, B-3, and B-4. Nearly sinusoidal waves of small amplitude and virtually permanent form could be generated; the more complicated waveforms with secondary crests result from nonlinear effects associated with finite wave amplitude. Features of these waveforms agree with the findings of Galvin (1971), except that Figure B-3 shows a secondary crest can exist for d/L = 0.124, which is contrary to his report. However, the secondary soliton (in Galvin's terminology) is very weak, explaining how it could have been overlooked in analyzing motion picture records. Because the generation and propagation of nonlinear shallow-water laboratory waves is a subject of continuing interest, these data will be compared to analyses in available literature.

Madsen (1971) presented a second-order analysis of the waves created by sinusoidally moving piston, in the case of $d/L < 0.1$ and the Stokes parameter, $S = (HL^2/2d^3) < 4\pi^2/3$, where H is the height of the primary generated wave, a Stokes second-order progressive wave at the frequency of the piston motion. His solution predicts observable secondary waves for $S > 2\pi^2/3$, caused by a second harmonic free wave propagating more slowly than the primary wave; the interference between the primary and secondary waves causes an approximately sinusoidal wave height variation away from the generator with a wavelength of L/2. Mei and Unluata (1972) analyzed the resonant interaction between the first and second harmonics off a sinusoidally moving piston in shallow water, finding the harmonics vary periodically in amplitude, with dimensionless beat length, B/L, exhibiting a complicated dependence on S. Their preliminary experimental

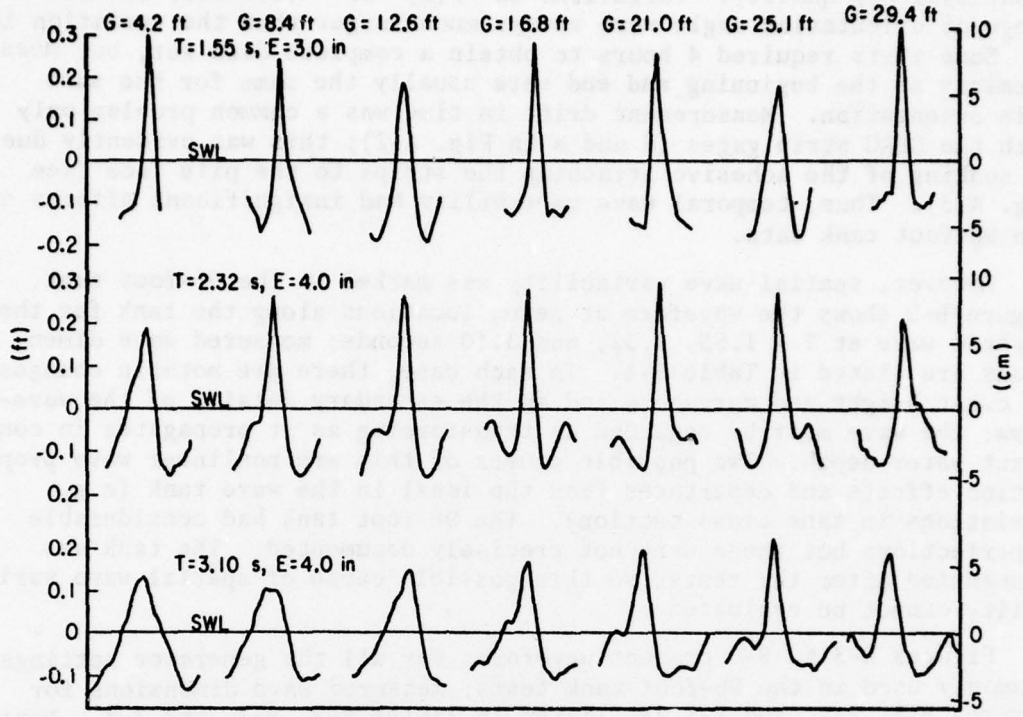

Figure B-2. Waveforms along 96-foot tank for three steep test waves. Stillwater depth = 1.00 foot.

Table B-1. Wave height, H, and crest height, W, of the waveforms shown in Figure B-2.

T = 1.55 s			T = 2.32 s		T = 3.10 s	
G (ft)	H (ft)	W (ft)	H (ft)	W (ft)	H (ft)	W (ft)
4.2	0.46	0.29	0.34	0.19	0.26	0.13
8.4	0.41	0.24	0.43	0.27	0.22	0.11
12.6	0.38	0.19	0.43	0.27	0.27	0.15
16.8	0.41	0.28	0.43	0.29	0.28	0.17
21.0	0.38	0.22	0.44	0.30	0.30	0.20
25.1	0.37	0.18	0.41	0.27	0.32	0.23
29.4	0.43	0.31	0.34	0.21	0.29	0.19

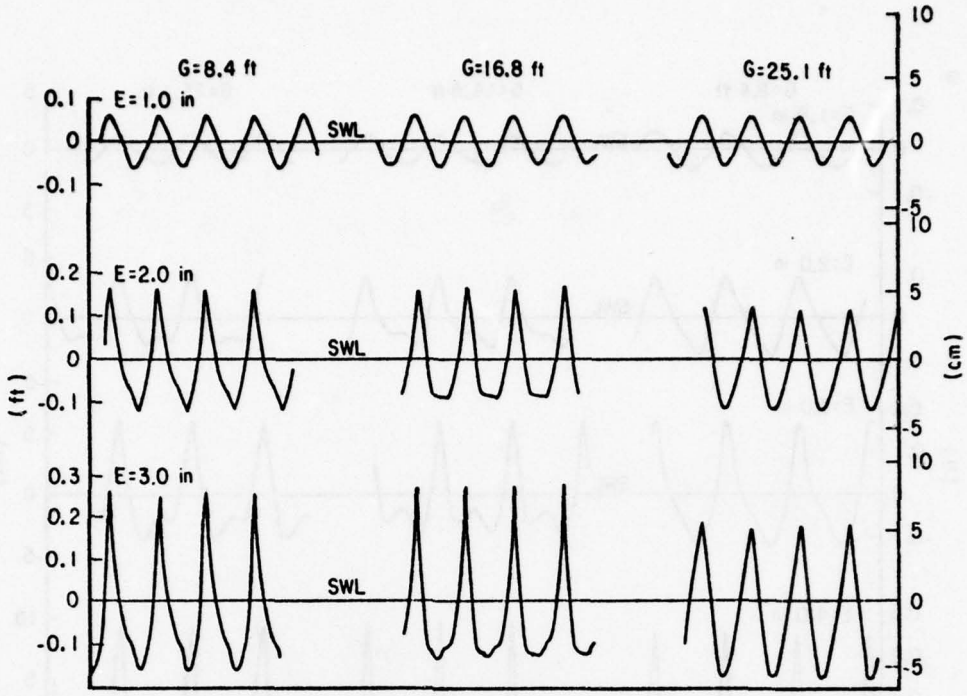

Figure B-3. T = 1.55-second test waves in 96-foot tank. Stillwater depth = 1.00 foot.

Table B-2. Wave height, H, and crest height, W, of the waveforms shown in Figure B-3 (T = 1.55 s, d = 1.00 ft).

Wavemaker eccentric, E (in)	G = 8.4 ft		G = 16.8 ft		G = 25.1 ft	
	H (ft)	W (ft)	H (ft)	W (ft)	H (ft)	W (ft)
1.0	0.125	0.066	0.118	0.065	0.115	0.064
2.0	0.285	0.168	0.256	0.168	0.240	0.120
3.0	0.426	0.259	0.406	0.276	0.362	0.178

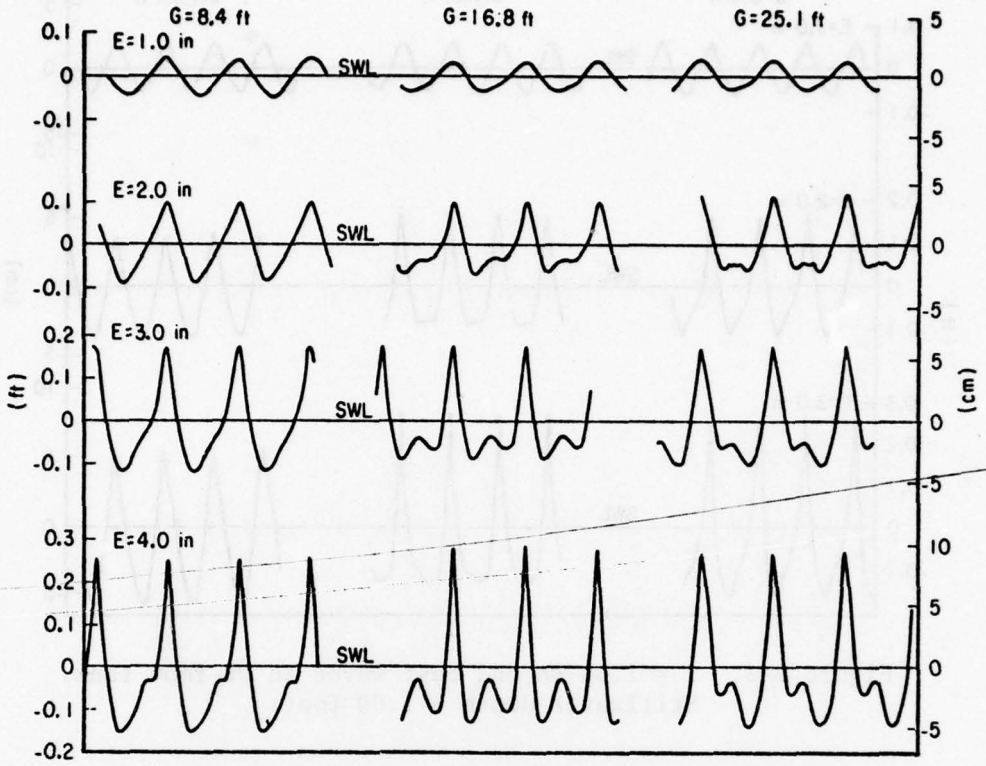

Figure B-4. T = 2.32-second test waves in 96-foot tank. Stillwater depth = 1.00 foot.

Table B-3. Wave height, H, and crest height, W, of the waveforms shown in Figure B-4 (T = 2.32 s, d = 1.00 ft).

Wavemaker eccentric, E (in)	G = 8.4 ft		G = 16.8 ft		G = 25.1 ft	
	H (ft)	W (ft)	H (ft)	W (ft)	H (ft)	W (ft)
1.0	0.092	0.045	0.071	0.036	0.083	0.050
2.0	0.195	0.105	0.170	0.104	0.181	0.119
3.0	0.303	0.180	0.273	0.183	0.285	0.183
4.0	0.427	0.266	0.430	0.290	0.417	0.275

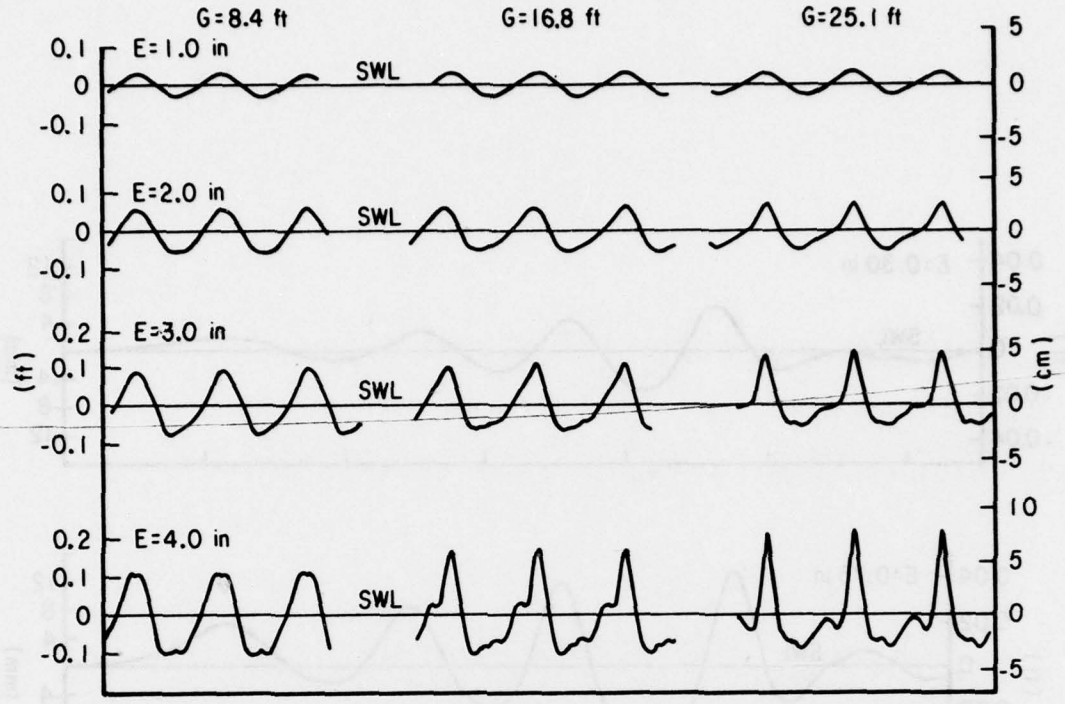

Figure B-5. T = 3.10-second test waves in 96-foot tank. Stillwater depth = 1.00 foot.

Table B-4. Wave height, H, and crest height, W, of the waveforms shown in Figure B-5 (T = 3.10 s, d = 1.00 ft).

Wavemaker eccentric, E (in)	G = 8.4 ft		G = 16.8 ft		G = 25.1 ft	
	H (ft)	W (ft)	H (ft)	W (ft)	H (ft)	W (ft)
1.0	0.058	0.026	0.059	0.029	0.064	0.035
2.0	0.113	0.056	0.114	0.060	0.131	0.078
3.0	0.176	0.098	0.191	0.117	0.208	0.146
4.0	0.222	0.114	0.285	0.180	0.311	0.216

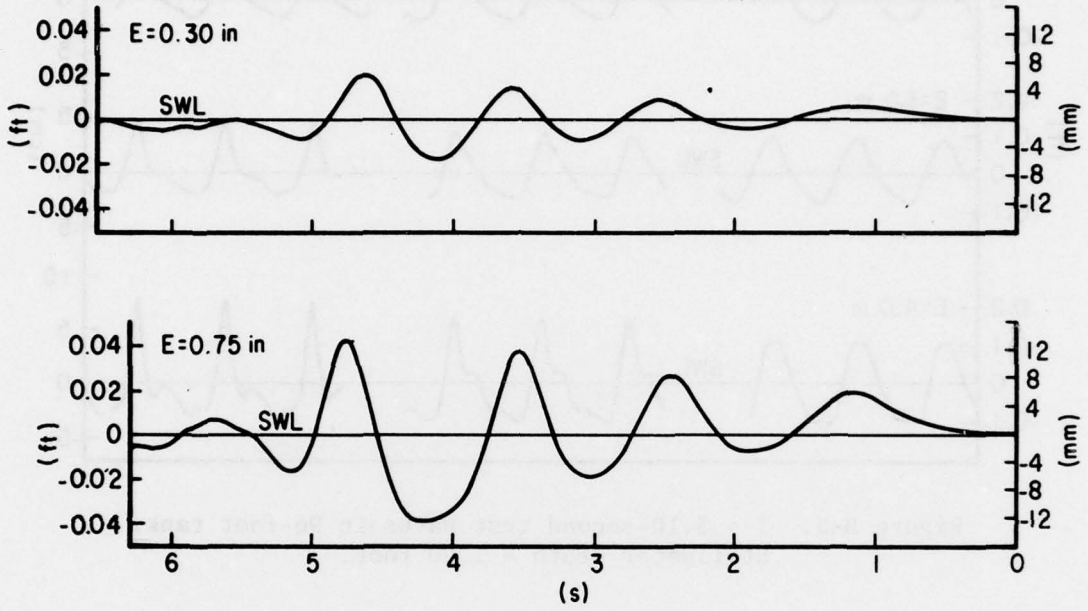

Figure B-6. Typical wave pulses used in 96-foot tank tests (with 6-inch-diameter pile). T = 1.00 second, d = 0.35 foot, G = 24.2 feet.

results showed general agreement with the theoretical expressions for the beat length and the second harmonic amplitude.

The present data support these analyses to some extent. Secondary crests are apparent when S is greater than about 10, although the critical value evidently depends slightly on d/L, for $0.05 < d/L < 0.13$. When a secondary crest is located halfway between the primary crests, the primary crest is higher and sharper, confirming that the primary and second harmonic waves are in phase there. However, the waveforms for various H at the same (L,d) combination (Figs. B-3, B-4, and B-5) fail to indicate a definite dependence of B/L on S. The waveform exhibits a more complicated fine structure as H increases, but there is no change in location of the secondary features and thus no change in the beat length. Table B-5 gives the beat length between locations of constructive interference shown in the three steep propagating waveforms presented in Figure B-2. The estimated beat length is approximately 3L/2, three times the prediction of Madsen (1971); however, these estimates are somewhat qualitative and pertain to situations more highly nonlinear than the stated range of validity of Madsen's analysis. There may be a slight decrease in beat length with increasing S, as Mei and Unluata (1972) predicted.

Table B-5. Beat lengths between primary and second harmonics for three steep test waves in 96-foot tank (estimated from Fig. B-2).

Wave period, T (s)	Dimensionless water depth, d/L	Dimensionless Stokes parameter, $HL^2/2d^3$	Dimensionless beat length, B/L
1.55	0.124	14	1.7
2.32	0.079	35	1.5
3.10	0.057	45	1.4

Several other nonlinear wave effects were observed in the 96-foot tank tests, although no quantitative data are available. After a steep crest passed a test pile, capillary waves were often radiated outward from the front half of the pile. Theoretical treatments by Longuet-Higgins (1963) and by Crapper (1970) have shown these waves can be generated where surface tension forces are accentuated due to a sharply curved free surface. The blockage of the propagating waveform at the pile causes an increased surface curvature. The resulting capillary waves are visible in some photos in Section II.

There was also some flow along steep crests in the 96-foot tank. A slight lump on the crest was observed to bounce from one side of the tank to the other as the crest propagated toward the beach. This lateral flow was apparently neither the transverse wave described by Madsen (1974) nor

the cross wave described by Mahoney (1972). Experiments by Barnard and Pritchard (1972) confirmed that a wavemaker moving at frequency ω, exciting a plane progressive wave train with wavelength L, may also generate a standing cross-wave field with frequency $\omega/2$ as a result of nonlinear resonance, if the tank width is greater than L. Madsen (1974) experimentally confirmed the possible occurrence of a standing transverse wave at the frequency of the generator motion if the tank width is greater than L/2. The tank width was never as large as L/2 in the 96-foot tank tests, and the lateral flow was observed with $b < (0.1)L$. The observed flow may have been due to a slight side motion of the somewhat loose-fitting, generating piston, or to the departures of the tank from a constant rectangular cross section. Because a slight leakage around the wavemaker can measurably affect generated wave height (Madsen, 1970), an asymmetric leakage could cause a significant initial variation in H across the tank. This, in turn, could cause an important lateral flow close to the generator. $W(\alpha)$ patterns markedly skewed about $\alpha = 0°$ were often recorded at G = 8.6 feet (see Fig. 24), while measurements at G = 25 feet gave patterns that were less skewed, but definitely not symmetric about $\alpha = 0°$ (James and Hallermeier, 1976).

Figure B-7 shows typical waveforms in the 85-foot tank tests; measured wave dimensions are listed in Table B-6. The short, steep beach in this tank was highly reflective in certain situations, resulting in marked wave variability both along and across the tank. Figure B-8 shows significant wave variability in the 85-foot tank. At T = 3.55 seconds, d = 2.33 feet, E = 2.5 inches (6.3 centimeters), and G ≃ 19 feet (5.7 meters), the wave action is distinctly different at the incident gage and the test pile locations, although they are separated by only 4.2 feet (1.3 meters) (Fig. 1). With this wave condition, the tank width is about half the wavelength, so this variability might be associated with the standing wave described by Madsen (1974). Other data obtained in the 85-foot tank was marred by an undesirable test situation. At T = 3.55 seconds, with the test pile at G ≃ 30 feet (9.1 meters), the pile was one wavelength from the generator and from the beach toe, so the incident and reflected waves superposed in phase. However, data of certain value were always obtained with wave pulses in the 85-foot tank. From certain other test data for the same tank, it was established that scale effects do not affect the conclusions about wave transformation from these model tests (see Sec. III).

In summary, the complicated nonlinear behavior of the test waves in the 96-foot tank should have had little effect on the conclusions presented in this report, since the transformation in space is not marked over a distance on the order of the pile cross-sectional dimension. The flow at any wave phase is approximately unidirectional for the thin test piles, and the waves may be regarded as having a permanent form locally. The crest height is the important characteristic of the waveform since it defines the peak horizontal flow velocity causing the peak water at the pile. Because the crest height varies as the wave propagates, this normalizing factor must be carefully selected for each test situation. The waveform features are of secondary importance to the present study, although the crest curvature in space must influence the accuracy of the unidirectional flow approximation.

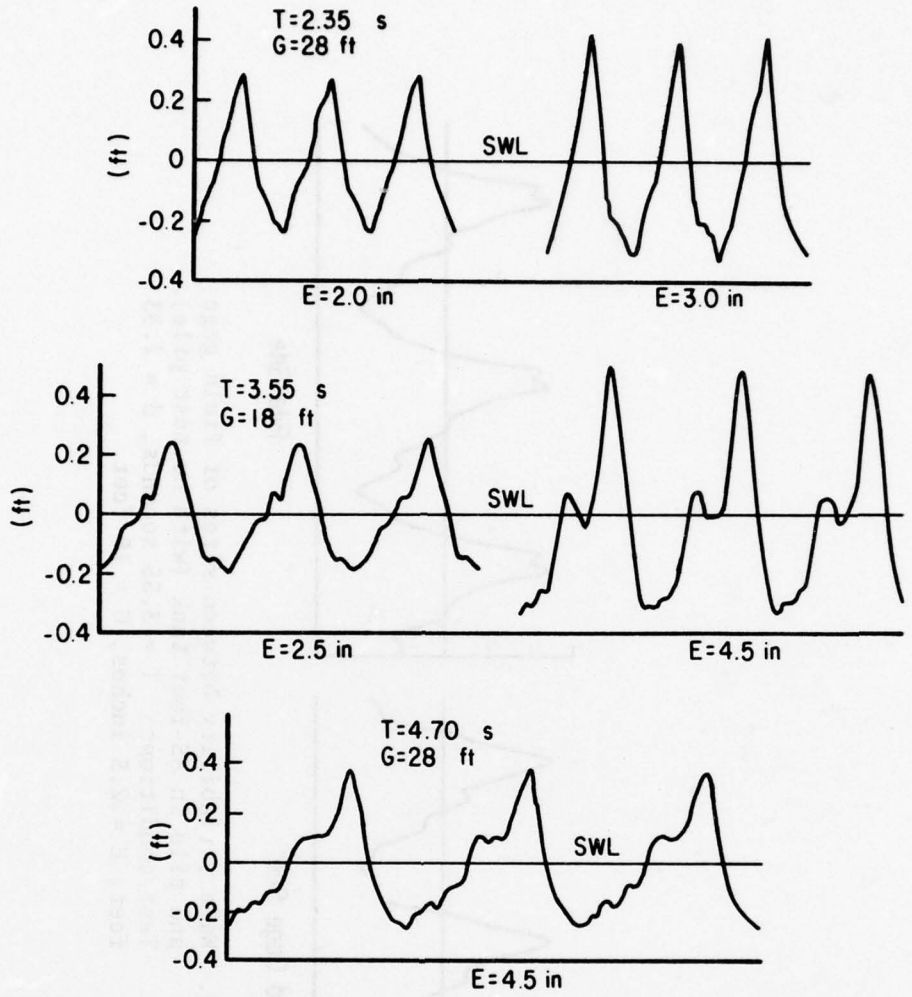

Figure B-7. Waveforms for five typical test waves at field gage in 85-foot tank. Stillwater depth = 2.33 feet.

Table B-6. Wave height, H, and crest height, W, of the waveforms shown in Figure B-7.

Test condition				
T (s)	E (in)	G (ft)	H (ft)	W (ft)
2.35	2.0	28	0.52	0.28
2.35	3.0	28	0.76	0.44
3.55	2.5	18	0.45	0.25
3.55	4.5	18	0.82	0.49
4.70	4.5	28	0.63	0.37

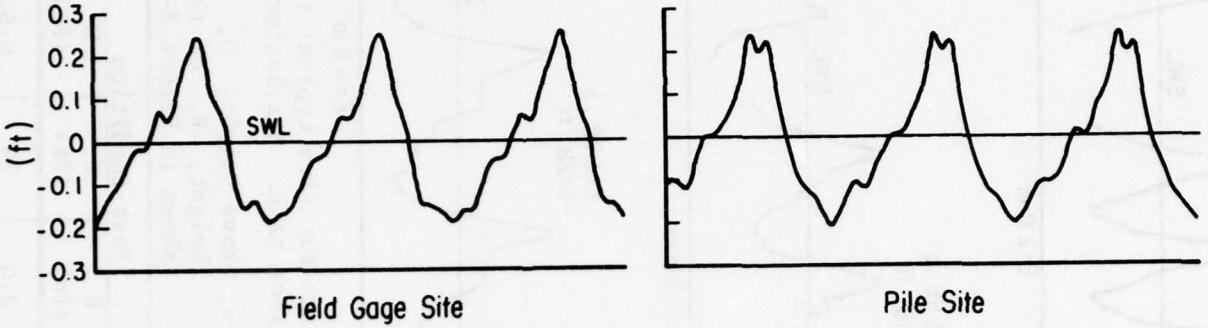

Figure B-8. Wave variability between sites of field gage and pile in 85-foot tank (with no test pile). Test conditions: T = 3.55 seconds, d = 2.33 feet, E = 2.5 inches, G ≈ 19 feet.

APPENDIX C

PEAK WATER DATA FOR SINGLE PILES IN SINGLE WAVE TRAIN

This appendix includes 73 rectilinear plots obtained from a simple computer program. The plots show 148 data sets of measured peak water versus pile orientation with respect to wave direction, with peak water normalized by the incident crest height. The original test records yielded incident crest height and peak water level (at each pile orientation angle), both measured above the SWL.

The plots include all data sets surviving a check of internal consistency of the test record. This check ensured that the strip-chart record of the incident wave did not display "excessive" change in SWL or wave height during the test. Typically, the sensitivity of the electrical gage was such that incident wave height was recorded at about 35 to 40 lines of the 50 lines on the strip chart. For convenience, an excessive change in height or SWL was defined as two or more lines; changes greater than this complicate the reduction of the test record and the production of accurate normalized plots. This check resulted in the deletion of a large number of data sets obtained in the 85-foot tank.

Some of the remaining data displayed nonclosure of the peak water pattern. Measurements at the same β at the beginning and end of a test were sometimes appreciably different. Tests were begun at $\beta = 0°$ or at $\beta = 90°$, and successive measurements were made at increasing β. Nonclosure was indicated as a jump in measurements near this starting angle, and was apparently due to residual wetting of the wafer electrical gage regularly used at the pile.

Some data sets for circular piles showed all normalized peak water measurements below 1.0. This occurred only for wetted paper or powder erosion records with small incident wave height, and was probably caused by a slight error in marking the SWL when the record was made.

On the following plots, individual tests are identified by a six-digit alphanumeric code. The first letter is G, W, or E, indicating electrical gage, wetted paper, or powder erosion record of peak water, respectively; tests with a leading E are one-wave records. The second letter is A if the test was done in the 96-foot tank, and B if the test was done in the 85-foot tank. The third character is the last number of the year, between 1970 and 1973, when the test was performed. The final three numbers indicate separate tests done in a certain year.

Each following plot shows only data for a certain pile with certain wave period and water depth.

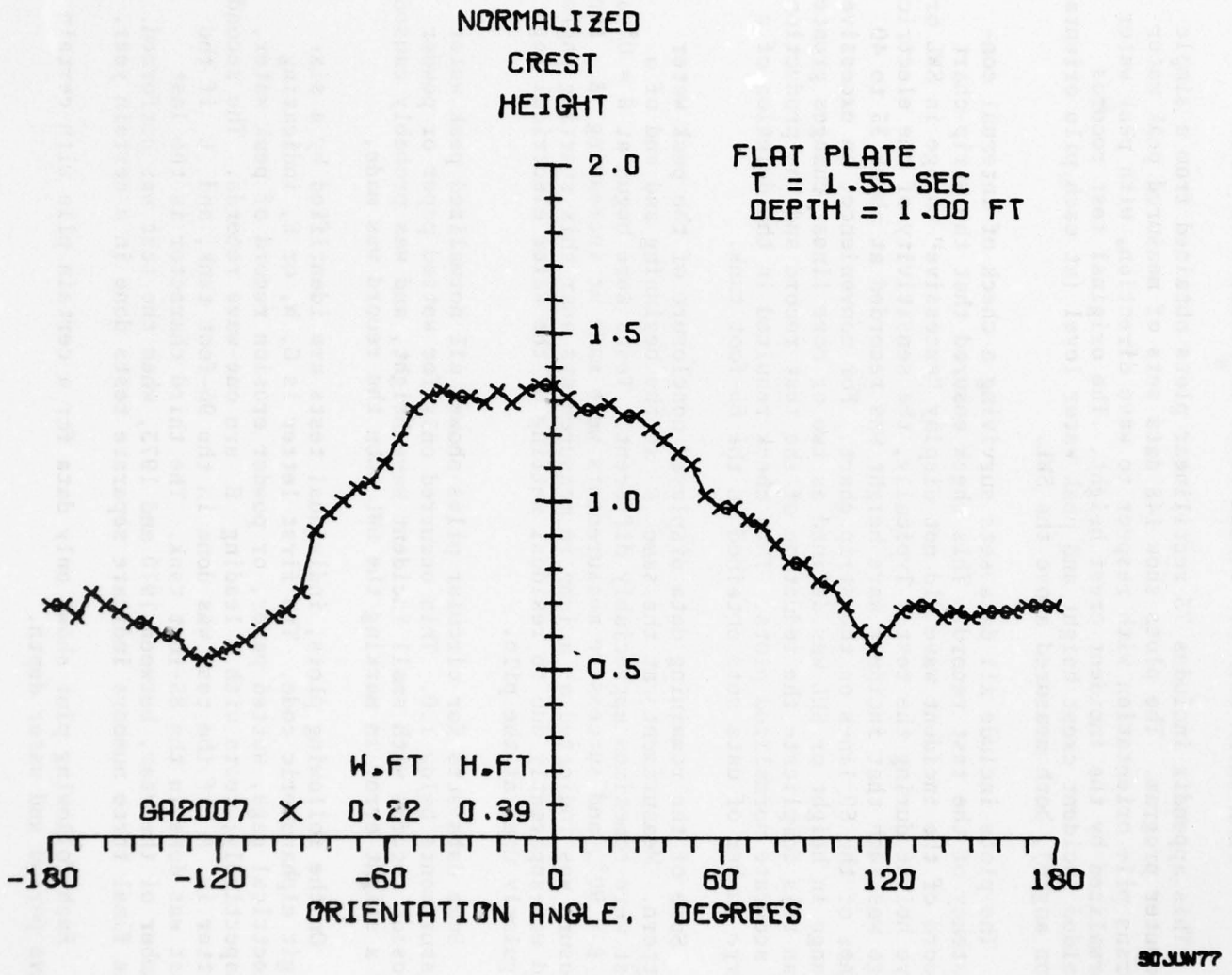
NORMALIZED
CREST
HEIGHT
FLAT PLATE
T = 1.55 SEC
DEPTH = 1.00 FT
2.0
1.5
1.0
0.5
W,FT H,FT
GA2007 X 0.22 0.39
-180
-120
-60
0
60
120
180
ORIENTATION ANGLE, DEGREES
30JUN77

AD-A055 409 COASTAL ENGINEERING RESEARCH CENTER FORT BELVOIR VA F/G 8/3
WAVE TRANSFORMATION AT ISOLATED VERTICAL PILES IN SHALLOW WATER--ETC(U)
MAR 78 R J HALLERMEIR, R E RAY

UNCLASSIFIED CERC-TP-78-1 NL

2 OF 2
AD
A055409

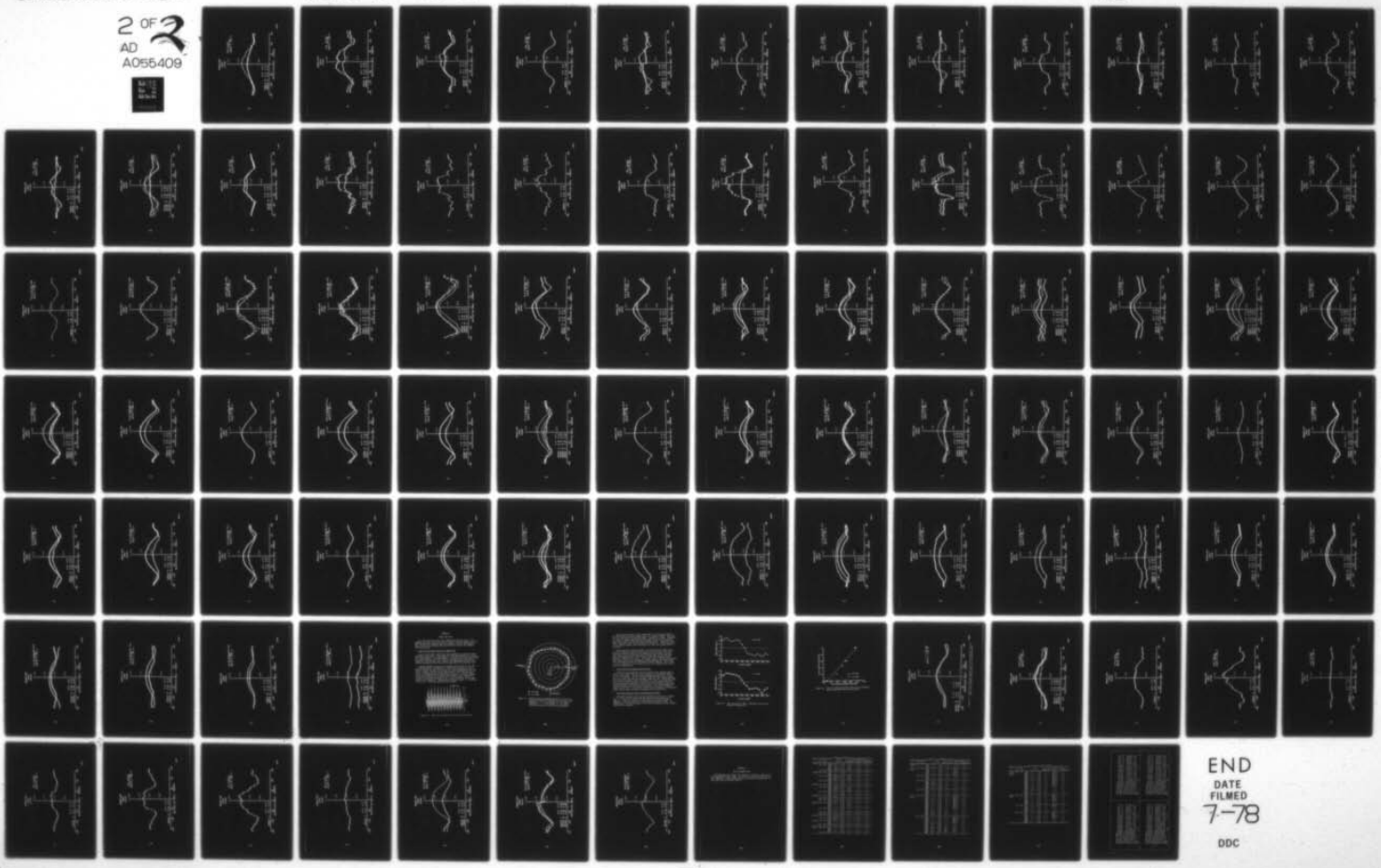

END
DATE
FILMED
7-78
DDC

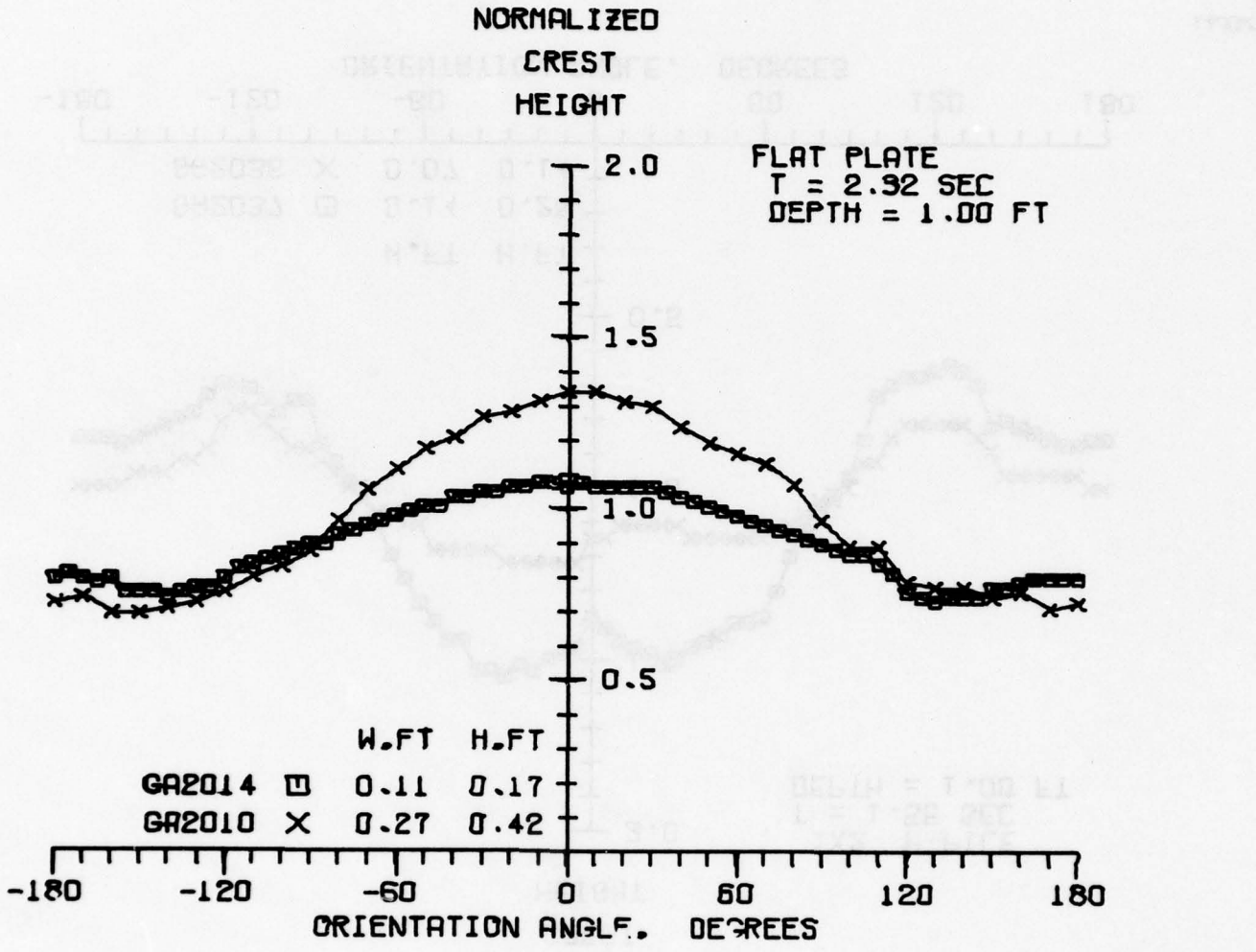
NORMALIZED
CREST
HEIGHT
FLAT PLATE
T = 2.32 SEC
DEPTH = 1.00 FT
2.0
1.5
1.0
0.5
W.FT H.FT
GA2014 0.11 0.17
GA2010 0.27 0.42
-180
-120
-60
0
60
120
180
ORIENTATION ANGLE, DEGREES
30JUN77

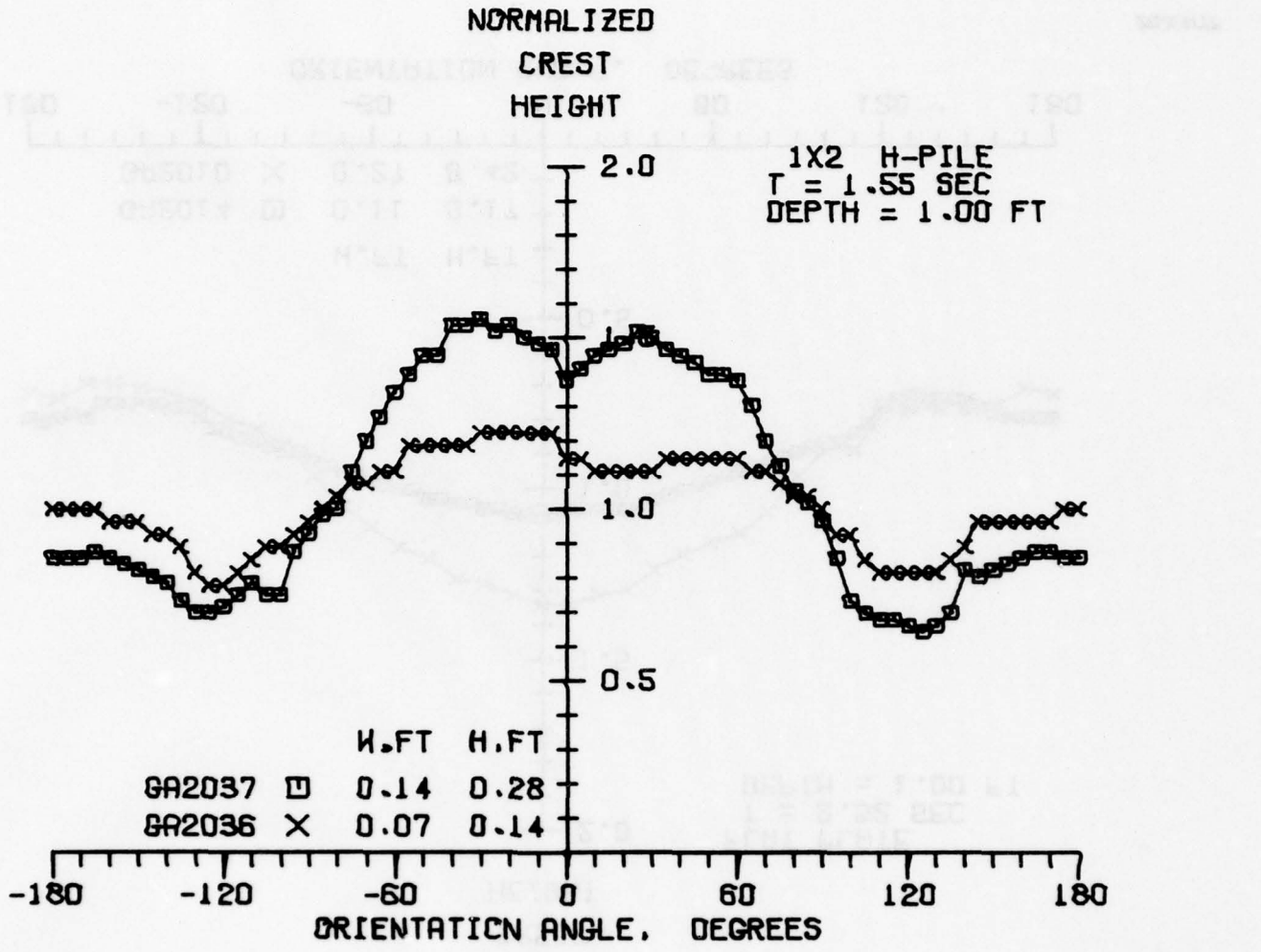
NORMALIZED
CREST
HEIGHT
1X2 H-PILE
T = 1.55 SEC
DEPTH = 1.00 FT
2.0
1.0
0.5
H,FT H,FT
GA2037 0.14 0.28
GA2036 0.07 0.14
-180
-120
-60
0
60
120
180
ORIENTATICN ANGLE, DEGREES
14JUN77

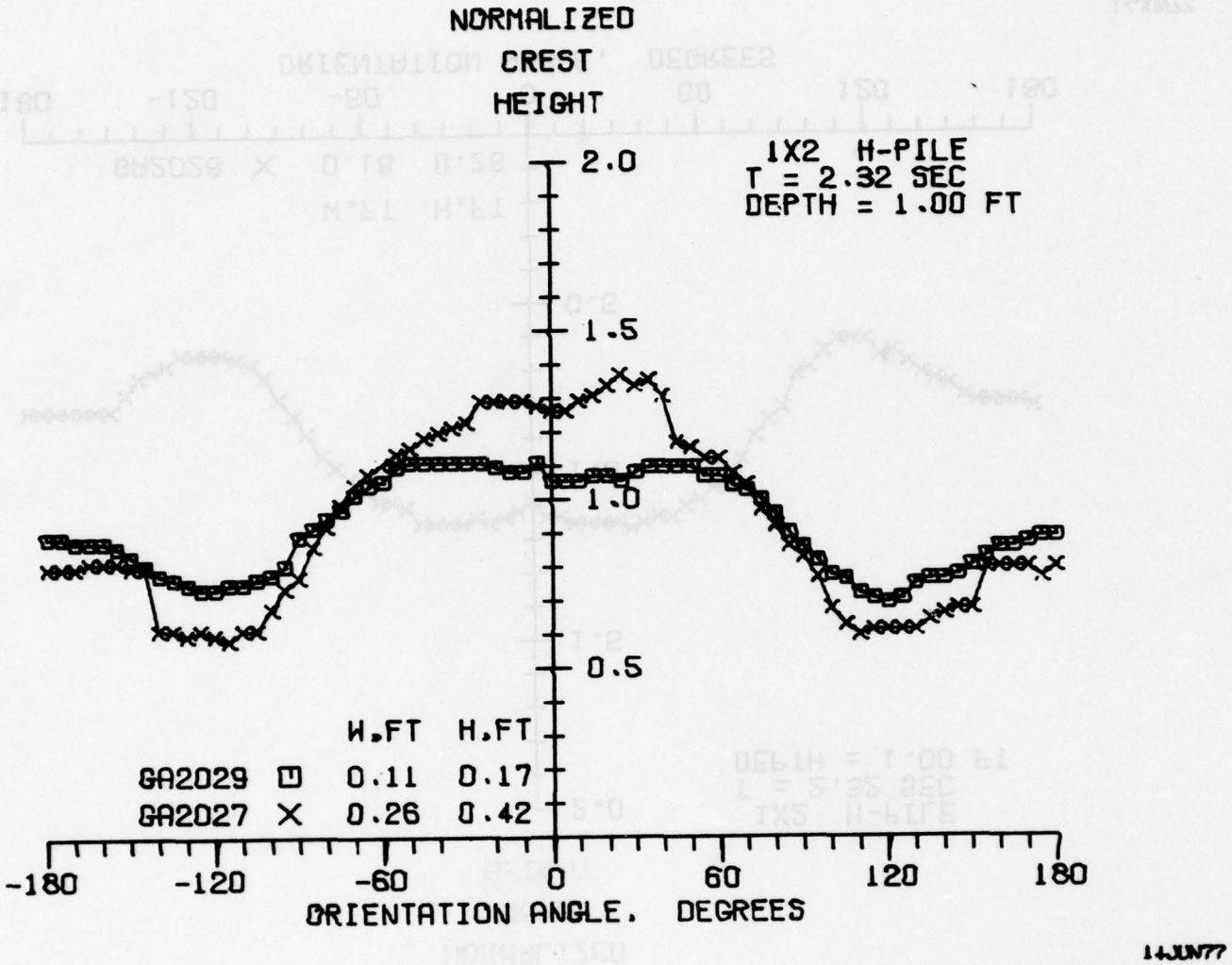
NORMALIZED
CREST
HEIGHT
1X2 H-PILE
T = 2.32 SEC
DEPTH = 1.00 FT
2.0
1.5
1.0
0.5
W.FT H.FT
GA2029 □ 0.11 0.17
GA2027 X 0.26 0.42
-180
-120
-60
0
60
120
180
ORIENTATION ANGLE. DEGREES
14JUN77

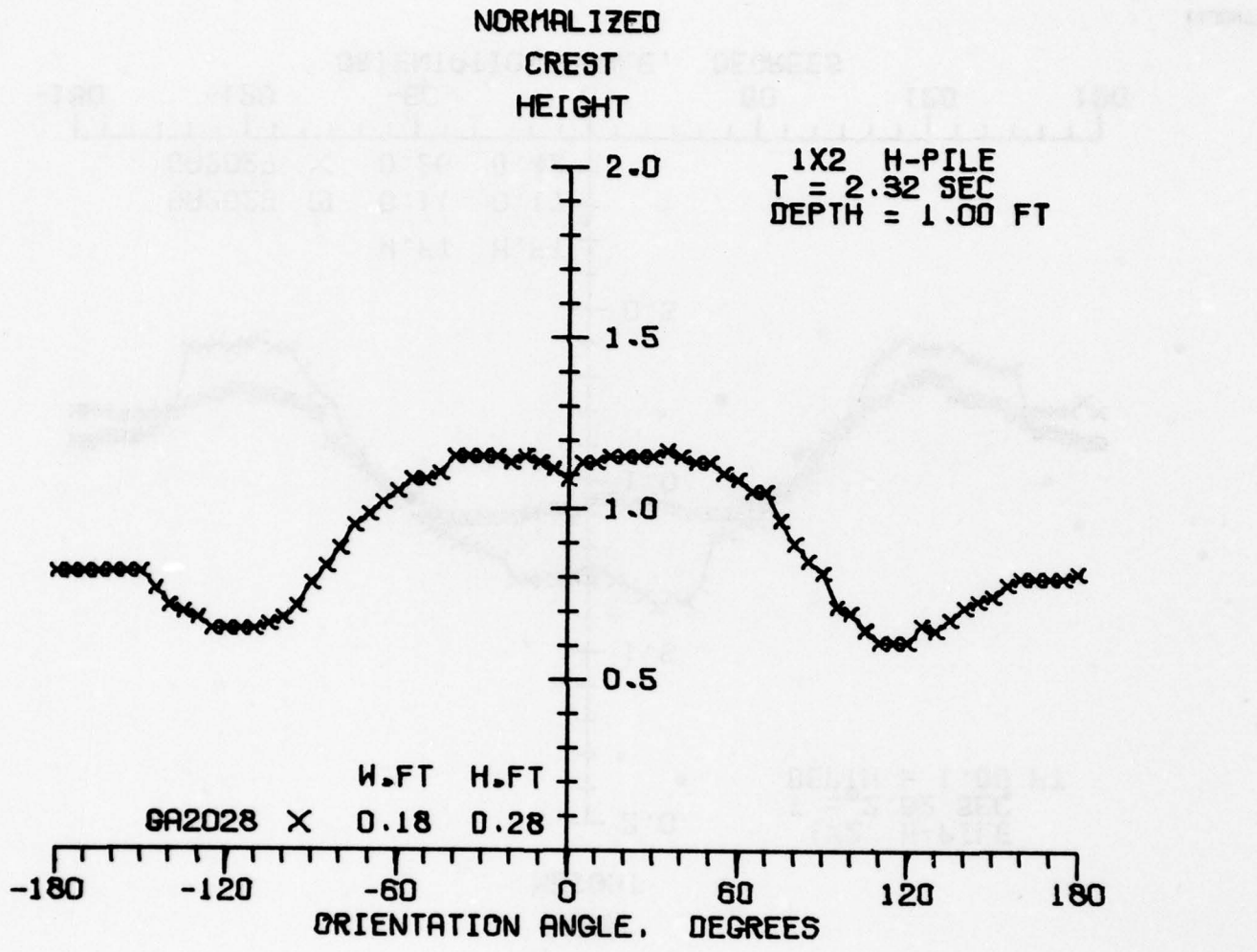
NORMALIZED
CREST
HEIGHT
1X2 H-PILE
T = 2.32 SEC
DEPTH = 1.00 FT
2.0
1.5
1.0
0.5
W,FT H,FT
GA2028 X 0.18 0.28
-180
-120
-60
0
60
120
180
ORIENTATION ANGLE, DEGREES
14JUN77

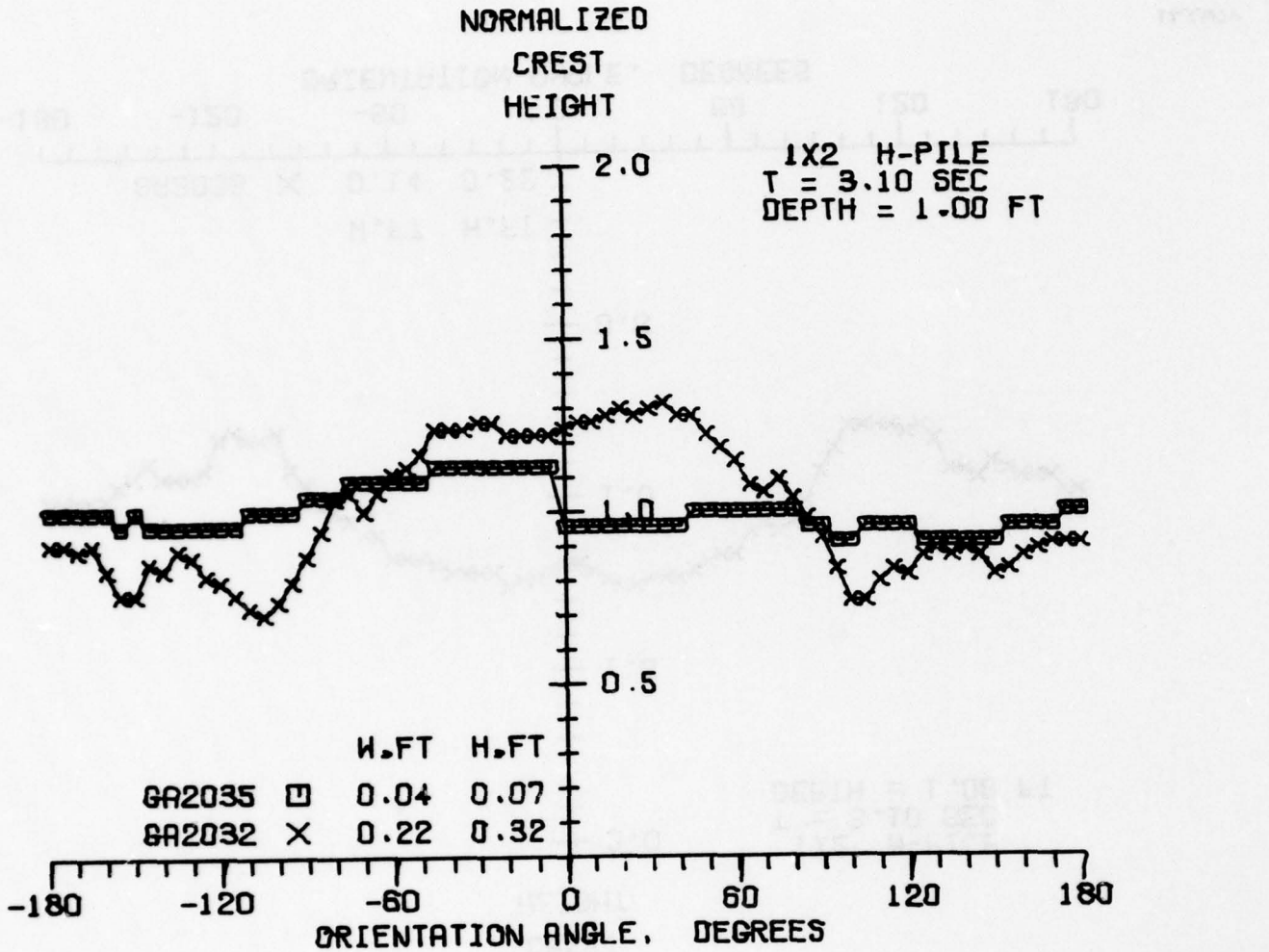
NORMALIZED
CREST
HEIGHT
1X2 H-PILE
T = 3.10 SEC
DEPTH = 1.00 FT
2.0
1.5
1.0
0.5
H,FT H,FT
GA2035 0.04 0.07
GA2032 0.22 0.32
-180
-120
-60
0
60
120
180
ORIENTATION ANGLE, DEGREES
14JUN77

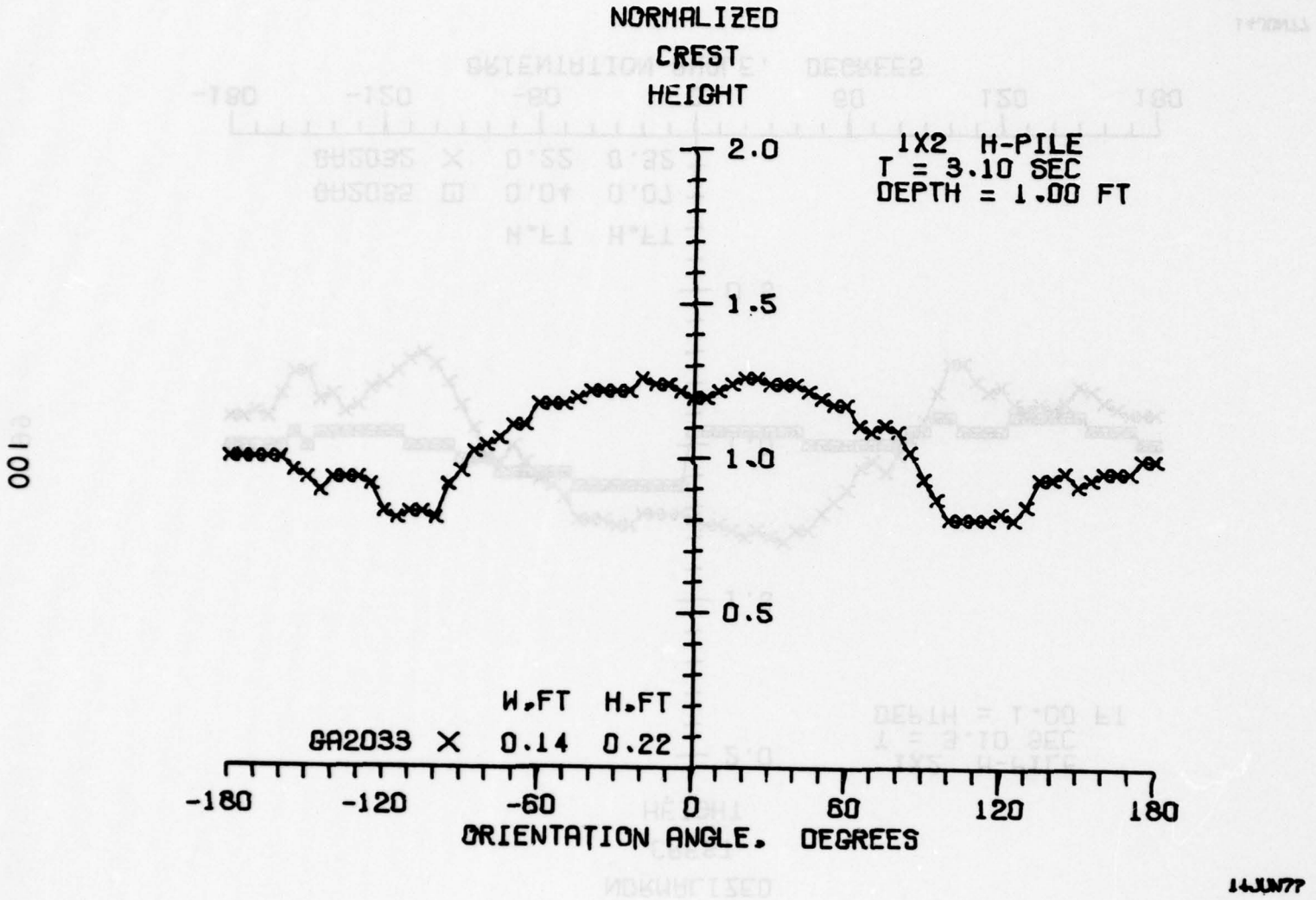
NORMALIZED
CREST
HEIGHT
1X2 H-PILE
T = 3.10 SEC
DEPTH = 1.00 FT
2.0
1.5
1.0
0.5
W,FT H,FT
GA2033 X 0.14 0.22
-180
-120
-60
0
60
120
180
ORIENTATION ANGLE, DEGREES
14JUN77

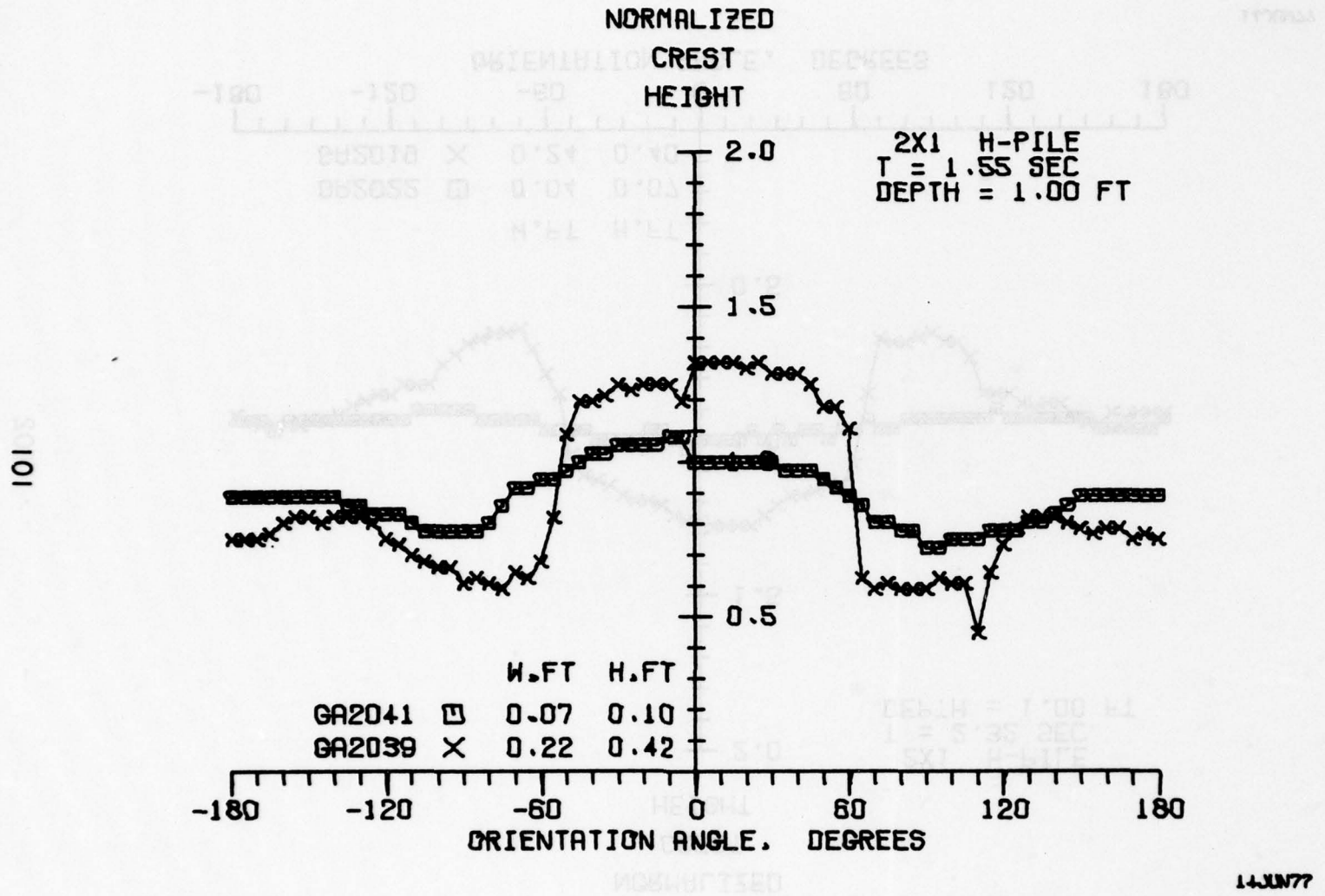
NORMALIZED
CREST
HEIGHT
2X1 H-PILE
T = 1.55 SEC
DEPTH = 1.00 FT
2.0
1.5
0.5
W.FT H.FT
GA2041 0.07 0.10
GA2039 0.22 0.42
-180
-120
-60
0
60
120
180
ORIENTATION ANGLE. DEGREES
14JUN77

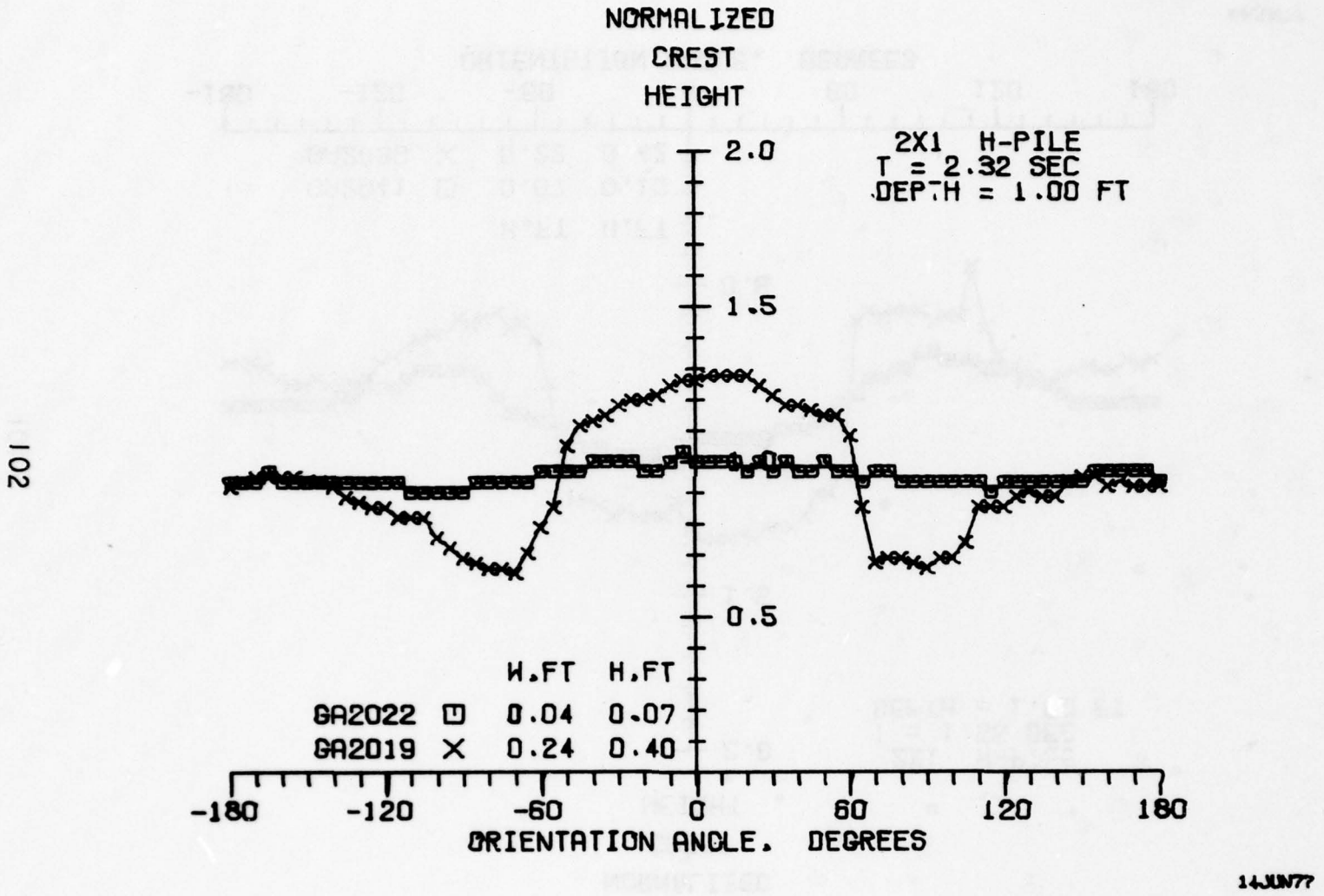
NORMALIZED
CREST
HEIGHT
2X1 H-PILE
T = 2.32 SEC
DEPTH = 1.00 FT
2.0
1.5
0.5
H,FT H,FT
GA2022 0.04 0.07
GA2019 0.24 0.40
-180
-120
-60
0
60
120
180
ORIENTATION ANGLE, DEGREES
14JUN77

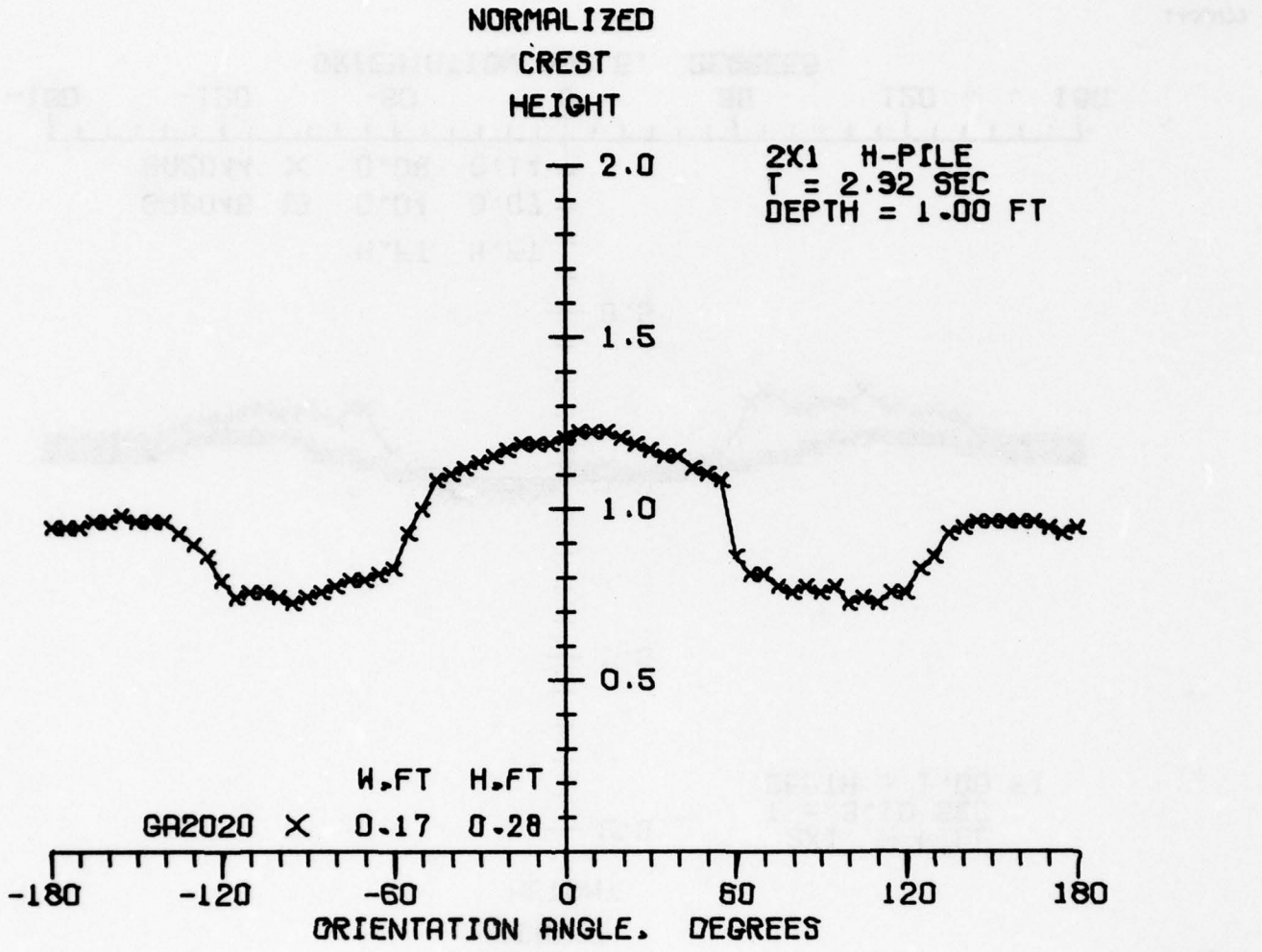
NORMALIZED
CREST
HEIGHT
2X1 H-PILE
T = 2.32 SEC
DEPTH = 1.00 FT
2.0
1.5
1.0
0.5
W.FT H.FT
GA2020 X 0.17 0.28
-180
-120
-60
0
60
120
180
ORIENTATION ANGLE. DEGREES
30JUN77

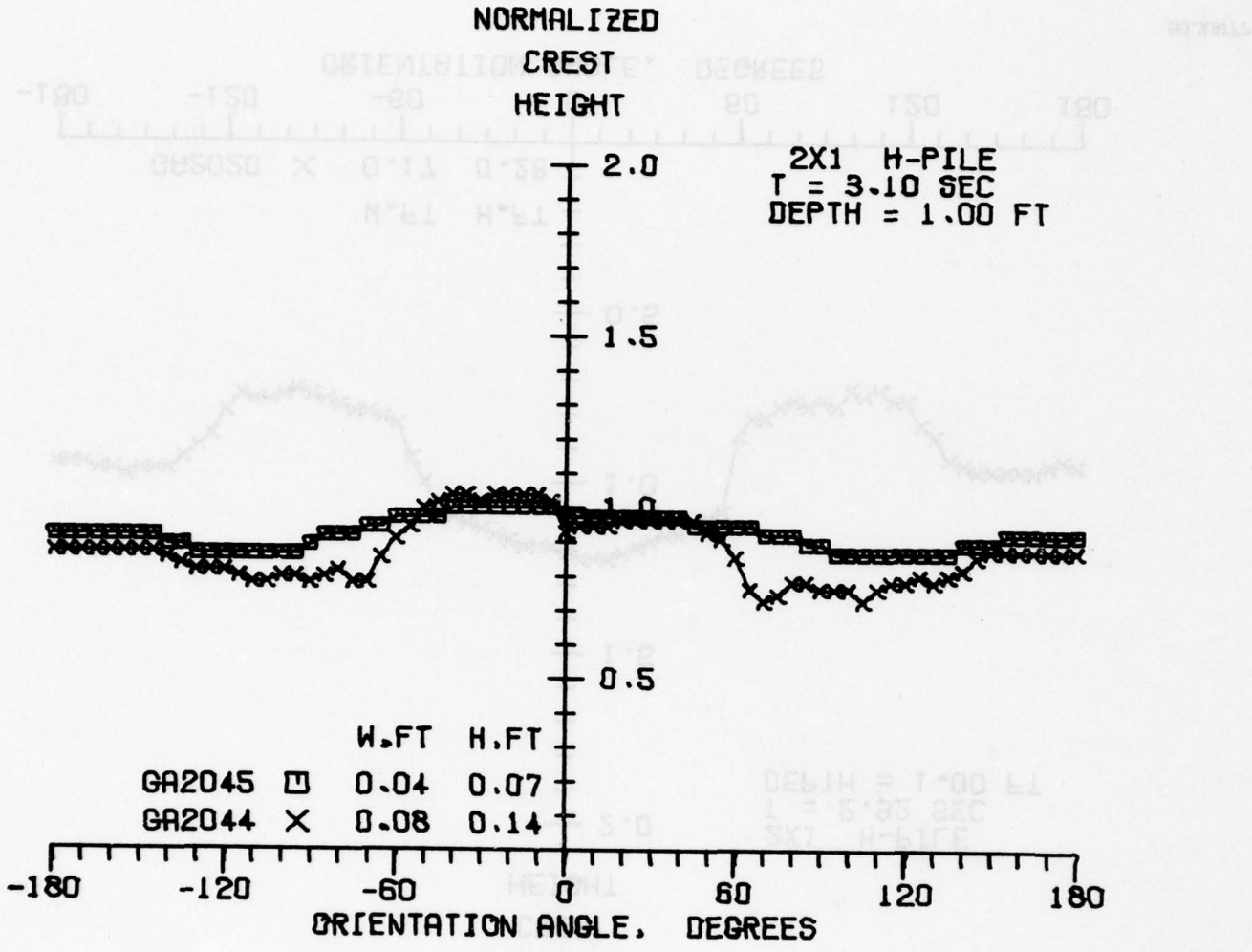
NORMALIZED
CREST
HEIGHT
2X1 H-PILE
T = 3.10 SEC
DEPTH = 1.00 FT
2.0
1.5
1.0
0.5
W,FT H,FT
GA2045 0.04 0.07
GA2044 0.08 0.14
-180
-120
-60
0
60
120
180
ORIENTATION ANGLE, DEGREES
14JUN77

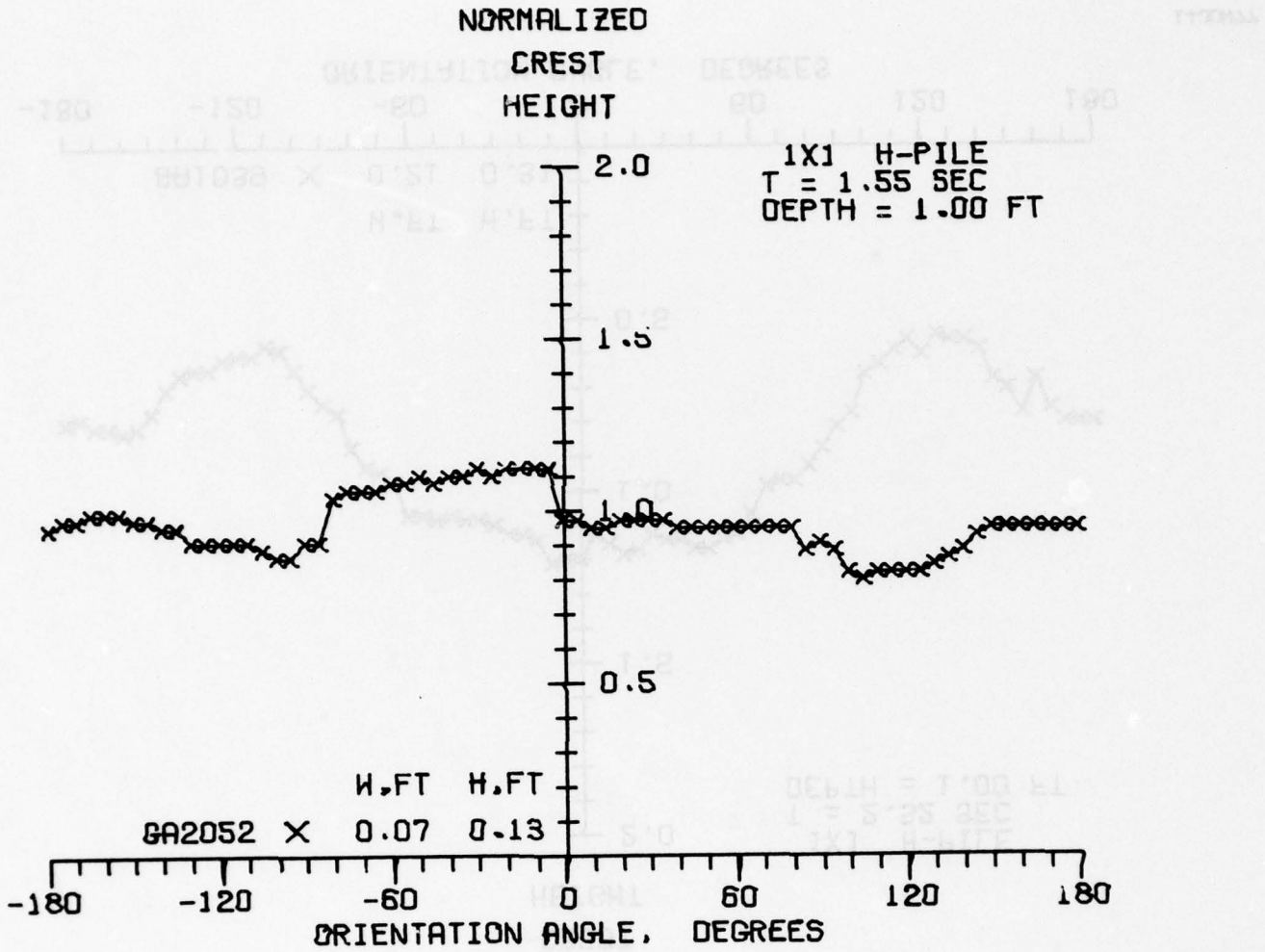
NORMALIZED
CREST
HEIGHT
1X1 H-PILE
T = 1.55 SEC
DEPTH = 1.00 FT
2.0
1.5
1.0
0.5
H,FT H,FT
GA2052 X 0.07 0.13
-180
-120
-60
0
60
120
180
ORIENTATION ANGLE, DEGREES
1 JUN77

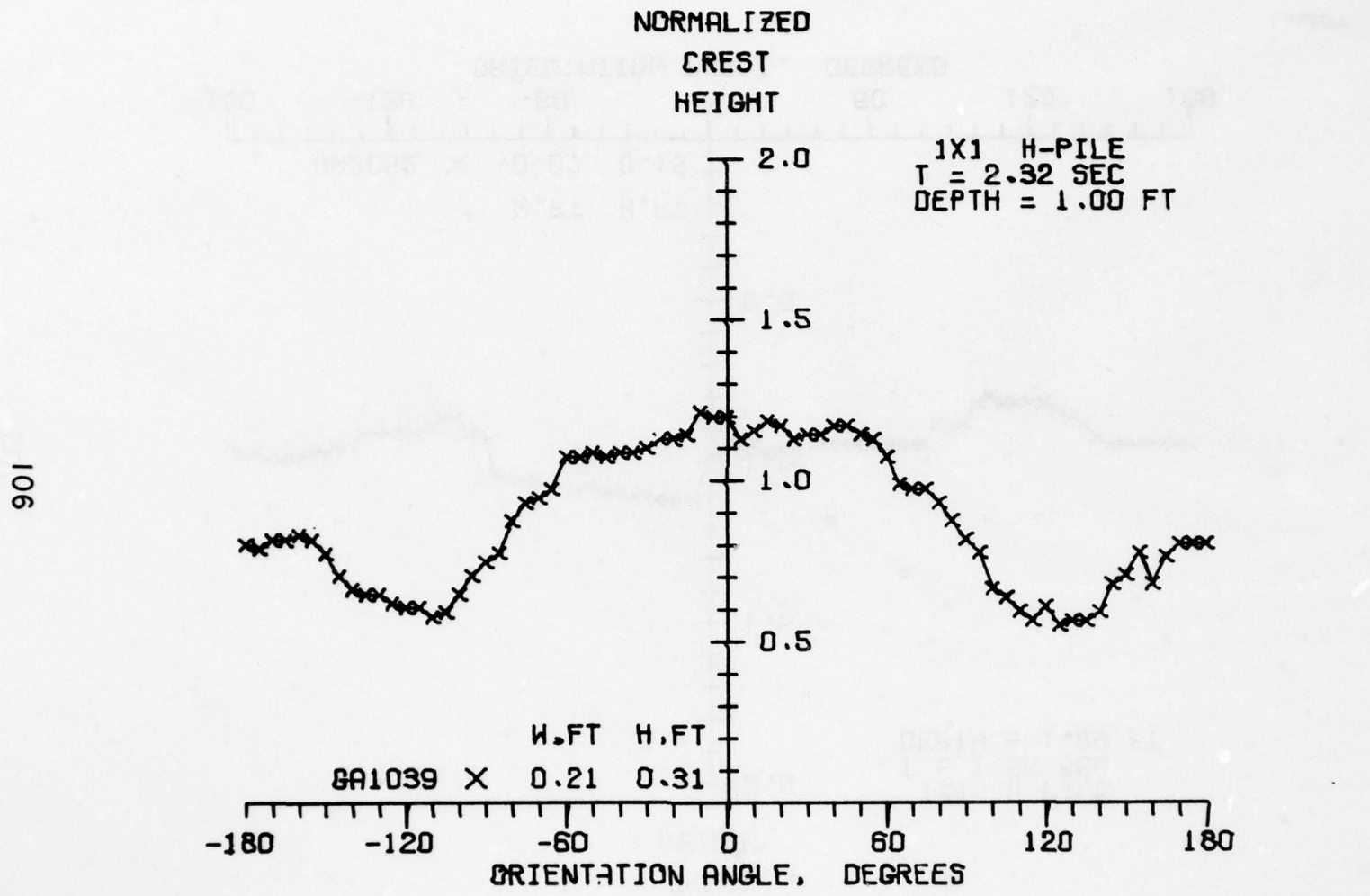
NORMALIZED
CREST
HEIGHT
1X1 H-PILE
T = 2.32 SEC
DEPTH = 1.00 FT
2.0
1.5
1.0
0.5
W,FT H,FT
GA1039 X 0.21 0.31
-180
-120
-60
0
60
120
180
ORIENTATION ANGLE, DEGREES
14JUN77

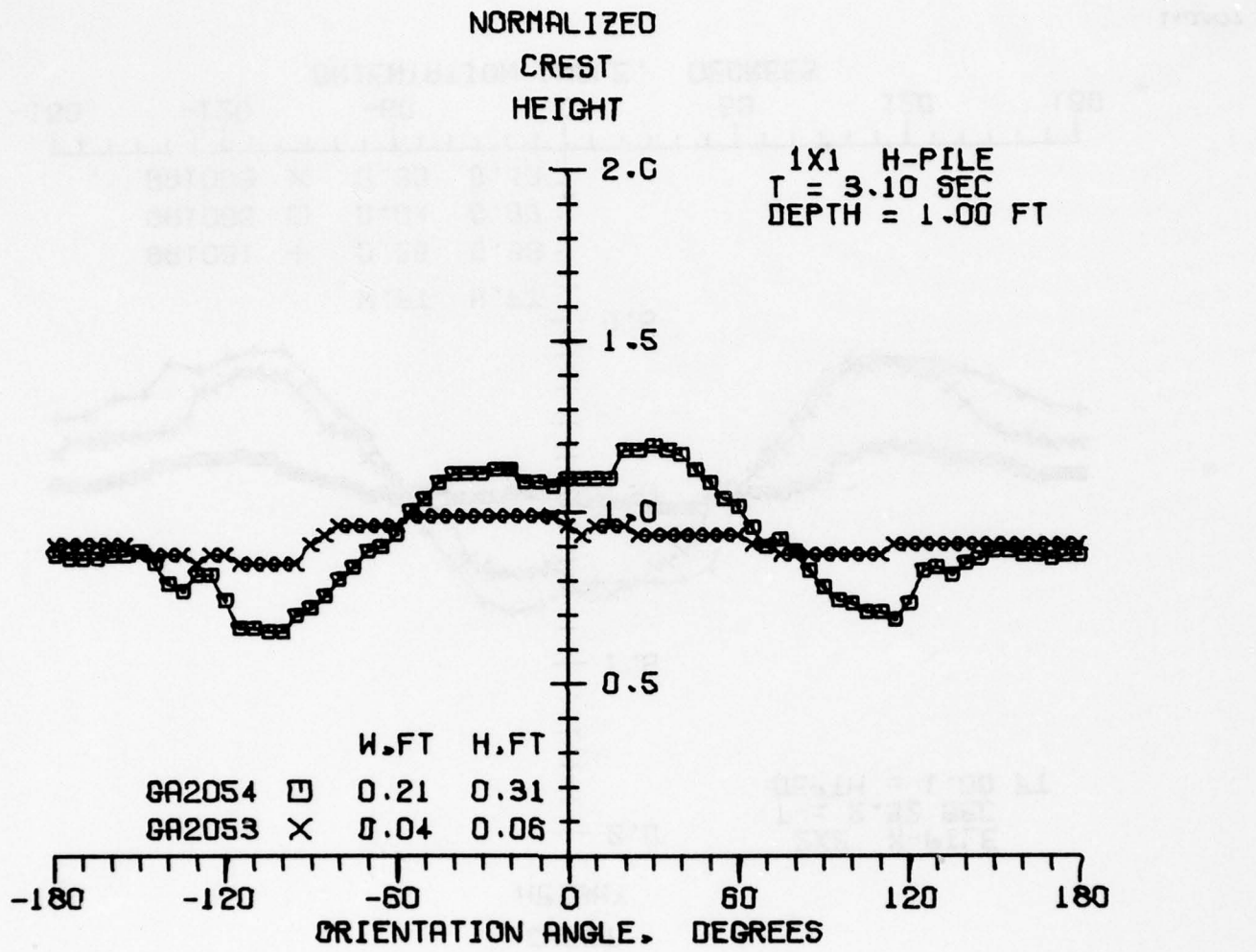
NORMALIZED
CREST
HEIGHT
1X1 H-PILE
T = 3.10 SEC
DEPTH = 1.00 FT
2.0
1.5
1.0
0.5
W,FT H,FT
GA2054 □ 0.21 0.31
GA2053 × 0.04 0.06
-180
-120
-60
0
60
120
180
ORIENTATION ANGLE, DEGREES
14JUN77

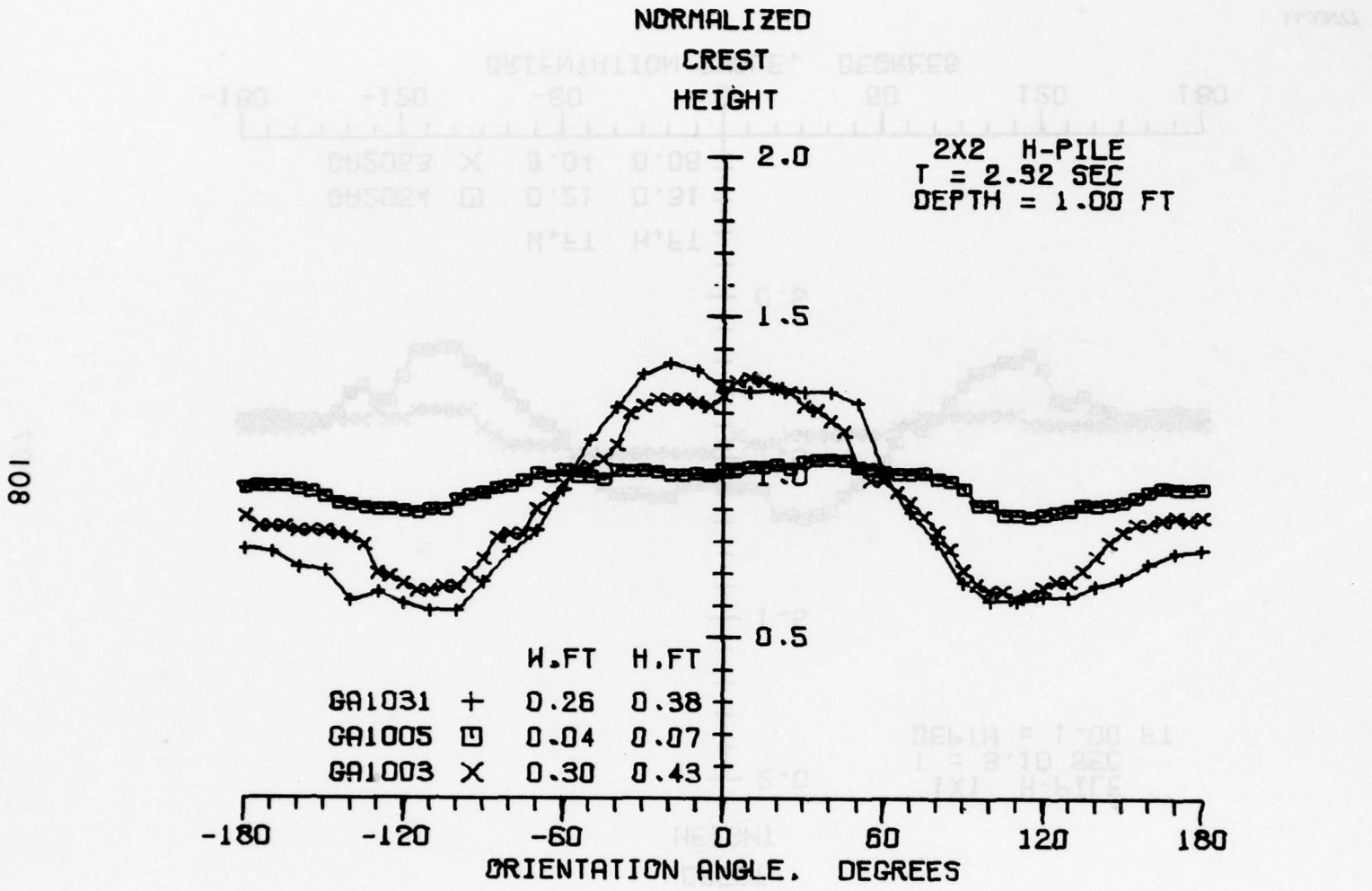
NORMALIZED
CREST
HEIGHT
2X2 H-PILE
T = 2.92 SEC
DEPTH = 1.00 FT
2.0
1.5
1.0
0.5
W.FT H.FT
GA1031 + 0.26 0.38
GA1005 □ 0.04 0.07
GA1003 X 0.30 0.43
-180
-120
-60
0
60
120
180
ORIENTATION ANGLE, DEGREES
14JUN77

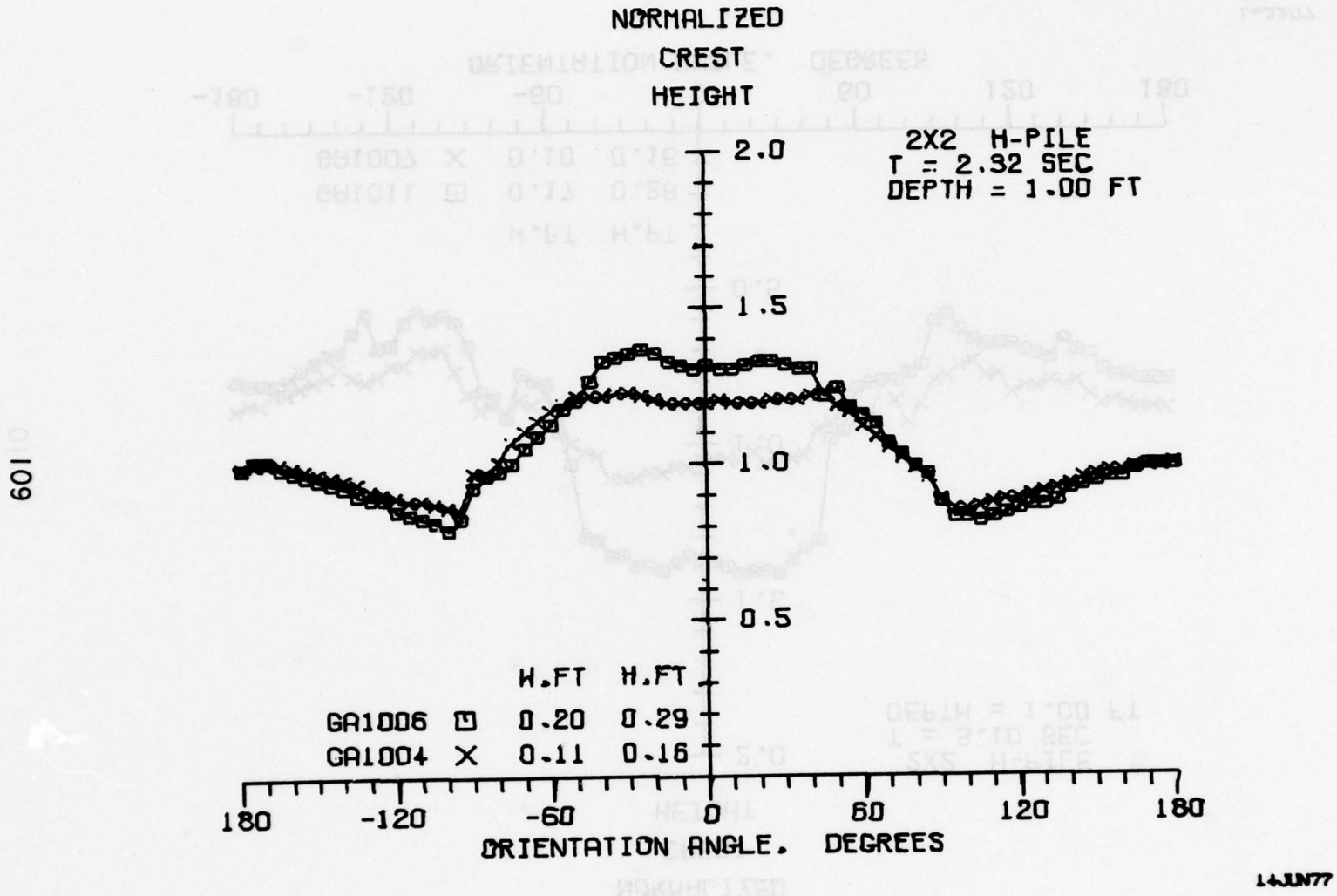
NORMALIZED
CREST
HEIGHT
2X2 H-PILE
T = 2.32 SEC
DEPTH = 1.00 FT
2.0
1.5
1.0
0.5
H.FT H.FT
GA1006 0.20 0.29
GA1004 0.11 0.16
180 -120 -60 0 60 120 180
ORIENTATION ANGLE. DEGREES
14JUN77

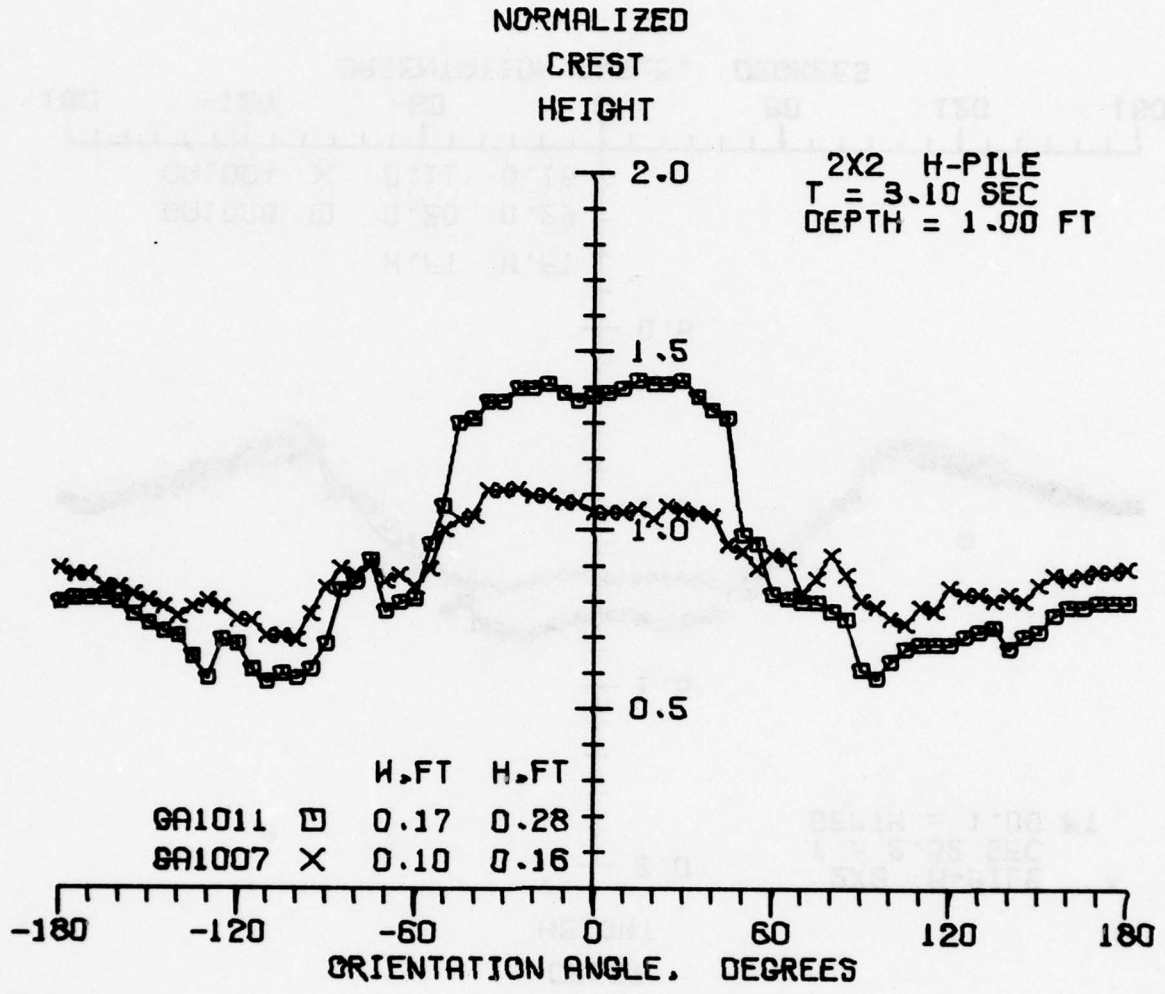
NORMALIZED
CREST
HEIGHT
2X2 H-PILE
T = 3.10 SEC
DEPTH = 1.00 FT
2.0
1.5
1.0
0.5
H,FT H,FT
GA1011 0.17 0.28
GA1007 0.10 0.16
-180
-120
-60
0
60
120
180
ORIENTATION ANGLE, DEGREES
14JUN77

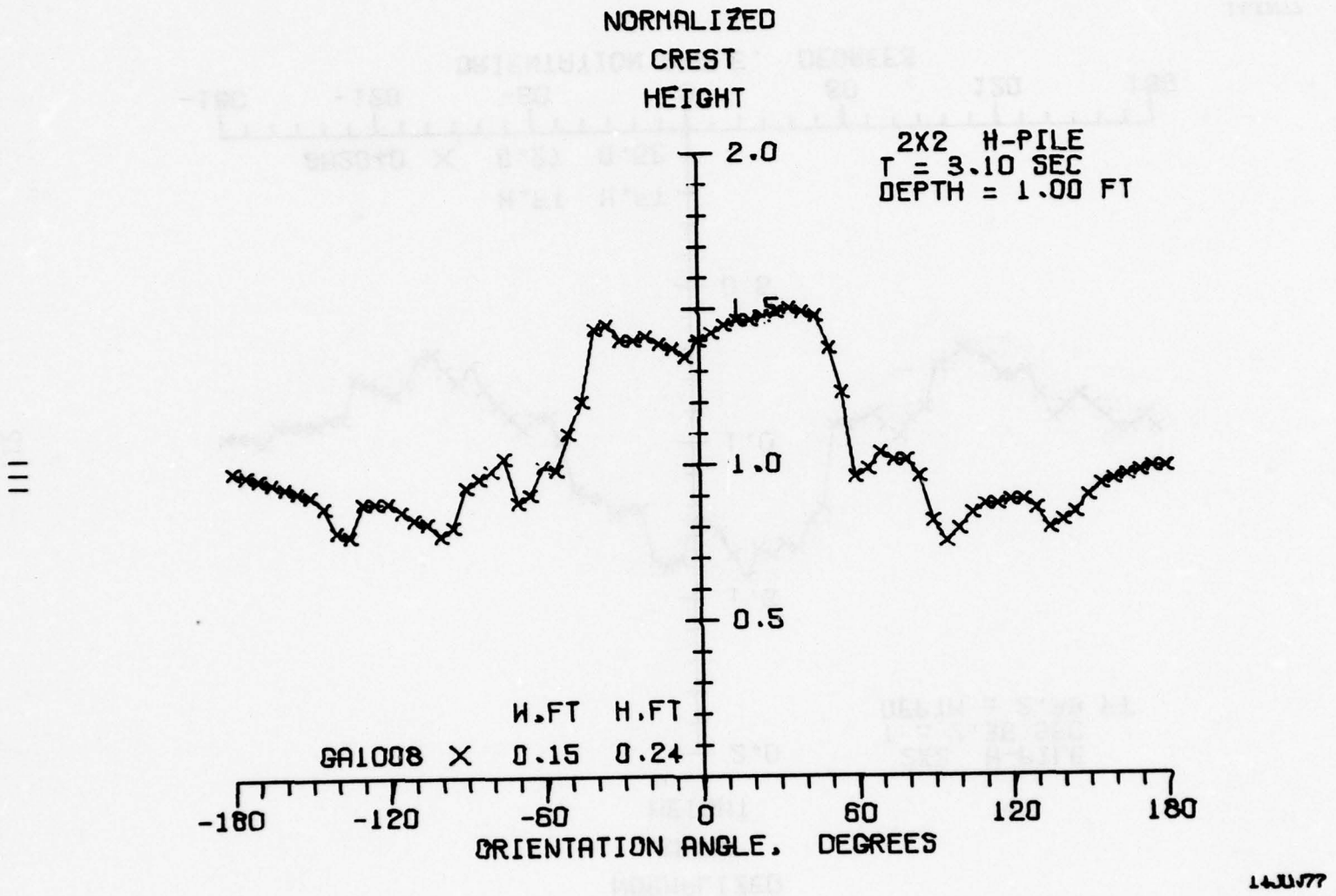
NORMALIZED
CREST
HEIGHT
2X2 H-PILE
T = 3.10 SEC
DEPTH = 1.00 FT
2.0
1.5
1.0
0.5
H,FT H,FT
GA1008 X 0.15 0.24
-180
-120
-60
0
60
120
180
ORIENTATION ANGLE, DEGREES

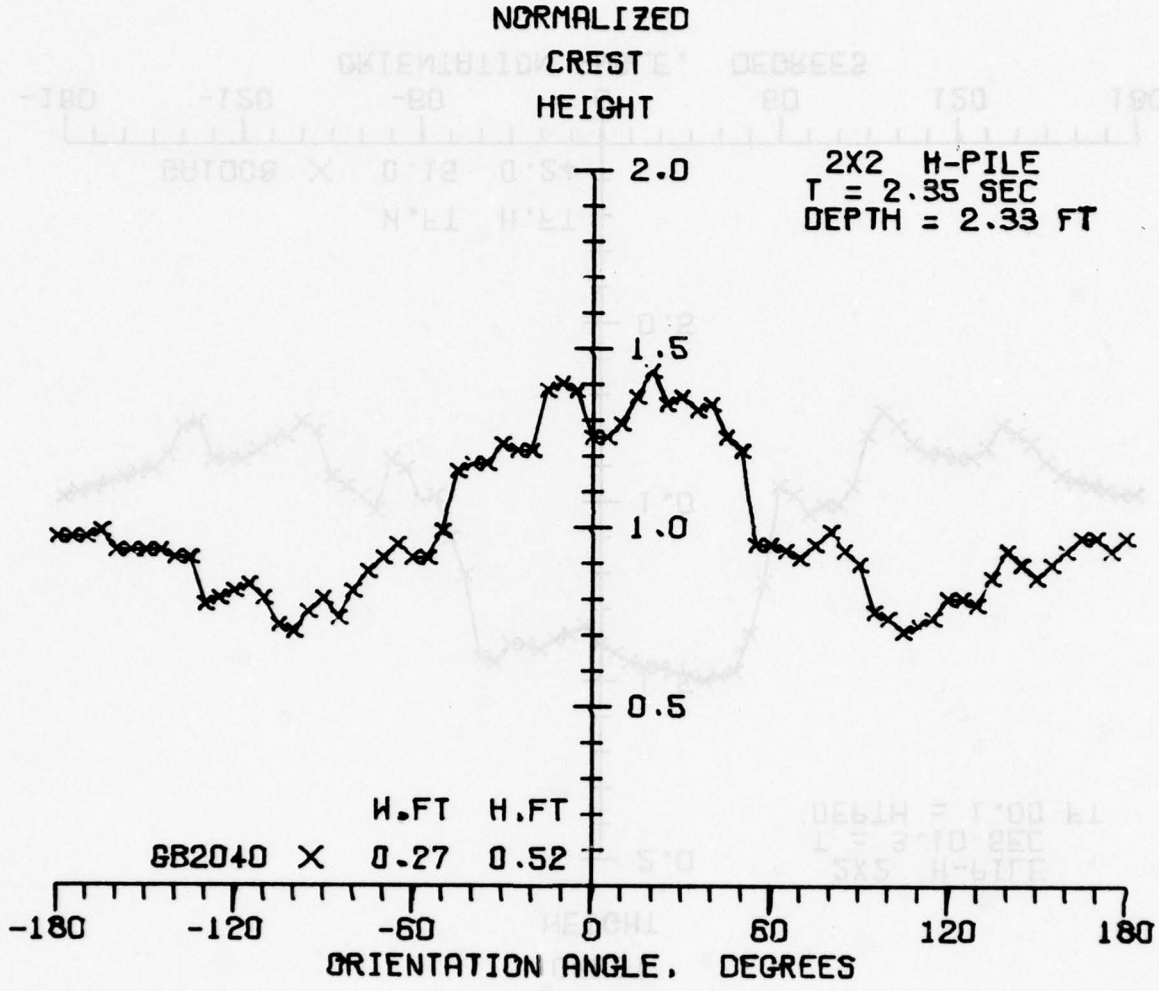
NORMALIZED
CREST
HEIGHT
2X2 H-PILE
T = 2.35 SEC
DEPTH = 2.33 FT
2.0
1.5
1.0
0.5
W,FT H,FT
GB2040 X 0.27 0.52
-180
-120
-60
0
60
120
180
ORIENTATION ANGLE, DEGREES
14JUN77

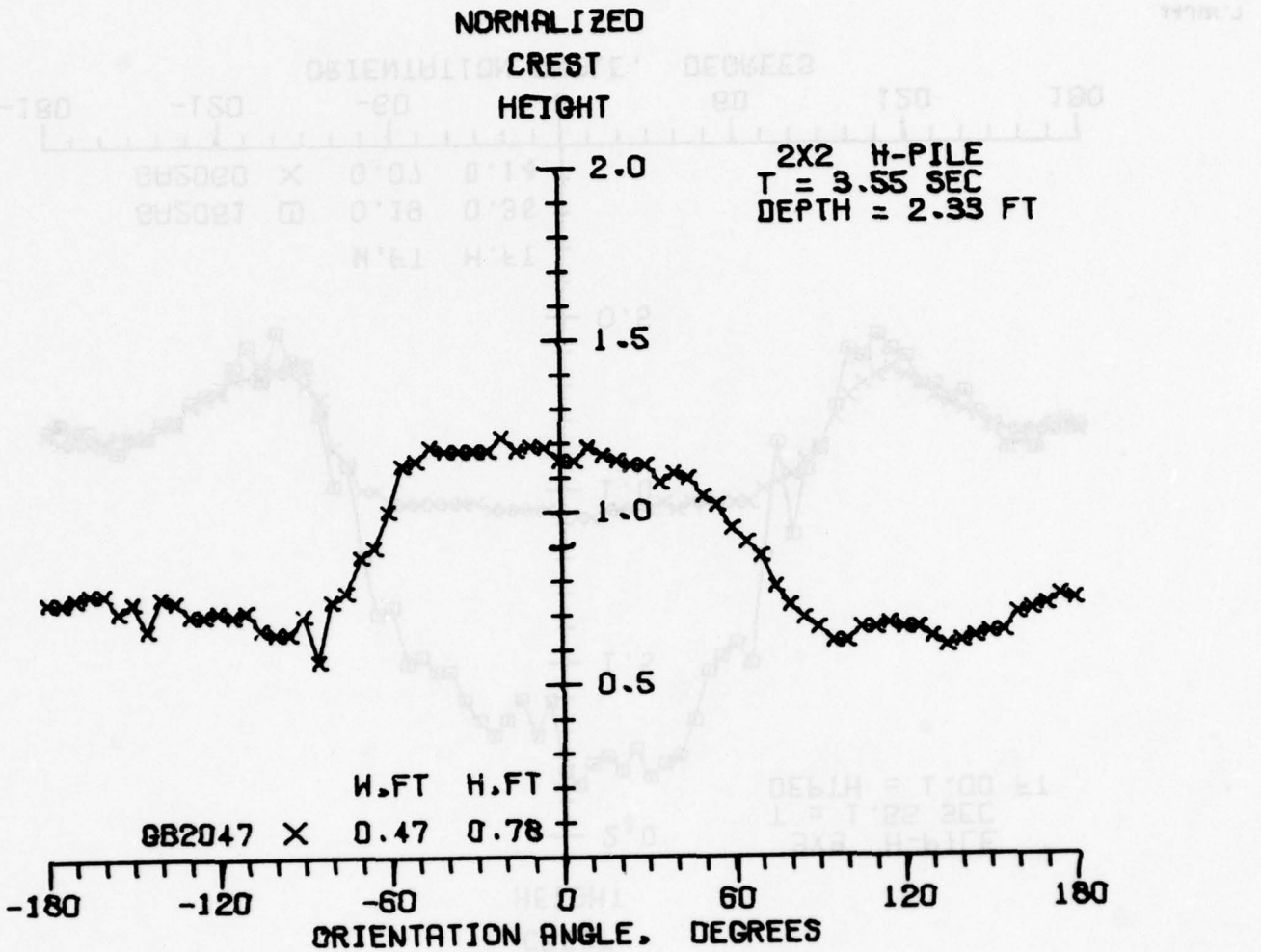
NORMALIZED
CREST
HEIGHT
2X2 H-PILE
T = 3.55 SEC
DEPTH = 2.33 FT
2.0
1.5
1.0
0.5
H,FT H,FT
GB2047 X 0.47 0.78
-180
-120
-60
0
60
120
180
ORIENTATION ANGLE, DEGREES
14JUN77

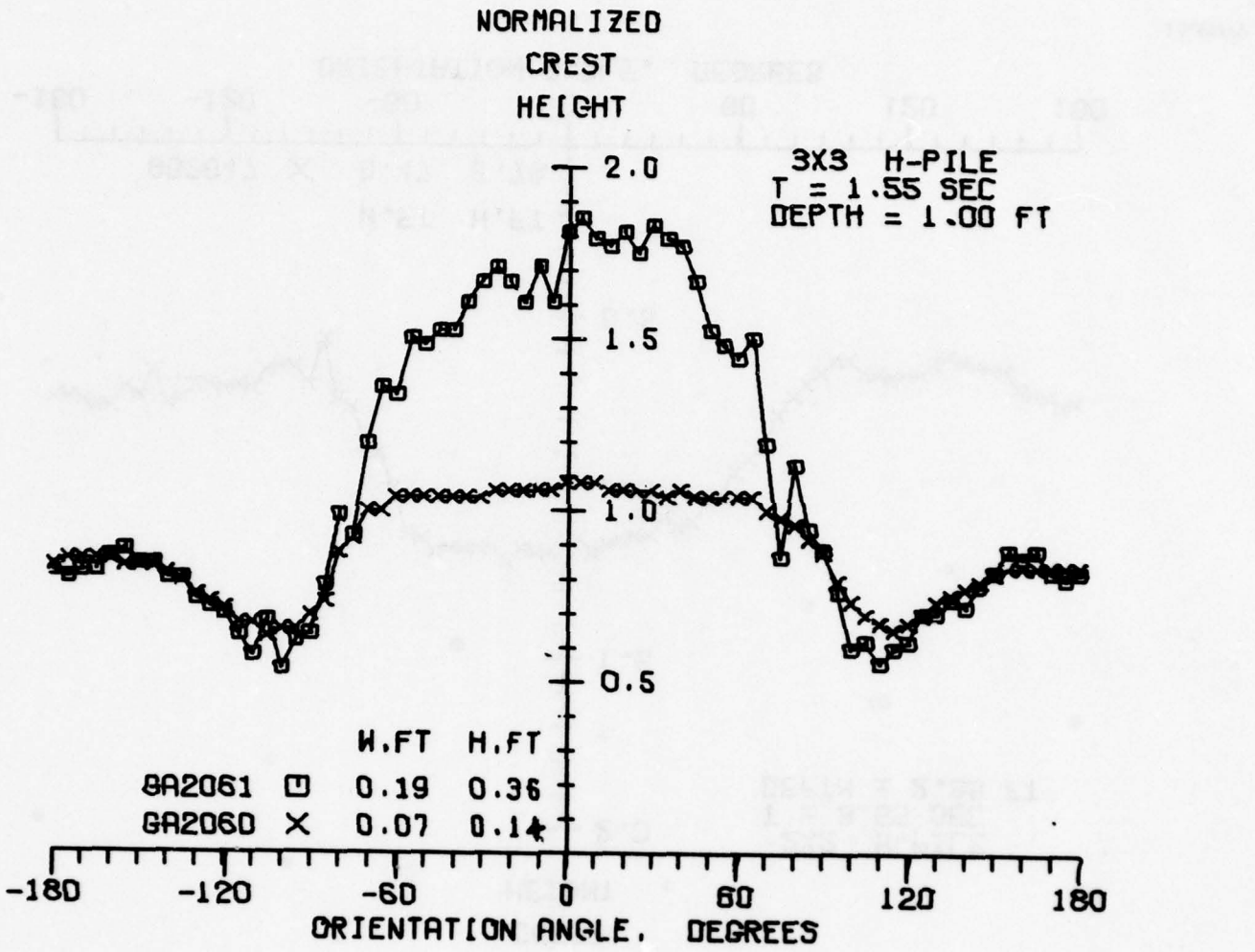
NORMALIZED
CREST
HEIGHT
3X3 H-PILE
T = 1.55 SEC
DEPTH = 1.00 FT
2.0
1.5
1.0
0.5
H,FT H,FT
GA2061 0.19 0.36
GA2060 0.07 0.14
-180
-120
-60
0
60
120
180
ORIENTATION ANGLE, DEGREES
14JUN.7

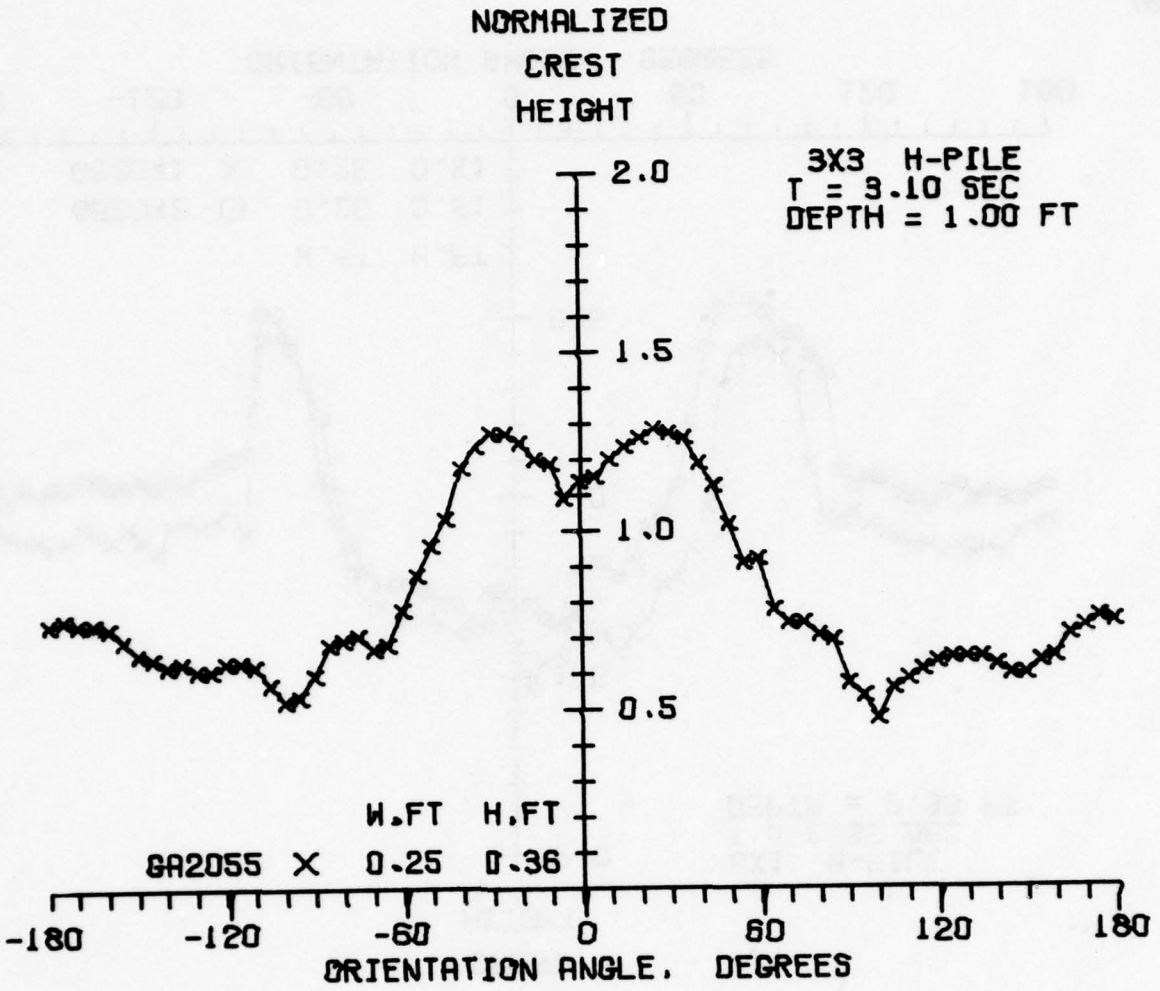
NORMALIZED
CREST
HEIGHT
3X3 H-PILE
T = 3.10 SEC
DEPTH = 1.00 FT
2.0
1.5
1.0
0.5
W.FT H.FT
GA2055 X 0.25 0.36
-180
-120
-60
0
60
120
180
ORIENTATION ANGLE, DEGREES

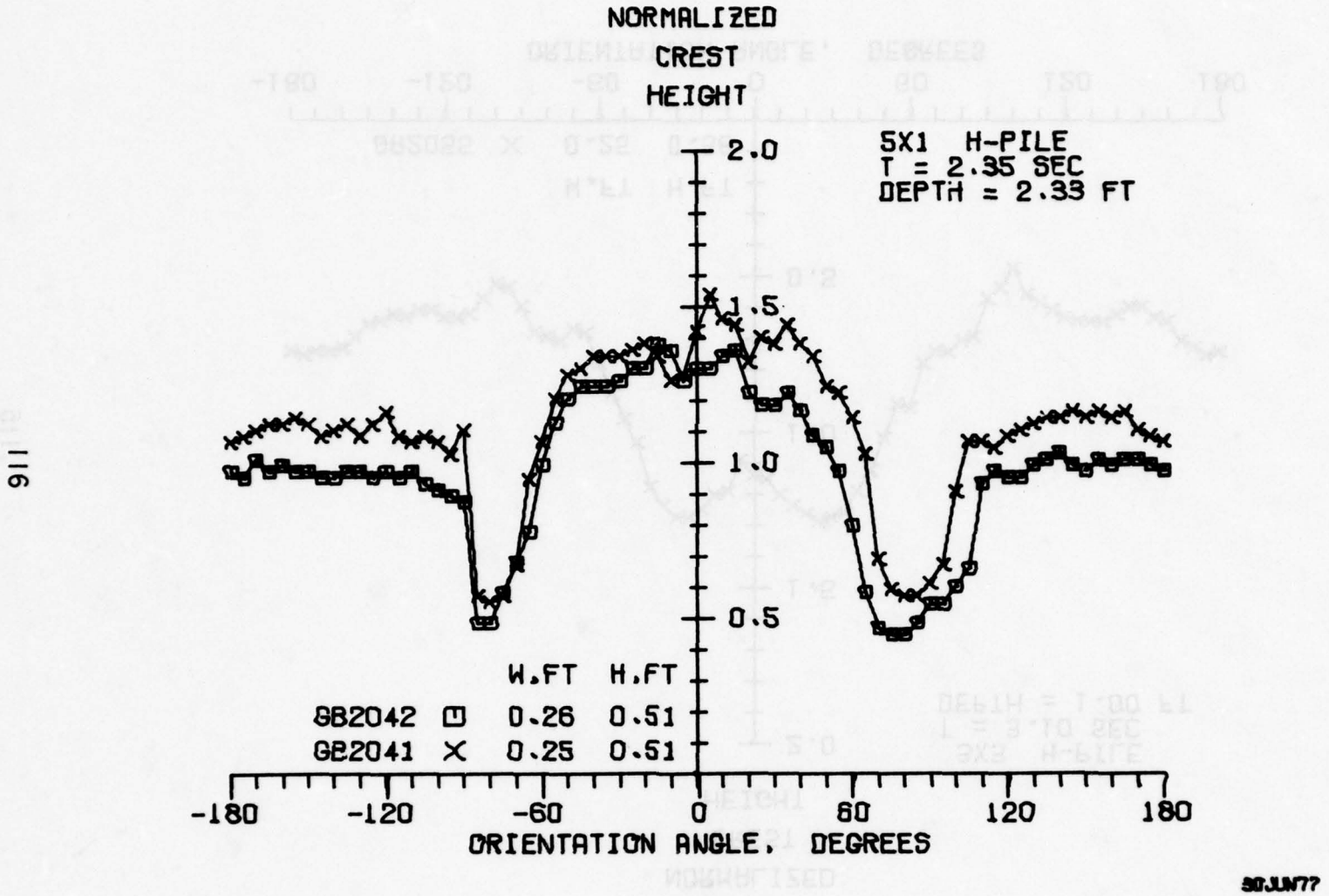
NORMALIZED
CREST
HEIGHT
5X1 H-PILE
T = 2.35 SEC
DEPTH = 2.33 FT
2.0
1.5
1.0
0.5
W.FT H.FT
GB2042 0.26 0.51
GB2041 0.25 0.51
-180
-120
-60
0
60
120
180
ORIENTATION ANGLE, DEGREES
30JUN77

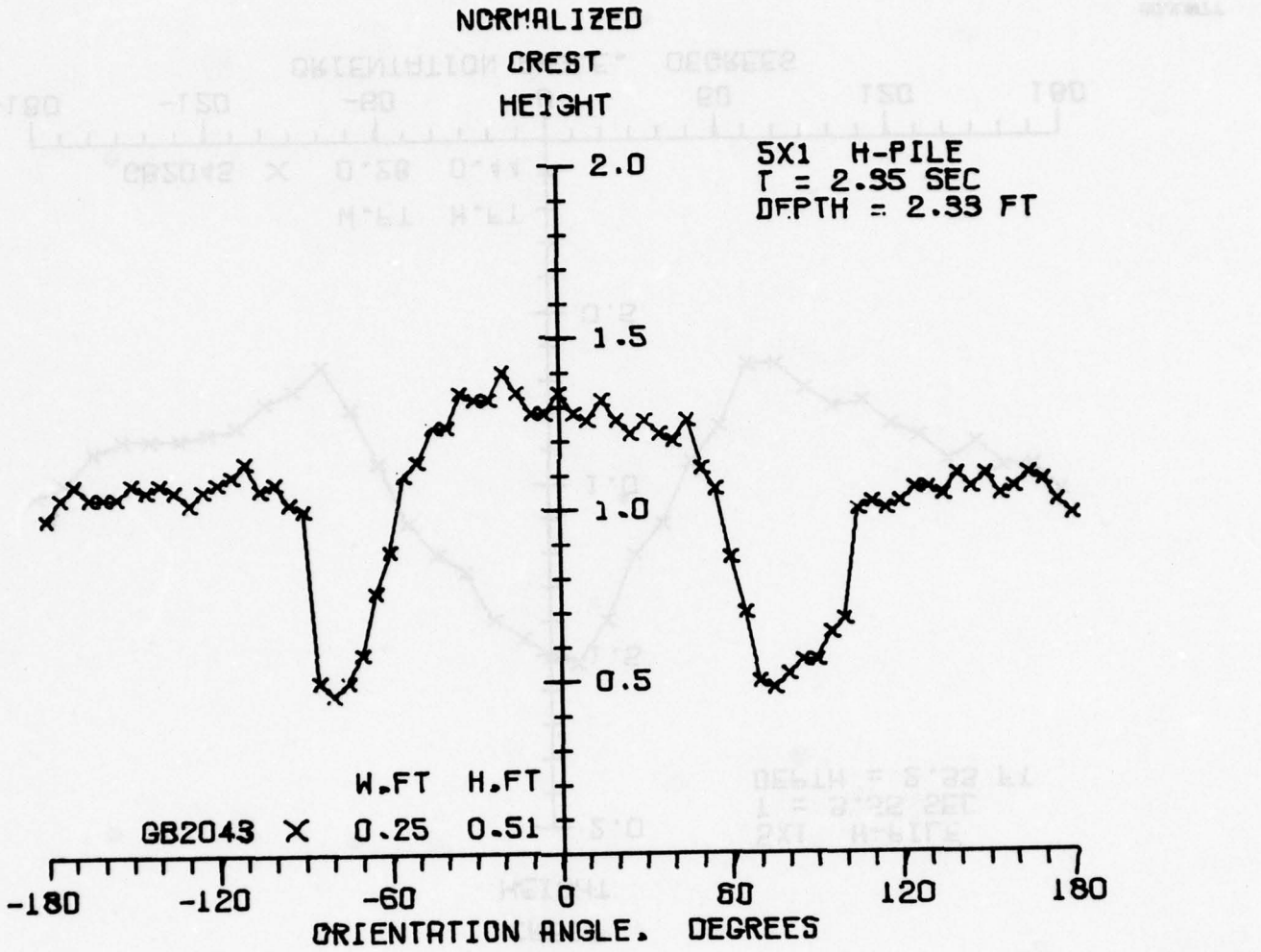
NORMALIZED
CREST
HEIGHT
5X1 H-PILE
T = 2.35 SEC
DEPTH = 2.33 FT
2.0
1.5
1.0
0.5
W.FT H.FT
GB2043 X 0.25 0.51
-180
-120
-60
0
60
120
180
ORIENTATION ANGLE. DEGREES
30JUN77

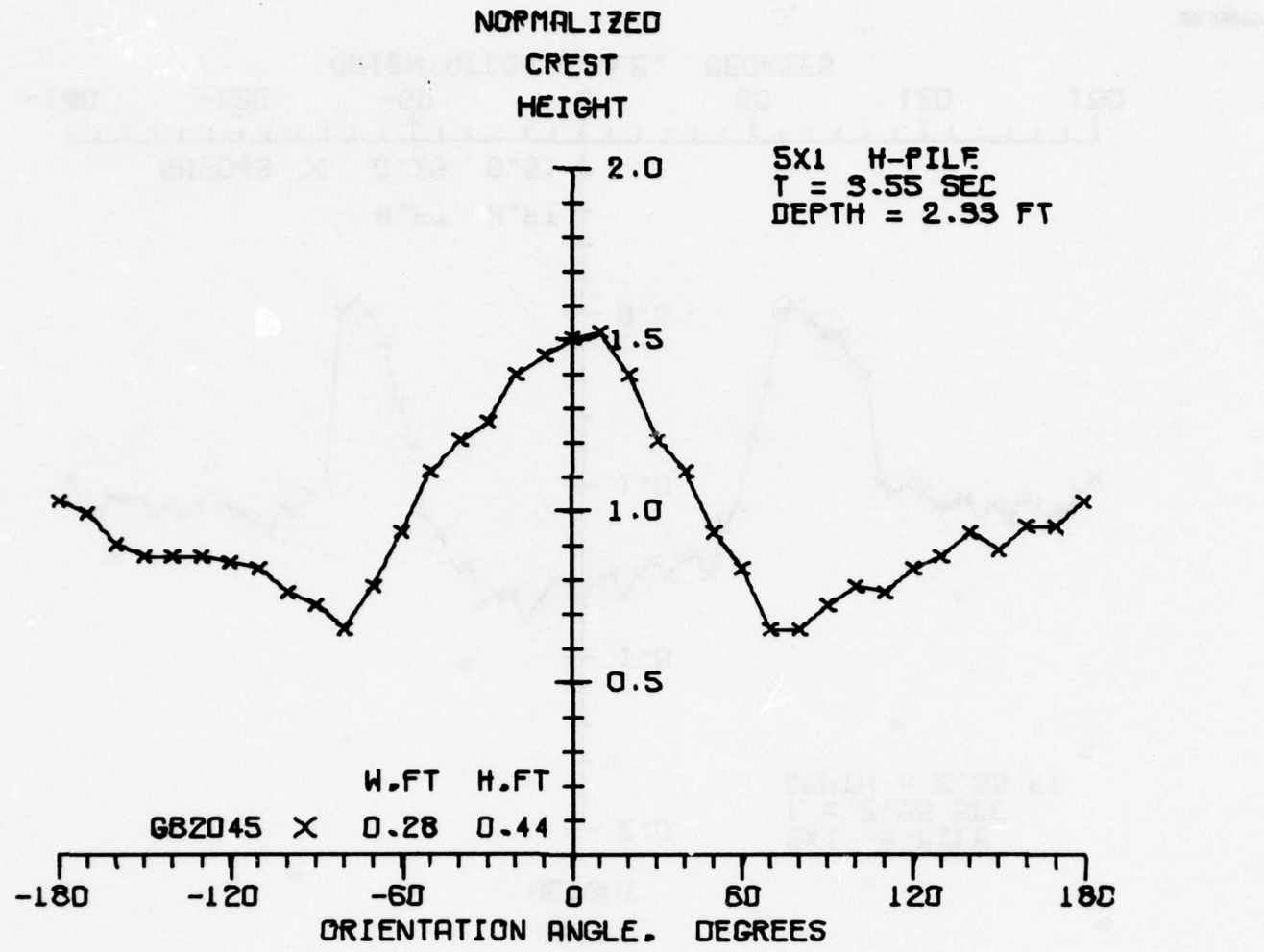
NORMALIZED
CREST
HEIGHT
5X1 H-PILE
T = 3.55 SEC
DEPTH = 2.33 FT
2.0
1.5
1.0
0.5
W.FT H.FT
GB2045 X 0.28 0.44
-180
-120
-60
0
60
120
180
ORIENTATION ANGLE. DEGREES
30JUN77

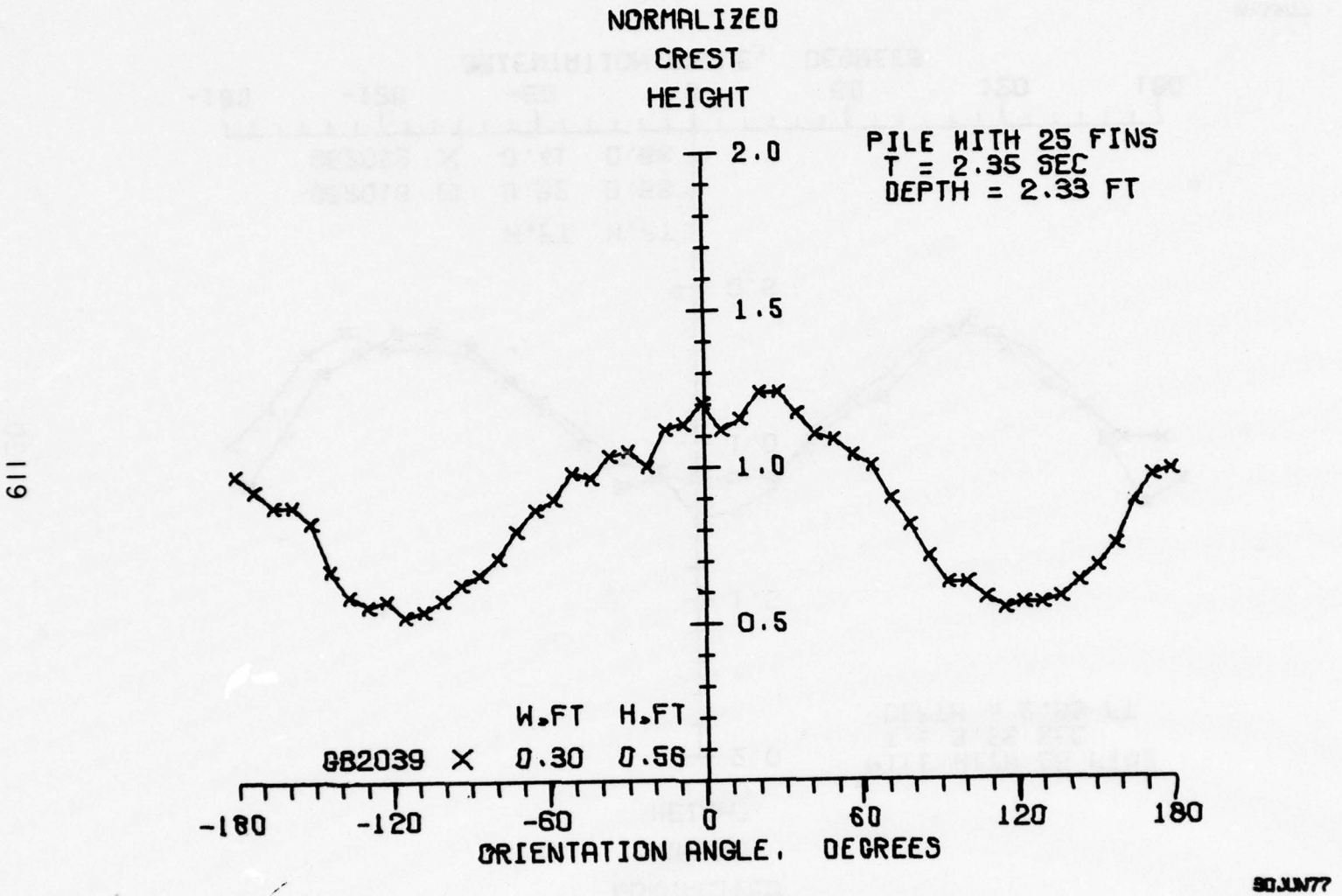
NORMALIZED
CREST
HEIGHT
PILE WITH 25 FINS
T = 2.35 SEC
DEPTH = 2.33 FT
2.0
1.5
1.0
0.5
W,FT H,FT
GB2039 X 0.30 0.56
-180
-120
-60
0
60
120
180
ORIENTATION ANGLE, DEGREES
30JUN77

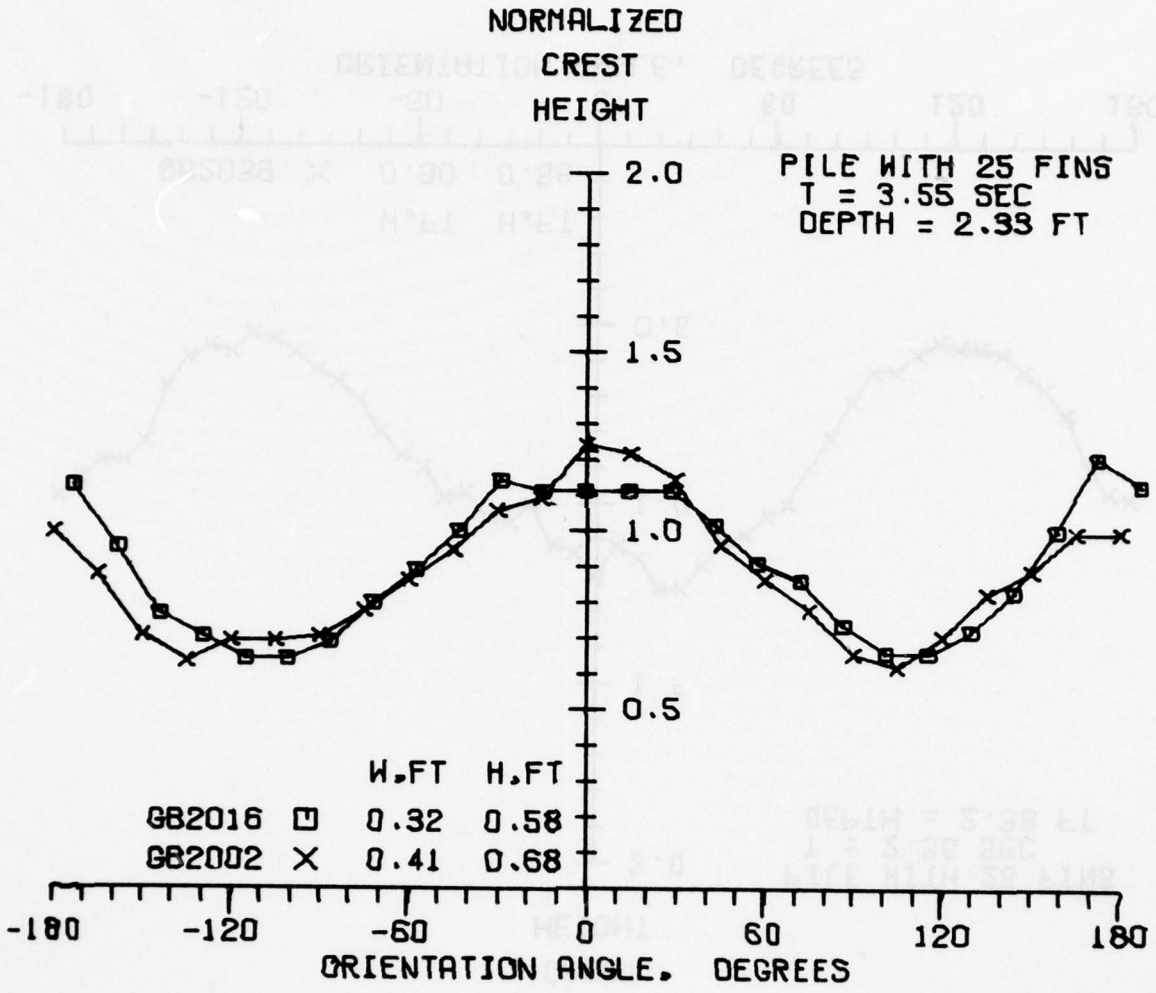
NORMALIZED
CREST
HEIGHT
PILE WITH 25 FINS
T = 3.55 SEC
DEPTH = 2.33 FT
2.0
1.5
1.0
0.5
W,FT H,FT
GB2016 0.32 0.58
GB2002 0.41 0.68
-180
-120
-60
0
60
120
180
ORIENTATION ANGLE, DEGREES
30JUN77

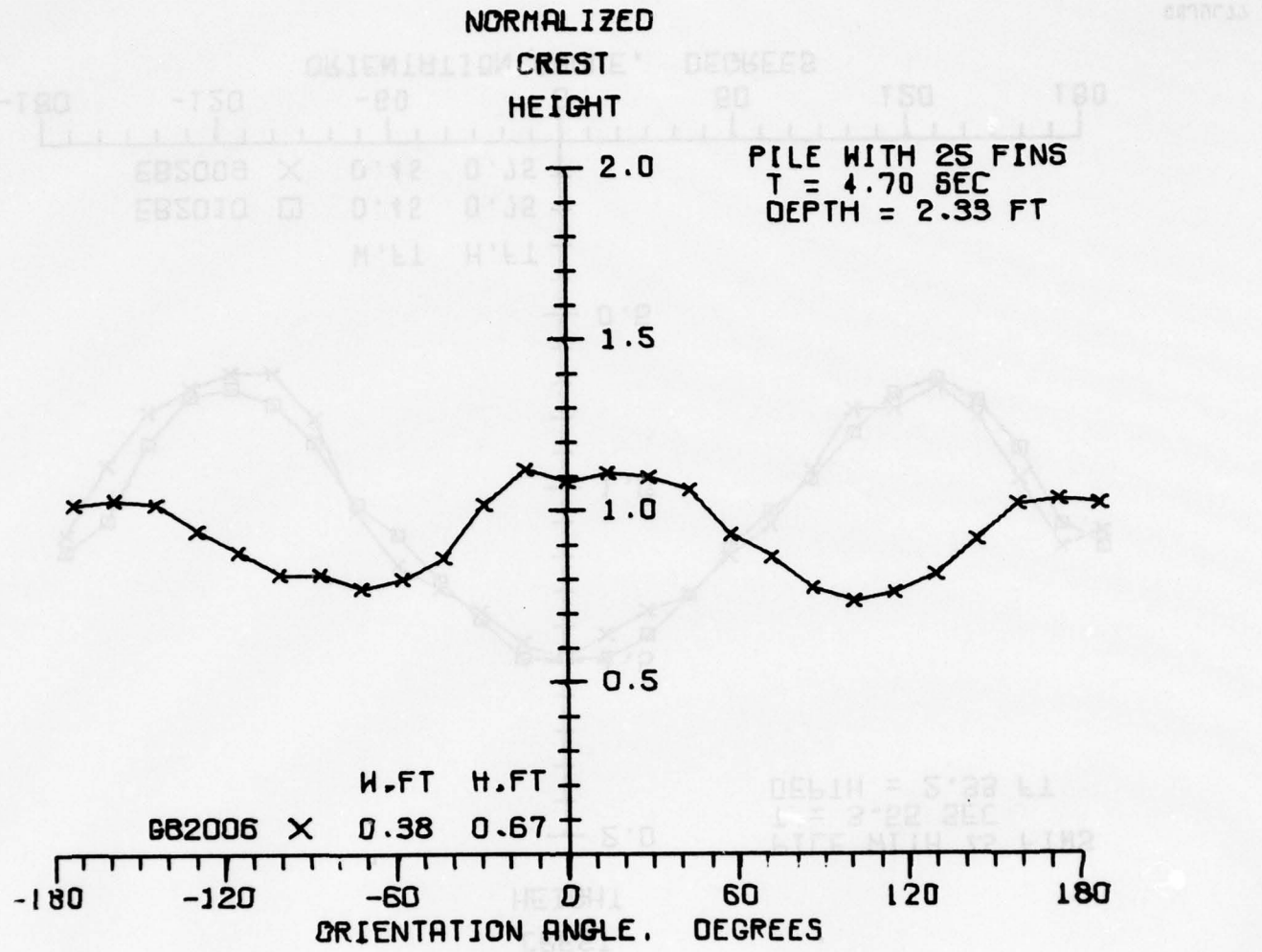
NORMALIZED
CREST
HEIGHT
PILE WITH 25 FINS
T = 4.70 SEC
DEPTH = 2.33 FT
2.0
1.5
1.0
0.5
W.FT H.FT
GB2006 X 0.38 0.67
-180
-120
-60
0
60
120
180
ORIENTATION ANGLE, DEGREES
30JUN77

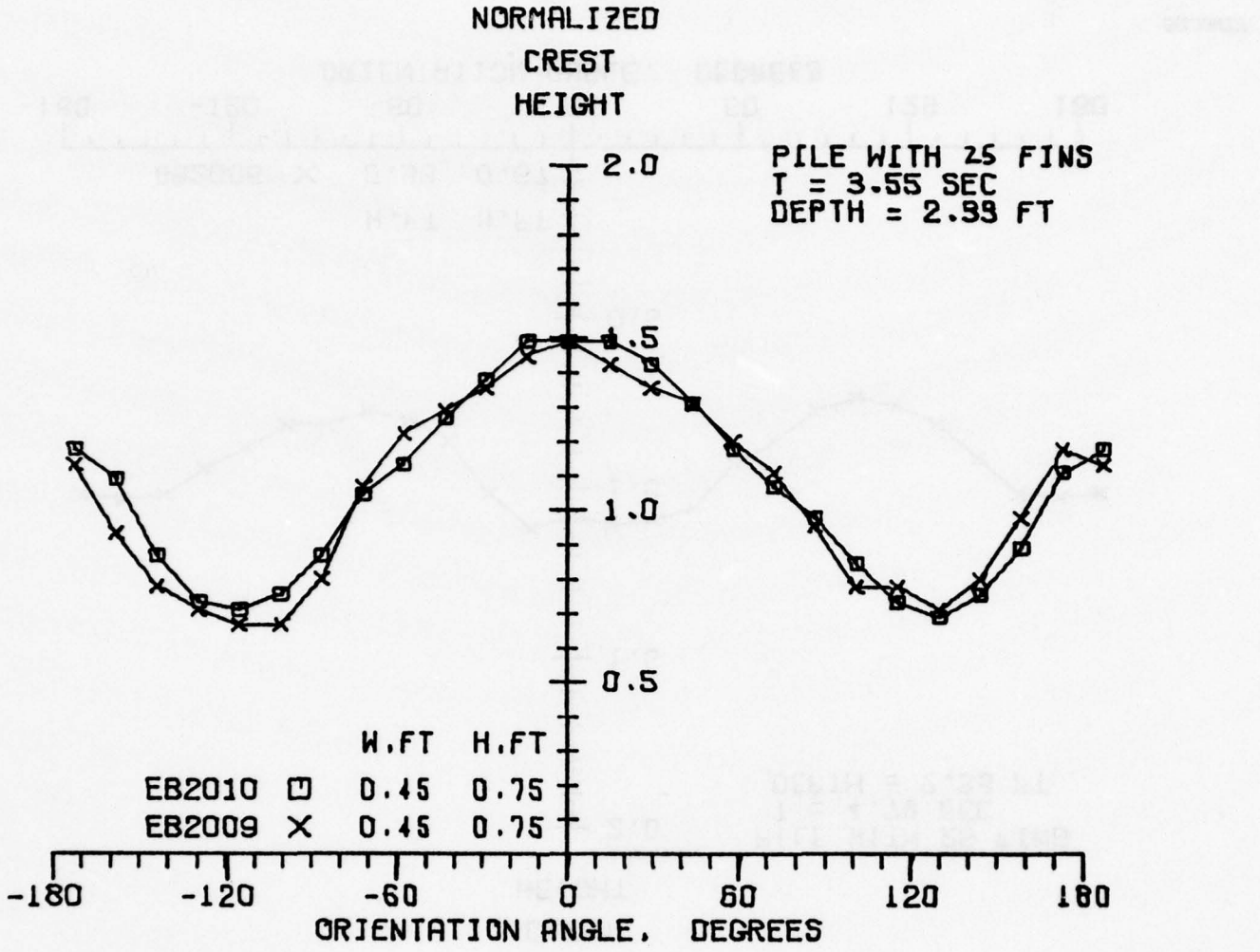
NORMALIZED
CREST
HEIGHT
PILE WITH 25 FINS
T = 3.55 SEC
DEPTH = 2.33 FT
2.0
1.5
1.0
0.5
W,FT H,FT
EB2010 0.45 0.75
EB2009 0.45 0.75
-180
-120
-60
0
60
120
180
ORIENTATION ANGLE, DEGREES
08JUL77

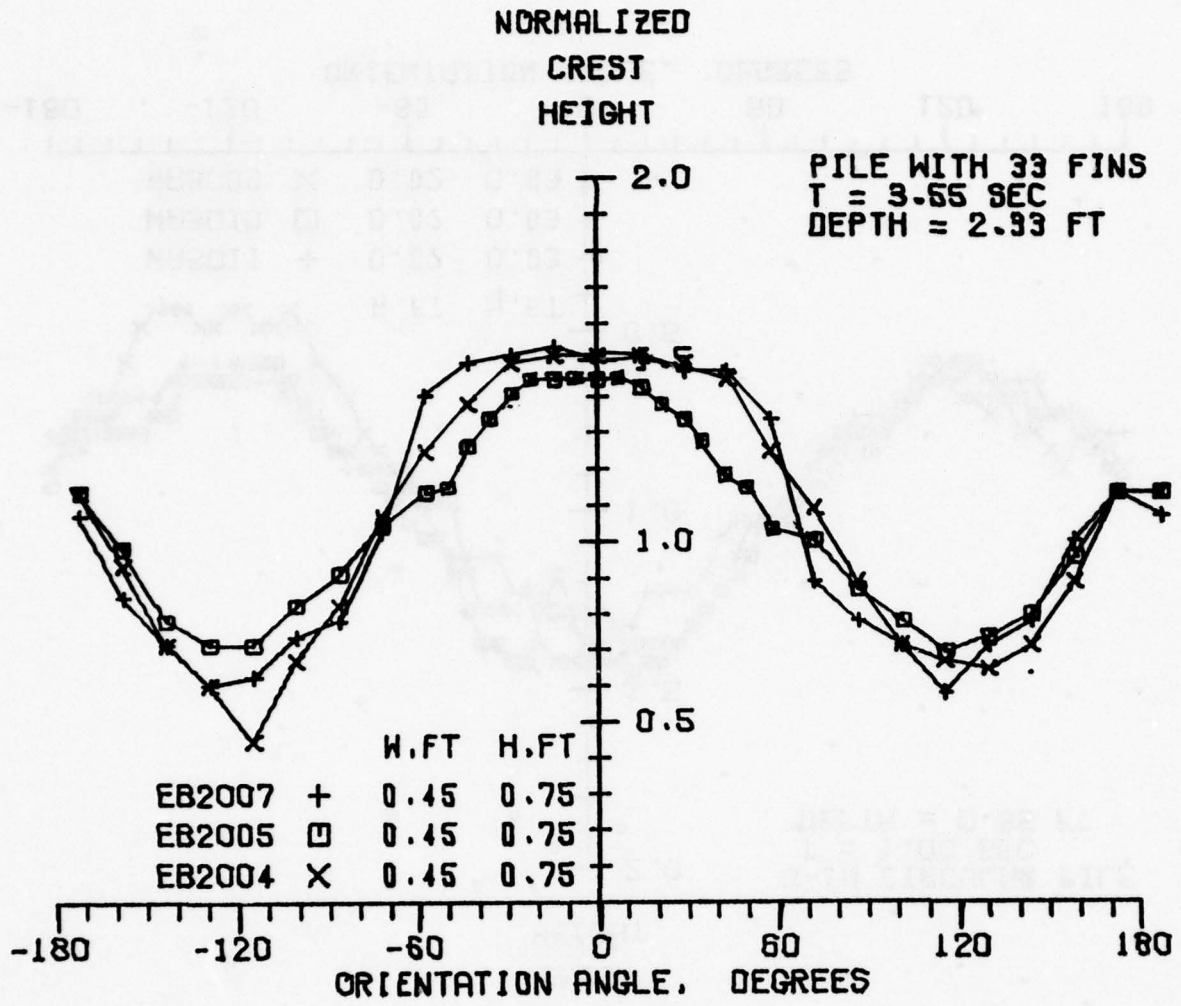
NORMALIZED
CREST
HEIGHT
PILE WITH 33 FINS
T = 3.55 SEC
DEPTH = 2.93 FT
2.0
1.0
0.5
W.FT H.FT
EB2007 + 0.45 0.75
EB2005 □ 0.45 0.75
EB2004 X 0.45 0.75
-180
-120
-60
0
60
120
180
ORIENTATION ANGLE, DEGREES
06JUL77

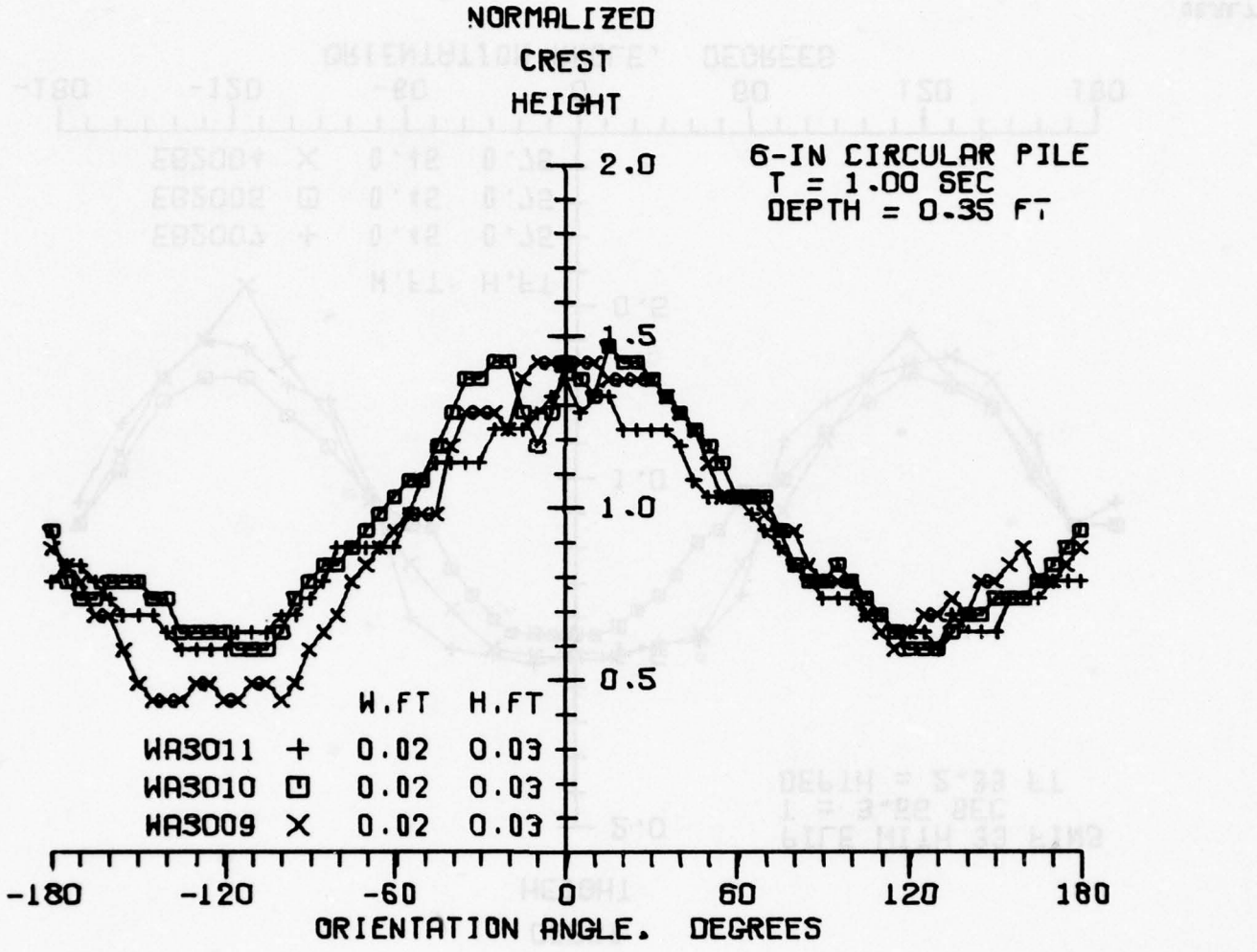
NORMALIZED
CREST
HEIGHT
6-IN CIRCULAR PILE
T = 1.00 SEC
DEPTH = 0.35 FT
2.0
1.5
1.0
0.5
W.FT H.FT
WA3011 + 0.02 0.03
WA3010 □ 0.02 0.03
WA3009 X 0.02 0.03
-180
-120
-60
0
60
120
180
ORIENTATION ANGLE. DEGREES
06JUL77

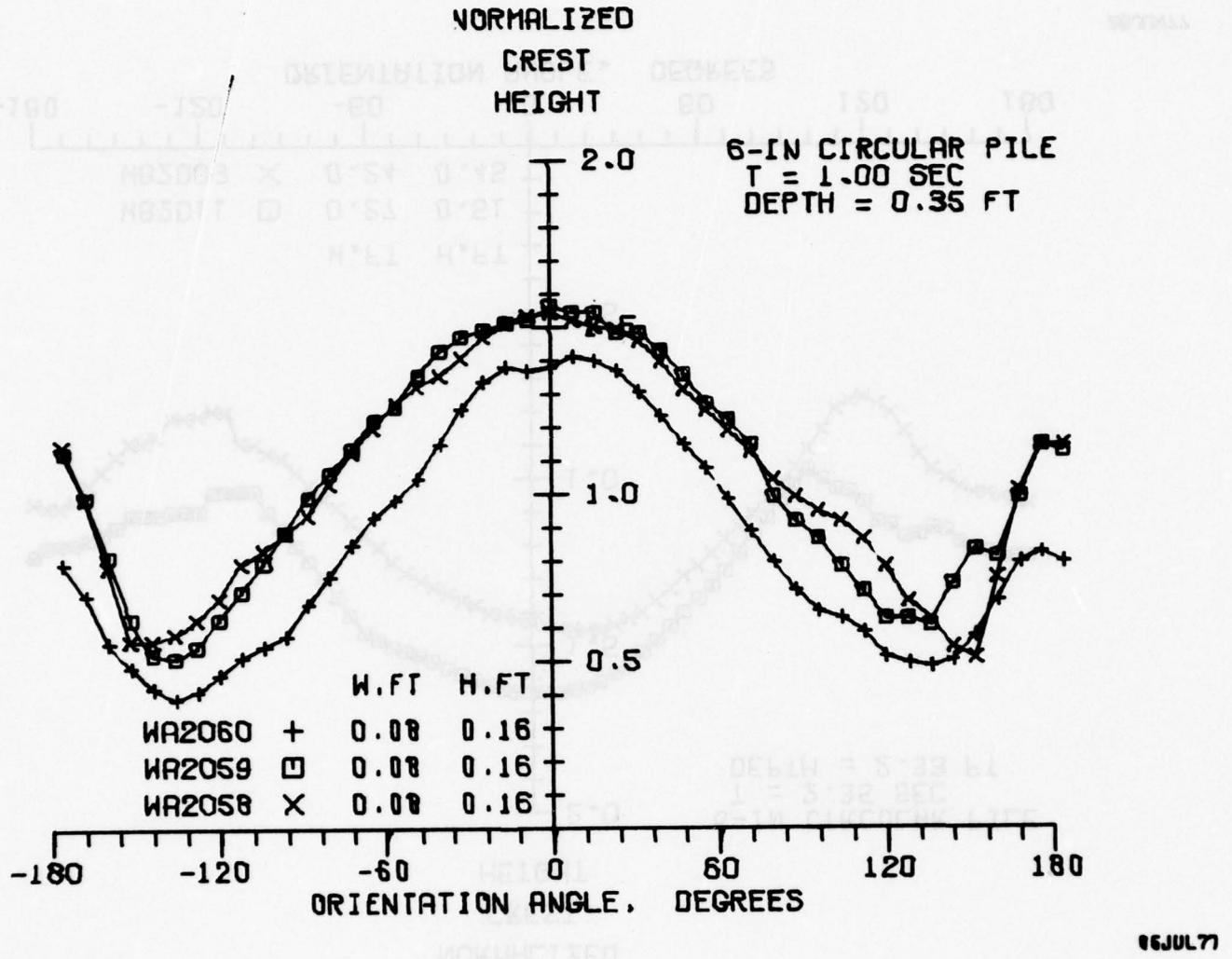
NORMALIZED
CREST
HEIGHT
6-IN CIRCULAR PILE
T = 1.00 SEC
DEPTH = 0.35 FT
2.0
1.0
0.5
W.FT H.FT
WA2060 + 0.08 0.16
WA2059 □ 0.08 0.16
WA2058 X 0.08 0.16
-180
-120
-60
0
60
120
180
ORIENTATION ANGLE, DEGREES
06JUL77

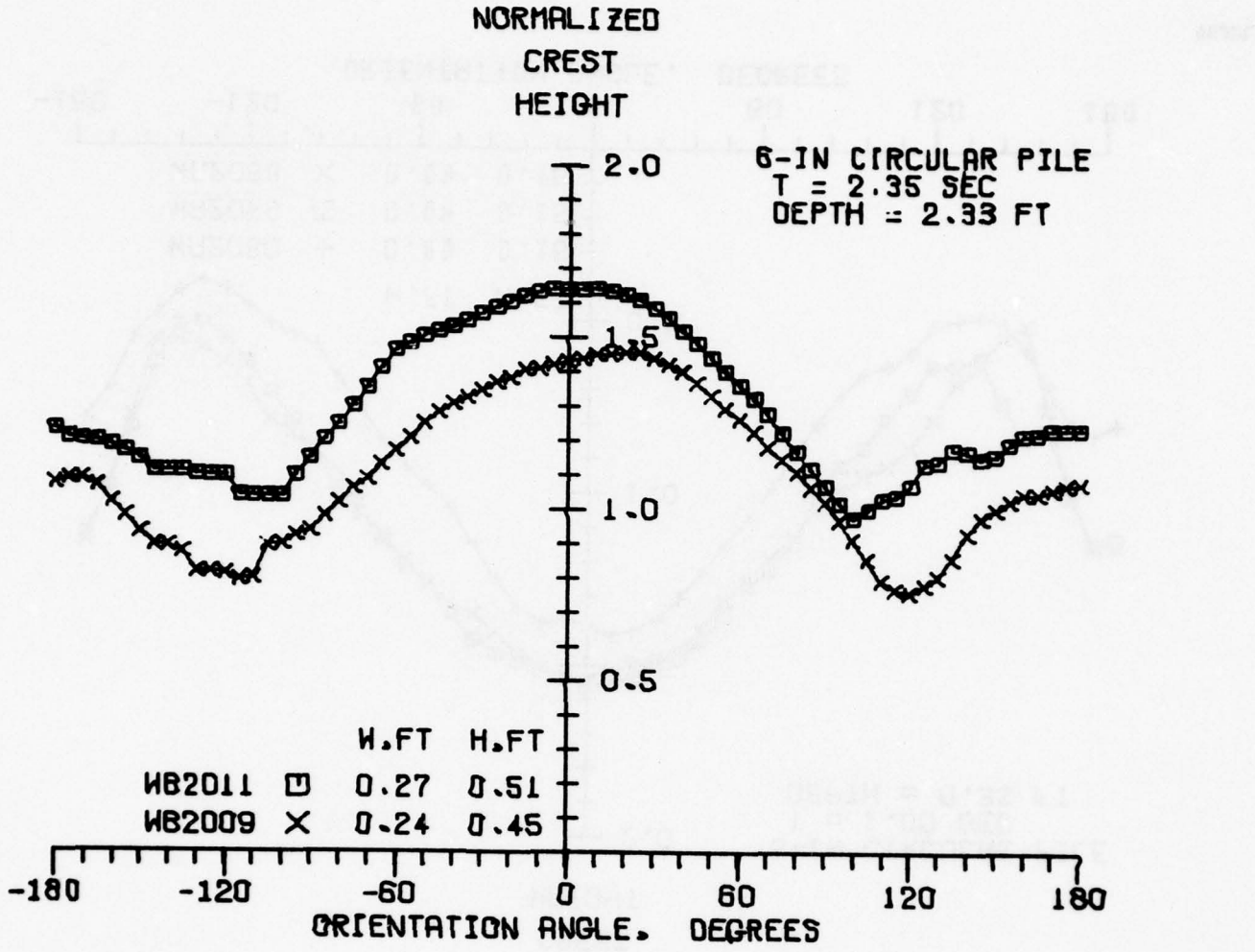
NORMALIZED
CREST
HEIGHT
6-IN CIRCULAR PILE
T = 2.35 SEC
DEPTH = 2.33 FT
2.0
1.5
1.0
0.5
W.FT H.FT
WB2011 0.27 0.51
WB2009 0.24 0.45
-180
-120
-60
0
60
120
180
ORIENTATION ANGLE, DEGREES
28JUN77

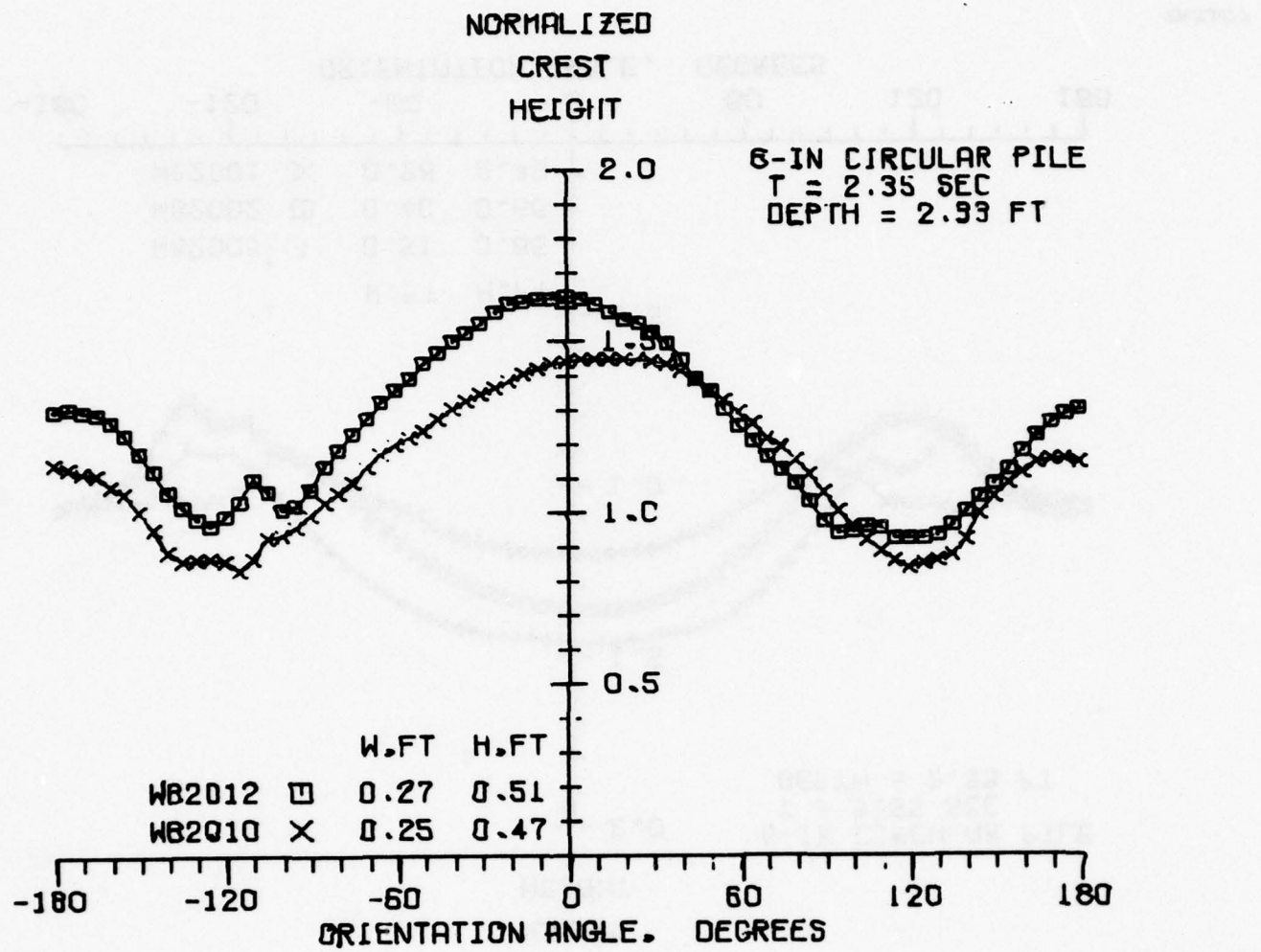
NORMALIZED
CREST
HEIGHT
6-IN CIRCULAR PILE
T = 2.35 SEC
DEPTH = 2.93 FT
2.0
1.5
1.0
0.5
W.FT H.FT
WB2012 0.27 0.51
WB2010 0.25 0.47
-180
-120
-60
0
60
120
180
ORIENTATION ANGLE, DEGREES
28JUN77

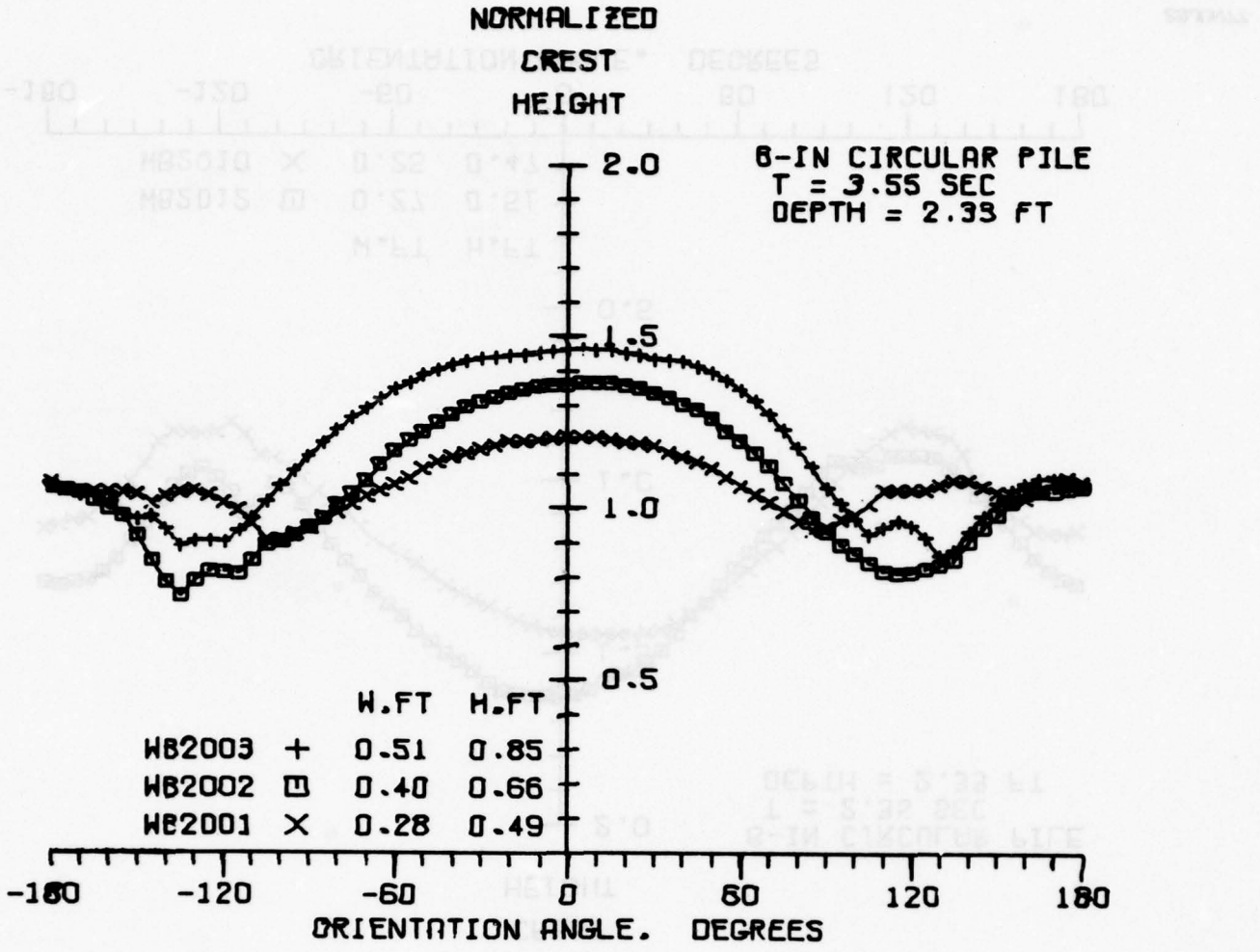
NORMALIZED
CREST
HEIGHT
8-IN CIRCULAR PILE
T = 3.55 SEC
DEPTH = 2.33 FT
2.0
1.5
1.0
0.5
W.FT H.FT
WB2003 + 0.51 0.85
WB2002 □ 0.40 0.66
WB2001 × 0.28 0.49
-180 -120 -60 0 60 120 180
ORIENTATION ANGLE. DEGREES
28JUN77

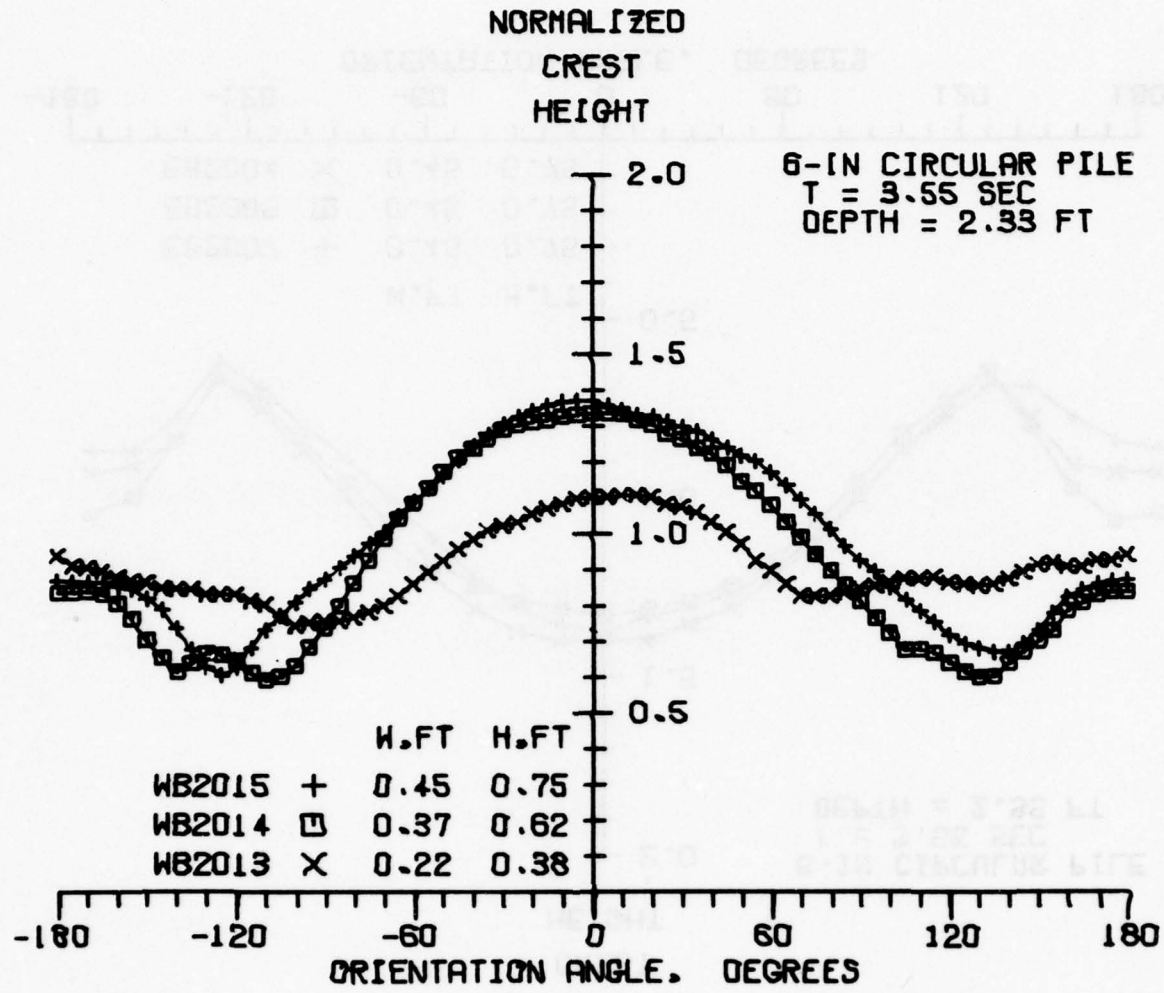
NORMALIZED
CREST
HEIGHT
6-IN CIRCULAR PILE
T = 3.55 SEC
DEPTH = 2.33 FT
2.0
1.5
1.0
0.5
W.FT H.FT
WB2015 + 0.45 0.75
WB2014 □ 0.37 0.62
WB2013 X 0.22 0.38
-180
-120
-60
0
60
120
180
ORIENTATION ANGLE. DEGREES
28JUN77

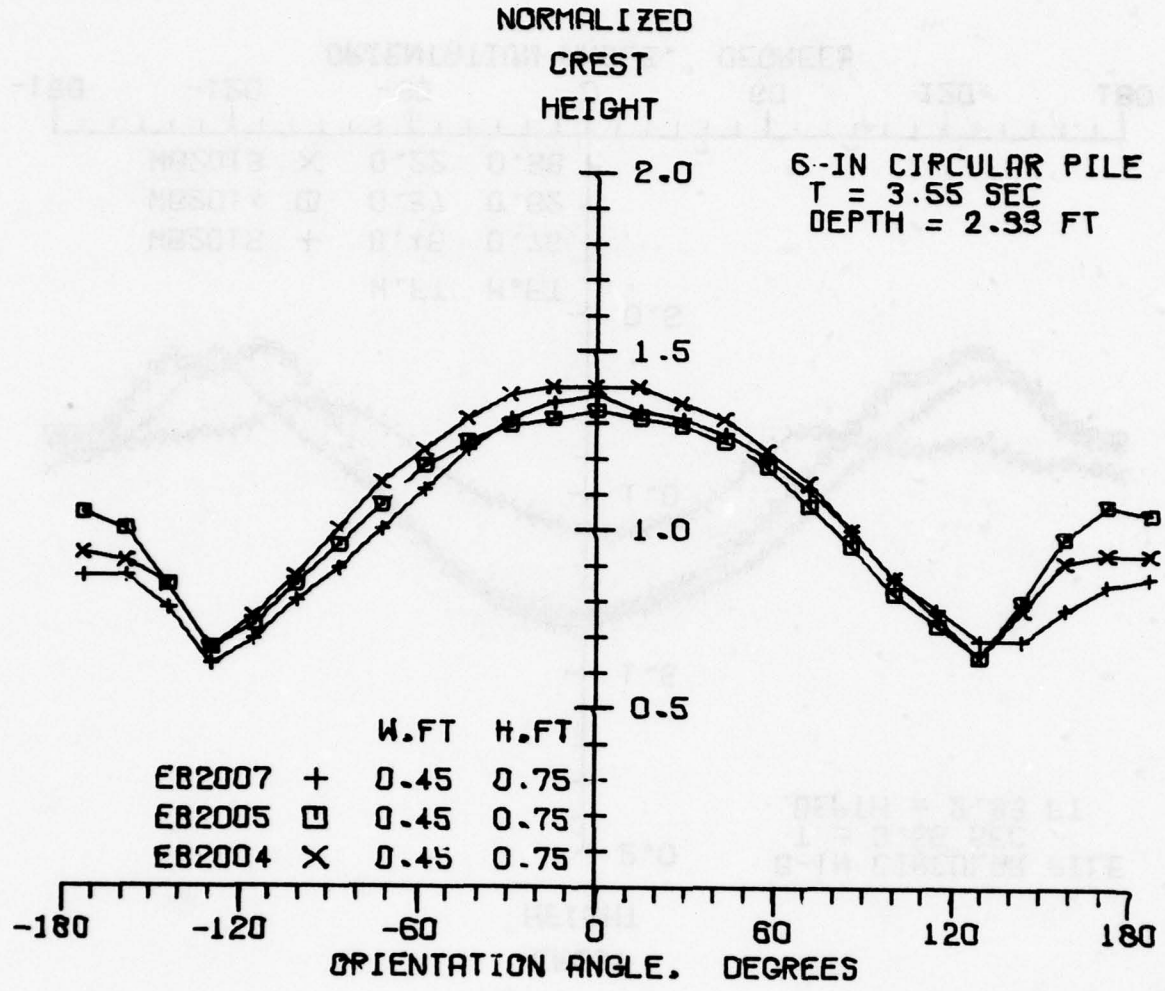
NORMALIZED
CREST
HEIGHT
6-IN CIRCULAR PILE
T = 3.55 SEC
DEPTH = 2.33 FT
2.0
1.5
1.0
0.5
W.FT H.FT
EB2007 + 0.45 0.75
EB2005 □ 0.45 0.75
EB2004 X 0.45 0.75
-180
-120
-60
0
60
120
180
ORIENTATION ANGLE, DEGREES
28JUN77

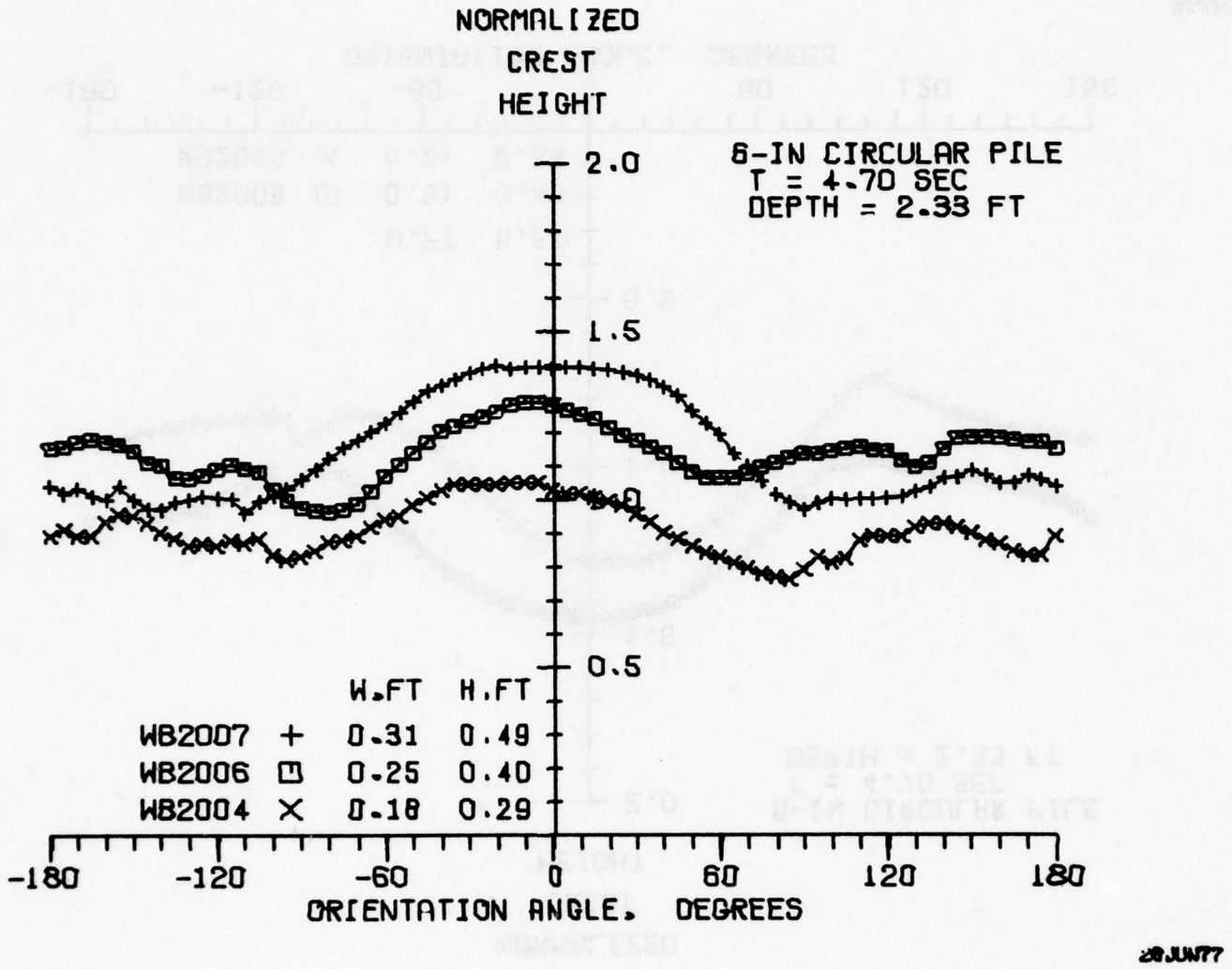
NORMALIZED
CREST
HEIGHT
6-IN CIRCULAR PILE
T = 4.70 SEC
DEPTH = 2.33 FT
2.0
1.5
1.0
0.5
W,FT H,FT
WB2007 + 0.31 0.49
WB2006 □ 0.25 0.40
WB2004 × 0.18 0.29
-180
-120
-60
0
60
120
180
ORIENTATION ANGLE, DEGREES
28JUN77

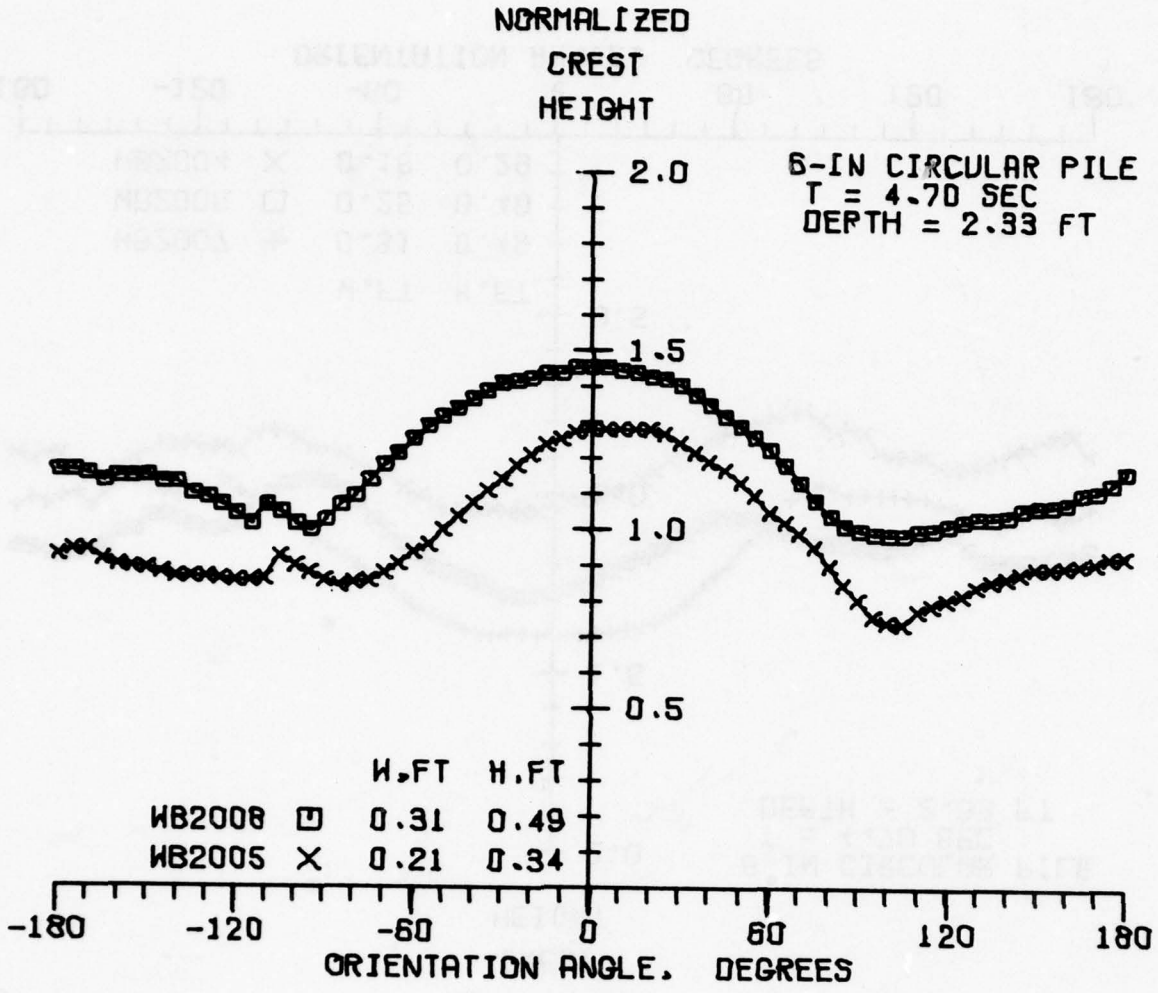
NORMALIZED
CREST
HEIGHT
6-IN CIRCULAR PILE
T = 4.70 SEC
DEPTH = 2.33 FT
2.0
1.5
1.0
0.5
W,FT H,FT
WB2008 0.31 0.49
WB2005 0.21 0.34
-180
-120
-60
0
60
120
180
ORIENTATION ANGLE, DEGREES
30JUN77

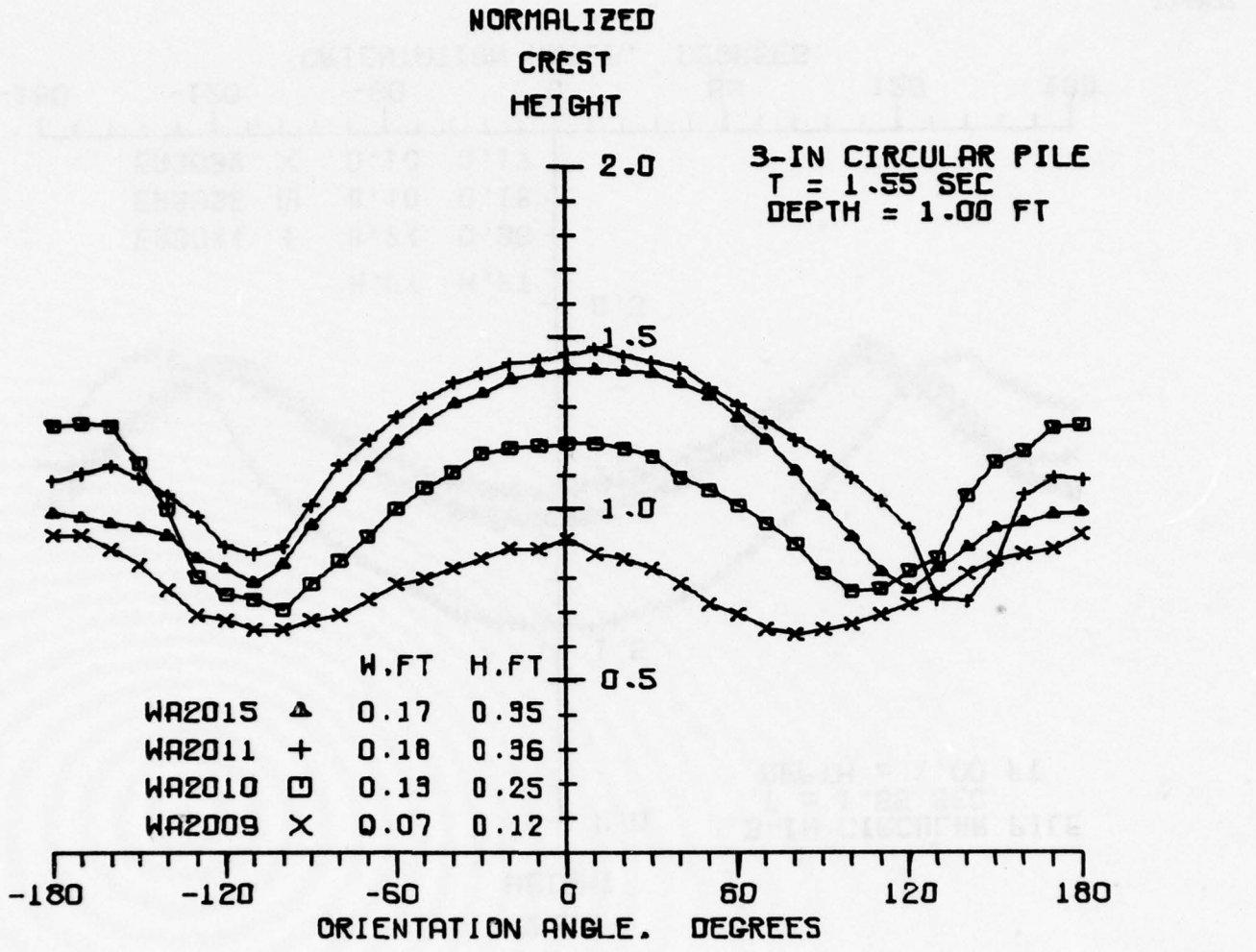
NORMALIZED
CREST
HEIGHT
3-IN CIRCULAR PILE
T = 1.55 SEC
DEPTH = 1.00 FT
2.0
1.5
1.0
0.5
W,FT H,FT
WA2015 0.17 0.35
WA2011 0.18 0.36
WA2010 0.13 0.25
WA2009 0.07 0.12
-180
-120
-60
0
60
120
180
ORIENTATION ANGLE. DEGREES
29JUN77

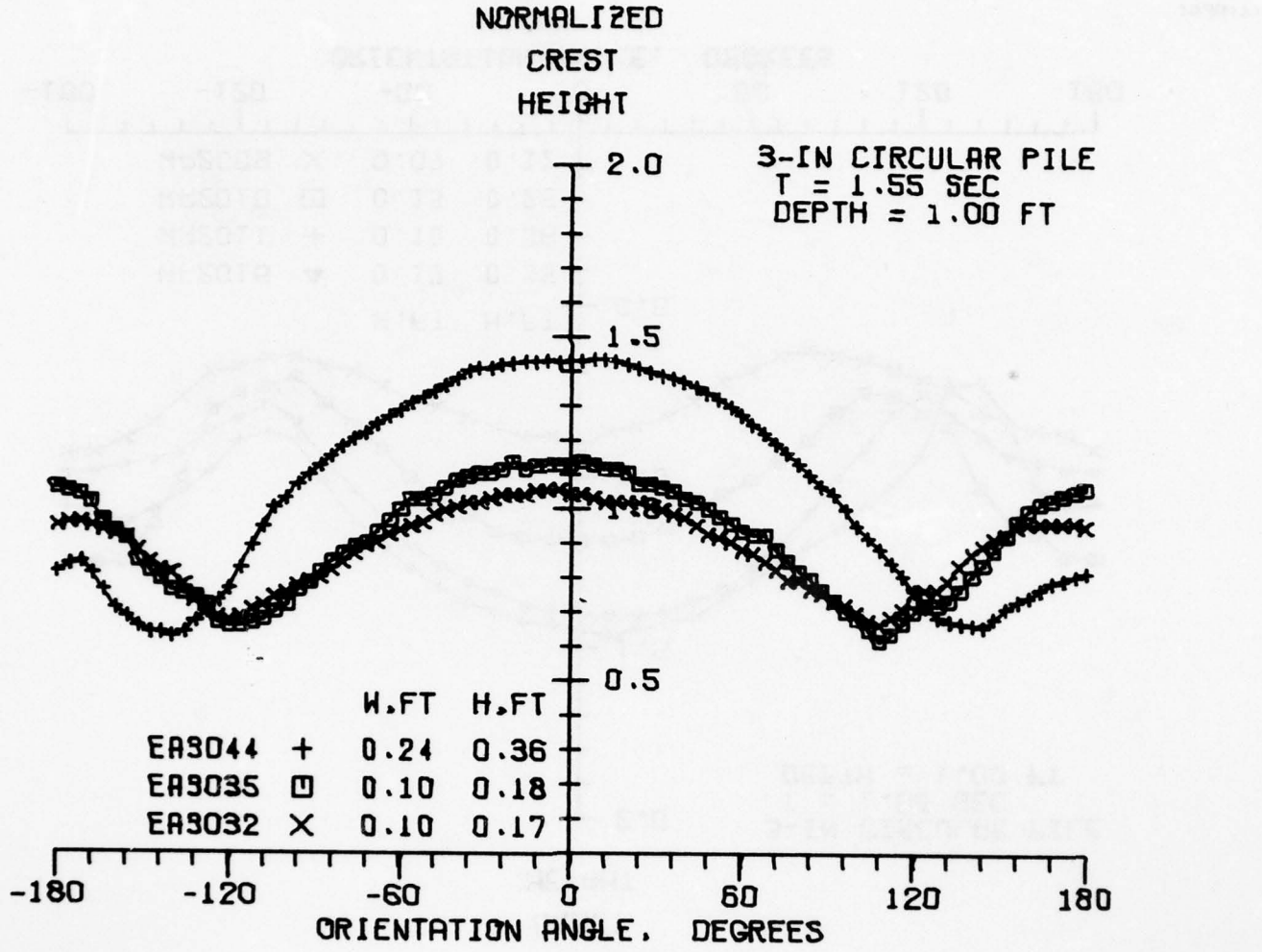
NORMALIZED
CREST
HEIGHT
3-IN CIRCULAR PILE
T = 1.55 SEC
DEPTH = 1.00 FT
2.0
1.5
1.0
0.5
W,FT H,FT
EA3044 + 0.24 0.36
EA3035 □ 0.10 0.18
EA3032 X 0.10 0.17
-180
-120
-60
0
60
120
180
ORIENTATION ANGLE, DEGREES
29JUN77

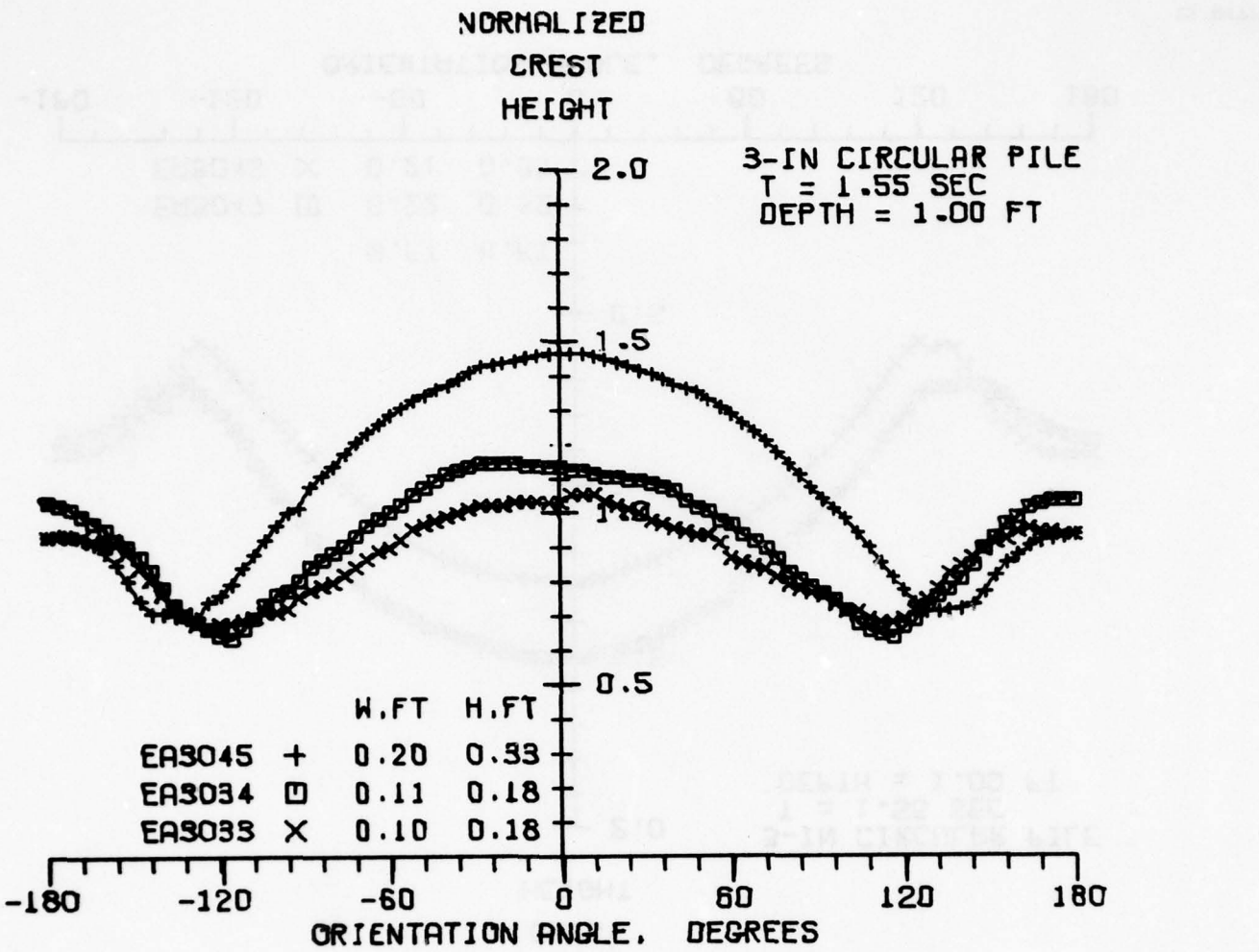
NORMALIZED
CREST
HEIGHT
3-IN CIRCULAR PILE
T = 1.55 SEC
DEPTH = 1.00 FT
2.0
1.5
1.0
0.5
W,FT H,FT
EA3045 + 0.20 0.33
EA3034 □ 0.11 0.18
EA3033 X 0.10 0.18
-180
-120
-60
0
60
120
180
ORIENTATION ANGLE, DEGREES
29JUN77

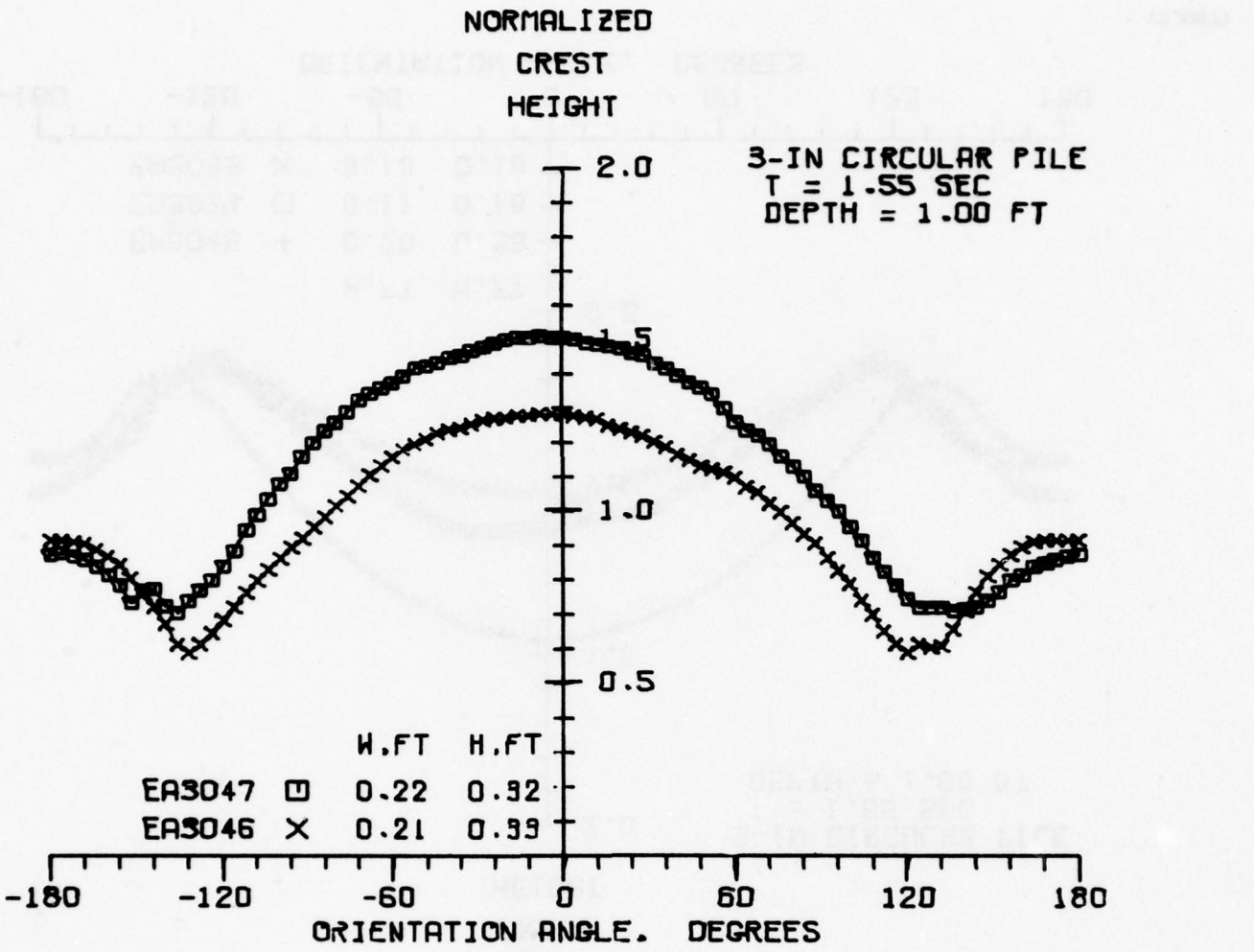
NORMALIZED
CREST
HEIGHT
3-IN CIRCULAR PILE
T = 1.55 SEC
DEPTH = 1.00 FT
2.0
1.5
1.0
0.5
W,FT H,FT
EA3047 □ 0.22 0.92
EA3046 X 0.21 0.99
-180 -120 -60 0 60 120 180
ORIENTATION ANGLE, DEGREES
23 JUN 77

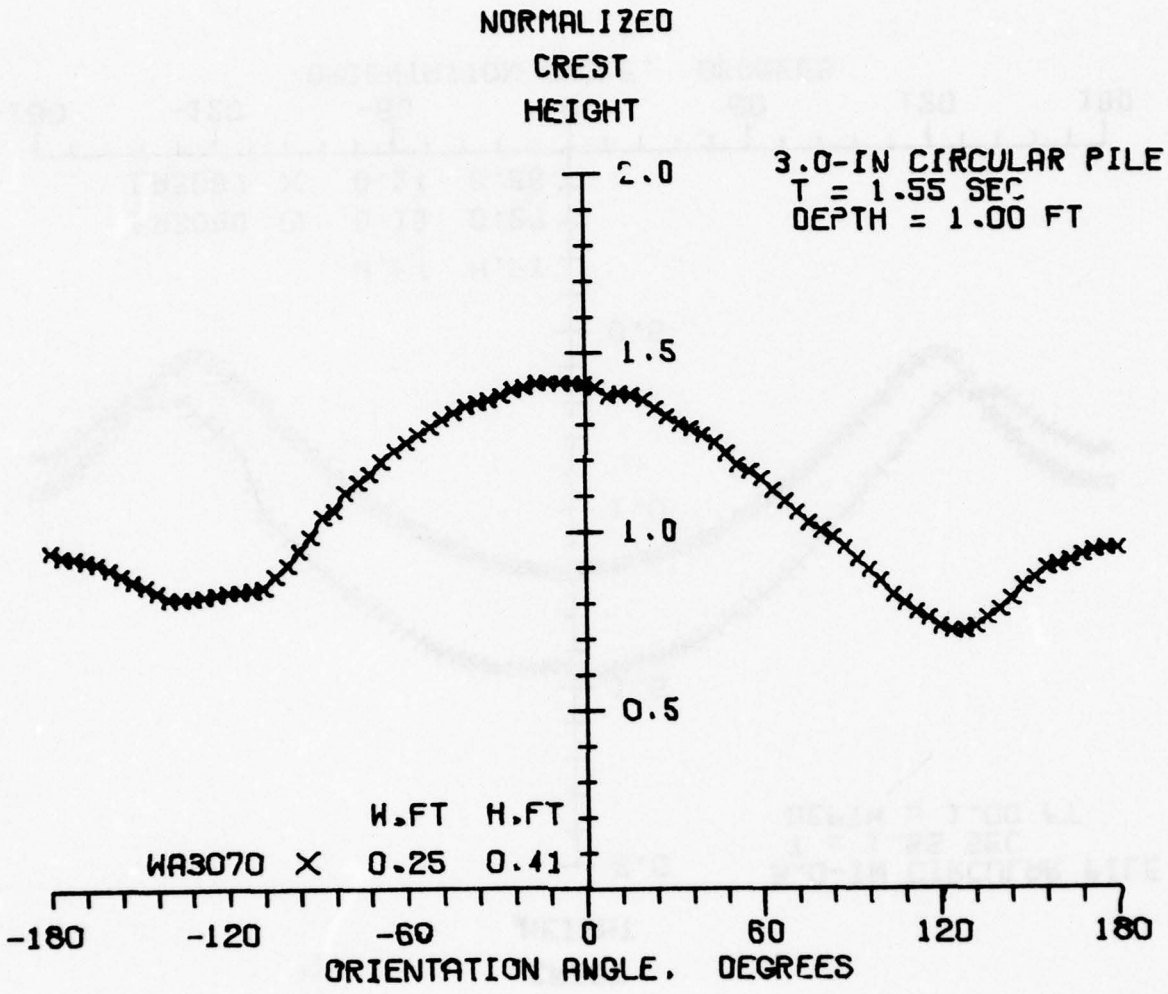
NORMALIZED
CREST
HEIGHT
3.0-IN CIRCULAR PILE
T = 1.55 SEC
DEPTH = 1.00 FT
2.0
1.5
1.0
0.5
W,FT H,FT
WA3070 X 0.25 0.41
-180
-120
-60
0
60
120
180
ORIENTATION ANGLE, DEGREES

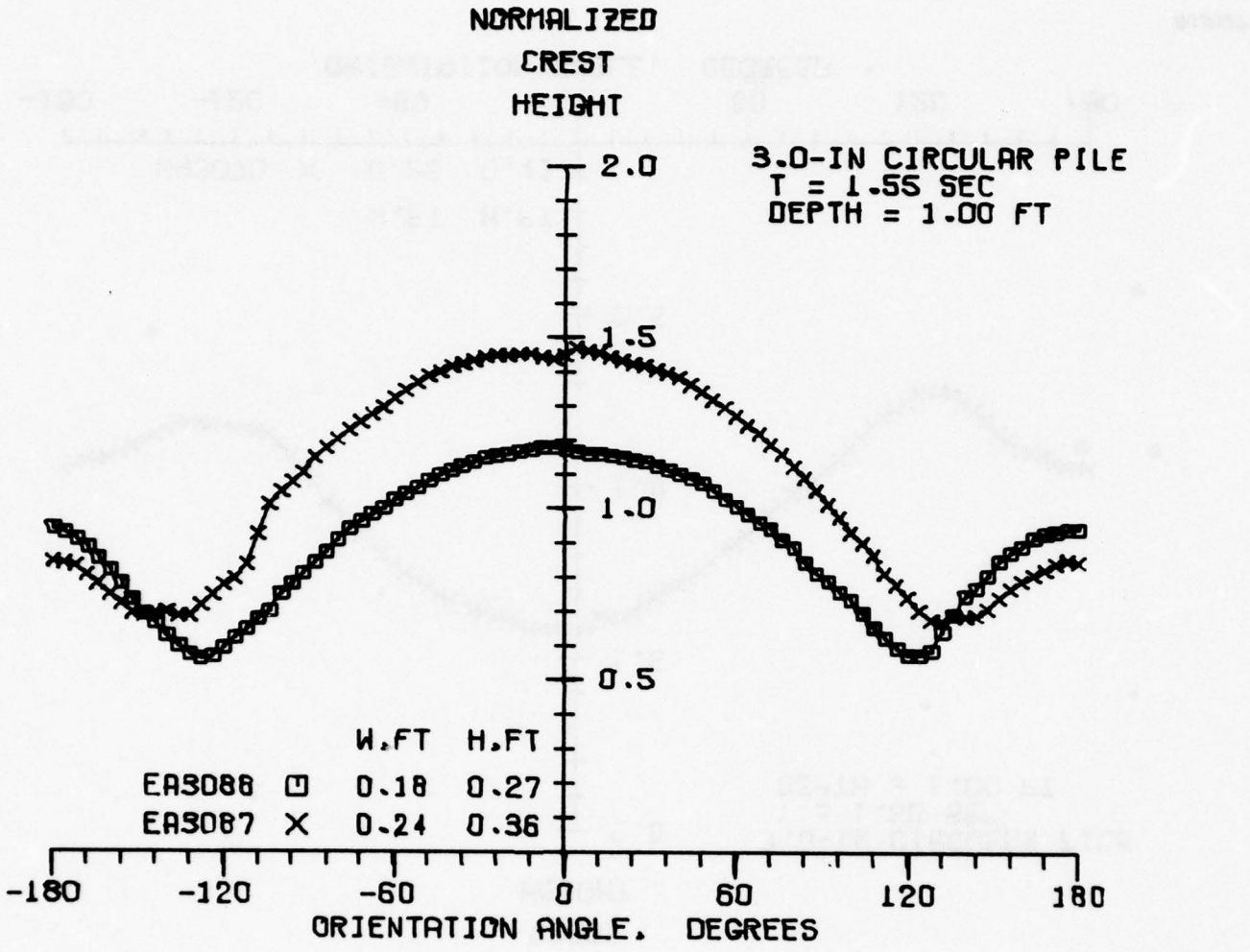
NORMALIZED
CREST
HEIGHT
3.0-IN CIRCULAR PILE
T = 1.55 SEC
DEPTH = 1.00 FT
2.0
1.5
1.0
0.5
W,FT H,FT
EA3088 0.18 0.27
EA3087 0.24 0.36
-180
-120
-60
0
60
120
180
ORIENTATION ANGLE, DEGREES
29JUN77

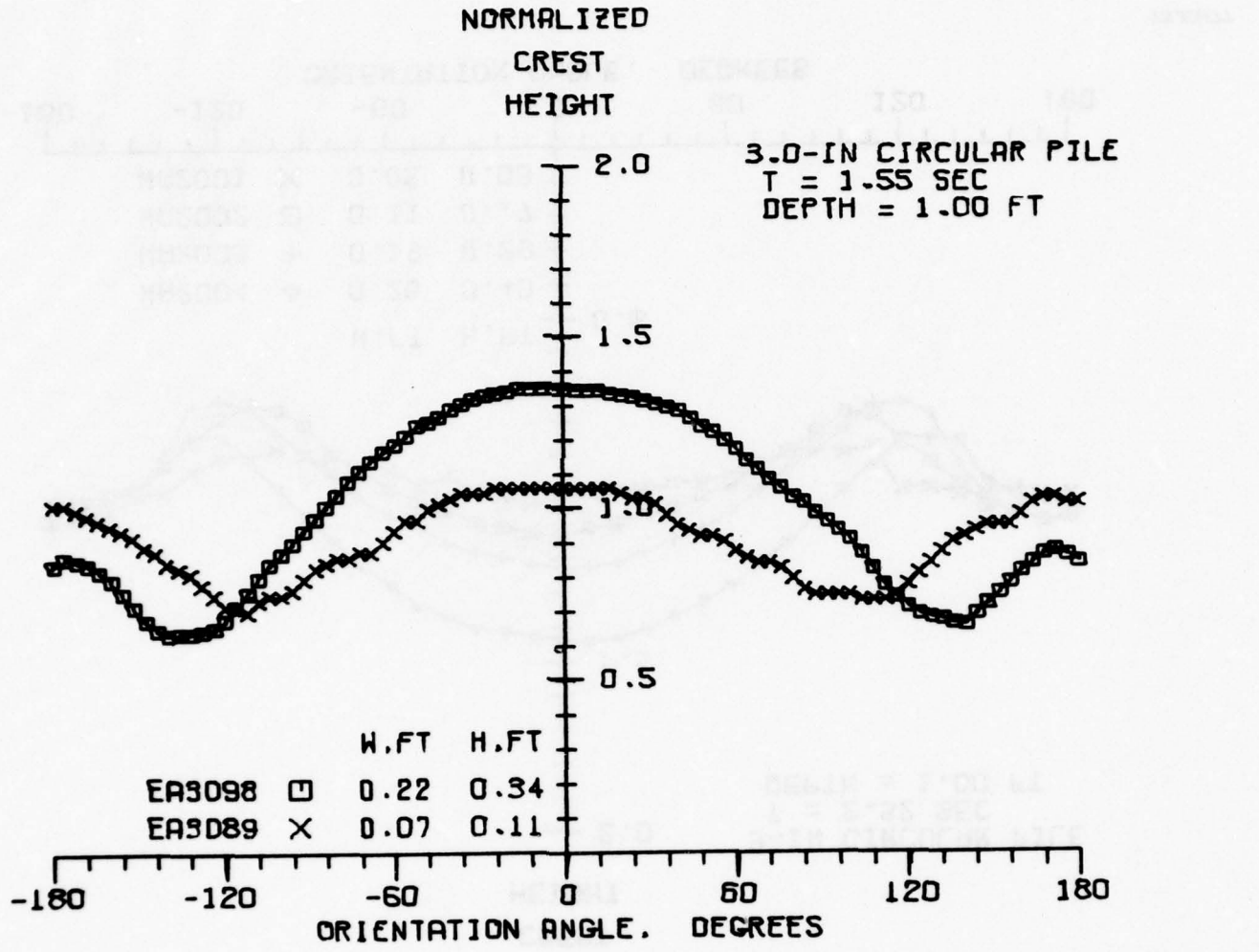
NORMALIZED
CREST
HEIGHT
3.0-IN CIRCULAR PILE
T = 1.55 SEC
DEPTH = 1.00 FT
2.0
1.5
1.0
0.5
W,FT H,FT
EA3098 □ 0.22 0.34
EA3D89 X 0.07 0.11
-180
-120
-60
0
60
120
180
ORIENTATION ANGLE. DEGREES
23JUN77

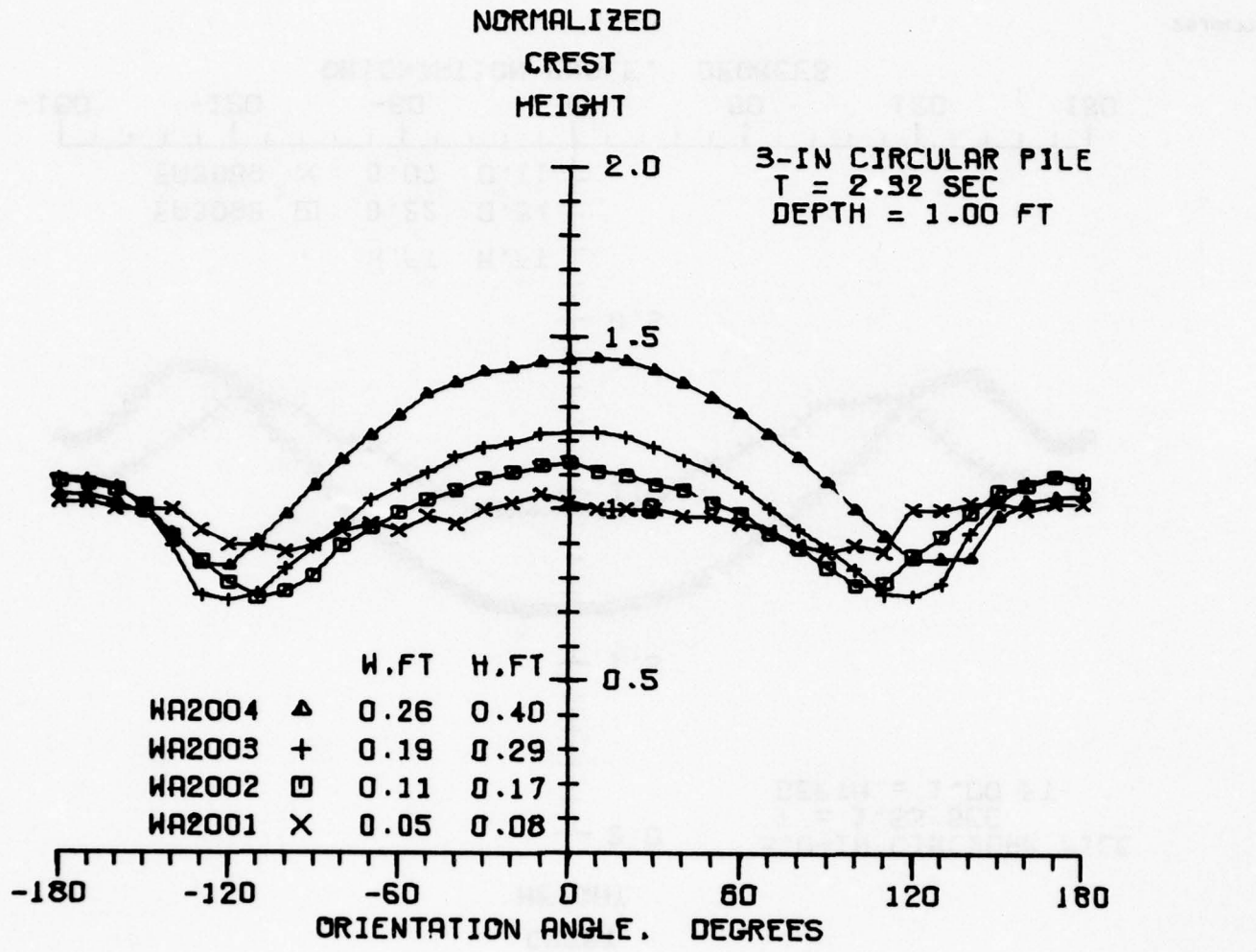
NORMALIZED
CREST
HEIGHT
3-IN CIRCULAR PILE
T = 2.32 SEC
DEPTH = 1.00 FT
2.0
1.5
1.0
0.5
W.FT H.FT
WA2004 0.26 0.40
WA2003 0.19 0.29
WA2002 0.11 0.17
WA2001 0.05 0.08
-180
-120
-60
0
60
120
180
ORIENTATION ANGLE, DEGREES
29JUN77

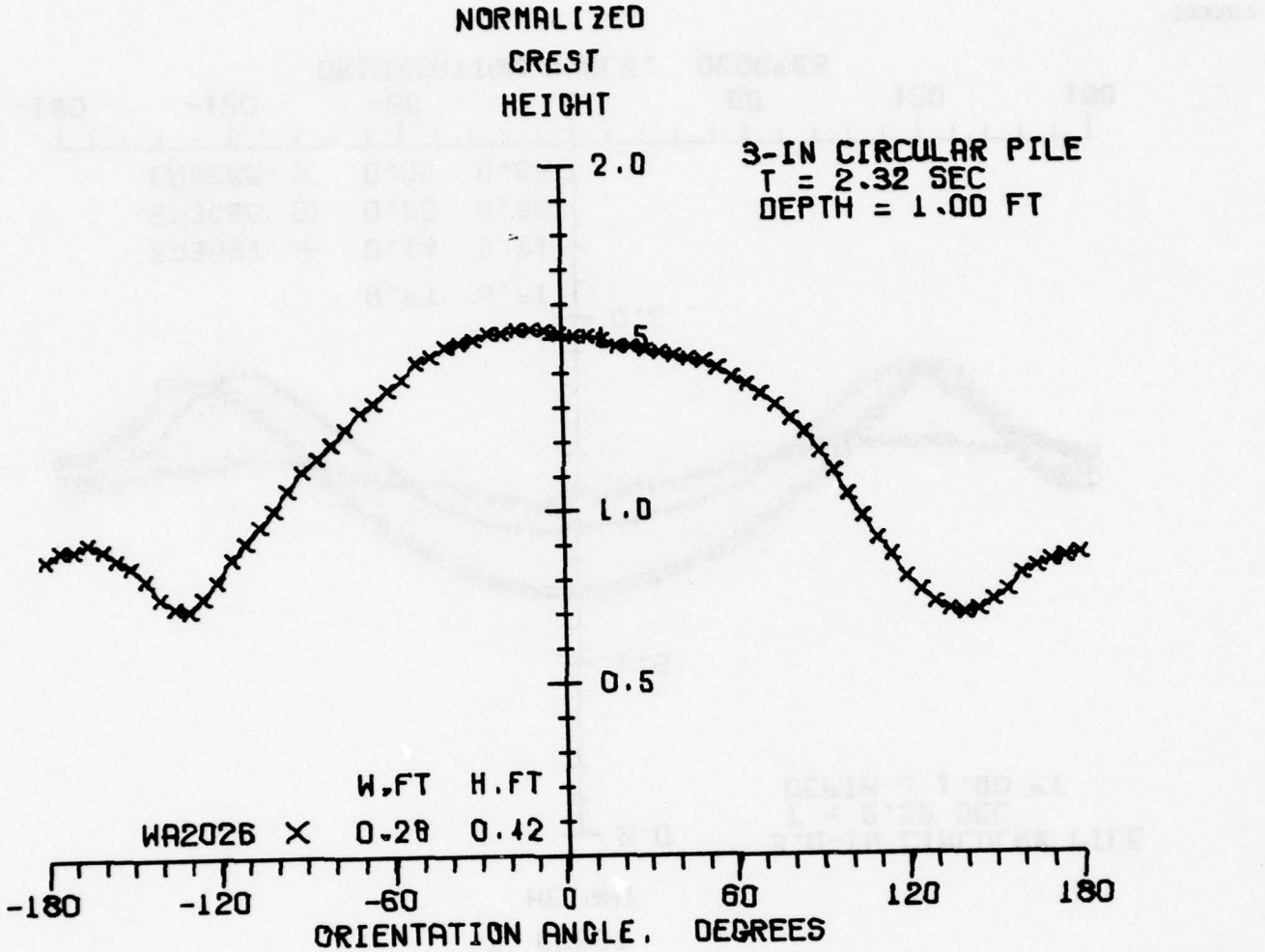
NORMALIZED
CREST
HEIGHT
3-IN CIRCULAR PILE
T = 2.32 SEC
DEPTH = 1.00 FT
2.0
1.5
1.0
0.5
W,FT H,FT
WA2026 X 0.28 0.42
-180
-120
-60
0
60
120
180
ORIENTATION ANGLE, DEGREES
06JUL77

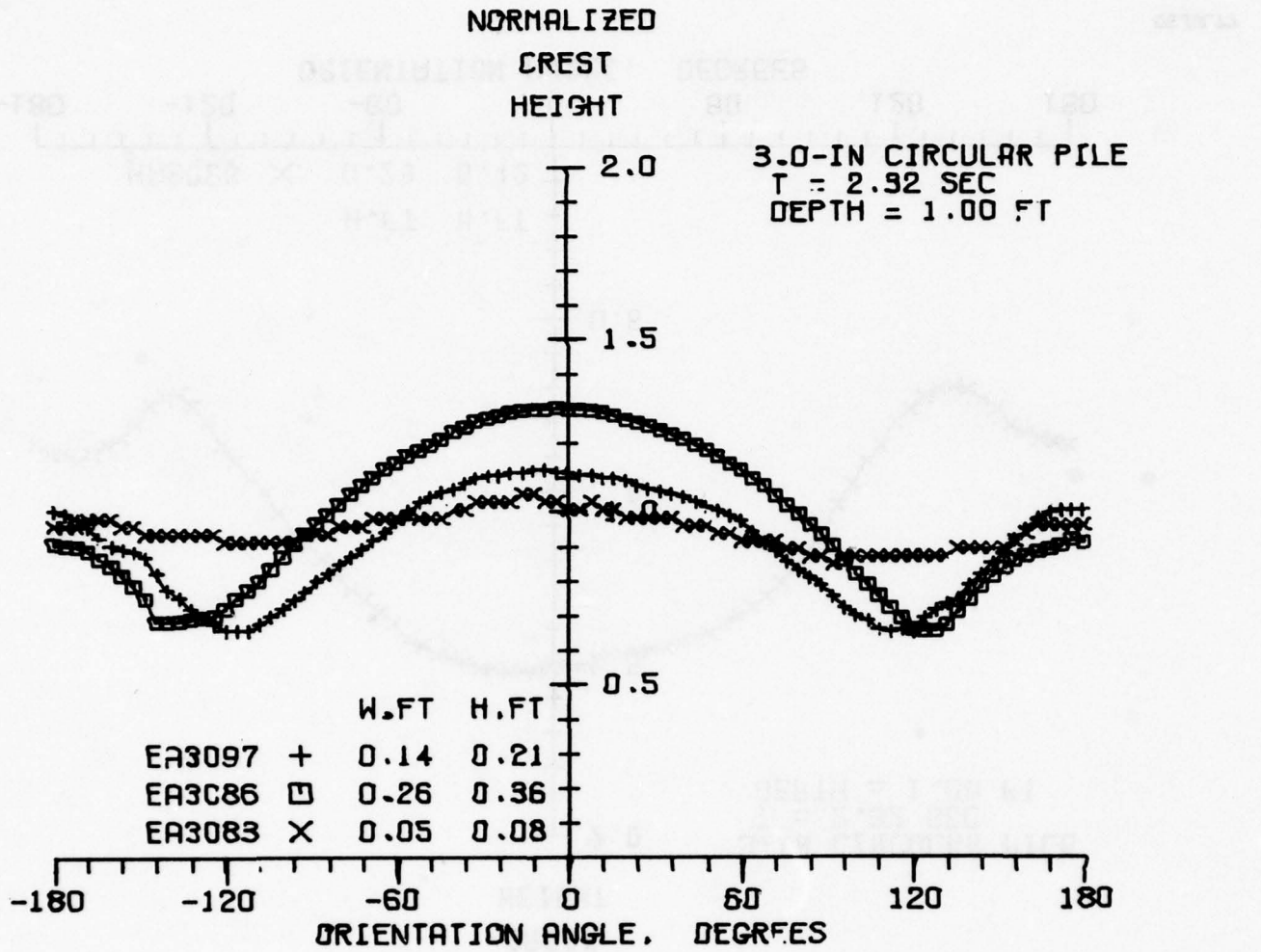
NORMALIZED
CREST
HEIGHT
3.0-IN CIRCULAR PILE
T = 2.92 SEC
DEPTH = 1.00 FT
2.0
1.5
0.5
W,FT H,FT
EA3097 + 0.14 0.21
EA3086 □ 0.26 0.36
EA3083 X 0.05 0.08
-180
-120
-60
0
60
120
180
ORIENTATION ANGLE, DEGREES
30JUN77

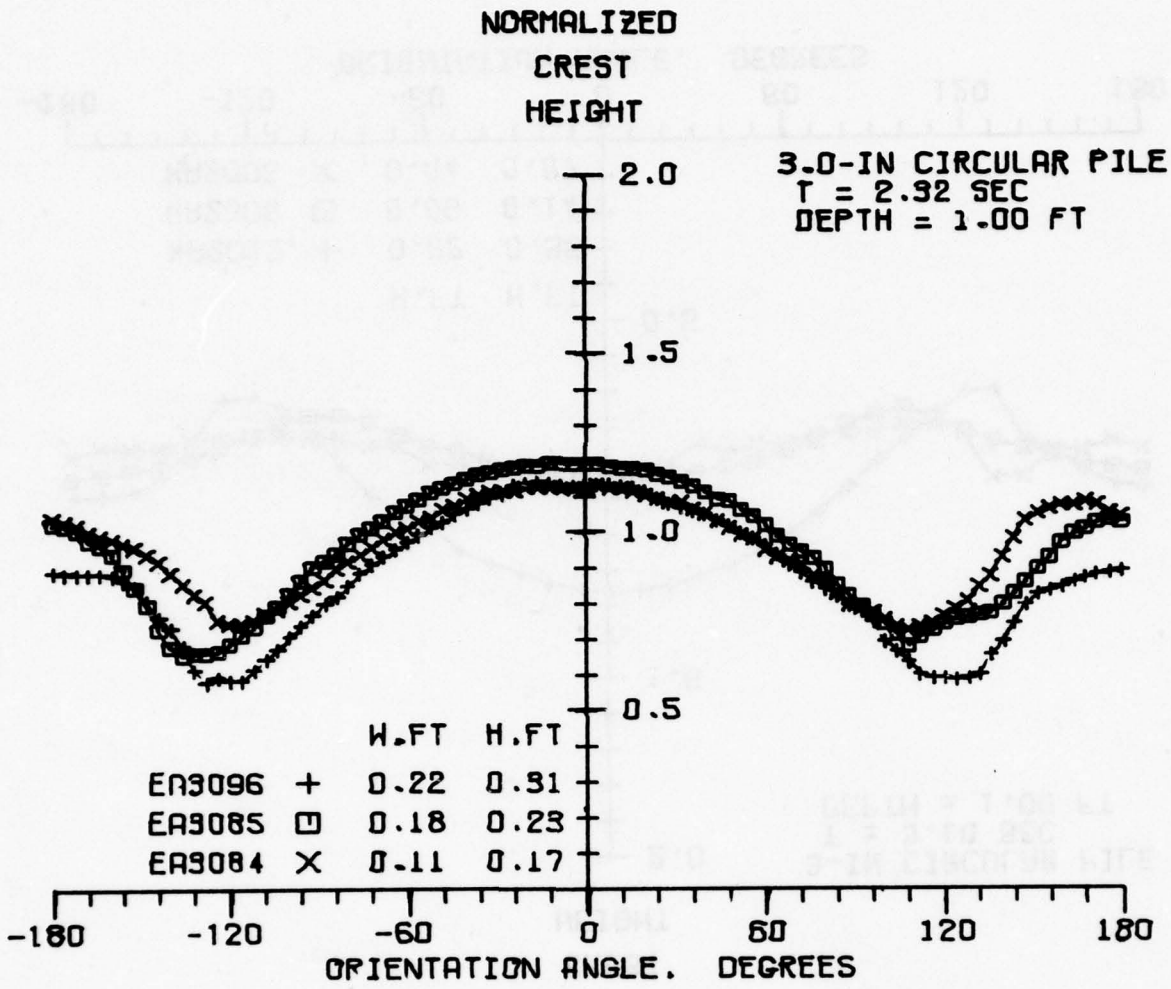
NORMALIZED
CREST
HEIGHT
3.0-IN CIRCULAR PILE
T = 2.32 SEC
DEPTH = 1.00 FT
2.0
1.5
1.0
0.5
W.FT H.FT
EA3096 + 0.22 0.31
EA3085 □ 0.18 0.23
EA3084 X 0.11 0.17
-180
-120
-60
0
60
120
180
ORIENTATION ANGLE. DEGREES
30JUN77

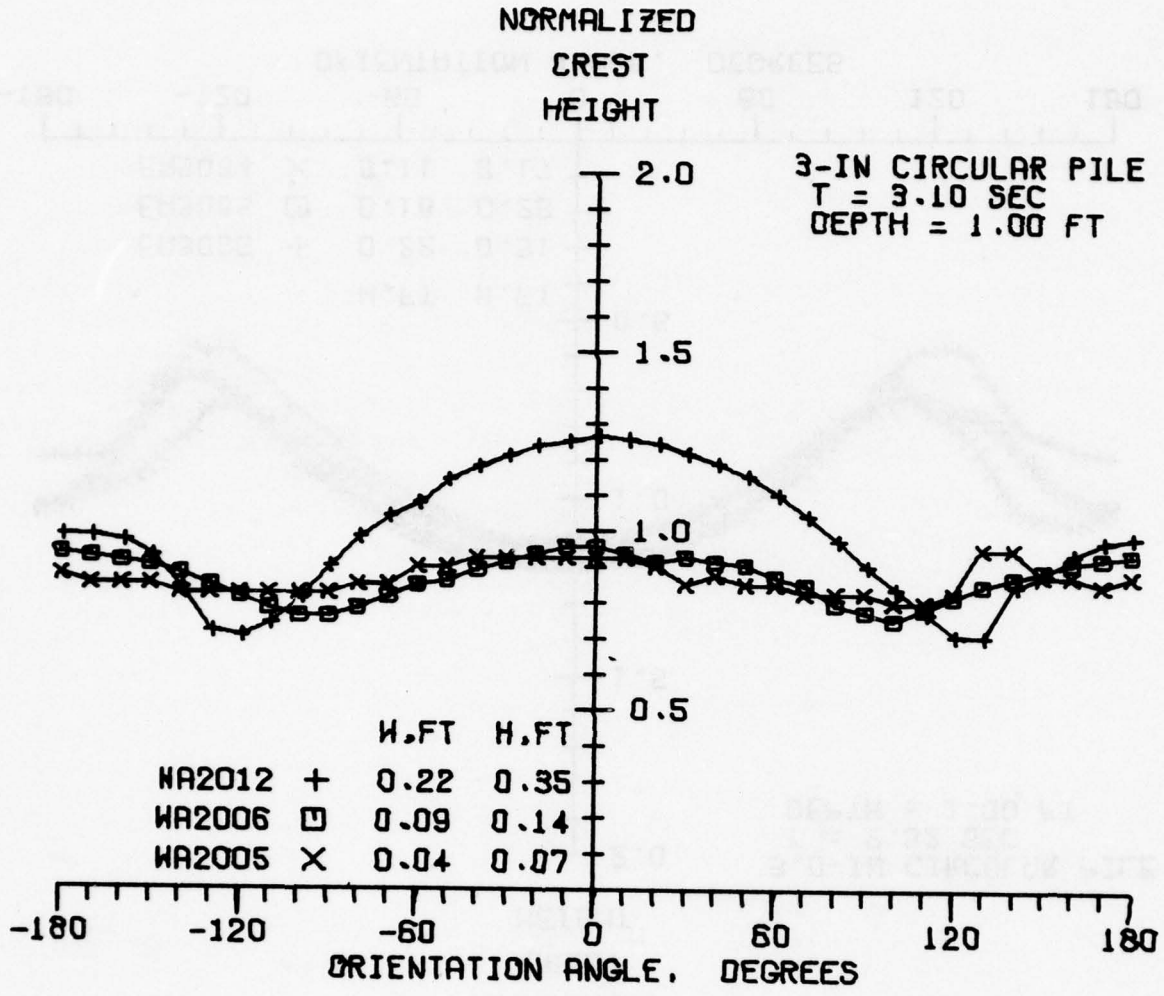
NORMALIZED
CREST
HEIGHT
3-IN CIRCULAR PILE
T = 3.10 SEC
DEPTH = 1.00 FT
2.0
1.5
1.0
0.5
H,FT H,FT
WA2012 + 0.22 0.35
WA2006 □ 0.09 0.14
WA2005 X 0.04 0.07
-180
-120
-60
0
60
120
180
ORIENTATION ANGLE, DEGREES
29JUN77

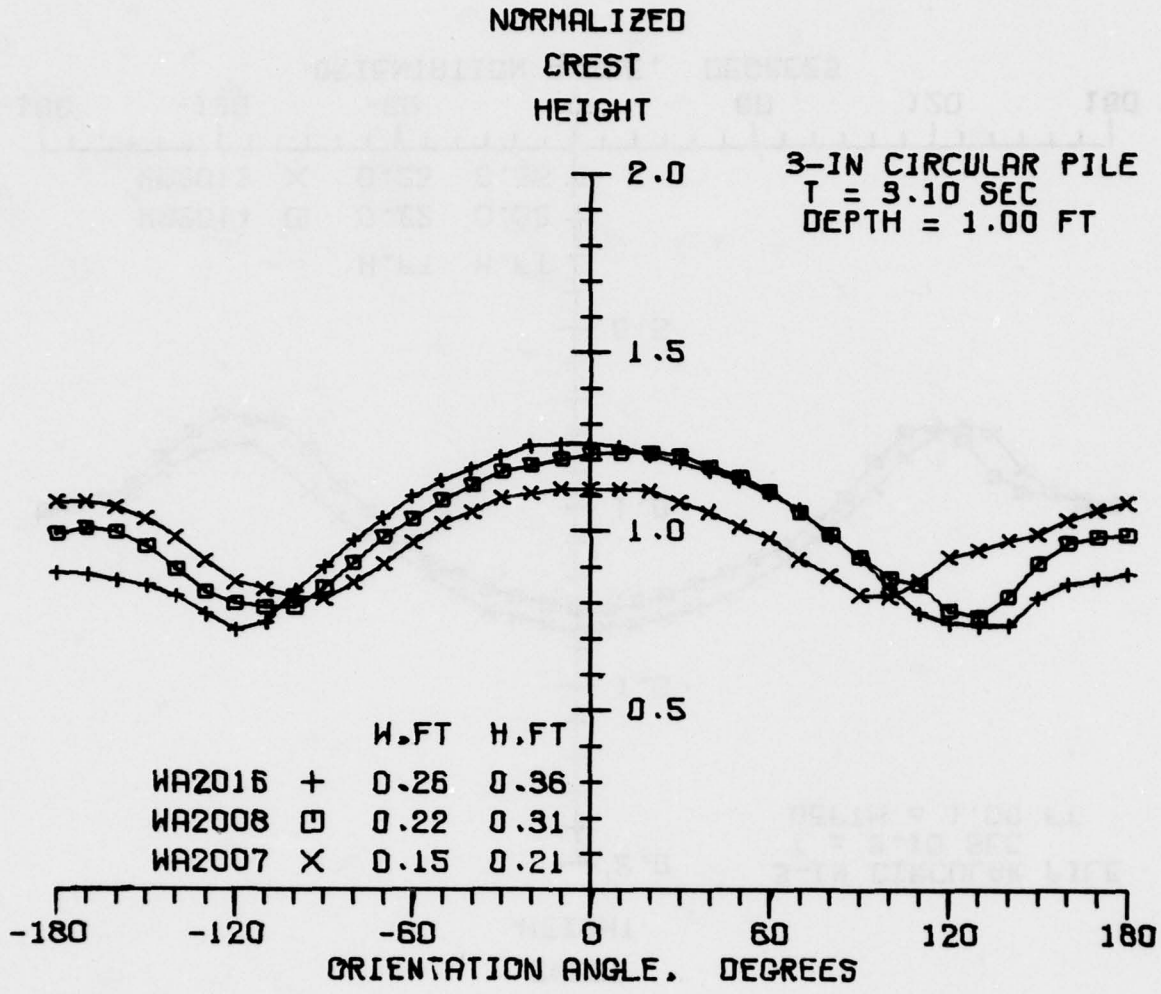
NORMALIZED
CREST
HEIGHT
3-IN CIRCULAR PILE
T = 3.10 SEC
DEPTH = 1.00 FT
2.0
1.5
1.0
0.5
H,FT H,FT
WA2016 + 0.26 0.36
WA2008 ⊡ 0.22 0.31
WA2007 X 0.15 0.21
-180
-120
-60
0
60
120
180
ORIENTATION ANGLE, DEGREES
28JUN77

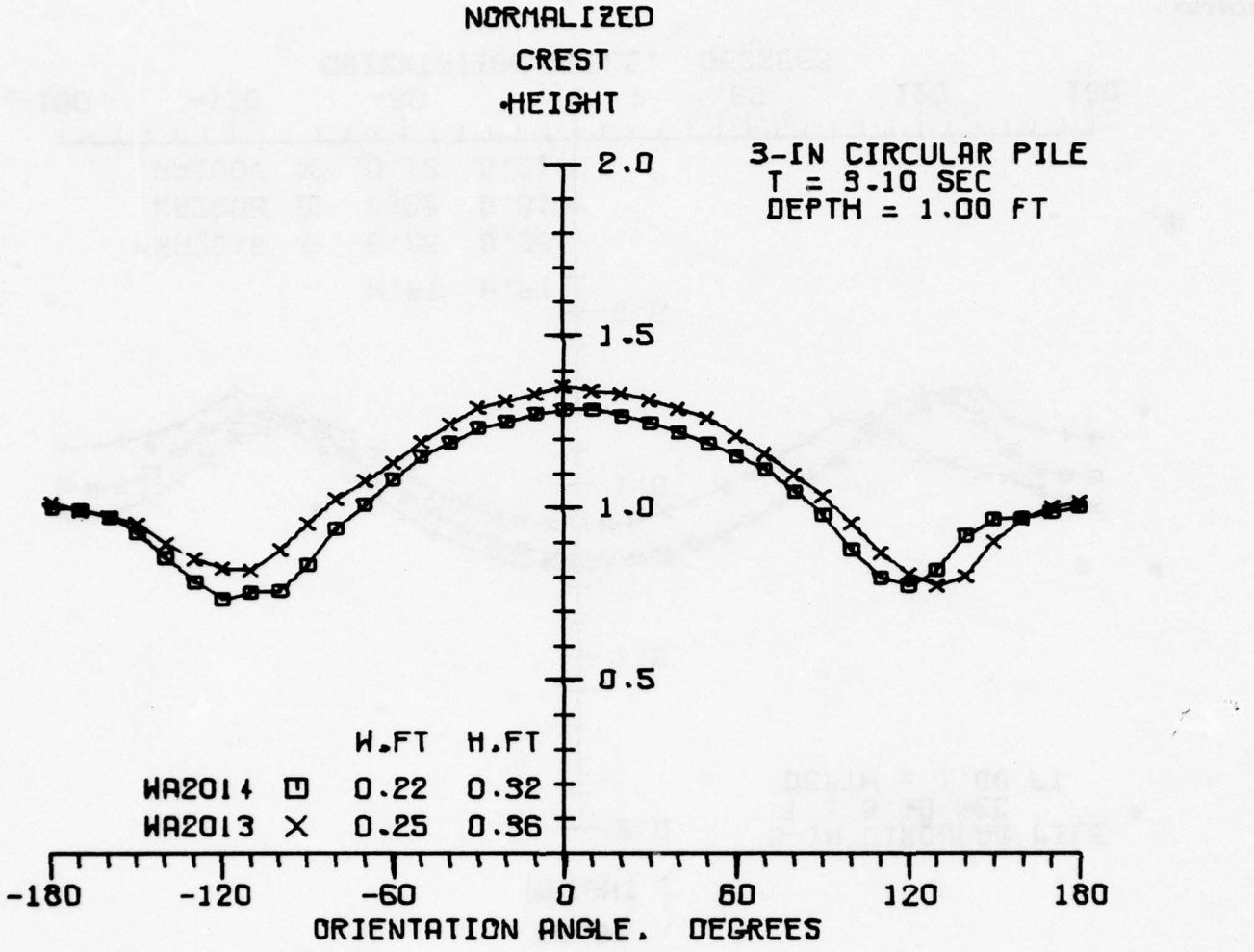
NORMALIZED
CREST
HEIGHT
3-IN CIRCULAR PILE
T = 3.10 SEC
DEPTH = 1.00 FT
2.0
1.5
1.0
0.5
H,FT H,FT
WA2014 0.22 0.32
WA2013 0.25 0.36
-180
-120
-60
0
60
120
180
ORIENTATION ANGLE, DEGREES
23JUN77

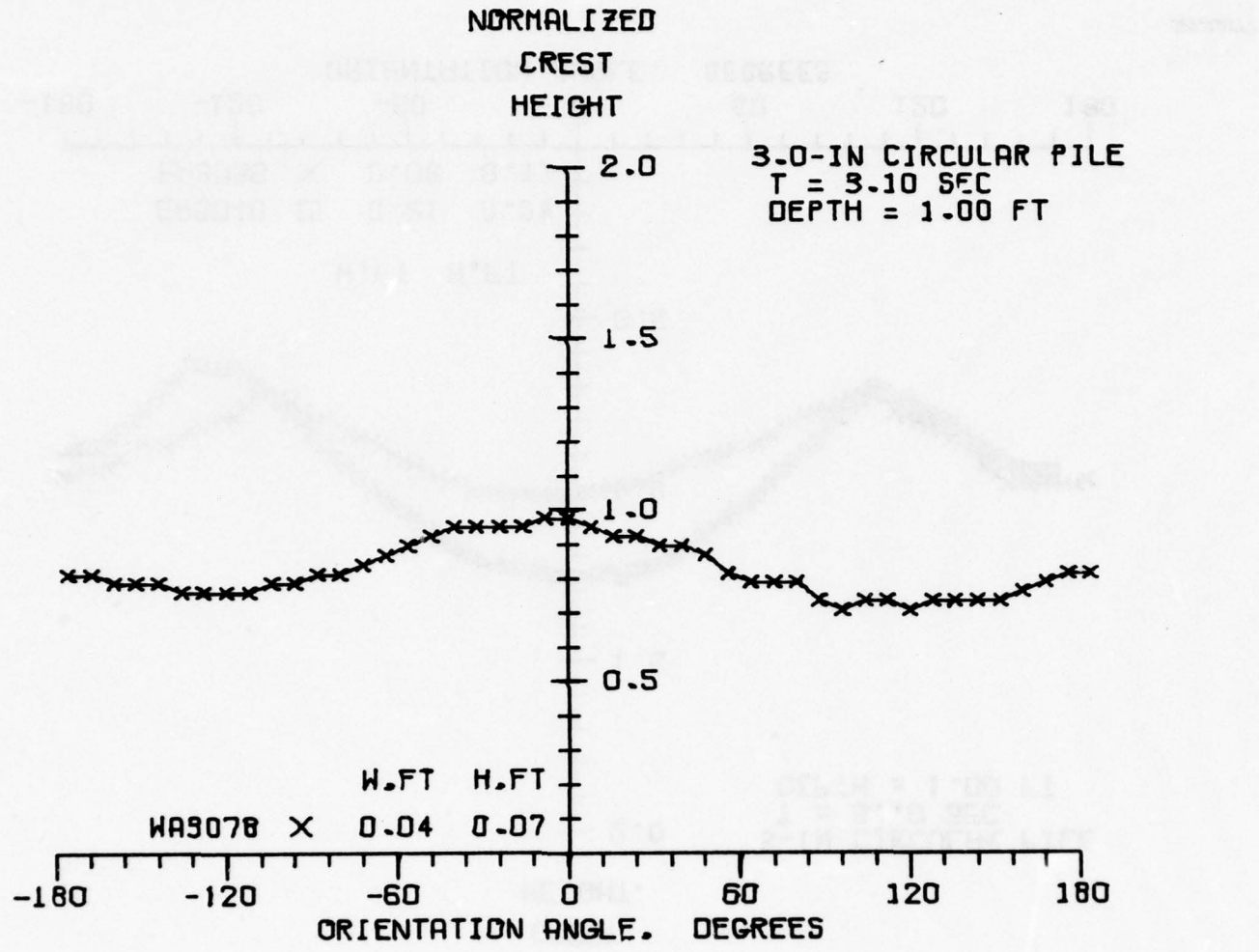
NORMALIZED
CREST
HEIGHT
3.0-IN CIRCULAR PILE
T = 3.10 SEC
DEPTH = 1.00 FT
2.0
1.5
1.0
0.5
W.FT H.FT
WA9078 X 0.04 0.07
-180
-120
-60
0
60
120
180
ORIENTATION ANGLE. DEGREES
28JUN77

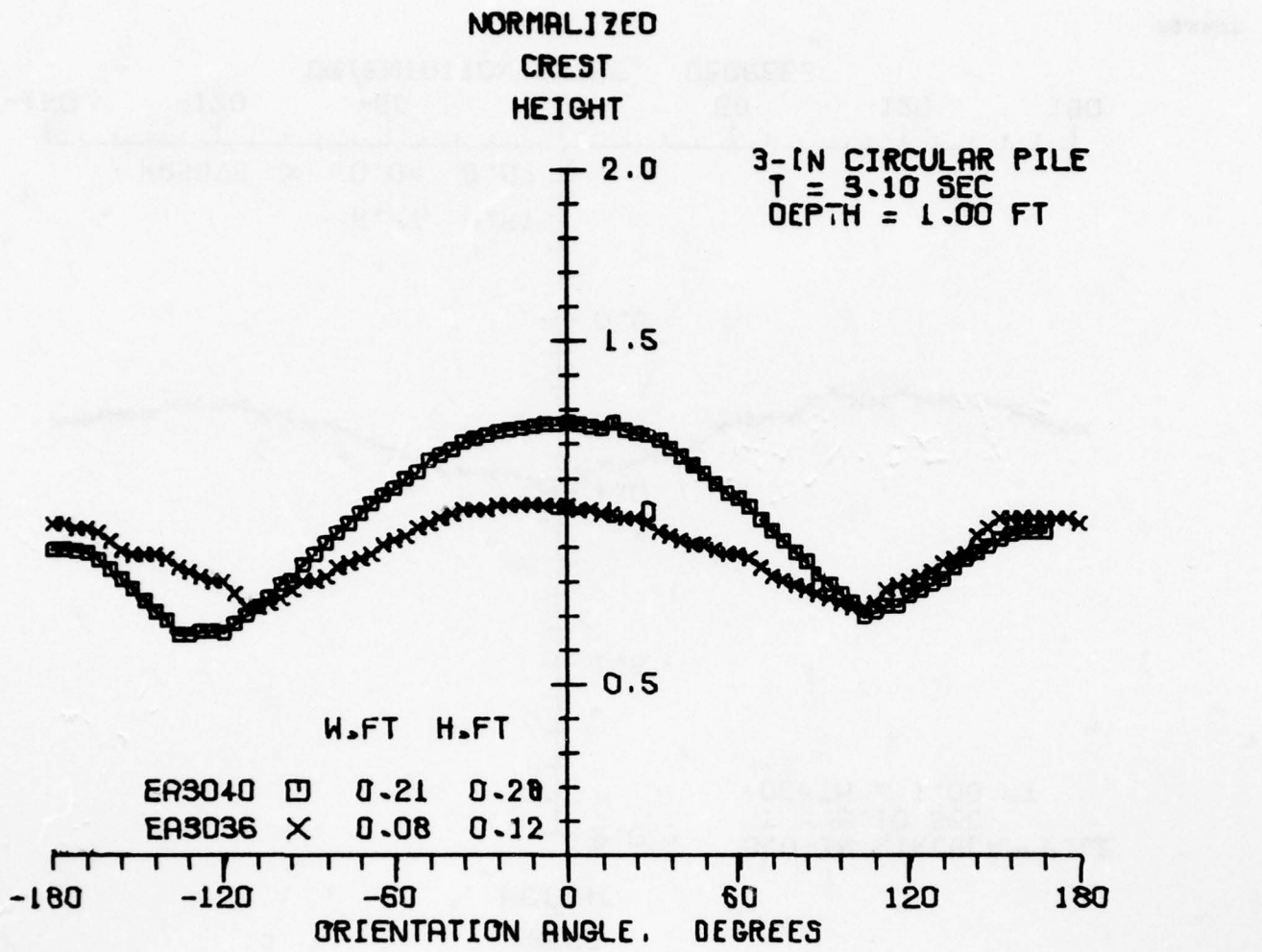
NORMALIZED
CREST
HEIGHT
3-IN CIRCULAR PILE
T = 3.10 SEC
DEPTH = 1.00 FT
2.0
1.5
1.0
0.5
W,FT H,FT
EA3040 □ 0.21 0.20
EA3036 × 0.08 0.12
-180
-120
-60
0
60
120
180
ORIENTATION ANGLE, DEGREES
SEJUN77

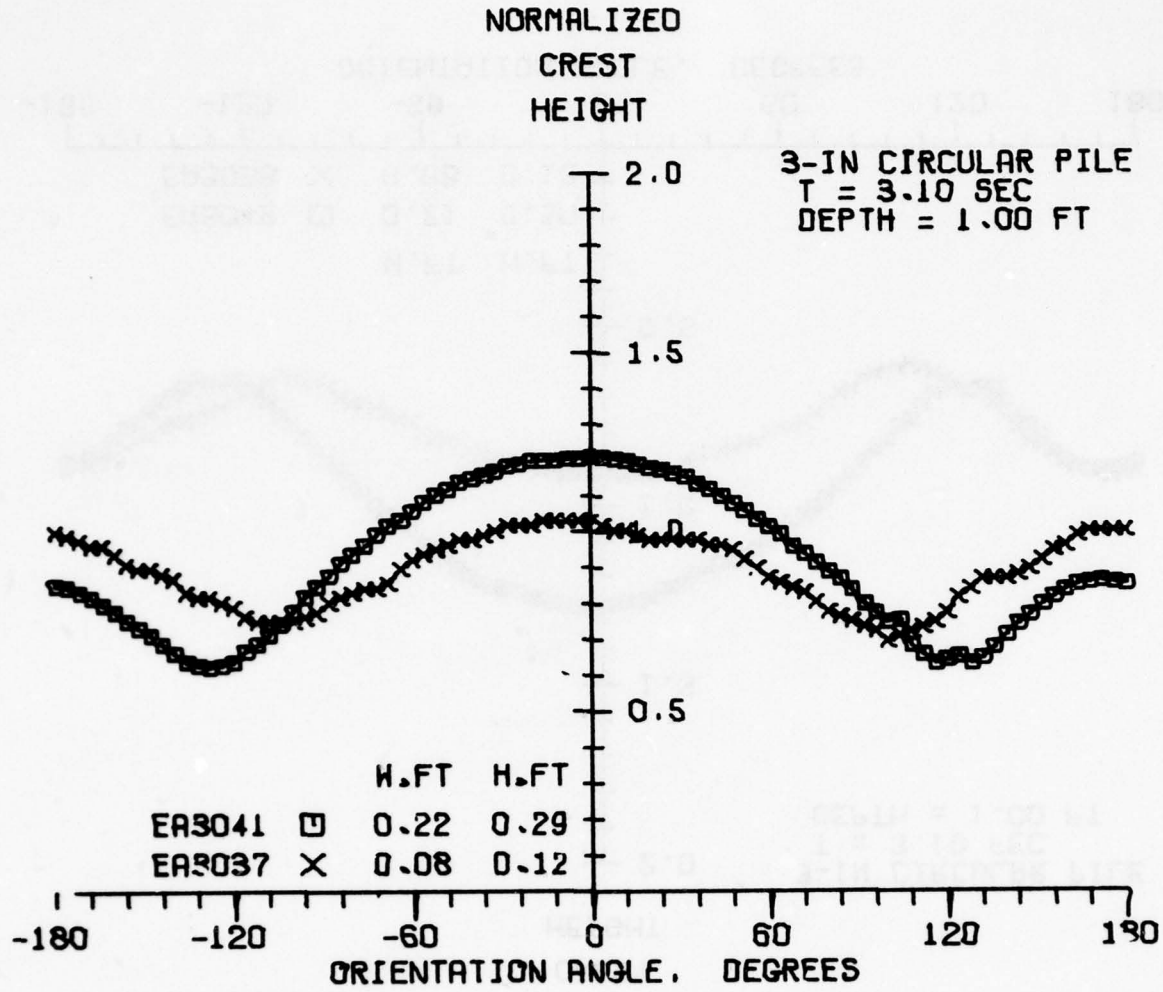
NORMALIZED
CREST
HEIGHT
3-IN CIRCULAR PILE
T = 3.10 SEC
DEPTH = 1.00 FT
2.0
1.5
1.0
0.5
H,FT H,FT
EA3041 □ 0.22 0.29
EA3037 × 0.08 0.12
-180
-120
-60
0
60
120
180
ORIENTATION ANGLE, DEGREES
08.XX.77

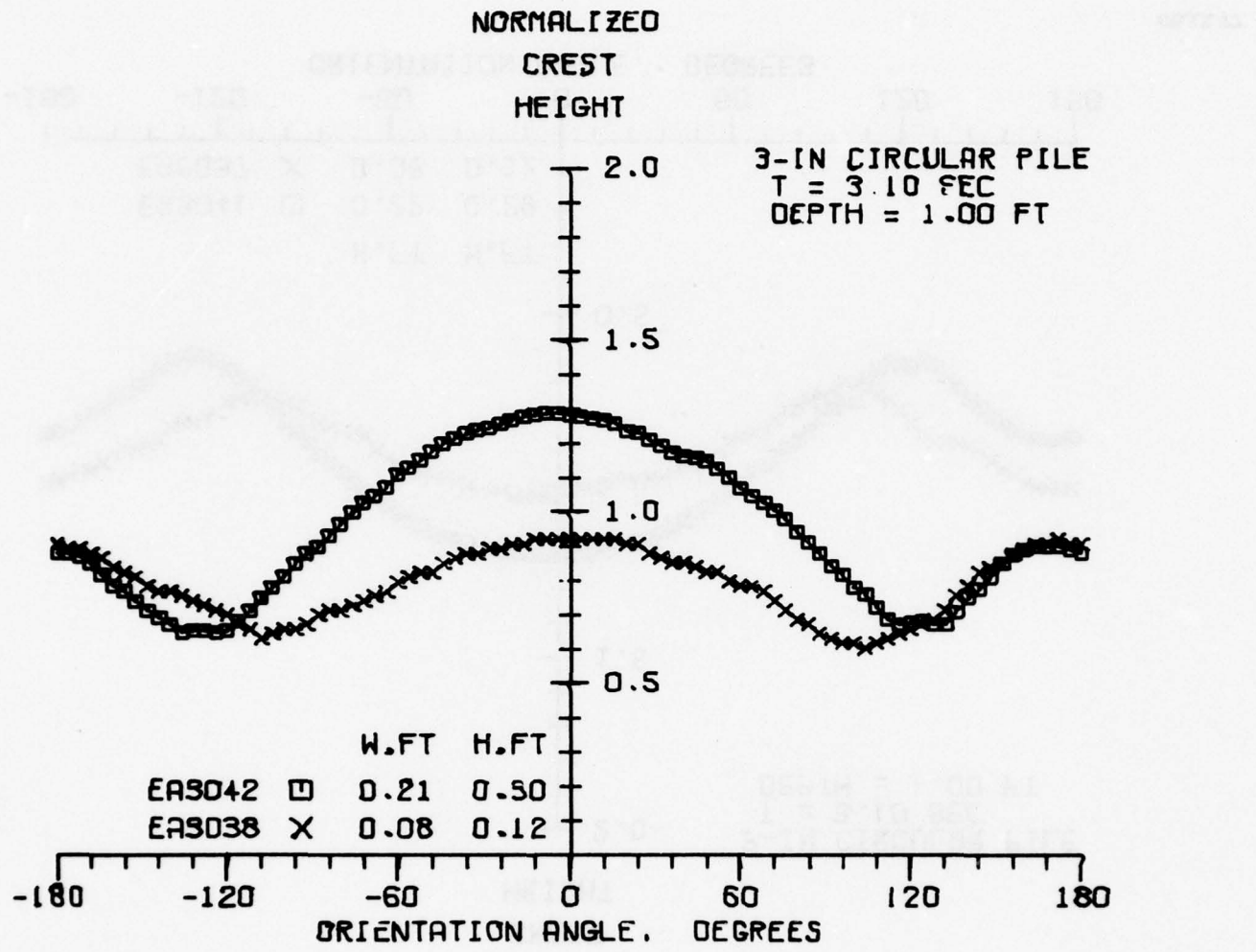
NORMALIZED
CREST
HEIGHT
3-IN CIRCULAR PILE
T = 3.10 SEC
DEPTH = 1.00 FT
2.0
1.5
1.0
0.5
W.FT H.FT
EA3042 0.21 0.50
EA3038 0.08 0.12
-180
-120
-60
0
60
120
180
ORIENTATION ANGLE, DEGREES
30JUN77

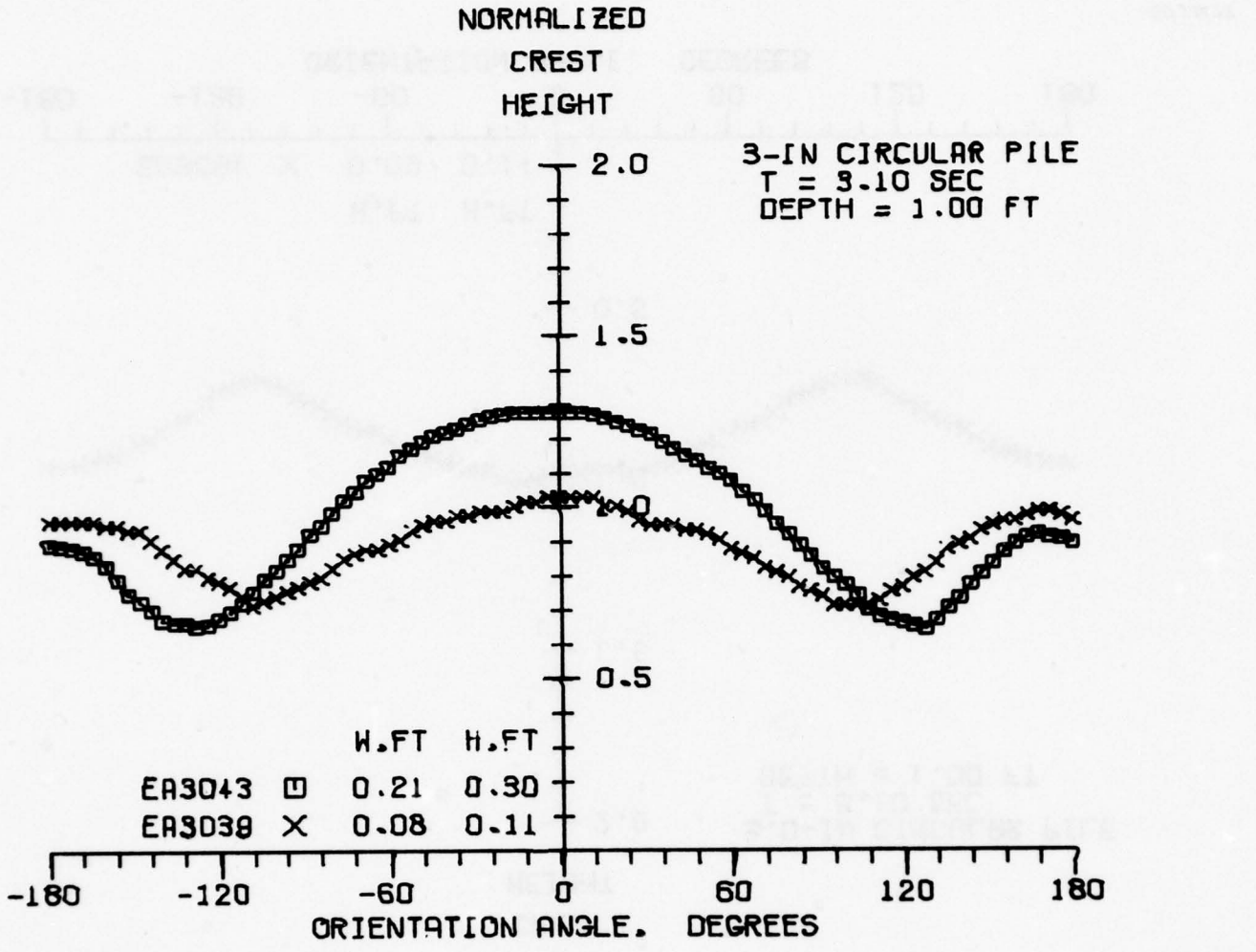
NORMALIZED
CREST
HEIGHT
3-IN CIRCULAR PILE
T = 3.10 SEC
DEPTH = 1.00 FT
2.0
1.5
1.0
0.5
W,FT H,FT
EA3043 0.21 0.30
EA3038 0.08 0.11
-180
-120
-60
0
60
120
180
ORIENTATION ANGLE, DEGREES
28JUN77

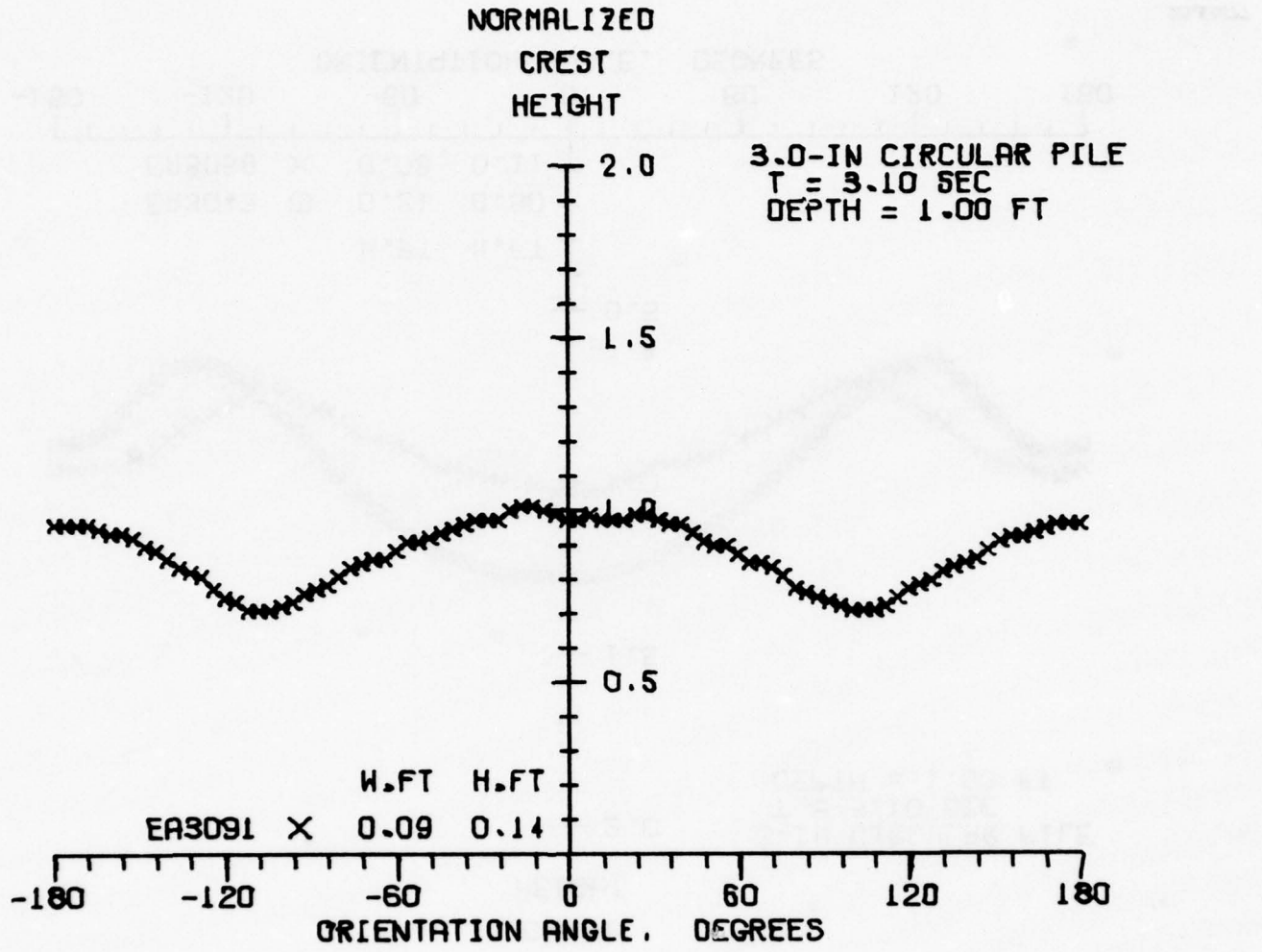
NORMALIZED
CREST
HEIGHT
3.0-IN CIRCULAR PILE
T = 3.10 SEC
DEPTH = 1.00 FT
2.0
1.5
1.0
0.5
W.FT H.FT
EA3091 X 0.09 0.14
-180
-120
-60
0
60
120
180
ORIENTATION ANGLE, DEGREES
9GJUN77

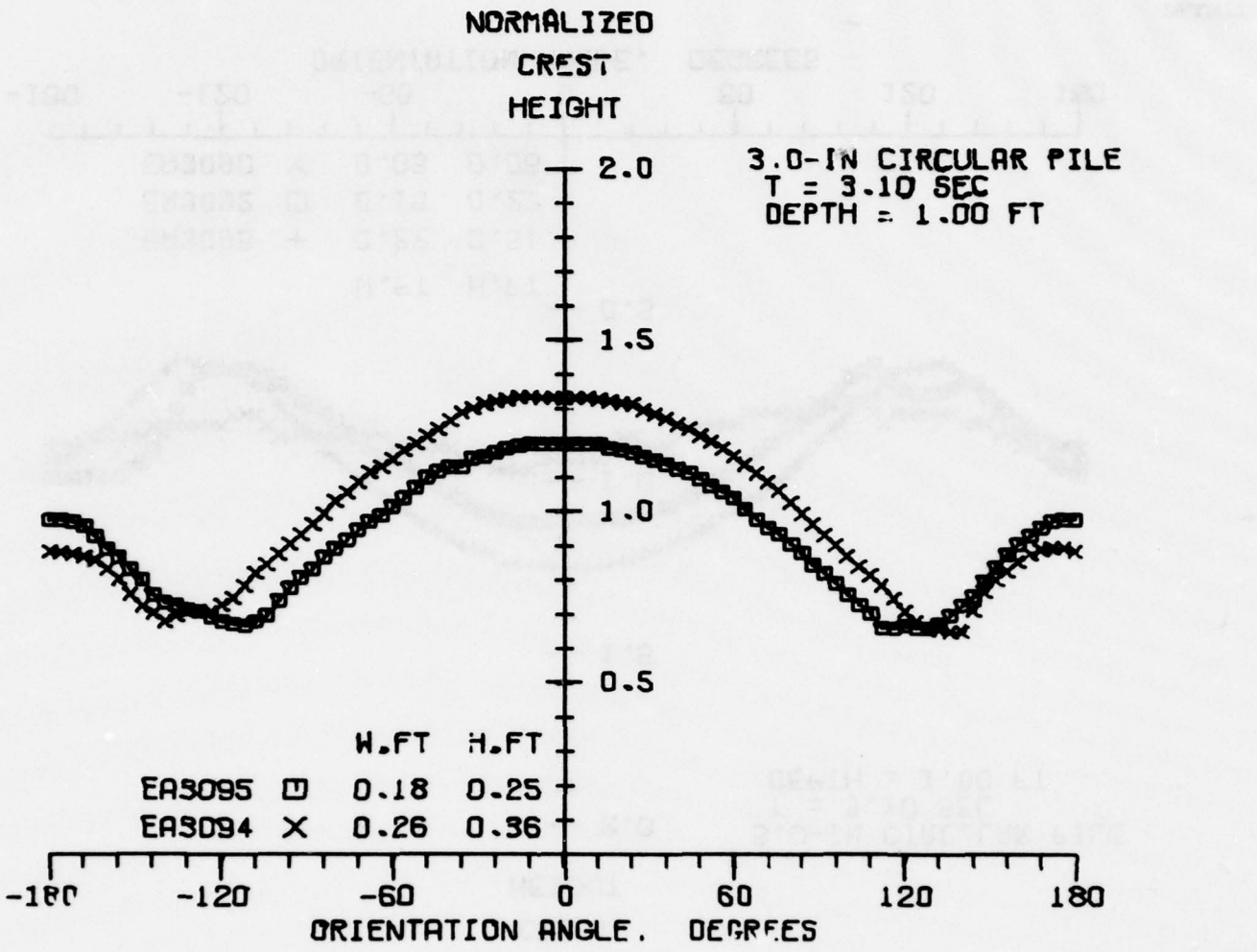
NORMALIZED
CREST
HEIGHT
3.0-IN CIRCULAR PILE
T = 3.10 SEC
DEPTH = 1.00 FT
2.0
1.5
1.0
0.5
W,FT H,FT
EA3095 □ 0.18 0.25
EA3094 X 0.26 0.36
-180
-120
-60
0
60
120
180
ORIENTATION ANGLE, DEGREES
30JUN77

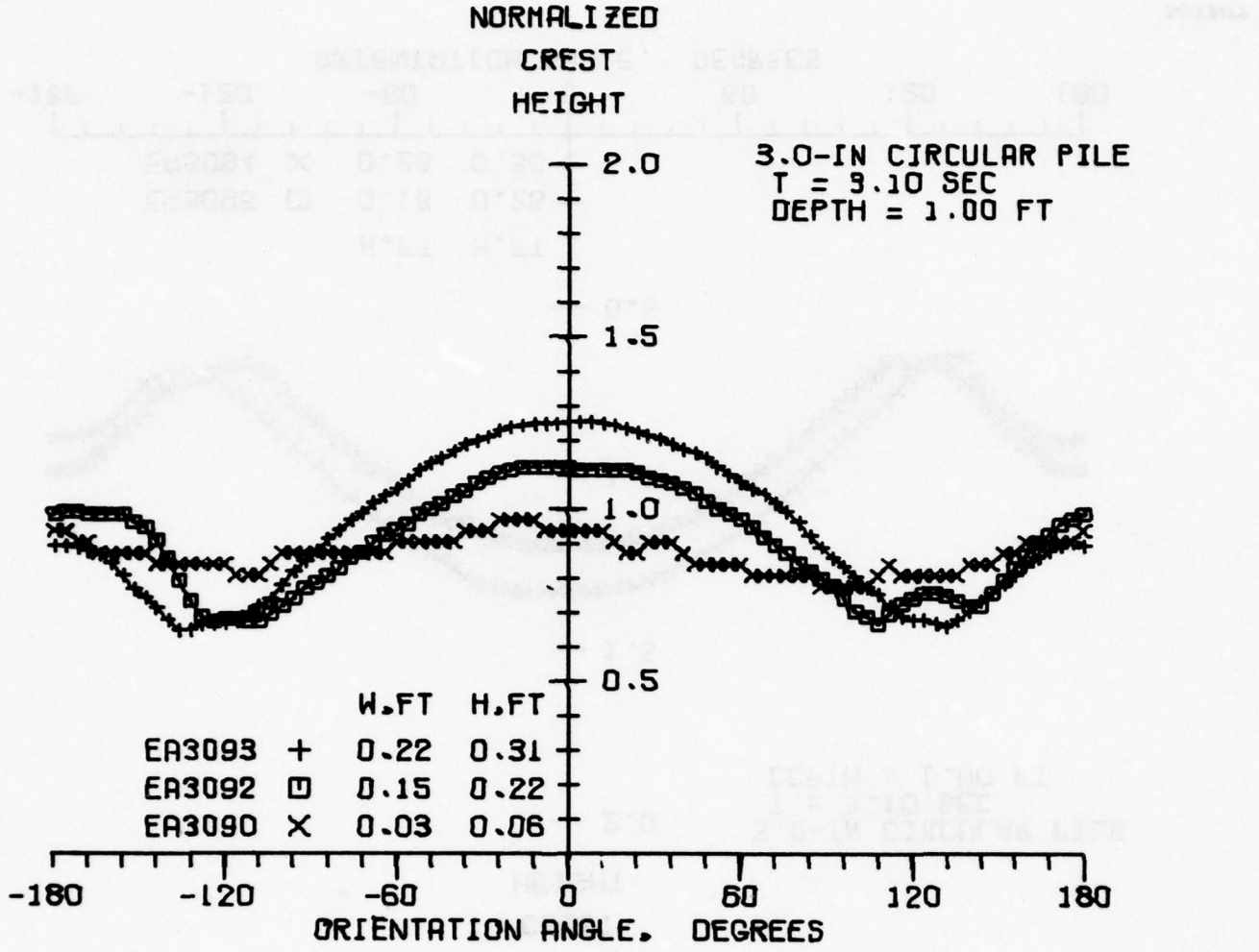
NORMALIZED
CREST
HEIGHT
3.0-IN CIRCULAR PILE
T = 9.10 SEC
DEPTH = 1.00 FT
2.0
1.5
1.0
0.5
W,FT H,FT
EA3093 + 0.22 0.31
EA3092 □ 0.15 0.22
EA3090 X 0.03 0.06
-180
-120
-60
0
60
120
180
ORIENTATION ANGLE, DEGREES
28JUN77

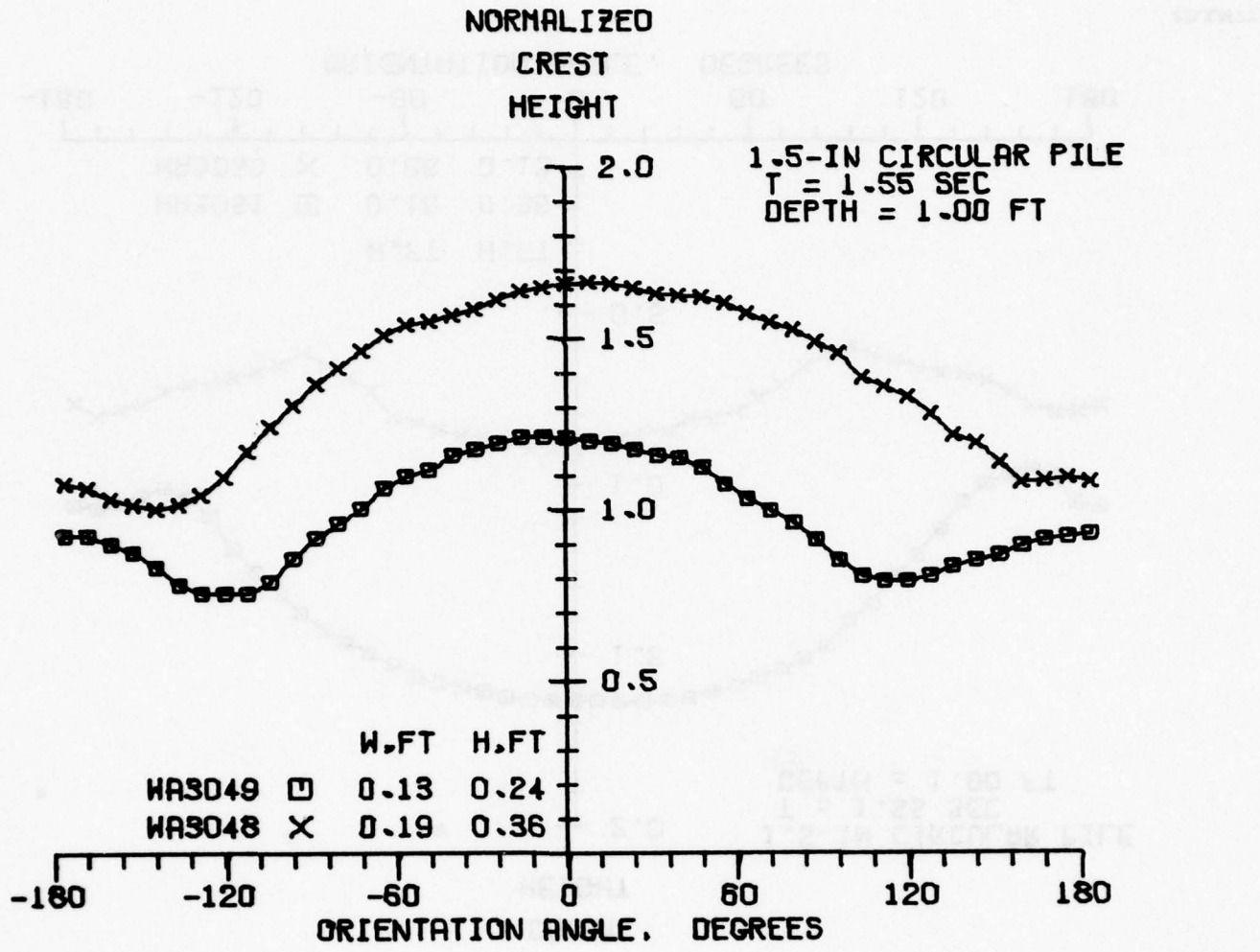
NORMALIZED
CREST
HEIGHT
1.5-IN CIRCULAR PILE
T = 1.55 SEC
DEPTH = 1.00 FT
2.0
1.5
1.0
0.5
W,FT H,FT
WA3049 0.13 0.24
WA3048 0.19 0.36
-180
-120
-60
0
60
120
180
ORIENTATION ANGLE, DEGREES
21JUN77

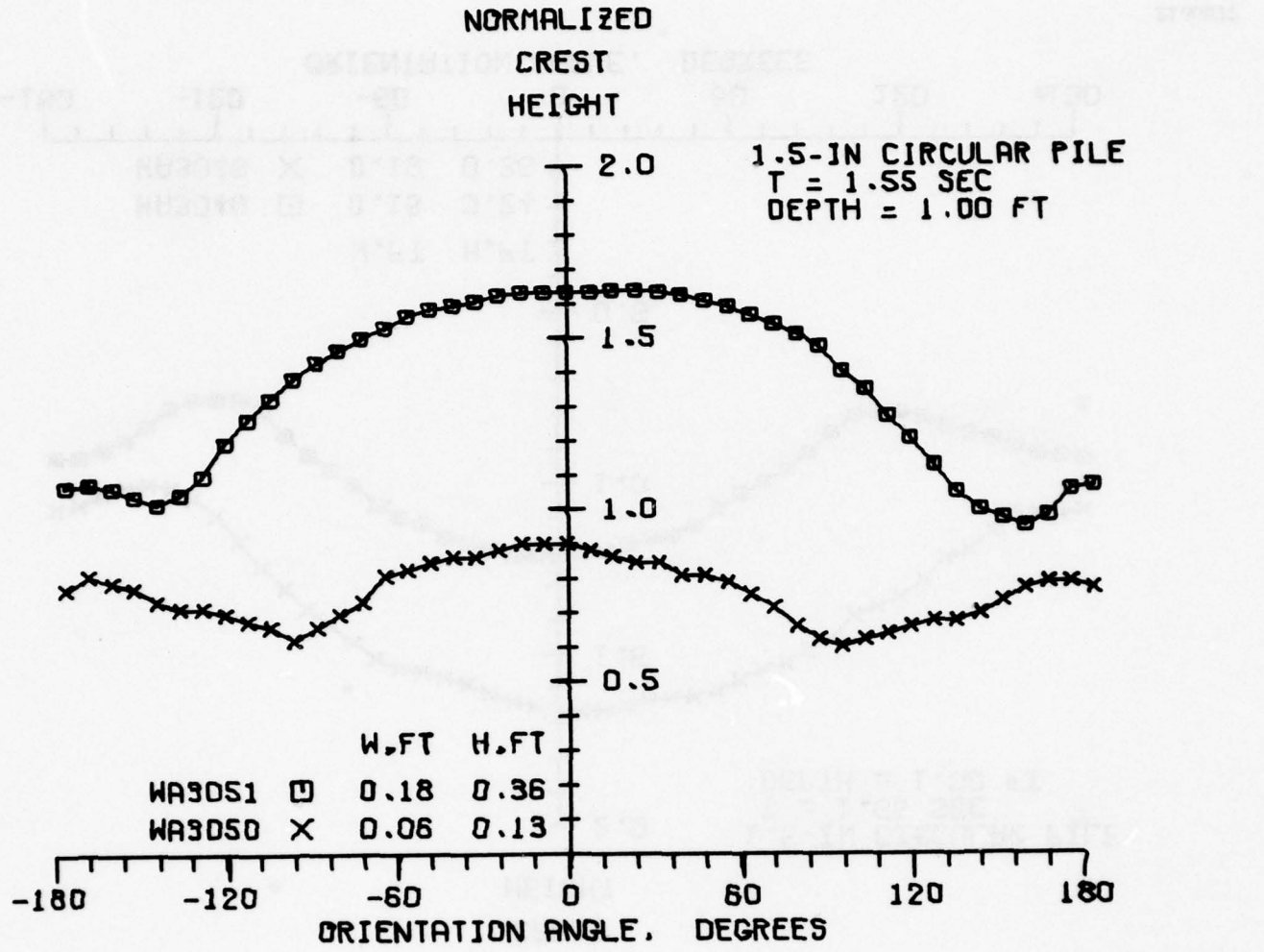
NORMALIZED
CREST
HEIGHT
1.5-IN CIRCULAR PILE
T = 1.55 SEC
DEPTH = 1.00 FT
2.0
1.5
1.0
0.5
W,FT H,FT
WA3DS1 0.18 0.36
WA3DS0 0.06 0.13
-180
-120
-60
0
60
120
180
ORIENTATION ANGLE, DEGREES
29JUN77

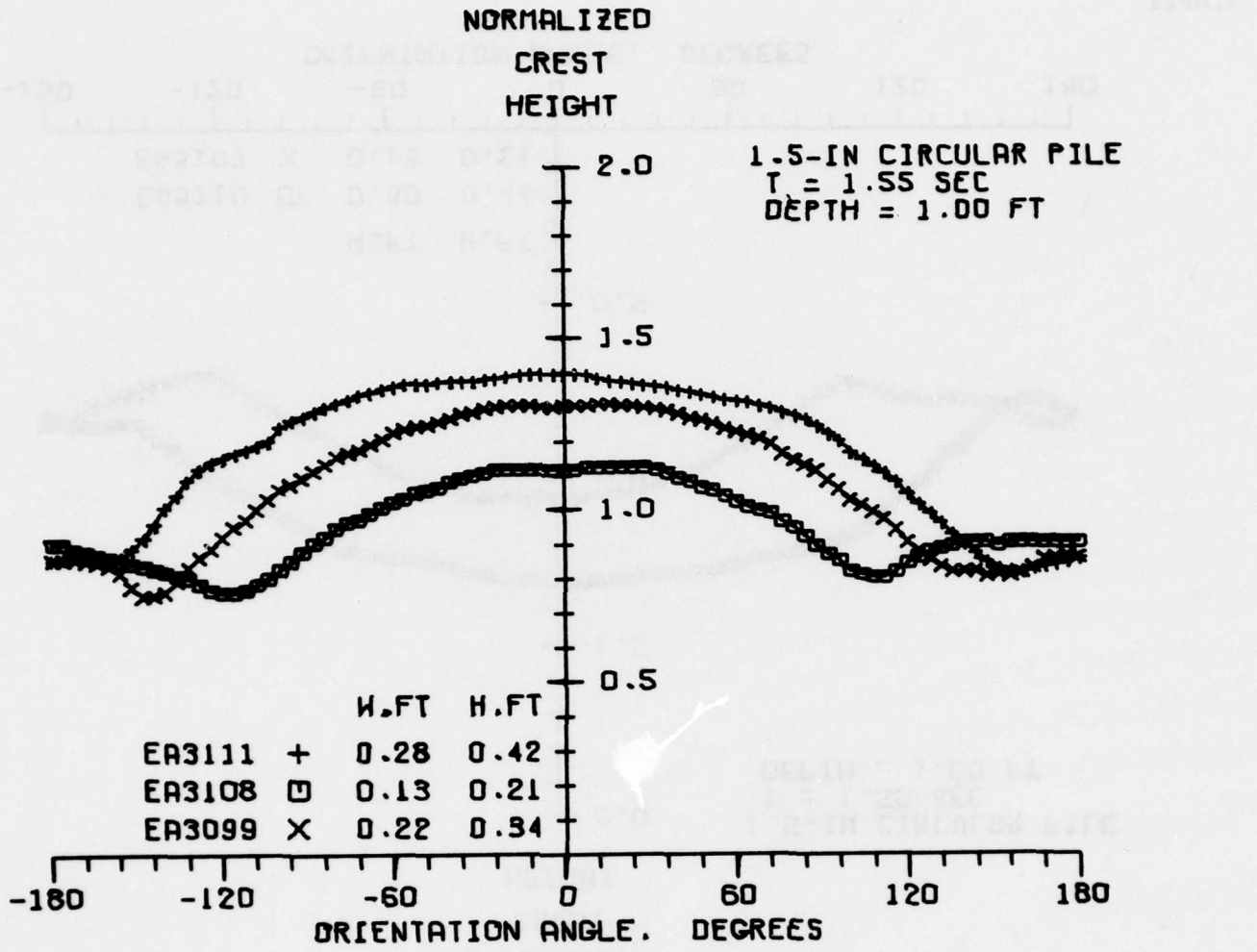
NORMALIZED
CREST
HEIGHT
1.5-IN CIRCULAR PILE
T = 1.55 SEC
DEPTH = 1.00 FT
2.0
1.5
1.0
0.5
H,FT H,FT
EA3111 + 0.28 0.42
EA3108 □ 0.13 0.21
EA3099 X 0.22 0.34
-180
-120
-60
0
60
120
180
ORIENTATION ANGLE. DEGREES
23JUN77

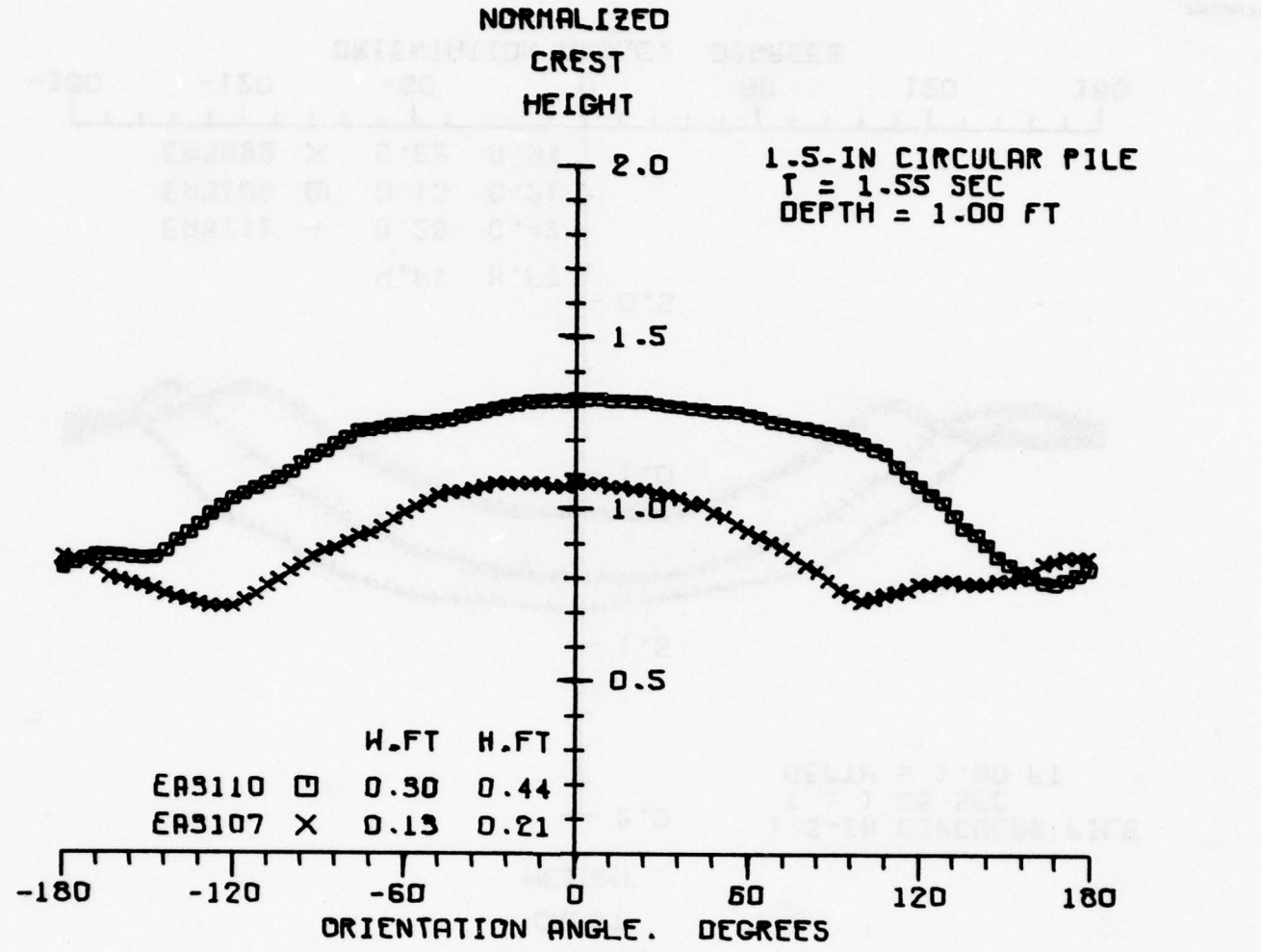
NORMALIZED
CREST
HEIGHT
1.5-IN CIRCULAR PILE
T = 1.55 SEC
DEPTH = 1.00 FT
2.0
1.5
1.0
0.5
W.FT H.FT
EA3110 □ 0.30 0.44
EA3107 X 0.13 0.21
-180 -120 -60 0 60 120 180
ORIENTATION ANGLE. DEGREES
23JUN77

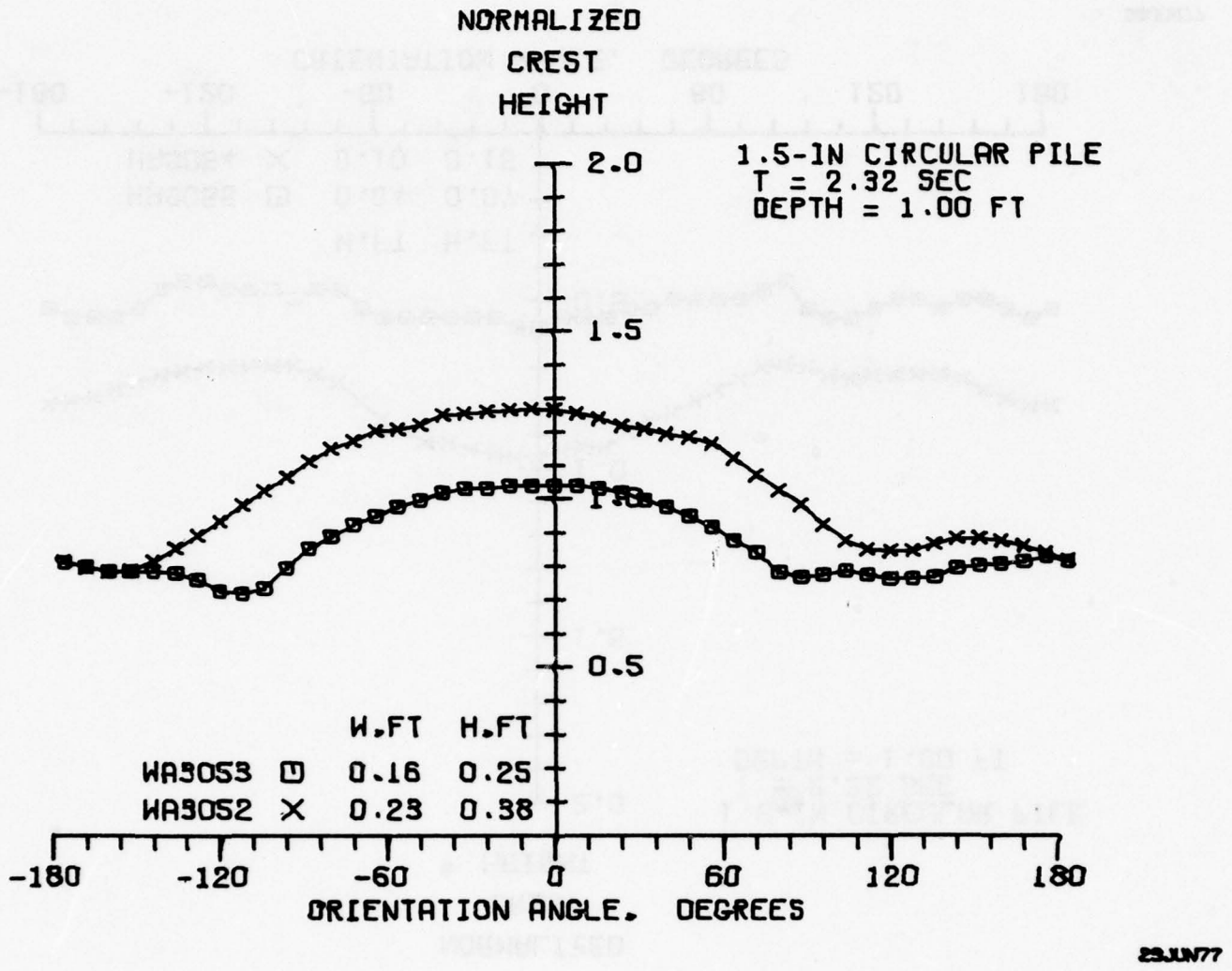
NORMALIZED
CREST
HEIGHT
1.5-IN CIRCULAR PILE
T = 2.32 SEC
DEPTH = 1.00 FT
2.0
1.5
1.0
0.5
W,FT H,FT
WA3053 0.16 0.25
WA3052 0.23 0.38
-180
-120
-60
0
60
120
180
ORIENTATION ANGLE, DEGREES
23JUN77

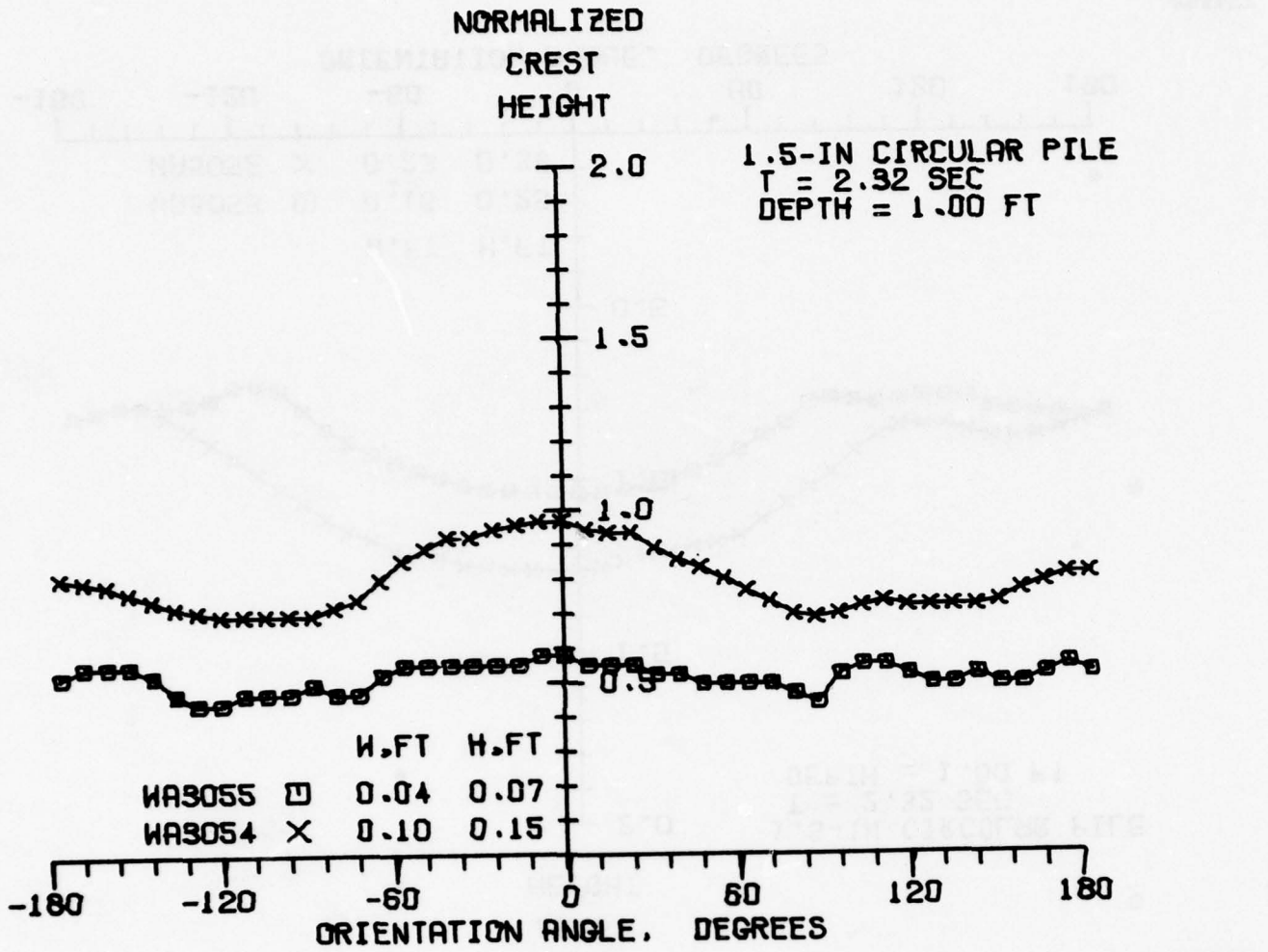
NORMALIZED
CREST
HEIGHT
1.5-IN CIRCULAR PILE
T = 2.32 SEC
DEPTH = 1.00 FT
2.0
1.5
1.0
0.5
H,FT H,FT
WA3055 0.04 0.07
WA3054 0.10 0.15
-180
-120
-60
0
60
120
180
ORIENTATION ANGLE, DEGREES
30JUN77

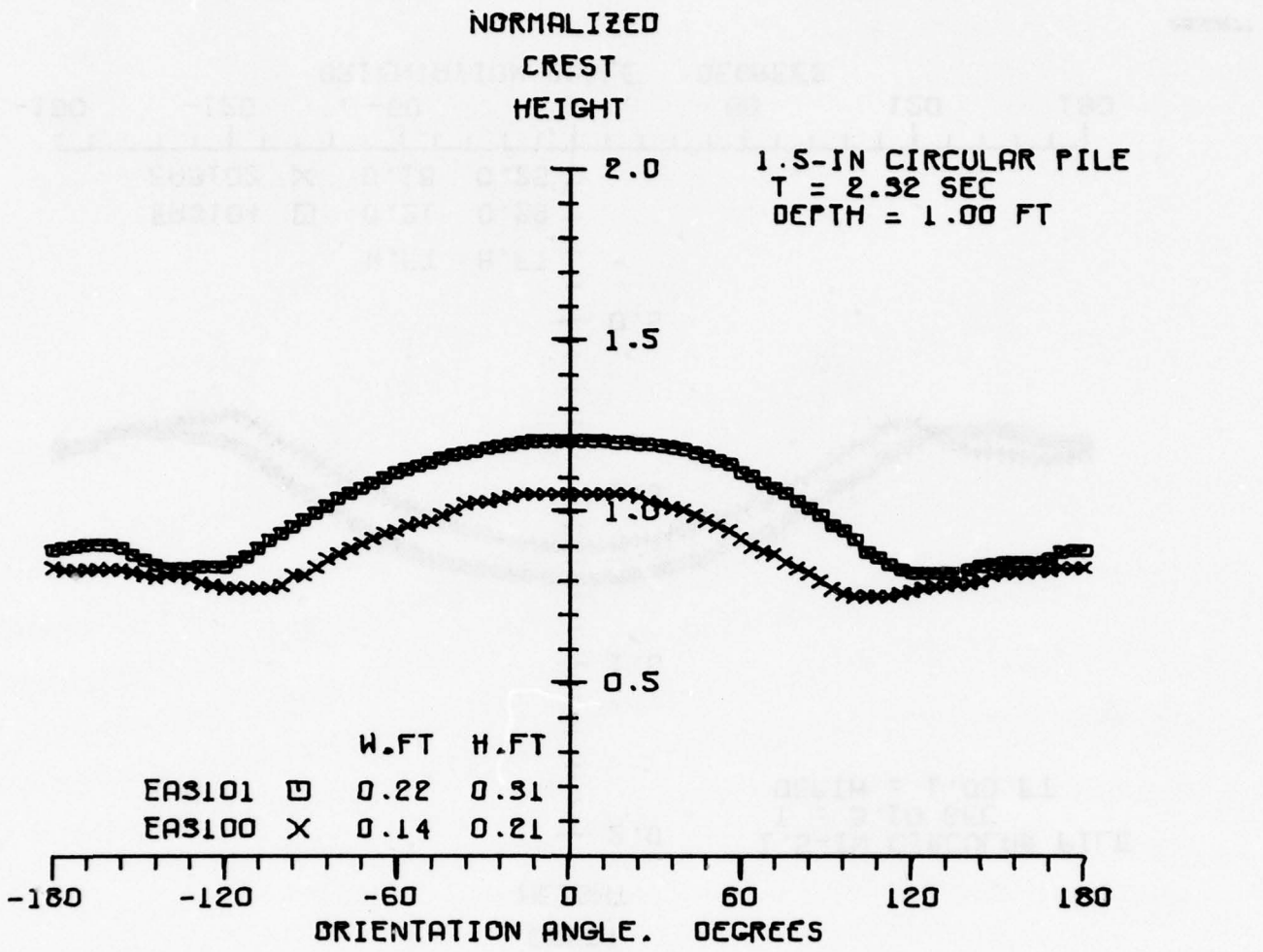
NORMALIZED
CREST
HEIGHT
1.5-IN CIRCULAR PILE
T = 2.32 SEC
DEPTH = 1.00 FT
2.0
1.5
1.0
0.5
W.FT H.FT
EAS101 0.22 0.31
EAS100 0.14 0.21
-180
-120
-60
0
60
120
180
ORIENTATION ANGLE. DEGREES
23JUN77

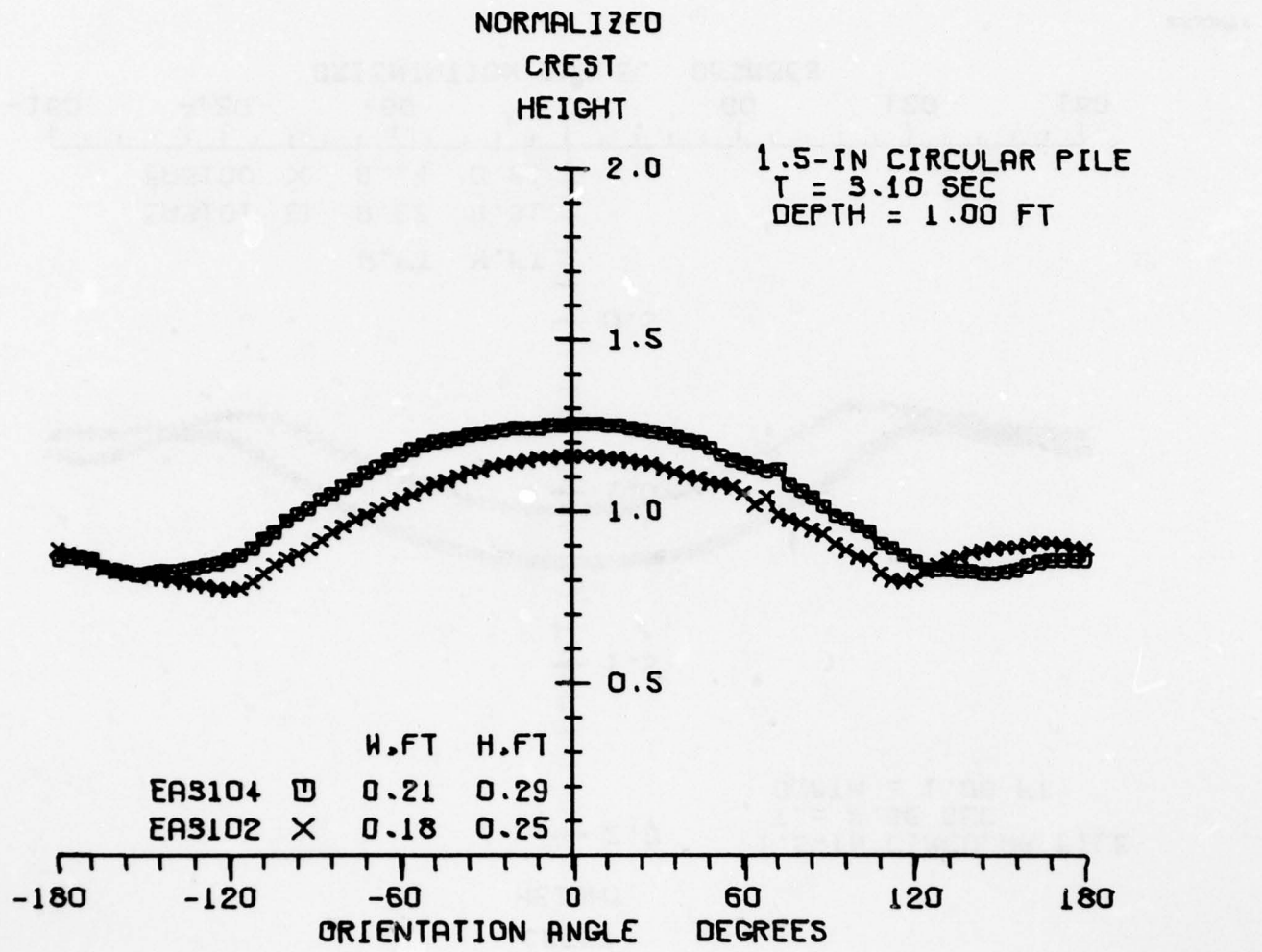
NORMALIZED
CREST
HEIGHT
1.5-IN CIRCULAR PILE
T = 3.10 SEC
DEPTH = 1.00 FT
2.0
1.5
1.0
0.5
W,FT H,FT
EAS104 0.21 0.29
EAS102 0.18 0.25
-180
-120
-60
0
60
120
180
ORIENTATION ANGLE DEGREES
29JUN77

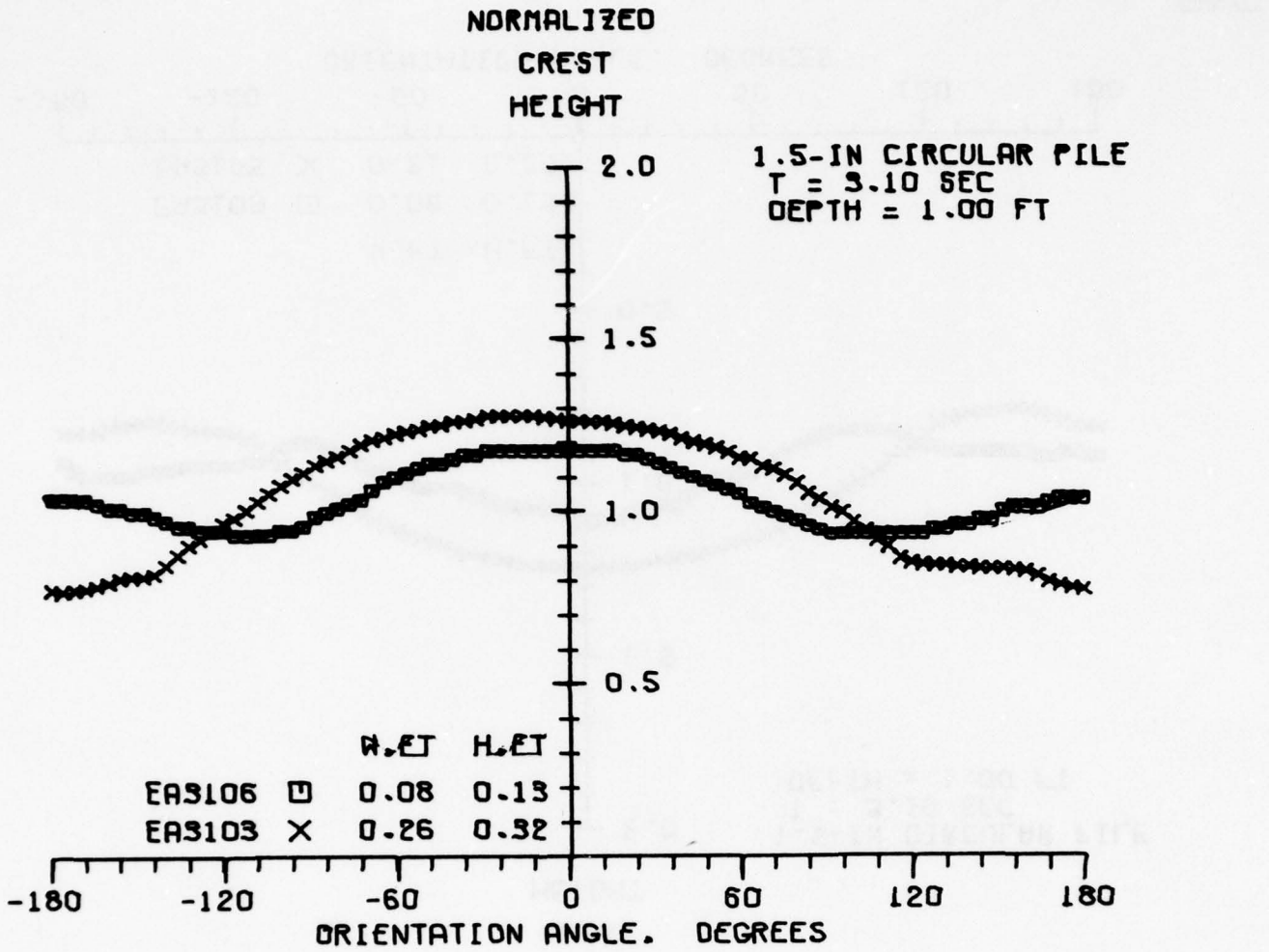
NORMALIZED
CREST
HEIGHT
1.5-IN CIRCULAR PILE
T = 3.10 SEC
DEPTH = 1.00 FT
2.0
1.5
1.0
0.5
W.ET H.ET
EA3106 0.08 0.13
EA3103 0.26 0.32
-180
-120
-60
0
60
120
180
ORIENTATION ANGLE. DEGREES
23JUN77

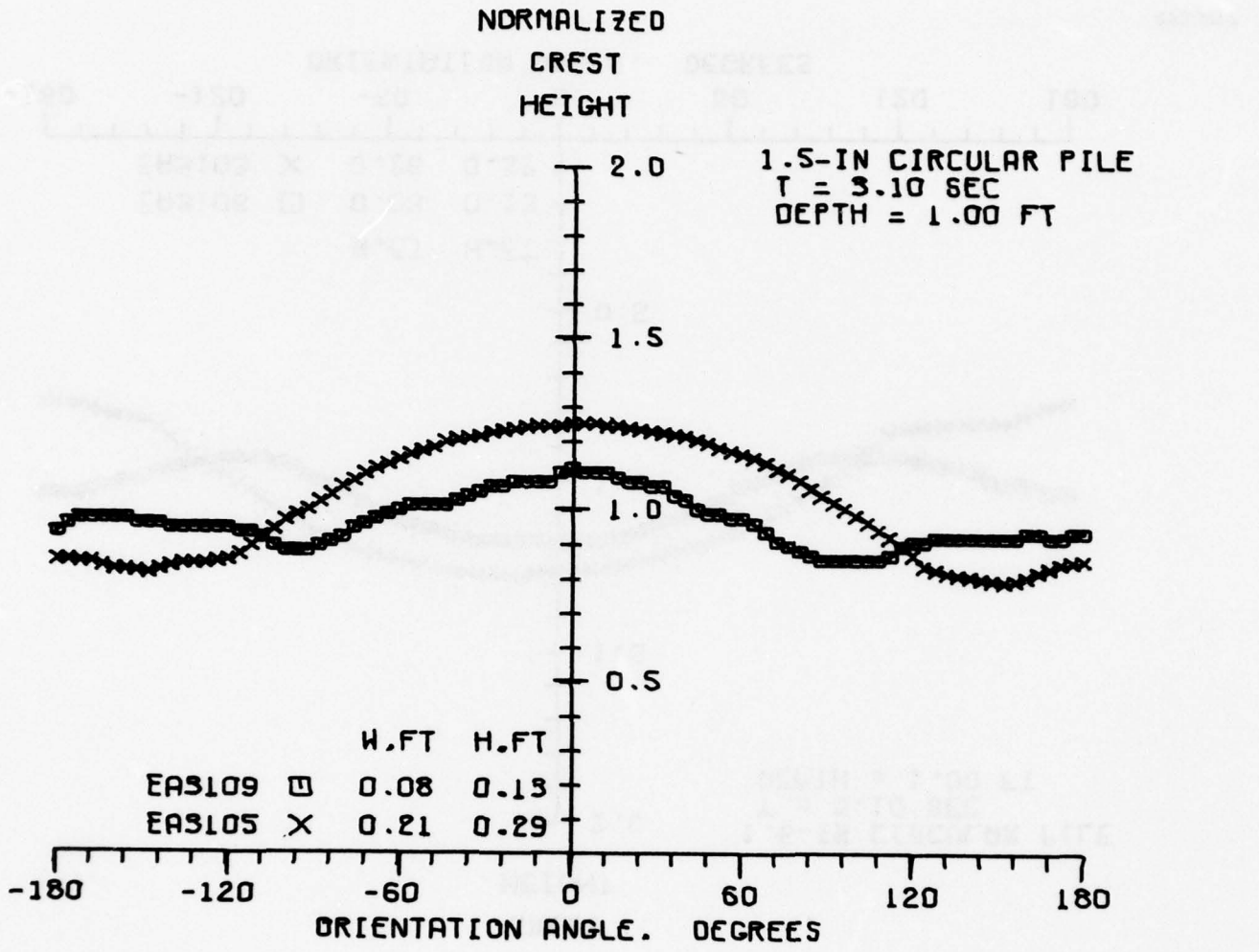
NORMALIZED
CREST
HEIGHT
1.5-IN CIRCULAR PILE
T = 3.10 SEC
DEPTH = 1.00 FT
2.0
1.5
1.0
0.5
W,FT H,FT
EAS109 0.08 0.13
EAS105 0.21 0.29
-180
-120
-60
0
60
120
180
ORIENTATION ANGLE, DEGREES
E3JUNTT

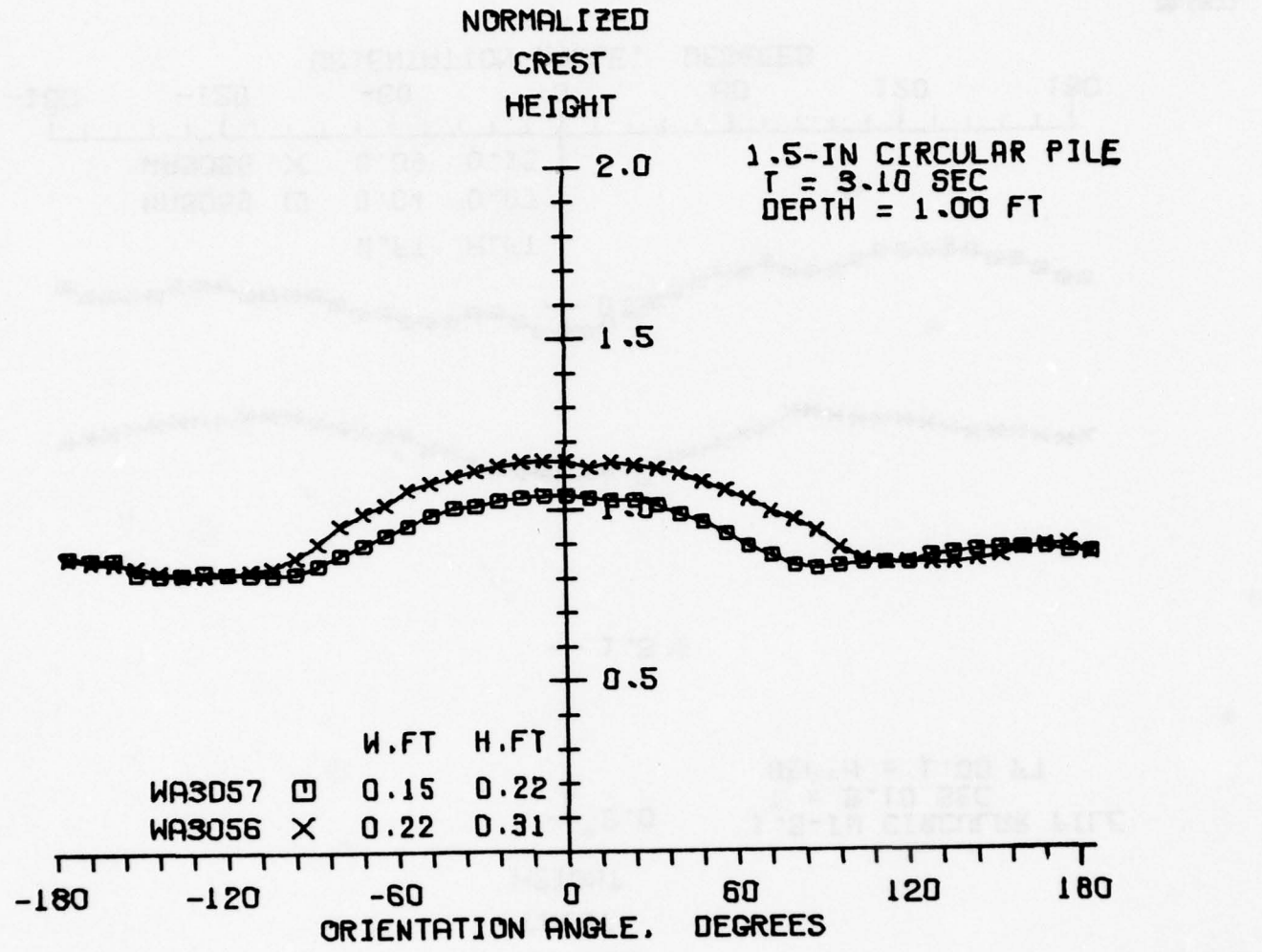
NORMALIZED
CREST
HEIGHT
1.5-IN CIRCULAR PILE
T = 3.10 SEC
DEPTH = 1.00 FT
2.0
1.5
1.0
0.5
W,FT H,FT
WA3057 □ 0.15 0.22
WA3056 X 0.22 0.31
-180
-120
-60
0
60
120
180
ORIENTATION ANGLE, DEGREES
29JUN77

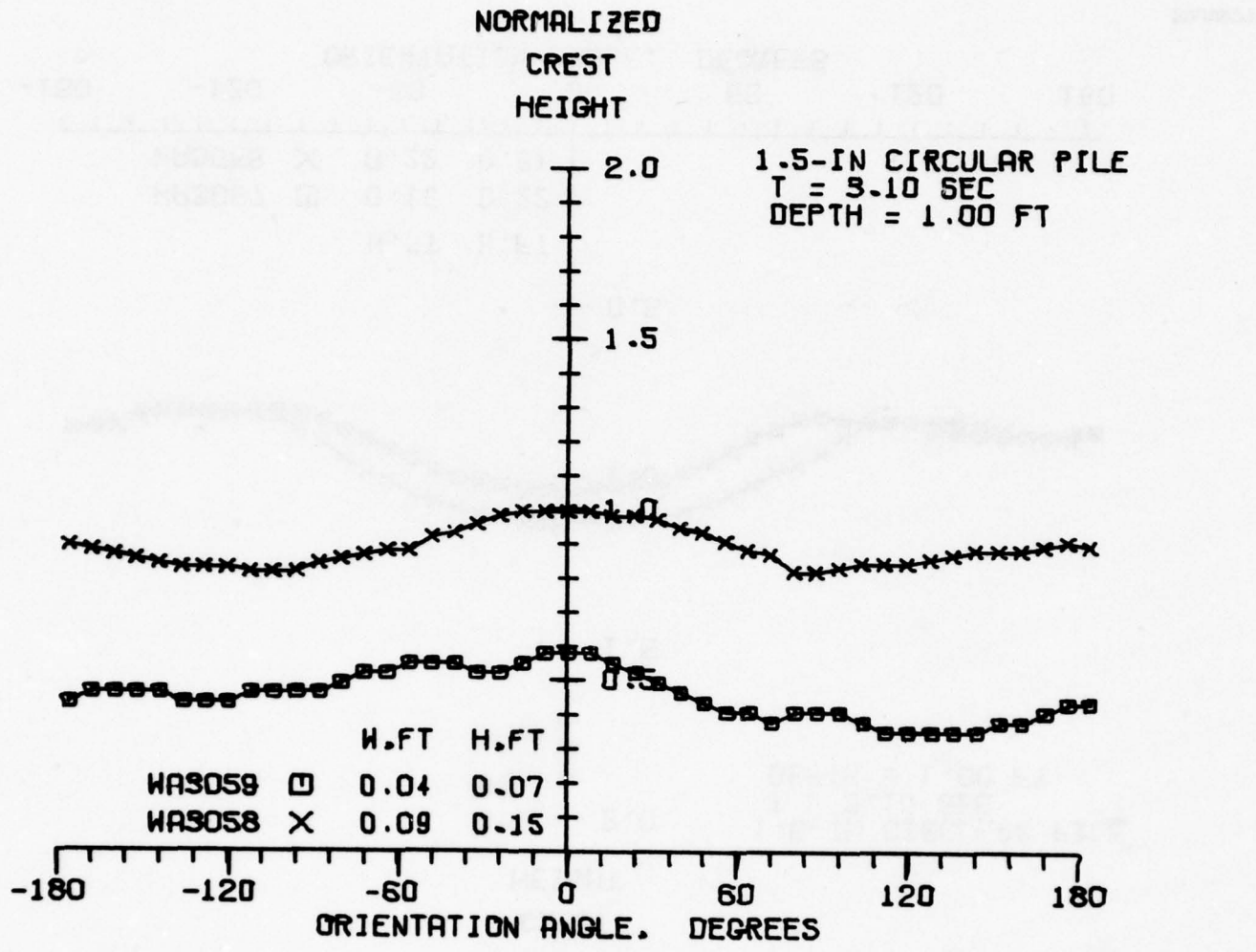
NORMALIZED
CREST
HEIGHT
1.5-IN CIRCULAR PILE
T = 3.10 SEC
DEPTH = 1.00 FT
2.0
1.5
1.0
0.5
W.FT H.FT
WA3058 □ 0.04 0.07
WA3058 X 0.09 0.15
-180
-120
-60
0
60
120
180
ORIENTATION ANGLE. DEGREES
29JUN77

APPENDIX D

OTHER TEST DATA

Two other series of tests were conducted during this study. This appendix discusses these test series, without a full presentation of the data obtained (the complete data are available at CERC), and presents plots of previously reported data which did not survive the internal consistency check.

1. Tests with Two-Wave Trains on a Single Pile.

Early in this study, some tests were conducted in an outdoor three-dimensional wave basin. These tests were initiated primarily to investigate scale effects on the measurements. The wave basin tests were plagued by various problems, and scale effect investigations were eventually completed in the 85-foot tank. However, one meaningful series of nine tests was conducted which could not be duplicated in the 85-foot tank.

Two wave generators were set to generate wave trains of 1.90- and 2.53-second periods, propagating at right angles past the test pile. Because the periods were in the ratio 3:4, and the generators were initially in phase, the wave trains constructively interfered at the pile with a 7.6-second period (see waveform in Fig. D-1). The peak wave height was measured from the gage record obtained in the pile channel, as the pile orientation was varied over the 360° range. Figure D-2 presents the patterns measured at the 1x1 and 2x2 H-piles in the same two-wave test situation. (The special orientation angle ψ is defined in Fig. D-2.) These two patterns closely agree.

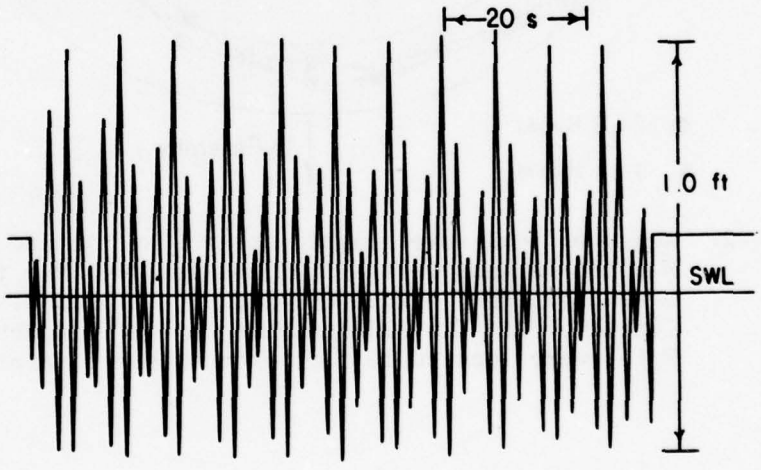

Figure D-1. Water level record in test with two wave trains.

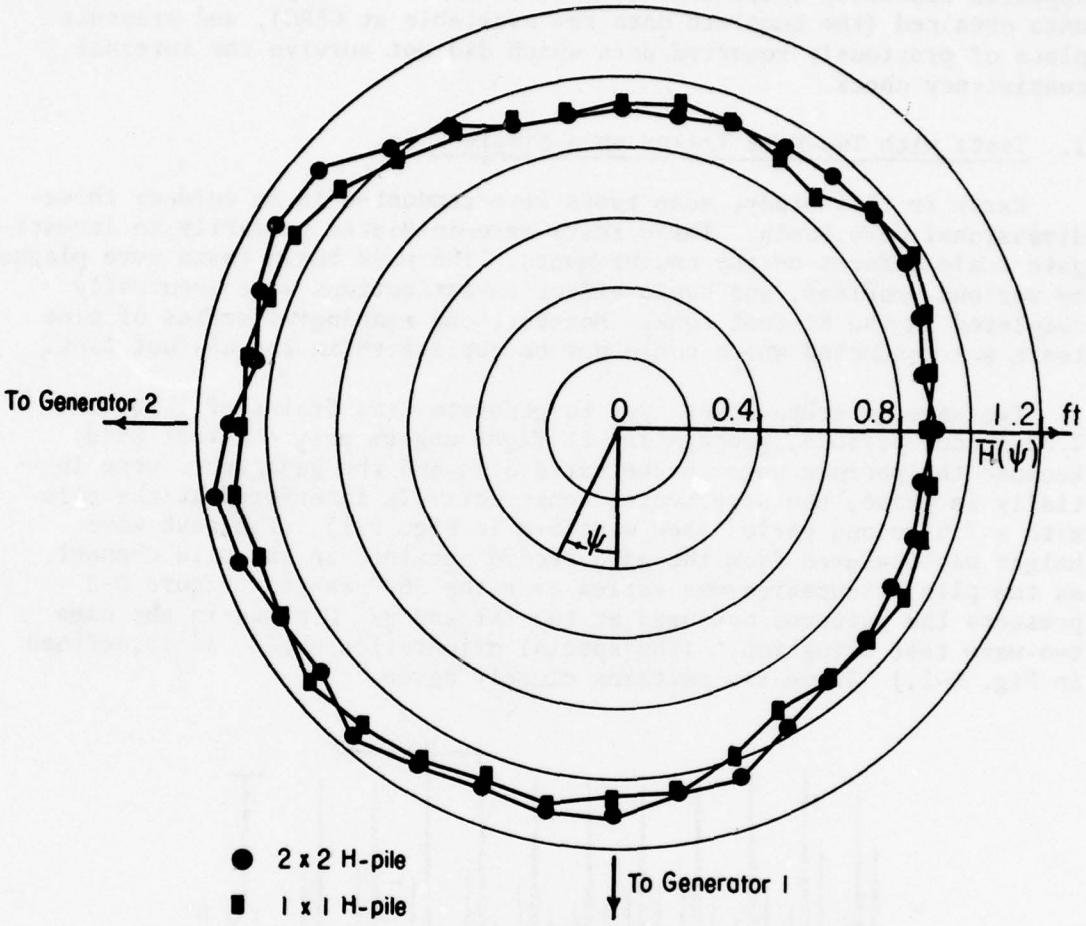

Figure D-2. Measured peak wave height patterns at 1x1 and 2x2 H-piles in same test situation with two wave trains. Generator 1: T = 2.53 seconds, E = 3.5 inches; Generator 2: T = 1.90 seconds, E = 3.0 inches. Piles were located 10 feet from each generator.

Galvin and Hallermeier (1972) introduced the zero-crossing method for determining the front symmetry point of a simple pattern. This uses the zero crossing of the quantity $[\overline{H}(\beta) - \overline{H}(\beta+180°)]$ or $[\overline{W}(\beta) - \overline{W}(\beta+180°)]$ to locate the angle separating the front from the back of the pattern; this angle is 90° away from the front symmetry point. Figure D-3 shows $[\overline{H}(\psi) - \overline{H}(\psi+180°)]$ for the two patterns in Figure D-2. Each pattern has a well-defined symmetry point located in the direction between the two generators.

Of the nine tests discussed here, five were run with either one or the other generator operating, and four were run with two wave trains. Figure D-4 shows the ratio of the computed velocity heads in the two wave trains versus the measured zero-crossing angle of the resulting peak wave height pattern. (The velocity heads were computed using McCowan's solitary wave theory.) The linear trend in Figure D-4 indicates that simple additive wave stagnation effects dominate the measured patterns at these two piles with relatively shallow channels. Also, there is little difference in test results with the two geometrically similar piles of different size.

2. Tests with Closely-Spaced Circular Piles.

Some tests were performed with two circular piles centered side-by-side in the 1.5-foot-wide wave tank, primarily to investigate effects of pile confinement. Center-to-center separations were 6 or 9 inches (0.15 or 0.23 meter), the two test piles sometimes had unequal diameter, and a wave pulse including one dominant crest was used. Electrical gages recorded the waveforms 2 feet (0.61 meter) in front of and behind the piles, and the peak waterlines on the piles were recorded by erosion of a powder deposit or wetting of a paper sleeve. The recorded peak waterlines show complicated variability, especially with piles of unequal diameter (Fig. D-5). These tests were basically extraneous to the present study, and no effort was made to interpret the resulting data.

3. Previously Reported Data of Unsatisfactory Quality.

Some data presented in Galvin and Hallermeier (1972) and in Figures 20, 27, and 28 of this report did not survive the consistency test (App. C). These data sets are of lower quality than those shown in Appendix C, but are valuable in illustrating qualitative trends. For completeness, the plots on pages 173 to 183 are presented in the standard format used in Appendix C.

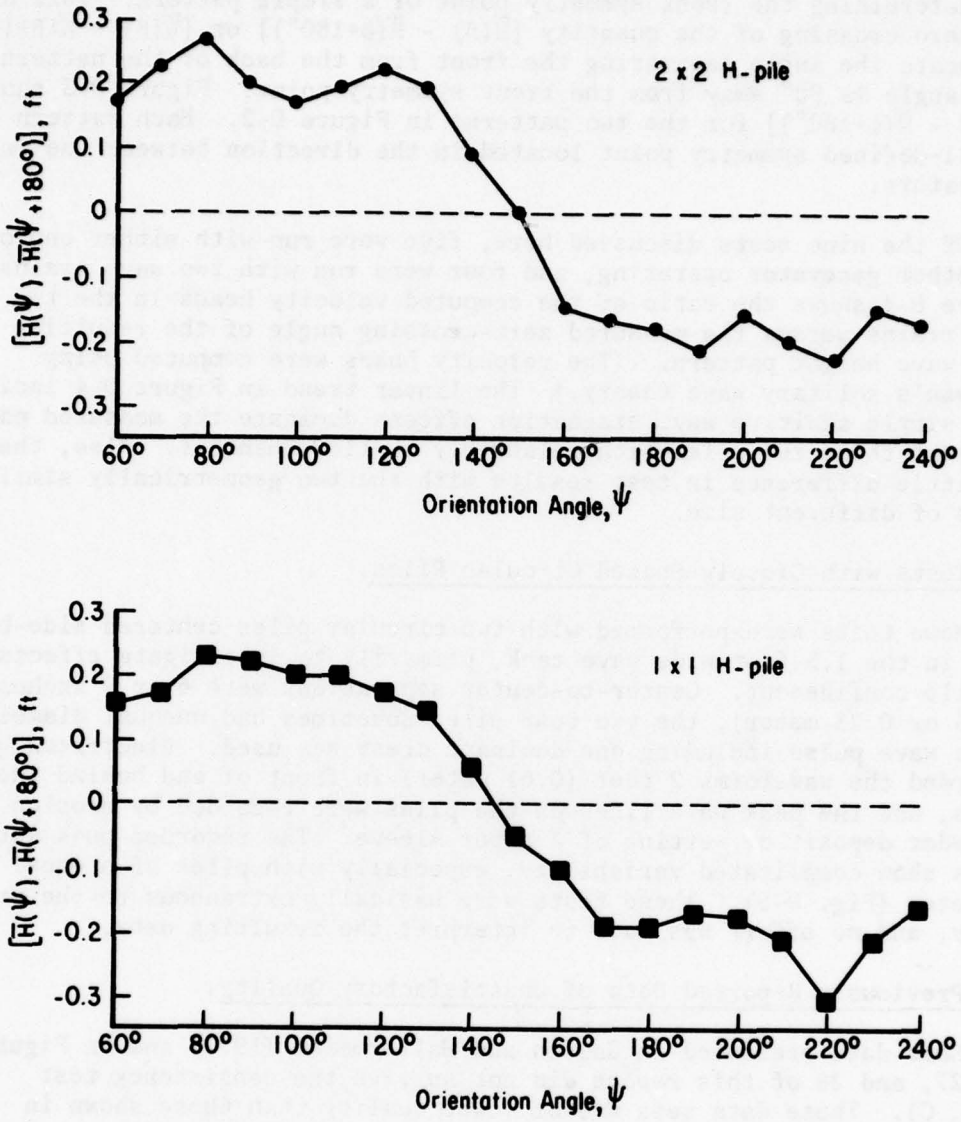

Figure D-3. Zero crossings of $[\overline{H}(\psi) - \overline{H}(\psi+180°)]$ for the two patterns in Figure D-2.

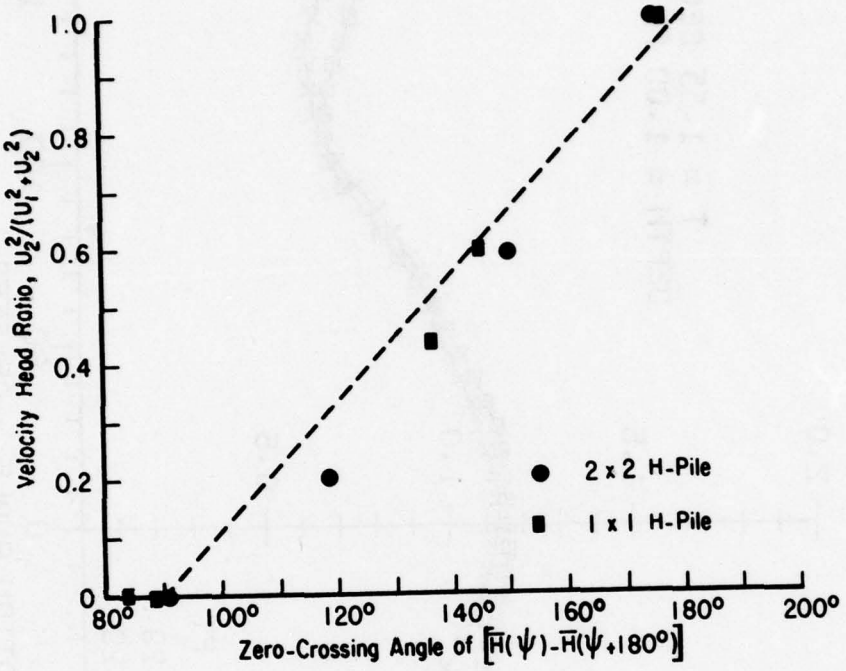

Figure D-4. Ratio of computed velocity heads of two orthogonal wave trains versus zero-crossing angle.

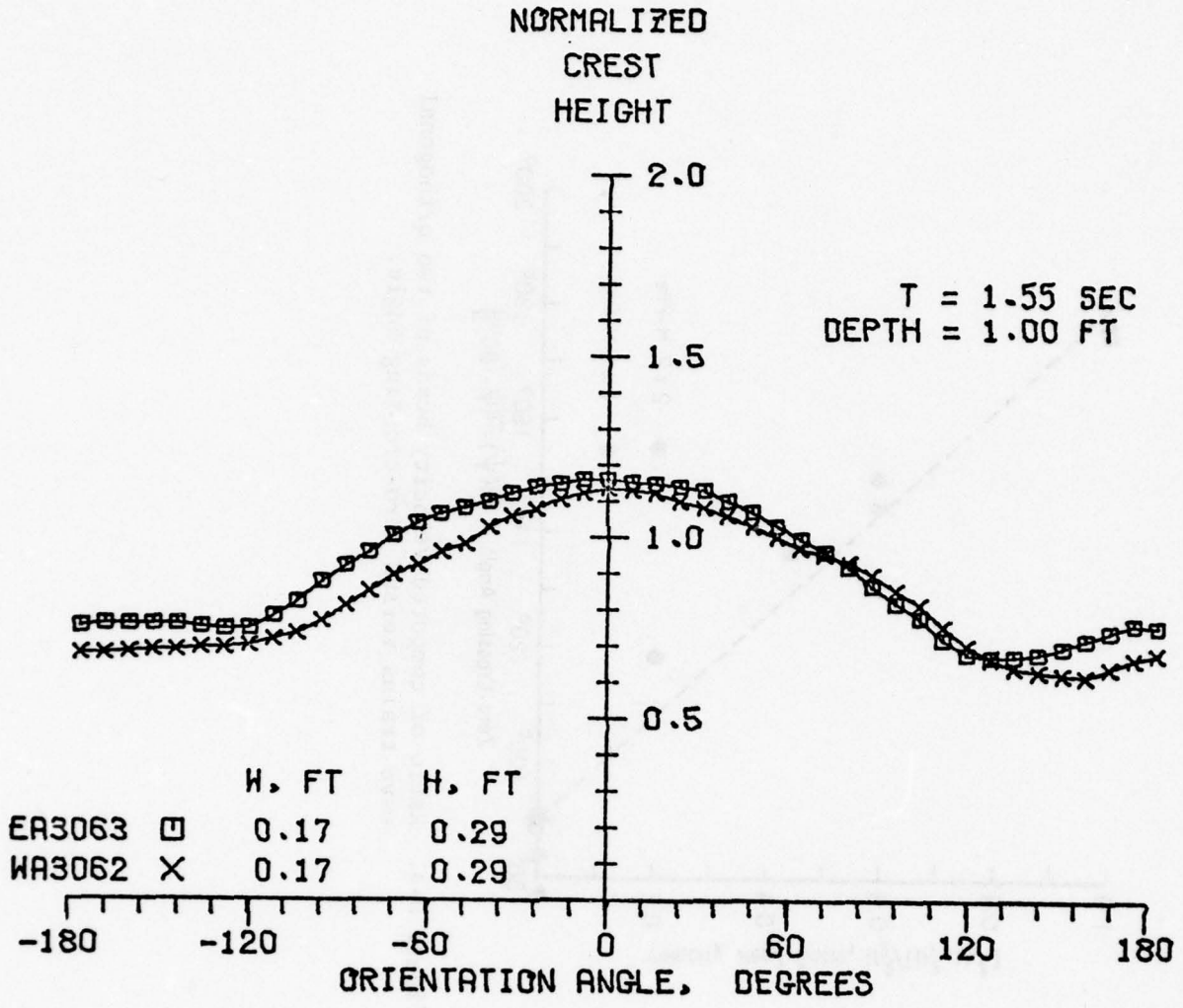

Figure D-5. Peak water around two side-by-side 1.5-inch-diameter circular piles, with 6 inches between centers in 1.5-foot-wide tank.

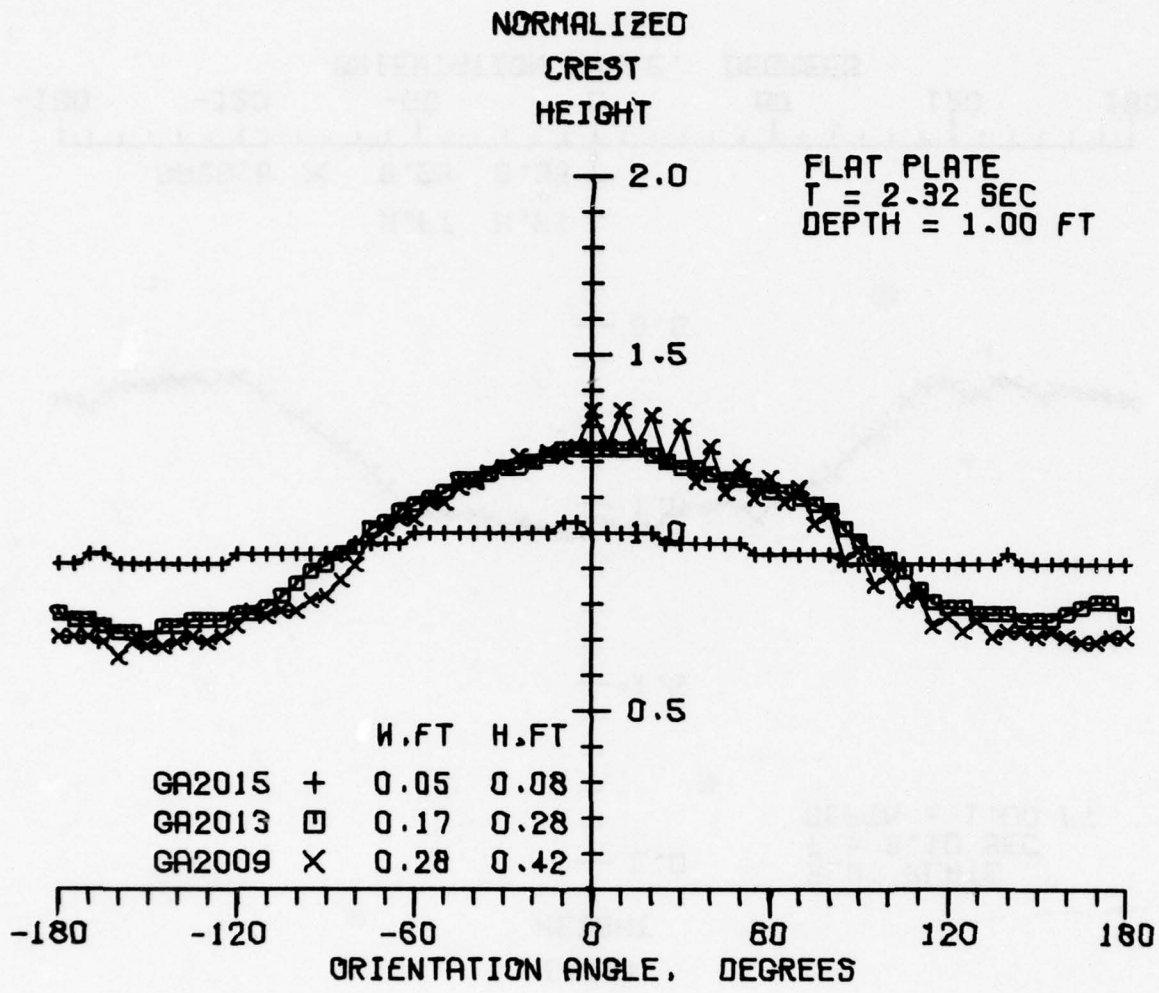
NORMALIZED
CREST
HEIGHT
FLAT PLATE
T = 2.32 SEC
DEPTH = 1.00 FT
2.0
1.5
1.0
0.5
W,FT H,FT
GA2015 + 0.05 0.08
GA2013 □ 0.17 0.28
GA2009 × 0.28 0.42
-180
-120
-60
0
60
120
180
ORIENTATION ANGLE, DEGREES
9JUN77

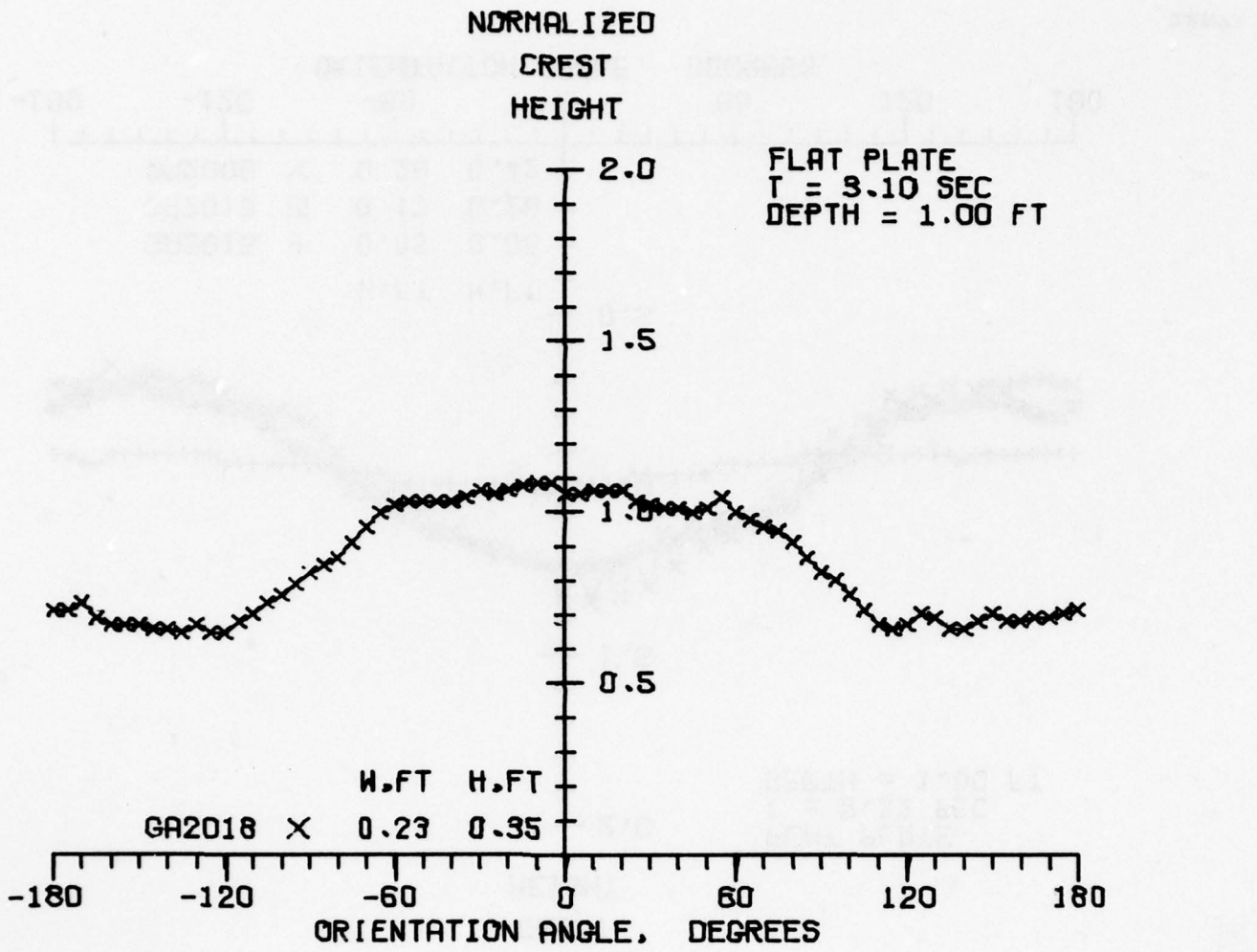
NORMALIZED
CREST
HEIGHT
FLAT PLATE
T = 3.10 SEC
DEPTH = 1.00 FT
2.0
1.5
1.0
0.5
W,FT H,FT
GA2018 X 0.23 0.35
-180
-120
-60
0
60
120
180
ORIENTATION ANGLE, DEGREES
9JUN77

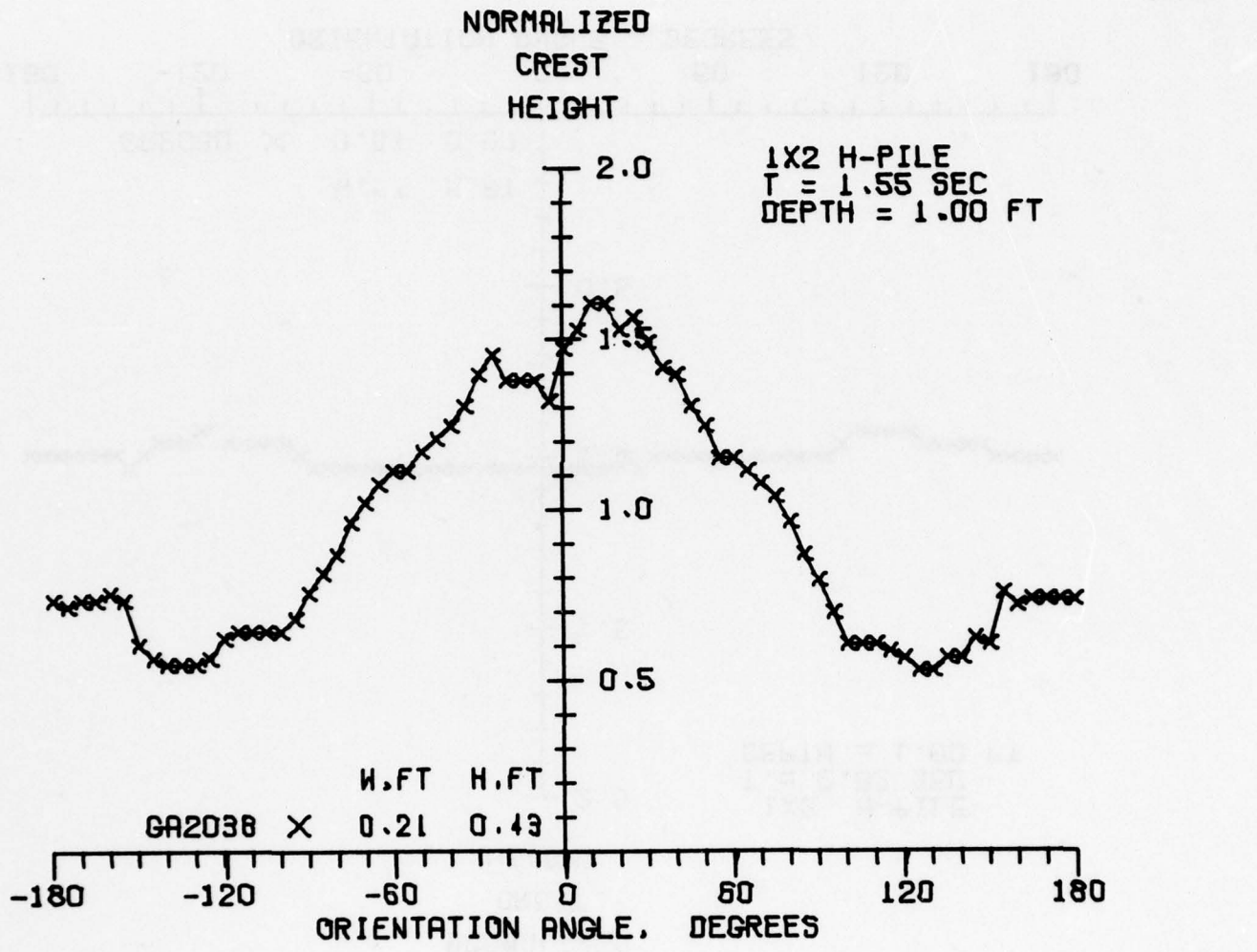
NORMALIZED
CREST
HEIGHT
1X2 H-PILE
T = 1.55 SEC
DEPTH = 1.00 FT
2.0
1.5
1.0
0.5
H,FT H,FT
GA2036 X 0.21 0.43
-180
-120
-60
0
60
120
180
ORIENTATION ANGLE, DEGREES
9JUN77

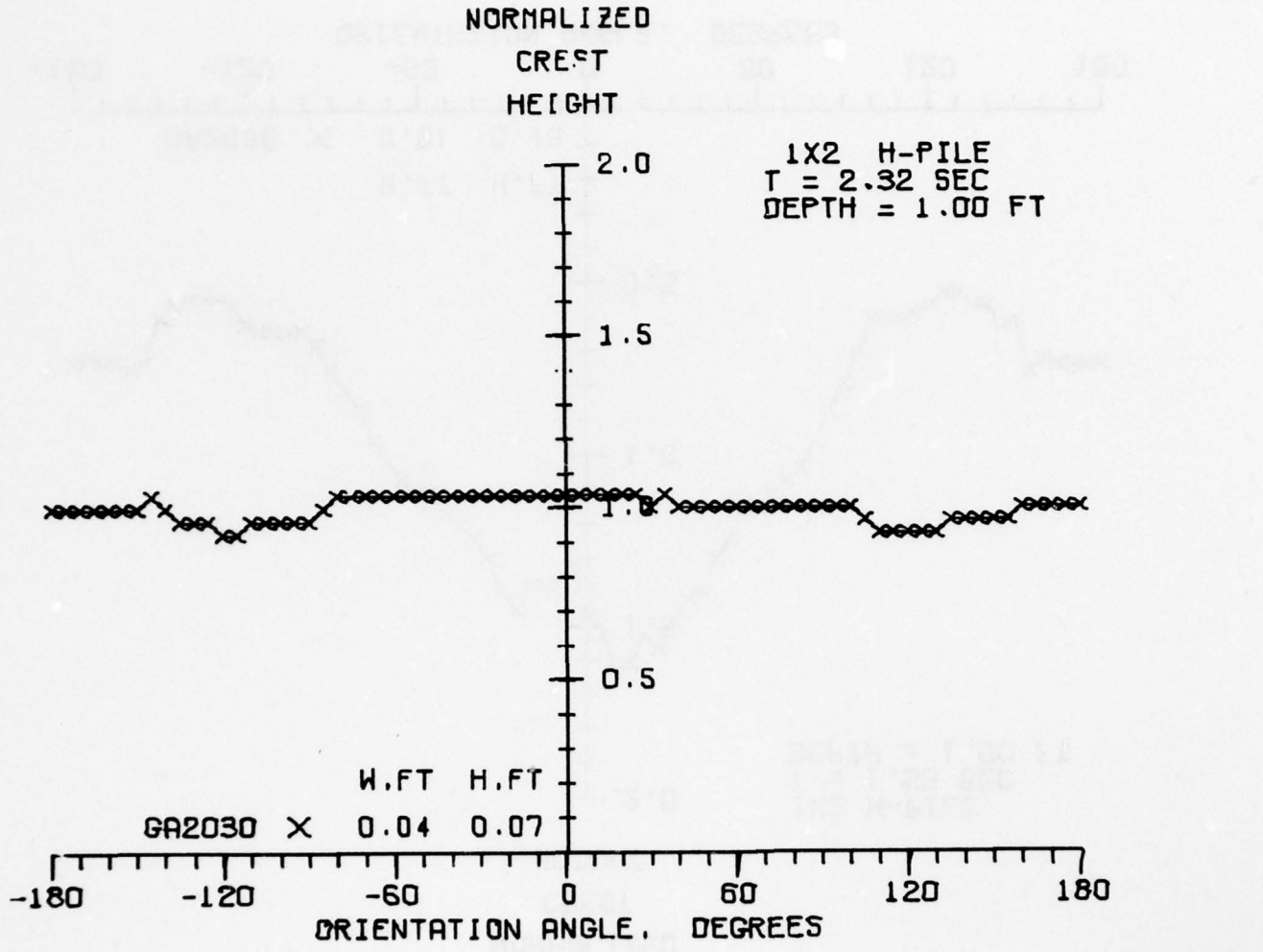
NORMALIZED
CREST
HEIGHT
1X2 H-PILE
T = 2.32 SEC
DEPTH = 1.00 FT
2.0
1.5
1.0
0.5
W,FT H,FT
GA2030 X 0.04 0.07
-180
-120
-60
0
60
120
180
ORIENTATION ANGLE, DEGREES
3JUN77

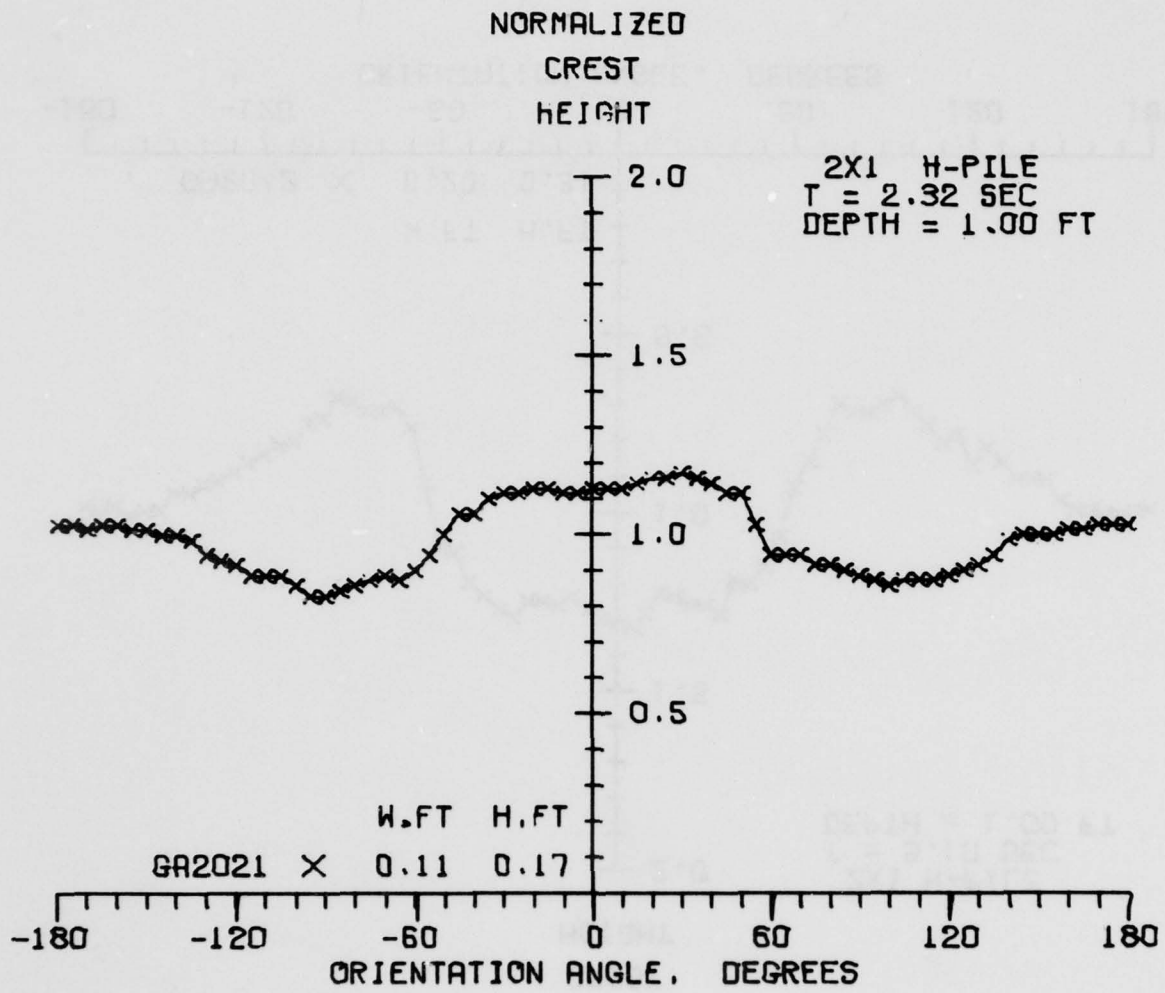
NORMALIZED
CREST
HEIGHT
2X1 H-PILE
T = 2.32 SEC
DEPTH = 1.00 FT
2.0
1.5
1.0
0.5
W,FT H,FT
GA2021 X 0.11 0.17
-180
-120
-60
0
60
120
180
ORIENTATION ANGLE, DEGREES
9JUN77

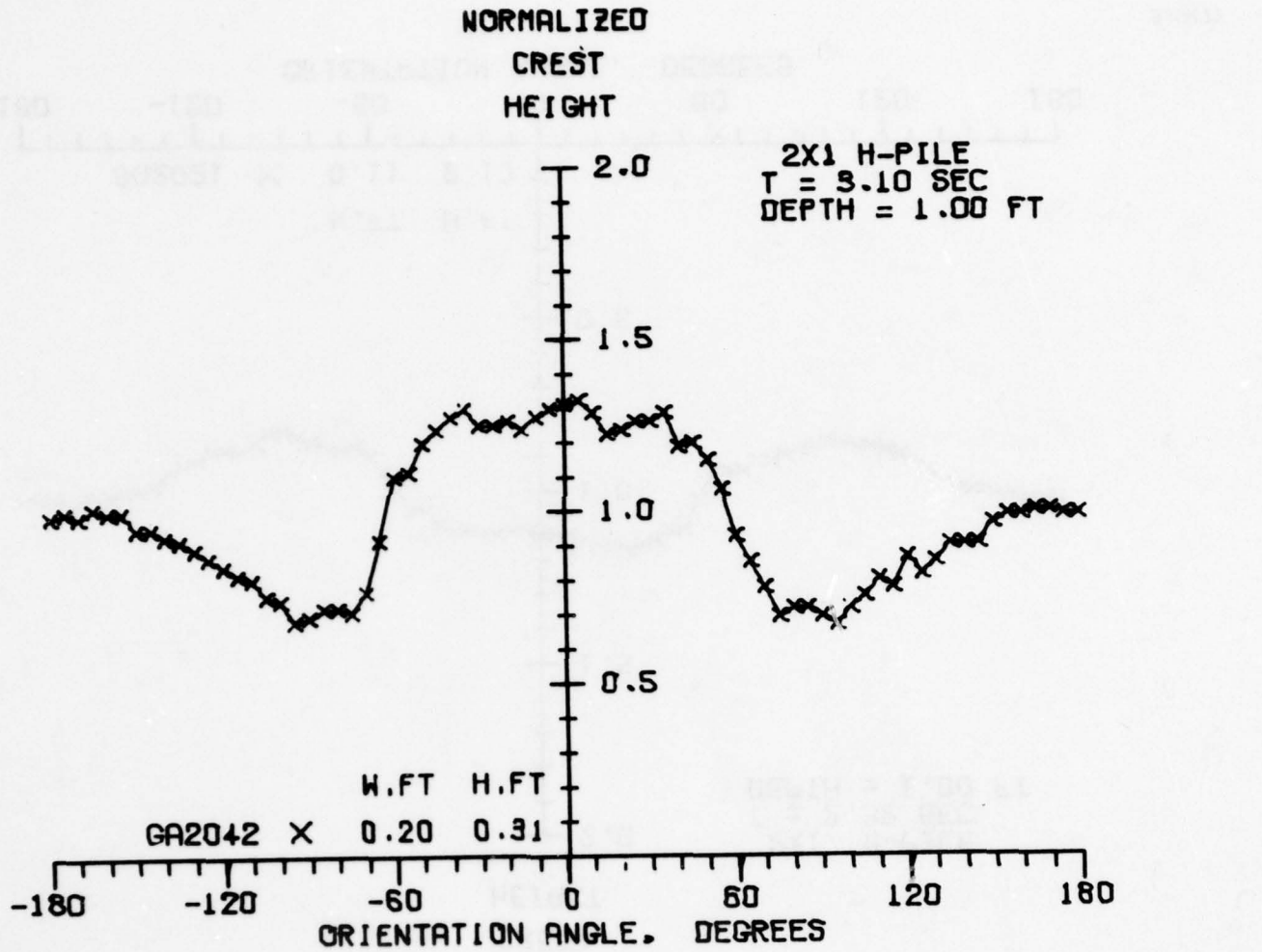
NORMALIZED
CREST
HEIGHT
2X1 H-PILE
T = 3.10 SEC
DEPTH = 1.00 FT
2.0
1.5
1.0
0.5
W.FT H.FT
GA2042 X 0.20 0.31
-180
-120
-60
0
60
120
180
ORIENTATION ANGLE, DEGREES
9JUN77

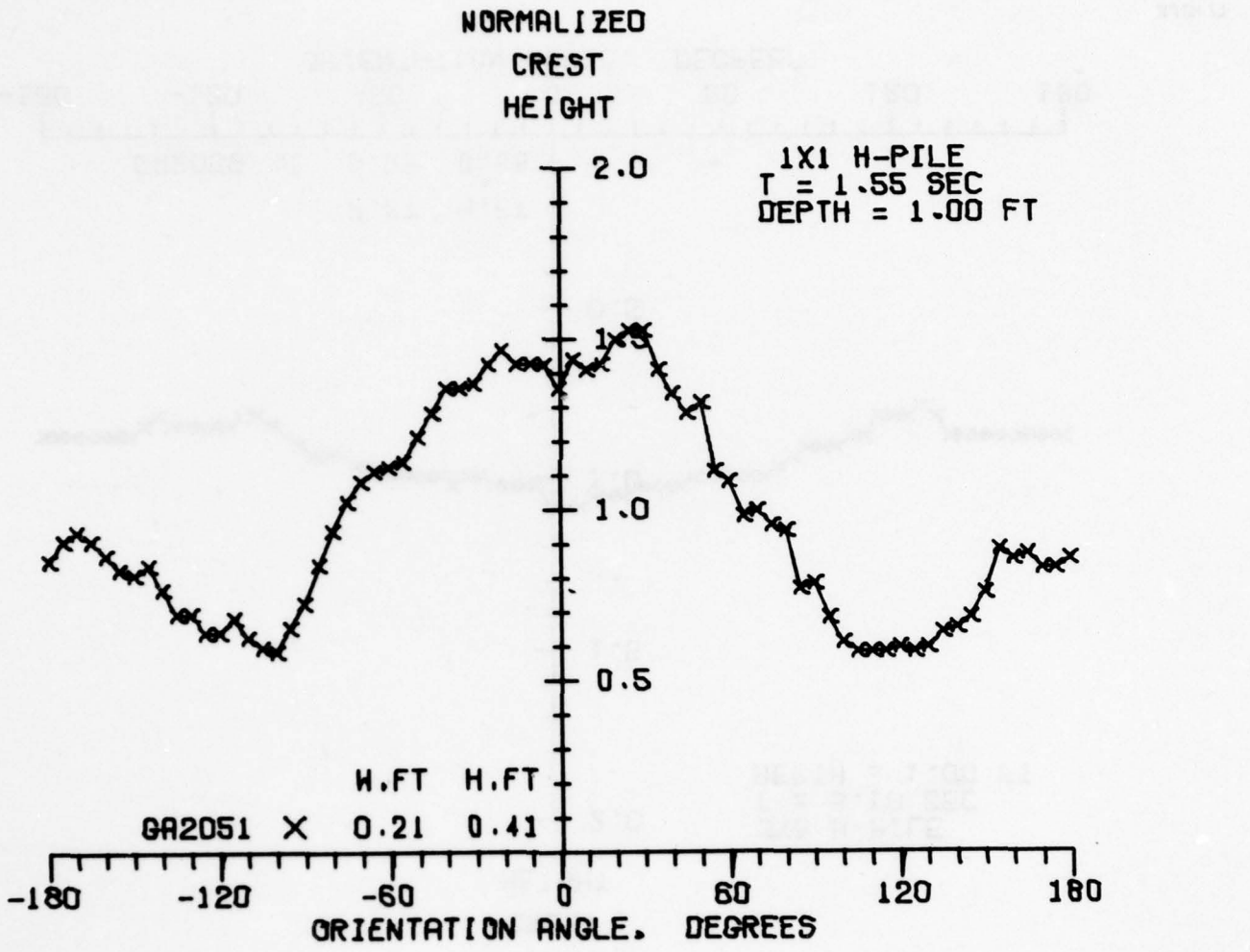
NORMALIZED
CREST
HEIGHT
1X1 H-PILE
T = 1.55 SEC
DEPTH = 1.00 FT
2.0
1.0
0.5
H,FT H,FT
GA2051 X 0.21 0.41
-180
-120
-60
0
60
120
180
ORIENTATION ANGLE, DEGREES
9JUN77

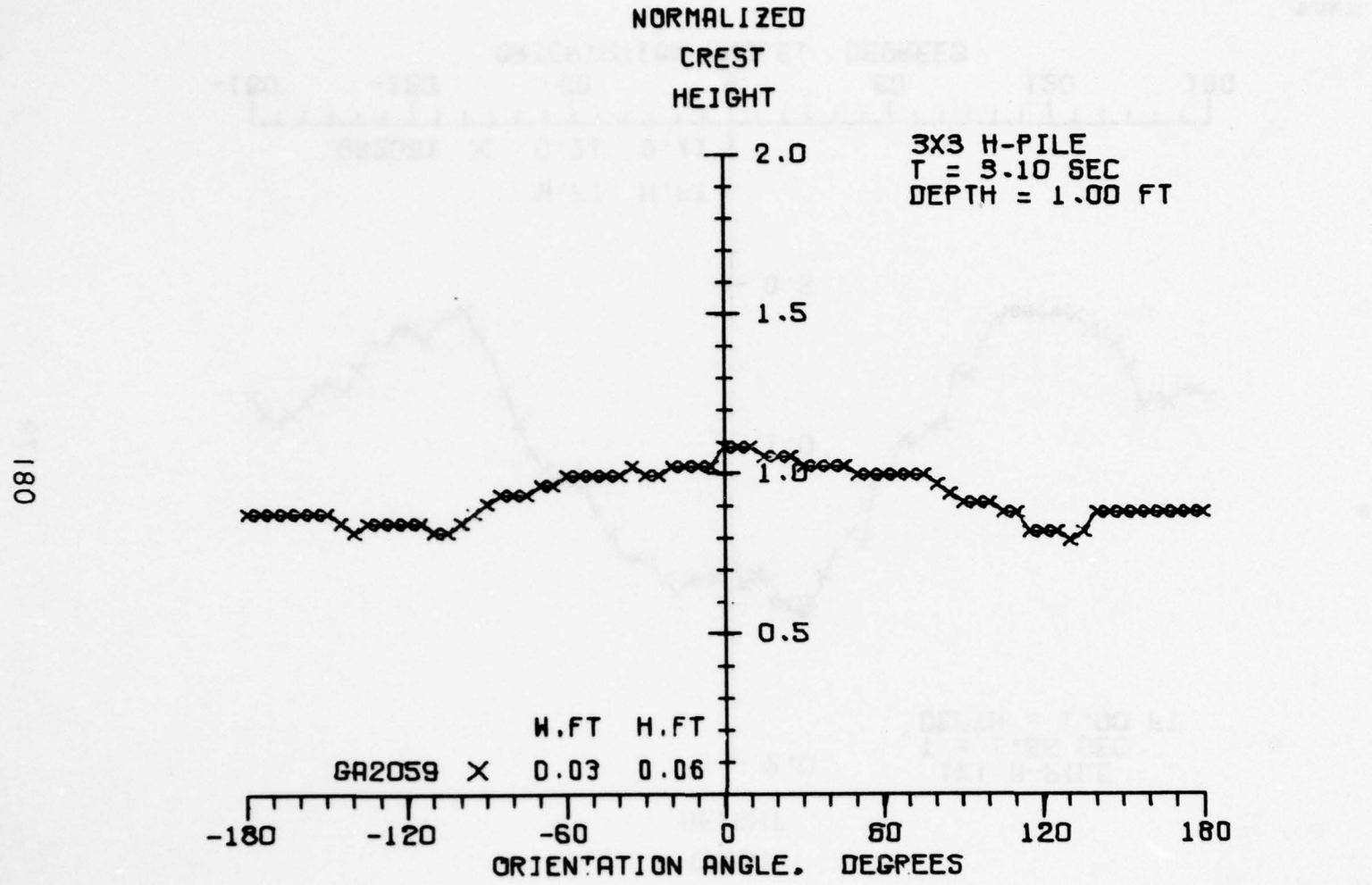
NORMALIZED
CREST
HEIGHT
3X3 H-PILE
T = 3.10 SEC
DEPTH = 1.00 FT
2.0
1.5
1.0
0.5
180
H,FT H,FT
GA2059 X 0.03 0.06
-180
-120
-60
0
60
120
180
ORIENTATION ANGLE, DEGREES
3JUN77

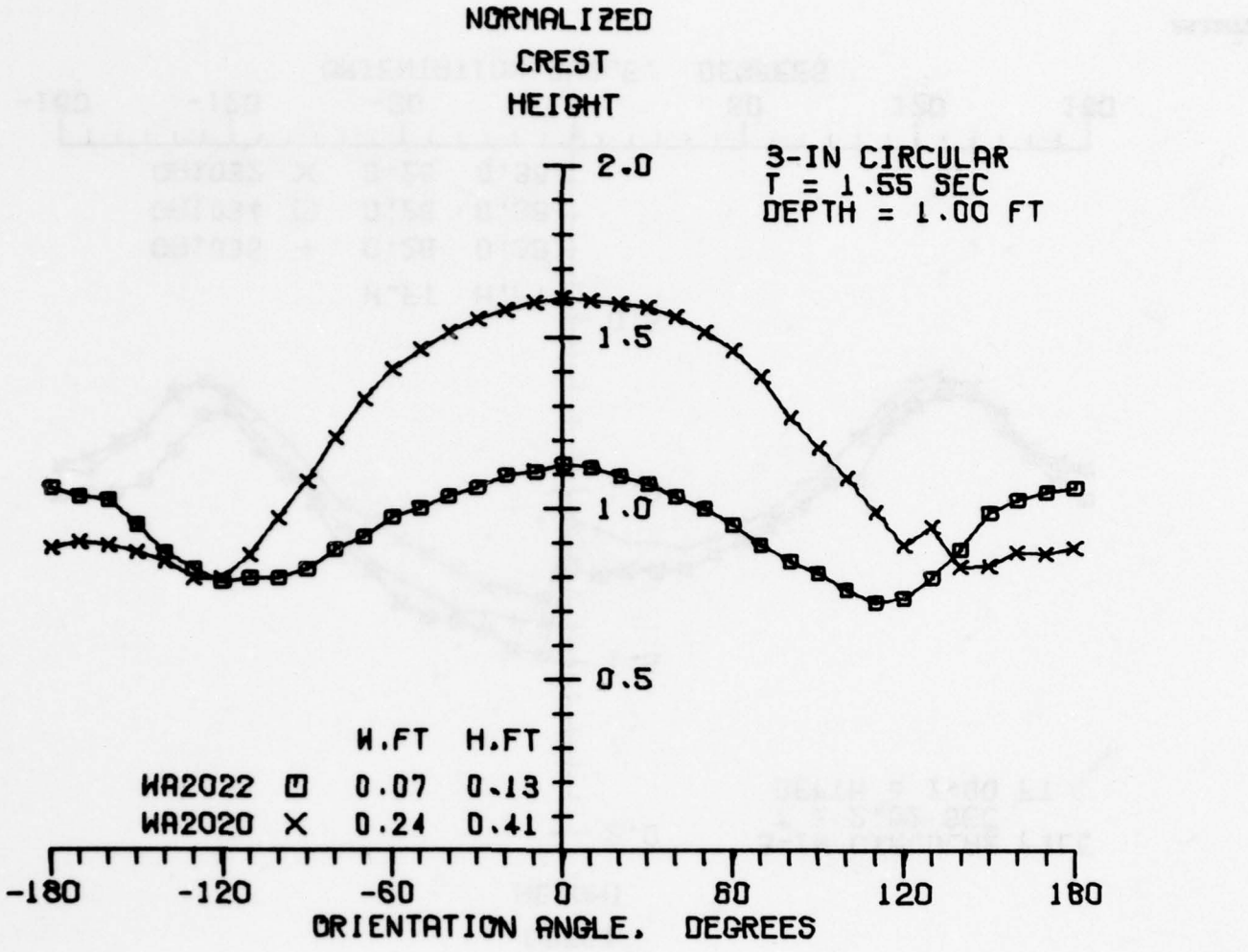
NORMALIZED
CREST
HEIGHT
3-IN CIRCULAR
T = 1.55 SEC
DEPTH = 1.00 FT
2.0
1.5
1.0
0.5
W.FT H.FT
WA2022 0.07 0.13
WA2020 0.24 0.41
-180
-120
-60
0
60
120
180
ORIENTATION ANGLE, DEGREES
9JUN77

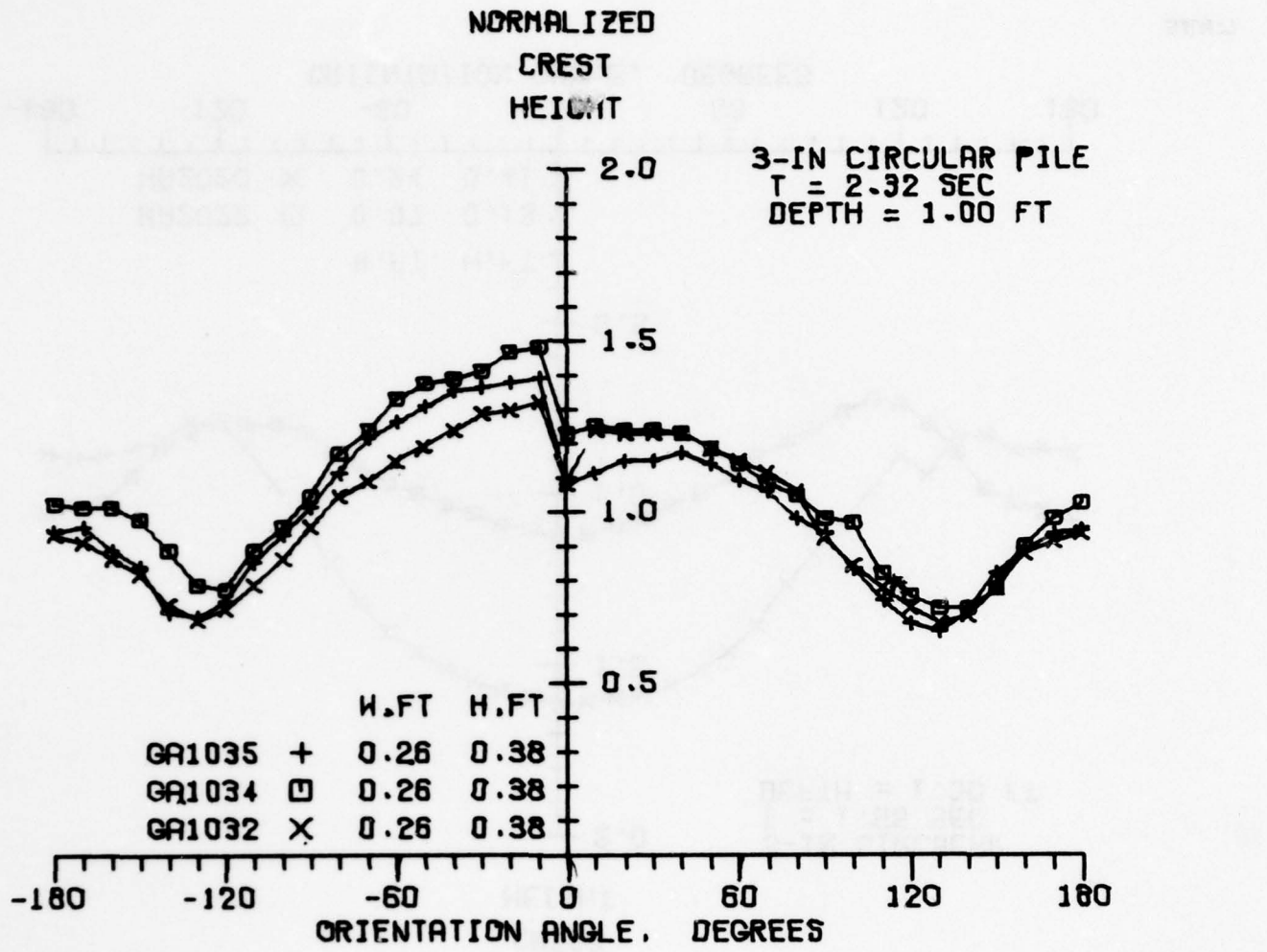
NORMALIZED
CREST
HEIGHT
3-IN CIRCULAR PILE
T = 2.32 SEC
DEPTH = 1.00 FT
2.0
1.5
1.0
0.5
H,FT H,FT
GA1035 + 0.26 0.38
GA1034 □ 0.26 0.38
GA1032 X 0.26 0.38
-180
-120
-60
0
60
120
180
ORIENTATION ANGLE, DEGREES
28JUN77

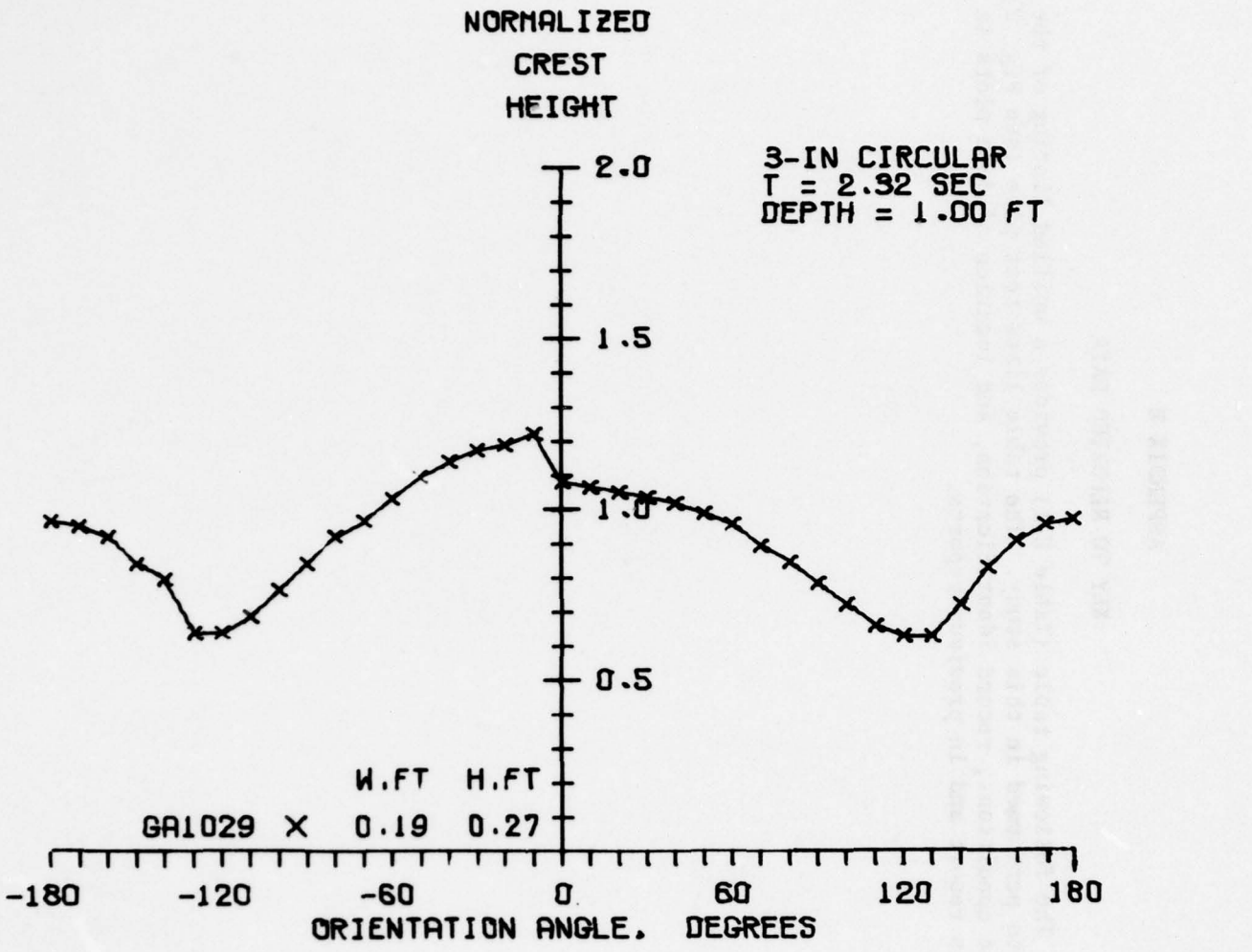
NORMALIZED
CREST
HEIGHT
3-IN CIRCULAR
T = 2.32 SEC
DEPTH = 1.00 FT
2.0
1.5
1.0
0.5
W.FT H.FT
GA1029 X 0.19 0.27
-180
-120
-60
0
60
120
180
ORIENTATION ANGLE, DEGREES
9JUN77

APPENDIX E

KEY TO REPORTED DATA

The following table (Table E-1) provides a unified listing of the tests performed in this study. The table lists test pile (see Fig. 2), test conditions, record identification, and location of data plots in this report and in previous reports.

Table E-1. Key to reported data.

Test pile	Test condition T (s)	Test condition d (ft)	Record I.D.	Plots in this report		Plots in previous reports: Galvin and Hallermeier (1972)	Hallermeier (1976)	James and Hallermeier (1976)
Flat plate	1.55	1.00	GA2007	Fig. 28	p. 94	-------	---------	-------
	2.32	1.00	GA2009	-------	p. 173	Fig. 13	---------	-------
			GA2010	Fig. 27	p. 95	-------	---------	-------
			GA2013	Figs. 6,27	p. 173	Fig. 13	---------	-------
			GA2014	Fig. 27	p. 95	Fig. 13	---------	-------
			GA2015	Fig. 27	p. 173	Fig. 13	---------	-------
	3.10	1.00	GA2018	Fig. 28	p. 174	-------	---------	-------
1x2 H-pile	1.55	1.00	GA2036	-------	p. 96	-------	---------	-------
			GA2037	-------	p. 96	-------	---------	-------
			GA2038	Fig. 28	p. 175	-------	---------	-------
	2.32	1.00	GA2027	Figs. 27,31	p. 97	Fig. 12	---------	-------
			GA2028	Figs. 6,8,27	p. 98	Fig. 12	---------	-------
			GA2029	Fig. 27	p. 97	Fig. 12	---------	-------
			GA2030	Fig. 27	p. 176	Fig. 12	---------	-------
	3.10	1.00	GA2032	Fig. 28	p. 99	-------	---------	-------
			GA2033	-------	p. 100	-------	---------	-------
			GA2035	-------	p. 99	-------	---------	-------
2x1 H-pile	1.55	1.00	GA2039	Fig. 28	p. 101	-------	---------	-------
			GA2041	-------	p. 101	-------	---------	-------
	2.32	1.00	GA2019	Figs. 27,31	p. 102	Fig. 10	---------	-------
			GA2020	Figs. 6,27	p. 103	Fig. 10	---------	-------
			GA2021	Fig. 27	p. 177	Fig. 10	---------	-------
			GA2022	Fig. 27	p. 102	Fig. 10	---------	-------
	3.10	1.00	GA2042	Fig. 28	p. 178	-------	---------	-------
			GA2044	-------	p. 104	-------	---------	-------
			GA2045	-------	p. 104	-------	---------	-------
1x1 H-pile	1.55	1.00	GA2051	Fig. 32	p. 179	-------	---------	-------
			GA2052	Fig. 32	p. 105	-------	---------	-------
	2.32	1.00	GA1039	Fig. 31	p. 106	-------	---------	-------
	3.10	1.00	GA2053	-------	p. 107	-------	---------	-------
			GA2054	Fig. 33	p. 107	-------	---------	-------
2x2 H-pile	2.32	1.00	GA1003	Fig. 31	p. 108	Fig. 11	---------	-------
			GA1004	-------	p. 109	Fig. 11	---------	-------
			GA1005	-------	p. 108	Fig. 11	---------	-------
			GA1006	-------	p. 109	Fig. 11	---------	-------
			GA1031	-------	p. 108	-------	---------	-------
	3.10	1.00	GA1007	-------	p. 110	-------	---------	-------
			GA1008	-------	p. 111	-------	---------	-------
			GA1011	Fig. 33	p. 110	Fig. 4	---------	-------
	2.35	2.33	GB2040	-------	p. 112	-------	---------	-------
	3.55	2.33	GB2047	-------	p. 113	-------	---------	-------
3x3 H-pile	1.55	1.00	GA2060	Fig. 20	p. 114	-------	---------	-------
			GA2061	Figs. 20,32	p. 114	-------	---------	-------
	3.10	1.00	GA2055	Fig. 20	p. 115	-------	---------	-------
			GA2059	Fig. 20	p. 180	-------	---------	-------
5x1 H-pile	2.35	2.33	GB2041	-------	p. 116	-------	---------	-------
			GB2042	-------	p. 116	-------	---------	-------
			GB2043	-------	p. 117	-------	---------	-------
	3.55	2.33	GB2045	Fig. 31	p. 118	-------	---------	-------
Pile with 25 fins	2.35	2.33	GB2039	-------	p. 119	-------	---------	-------
	3.55	2.33	EB2009	-------	p. 122	-------	---------	-------
			EB2010	-------	p. 122	-------	---------	-------
			GB2002	-------	p. 120	-------	---------	-------
			GB2016	-------	p. 120	-------	---------	-------
	4.70	2.33	GB2006	-------	p. 121	-------	---------	-------

Table E-1. Key to reported data.--continued

Test pile	Test condition T (s)	Test condition d (ft)	Record I.D.	Plots in this report		Plots in previous reports: Galvin and Hallermeier (1972)	Plots in previous reports: Hallermeier (1976)	Plots in previous reports: James and Hallermeier (1976)
Pile with 33 fins	3.55	2.33	EB2004	Fig. 26	p. 123	-------	---------	-------
			EB2005	-------	p. 123	-------	---------	-------
			EB2007	-------	p. 123	-------	---------	-------
6-in circular	1.00	0.35	WA2058	-------	p. 125	-------	Fig. 2a	-------
			WA2059	-------	p. 125	-------	Fig. 2a	-------
			WA2060	-------	p. 125	-------	Fig. 2a	-------
			WA3009	-------	p. 124	-------	Fig. 2a	-------
			WA3010	-------	p. 124	-------	Fig. 2a	-------
			WA3011	-------	p. 124	-------	Fig. 2a	-------
	2.35	2.33	WB2009	-------	p. 125	-------	---------	-------
			WB2010	-------	p. 126	-------	---------	-------
			WB2011	-------	p. 125	-------	---------	-------
			WB2012	-------	p. 126	-------	---------	-------
	3.55	2.33	EB2004	-------	p. 130	-------	---------	-------
			EB2005	Fig. 26	p. 130	-------	---------	-------
			WB2001	Fig. 23	p. 128	-------	---------	-------
			WB2002	Fig. 23	p. 128	-------	---------	-------
			WB2003	Figs. 23,24	p. 128	Fig. 14	---------	-------
			WB2013	-------	p. 129	-------	---------	-------
			WB2014	-------	p. 129	-------	---------	-------
			WB2015	-------	p. 129	-------	---------	-------
	4.70	2.33	WB2004	-------	p. 131	-------	---------	-------
			WB2005	-------	p. 132	-------	---------	-------
			WB2006	-------	p. 131	-------	---------	-------
			WB2007	-------	p. 131	-------	---------	-------
			WB2008	-------	p. 132	-------	---------	-------
3-in circular	1.55	1.00	EA3032	-------	p. 134	-------	Figs. 4,5	-------
			EA3033	-------	p. 135	-------	Figs. 4,5	-------
			EA3034	-------	p. 135	-------	Figs. 4,5	-------
			EA3035	Fig. 25	p. 134	-------	Figs. 4,5	Fig. 2a
			EA3044	-------	p. 134	-------	Figs. 4,5	-------
			EA3045	-------	p. 135	-------	Figs. 4,5	-------
			EA3046	-------	p. 136	-------	Figs. 4,5	-------
			EA3047	Fig. 2	p. 136	-------	Figs. 4,5	Fig. 2d
			EA3087	-------	p. 138	-------	Figs. 4,5	-------
			EA3088	-------	p. 138	-------	Figs. 4,5	-------
			EA3089	-------	p. 139	-------	Figs. 4,5	-------
			EA3098	-------	p. 139	-------	Figs. 4,5	-------
			WA2009	-------	p. 133	-------	---------	-------
			WA2010	-------	p. 133	-------	---------	-------
			WA2011	-------	p. 133	-------	---------	-------
			WA2015	Fig. 22	p. 133	Fig. 8	---------	-------
			WA2020	Fig. 20	p. 181	-------	---------	-------
			WA2022	Fig. 20	p. 181	-------	---------	-------
			WA3070	-------	p. 137	-------	---------	-------
	2.32	1.00	EA3083	-------	p. 142	-------	Figs. 4,5	-------
			EA3084	-------	p. 143	-------	Figs. 4,5	-------
			EA3085	-------	p. 143	-------	Figs. 4,5	-------
			EA3086	-------	p. 142	-------	Figs. 4,5	-------
			EA3096	-------	p. 143	-------	Figs. 4,5	-------
			EA3097	-------	p. 142	-------	Figs. 4,5	-------
			GA1029	Figs. 6,8	p. 183	-------	---------	-------
			GA1032	-------	p. 182	-------	---------	-------
			GA1034	-------	p. 182	-------	---------	-------
			GA1035	-------	p. 182	-------	---------	-------
			WA2001	Fig. 21	p. 140	Fig. 9	Fig. 2b	-------
			WA2002	Fig. 21	p. 140	Fig. 9	Fig. 2b	-------
			WA2003	-------	p. 140	Fig. 9	---------	-------
			WA2004	Fig. 21	p. 140	Fig. 9	Fig. 2b	-------
			WA2012	Fig. 22	p. 144	Fig. 8	---------	-------
			WA2026	Fig. 24	p. 141	-------	---------	-------

Table E-1. Key to reported data.--continued

Test pile	Test condition		Record I.D.	Plots in this report		Plots in previous reports		
	T (s)	d (ft)				Galvin and Hallermeier (1972)	Hallermeier (1976)	James and Hallermeier (1976)
3-in circular (continued)	3.10	1.00	EA3036	Fig. 7	p. 148	-------	Figs. 4,5	-------
			EA3037	-------	p. 149	-------	Figs. 4,5	-------
			EA3038	-------	p. 150	-------	Figs. 4,5	-------
			EA3039	Fig. 25	p. 151	-------	Figs. 4,5	Fig. 2b
			EA3040	-------	p. 148	-------	Figs. 4,5	-------
			EA3041	-------	p. 149	-------	Figs. 4,5	-------
			EA3042	-------	p. 150	-------	Figs. 4,5	-------
			EA3043	Figs. 7,25	p. 151	-------	Figs. 4,5	Fig. 2c
			EA3090	-------	p. 154	-------	Figs. 4,5	-------
			EA3091	-------	p. 152	-------	Figs. 4,5	-------
			EA3092	-------	p. 154	-------	Figs. 4,5	-------
			EA3093	-------	p. 154	-------	Figs. 4,5	-------
			EA3094	-------	p. 153	-------	Figs. 4,5	-------
			EA3095	-------	p. 153	-------	Figs. 4,5	-------
			WA2005	Fig. 20	p. 144	-------	----------	-------
			WA2006	-------	p. 144	-------	----------	-------
			WA2007	-------	p. 145	-------	----------	-------
			WA2008	Fig. 20	p. 145	-------	----------	-------
			WA2013	-------	p. 146	-------	----------	-------
			WA2014	-------	p. 146	-------	----------	-------
			WA2016	Fig. 22	p. 145	Fig. 8	----------	-------
			WA3078	-------	p. 147	-------	----------	-------
1.5-in circular	1.55	1.00	EA3099	-------	p. 157	-------	Figs. 4,5	-------
			EA3107	-------	p. 158	-------	Figs. 4,5	-------
			EA3108	-------	p. 157	-------	Figs. 4,5	-------
			EA3110	-------	p. 158	-------	Figs. 4,5	-------
			EA3111	-------	p. 157	-------	Figs.3,4,5	-------
			WA3048	-------	p. 155	-------	Figs. 4,5	-------
			WA3049	-------	p. 155	-------	----------	-------
			WA3050	-------	p. 156	-------	----------	-------
			WA3051	-------	p. 156	-------	Figs. 4,5	-------
	2.32	1.00	EA3100	-------	p. 161	-------	Figs. 4,5	-------
			EA3101	-------	p. 161	-------	Figs. 4,5	-------
			WA3052	Fig. 11	p. 159	-------	----------	-------
			WA3053	-------	p. 159	-------	----------	-------
			WA3054	-------	p. 160	-------	----------	-------
			WA3055	-------	p. 160	-------	----------	-------
	3.10	1.00	EA3102	-------	p. 162	-------	Figs. 4,5	-------
			EA3103	-------	p. 163	-------	Figs. 4,5	-------
			EA3104	-------	p. 162	-------	Figs. 4,5	-------
			EA3105	-------	p. 164	-------	Figs. 4,5	-------
			EA3106	-------	p. 163	-------	Figs. 4,5	-------
			EA3109	-------	p. 164	-------	Figs. 4,5	-------
			WA3056	-------	p. 165	-------	----------	-------
			WA3057	-------	p. 165	-------	----------	-------
			WA3058	-------	p. 166	-------	----------	-------
			WA3059	-------	p. 166	-------	----------	-------

Hallermeier, Robert J.
Wave transformation at isolated vertical piles in shallow water / by Robert J. Hallermeier and Robert E. Ray. – Fort Belvoir, Va. : U.S. Coastal Engineering Research Center ; Springfield, Va. : available from National Technical Information Service, 1978.
187 p. : ill. (Technical paper – U.S. Coastal Engineering Research Center ; no. 78-1)
Bibliography : p. 69.
This report presents the results of a laboratory investigation of wave height measurements at an isolated pile. The investigation was motivated by the possibility that wave transformation near a pile can be used to measure nearshore wave directions. Twelve different vertical piles were tested, including circular, circular with radial fins, and various H-sections.
1. Wave transformation. 2. Wave forces. 3. Wave runup. 4. Wave gages. 5. Wave direction. I. Title. II. Ray, Robert E., joint author. III. U.S. Coastal Engineering Research Center. Technical paper no. 78-1.
TC203 .U581tp no. 78-1 627

Hallermeier, Robert J.
Wave transformation at isolated vertical piles in shallow water / by Robert J. Hallermeier and Robert E. Ray. – Fort Belvoir, Va. : U.S. Coastal Engineering Research Center ; Springfield, Va. : available from National Technical Information Service, 1978.
187 p. : ill. (Technical paper – U.S. Coastal Engineering Research Center ; no. 78-1)
Bibliography : p. 69.
This report presents the results of a laboratory investigation of wave height measurements at an isolated pile. The investigation was motivated by the possibility that wave transformation near a pile can be used to measure nearshore wave directions. Twelve different vertical piles were tested, including circular, circular with radial fins, and various H-sections.
1. Wave transformation. 2. Wave forces. 3. Wave runup. 4. Wave gages. 5. Wave direction. I. Title. II. Ray, Robert E., joint author. III. U.S. Coastal Engineering Research Center. Technical paper no. 78-1.
TC203 .U581tp no. 78-1 627

188

Hallermeier, Robert J.
Wave transformation at isolated vertical piles in shallow water / by Robert J. Hallermeier and Robert E. Ray. – Fort Belvoir, Va. : U.S. Coastal Engineering Research Center ; Springfield, Va. : available from National Technical Information Service, 1978.
187 p. : ill. (Technical paper – U.S. Coastal Engineering Research Center ; no. 78-1)
Bibliography : p. 69.
This report presents the results of a laboratory investigation of wave height measurements at an isolated pile. The investigation was motivated by the possibility that wave transformation near a pile can be used to measure nearshore wave directions. Twelve different vertical piles were tested, including circular, circular with radial fins, and various H-sections.
1. Wave transformation. 2. Wave forces. 3. Wave runup. 4. Wave gages. 5. Wave direction. I. Title. II. Ray, Robert E., joint author. III. U.S. Coastal Engineering Research Center. Technical paper no. 78-1.
TC203 .U581tp no. 78-1 627

Hallermeier, Robert J.
Wave transformation at isolated vertical piles in shallow water / by Robert J. Hallermeier and Robert E. Ray. – Fort Belvoir, Va. : U.S. Coastal Engineering Research Center ; Springfield, Va. : available from National Technical Information Service, 1978.
187 p. : ill. (Technical paper – U.S. Coastal Engineering Research Center ; no. 78-1)
Bibliography : p. 69.
This report presents the results of a laboratory investigation of wave height measurements at an isolated pile. The investigation was motivated by the possibility that wave transformation near a pile can be used to measure nearshore wave directions. Twelve different vertical piles were tested, including circular, circular with radial fins, and various H-sections.
1. Wave transformation. 2. Wave forces. 3. Wave runup. 4. Wave gages. 5. Wave direction. I. Title. II. Ray, Robert E., joint author. III. U.S. Coastal Engineering Research Center. Technical paper no. 78-1.
TC203 .U581tp no. 78-1 627

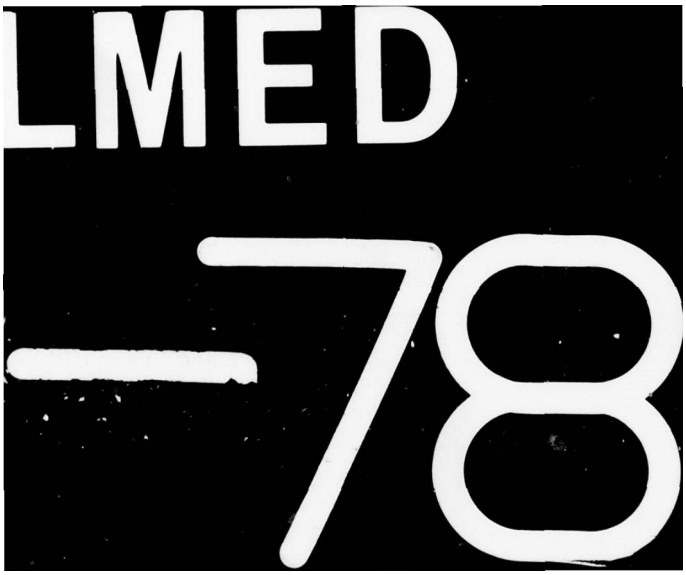
LMED
78